The development of quartz crystal microbalance based chemical sensors

Drake, Philip

Award date:
2000

Awarding institution:
University of Bath

The Development of Quartz Crystal Microbalance Based Chemical Sensors

submitted by Philip Drake
for the degree of PhD
of the University of Bath
2000

ProQuest LLC
789 East Eisenhower Parkway
P.O. Box 1346
Ann Arbor, MI 48106-1346

Summary

Chemical sensors based on the quartz crystal microbalance are investigated. Two liquid phase and two gas phase sensor systems are utilised with the main focus of the work towards the development of the liquid phase systems.

The two liquid phase systems are based on crown ether containing copolymer coatings that respond selectively to $K^+_{(aq)}$ over the other Group I ions $Na^+_{(aq)}$ and $Li^+_{(aq)}$. The uptake of the resins for $K^+_{(aq)}$ was in the order of 1000 μg per gram of the resin. The equilibrium constant for the crown ether complex formation with $K^+_{(aq)}$ is found to be 1554 ± 617 dm^3mol^{-1}. The 18-crown-6 copolymer is successfully synthesised on the surface of a QCM resonator with selectivity over other Group I ions maintained. The sensitivity of the sensor is estimated to be 0.2 ppm over the concentration range of 0-2000 ppm. The sensor is also employed in an FIA system to monitor the concentration of $K^+_{(aq)}$ injected into the flow.

The two gas phase systems are based on cyclodextrin (CD) and azobenzene dye coatings. The cyclodextrin based sensors are designed to respond generally to volatile organic species (VOCs) and more specifically alcohol vapours. The azobenzene dye coating is designed to respond selectively to NO_x gas.

For the cyclodextrin system three resonators are coated with 2.46 μg, 2.66 μg and 1.39 μg of α-CD, β-CD and amylose respectively. The response factor associated with the exposure of the resonators to VOCs is calculated. For α-CD the methanol response factor is 5.30 Hz Sec μg^{-1} with all other non-alcoholic VOCs less than 0.50 Hz Sec μg^{-1}. For β-CD the methanol response factor is 3.03 Hz Sec μg^{-1}, again with all other non-alcoholic VOCs less then 0.60 Hz Sec μg^{-1}. The amylose sensor had response factors less than 0.70 Hz Sec μg^{-1} for all VOCs.

For the $NO_{x(gas)}$ system several resonators are coated with Langmuir-Blodgett, (LB), films of the azobenzene dye. The mass of the films are estimated to be 0.17 μg, 0.97 μg and 1.50 μg. The resonators are utilised to determine θ; the ratio of occupied binding sites to the total available binding sites after the films were exposed to 100 ppm $NO_{x(gas)}$. This is found to be $\theta = 0.433 \pm 0.018$. The detection limit for $NO_{x(gas)}$ is about 1 ppm.

I would like to dedicate this thesis to Dan-Lin whose love and support was an endless source of inspiration.

You may have been far away,
but you were never far from my thoughts!

Acknowledgements

I would like to thank Gareth Price for giving me the opportunity to work in this interesting and rewarding area, for his expert supervision and guidance, good humour and satirical remarks! I would also like to thank the University of Bath for providing the financial support.

My thanks also go out to Mike Bailes for building the QCM and writing the operating software and to Alan Carver for running the AES, AAS and CHN analysis of all the samples.

Finally I would like to thank my lab colleagues, Simon H and Simon C, David B and David S and my two house mates, Claire and Roger for making my time in Bath extremely enjoyable and Suki, Claire, Zareen, Sharon, Matt, Jim and Duncan for all the weekends away.

CHAPTER ONE

INTRODUCTION AND THEORY

CHAPTER TWO

EXPERIMENTAL

CHAPTER THREE

CROWN ETHER BASED $K^+_{(aq)}$ SENSORS

CHAPTER FOUR

GAS PHASE QCM-BASED CHEMICAL SENSORS

CHAPTER FIVE

CONCLUSION AND FURTHER WORK

INTRODUCTION AND THEORY

CHAPTER ONE

1.1 Chemical Sensors

An interesting trend of the modern society is the desire to take control. To control the level of fluoride in their drinking water, to control the temperature of the office building, to control and understand every aspect of the environment in which they live, work and play. This quest requires the acquisition and the processing of vast amounts of information associated with different circumstances and different events. The complex data manipulation required for this 'control' is only conceivable because of the super computers so widely available in today's high-tech world. The processing power and data storage facility of these devises far exceeds that of their early predecessors. Chemical sensors form part of this information revolution and contribute to a data acquisition process in which some insight is obtained about the chemical composition of a system in real time. Like most aspects of modern science this insight owes its existence to the data processing powers of neoteric computers. Without these devices the endless amount of raw data collected could not be processed and the subsequent analysis could not be performed.

The term 'chemical sensor' can be somewhat misleading and is used in the scientific community to describe a variety of devices. For this reason a brief attempt will be made to clarify the meaning of the term 'chemical sensor' and provide a definition for the purpose of this dissertation.

Sensors, in general, can be defined as anything that receives a signal or stimulus and responds to it [1]. They can be divided into two main subsets, physical sensors for purposes such as measurement of temperature, pressure, or magnetic flux, and chemical sensors such as glucose, CO_2 gas and pH meters. Physical sensors, as their name suggests, respond to changes in the physical environment, a temperature increase for example. They offer no correlation between the physical change and any chemical reaction that may have caused that change. A chemical sensor on the other hand is a device that responds to a particular chemical species and can be used for the qualitative or quantitative analysis of that species, in either the gas phase or the liquid phase. The useful information obtained is primarily the concentration or activity of the species of interest, however, this can often be related to other aspects of the system.

Chemical sensors generally consist of two distinct components that perform two separate tasks; these are selection followed by conversion. The first step, selection, is the mechanism employed by the sensor to identify and recognise the species of interest. The conversion step is the translation of the physical or chemical signal generated by the recognition process into a signal that can be recorded and interpreted by the operator. The transducer performs this task. Sensors can therefore be further categorised by either the mechanism used for selection or the type of transducer employed. A brief overview of the various transducers available will be presented in the following pages before a more detailed review on the specific method employed for the work covered in this dissertation.

1.2 Transducers Utilised in Chemical Sensors

Each individual method of transduction requires a different type of input signal, therefore the sensors developed based on each transducer vary considerably in their operating conditions and sensitivity. Each type has its own specific requirements, its own advantages and disadvantages.

The transducer is the element of the sensor that receives the physical or chemical signal generated during the recognition process. The signal is then translated and amplified to form an output signal. This output signal is related via some mathematical function to the concentration of the target species, hence, a real time read out can be obtained of the concentration, and any changes or fluctuations in the concentration that may have occurred during the period of analysis. The various categories of transducers available are listed and summarised below.

1.2.1 Electrochemical

Electrochemical transducers [2] are the most widely utilised in chemical sensor applications. This is probably related to the fact that this is also the oldest group of transducers and to date many chemical sensors based on electrochemical devices are commercially available. The transducers rely on the variation of an electrochemical property within the system. This variation can occur in any of three electrical properties, current, conductance and potential difference. The knowledge and

understanding of these three electrochemical properties can be attributed to the works of Heyrovsky [3], Faraday [4] and Nernst [5], with the three properties leading to amperometric, conductimetric and potentiometric devices respectively. Examples of chemical sensors based on these three electrochemical properties include, solid electrolyte gas sensors [6][7] for amperometric devices, semiconductor-based gas sensors [8][9][10] for conductimetric devices and ion-selective electrodes [11] or ion-selective field effect transistors [12] for potentiometric devices. The huge scope and amount of work carried out on electrochemical sensors means that a simple paragraph can not cover every aspect, however, a brief attempt will be made to illustrate the important points and provide examples where appropriate.

The greatest advancements have been in the field of potentiometric devices and amperometric devices. Commercially available chemical sensors based on potentiometric systems find extensive applications in areas such as environmental analysis [13], and particularly in the field of medical analysis [14]. Sodium and potassium are the two most important electrolyte ions in biological fluids, potentiometric chemical sensors are routinely used to analyse solutions for both of these ions. The sensors are based on polymer membrane ion-selective electrodes. The polymer membrane contains a selective ionophore that transports the required species across an interface. The K^+ ionophore is the depsipeptide antibiotic valinomycin which forms a stable 1:1 complex with K^+ selectively over Na^+. The valinomycin membrane transports K^+ about $5x10^3$ times greater than Na^+. The normal range for the concentration of K^+ in adult blood serum is about 3.5-5.0 mM and the concentration of Na^+ about 135-145 mM, thus, this high K^+ selectivity, imparted by the valinomycin, is vital for the sensors useful application. These sensors replaced the flame photometer method previously employed for the clinical determination of K^+ in blood serum. The ion-selective sensors can be operated *in situ* and without excessive operator training, improving both the ease and speed of analysis.

The glucose biosensor [15] is perhaps the most successful amperometric-based sensor. The latest developments have realised the ultimate aim of all chemical sensor research. The production of a commercially available, hand held, easy to use and reliable device. The sensor analyses whole blood for the determination of

glucose levels and can be used by diabetics without supervision in the privacy of their own home. The sensor operates by monitoring the current flow that occurs during the glucose oxidase (GOD) catalysed oxidation of glucose to gluconic acid [16]. The redox process is mediated by the presence of a ferrocene derivative that reproduces the GOD and eliminates the need for oxygen. It is the presence of this mediator that led to the final commercial sensor. Previous glucose biosensors relied on dissolved oxygen to mediate the redox reaction between GOD and glucose. This hampered the biosensor as the oxygen content of blood varies considerably from patient to patient. The ferrocene also allowed the redox reaction to be catalysed at a lower potential +160 mV as opposed to +600 mV. This also improved the sensor reliability, as several impurities in human blood are redox active at +600mV. The sensor is sensitive to glucose concentrations down to 2 ppm, diabetics have blood glucose levels in the range 360-5400 ppm well above the sensor's detection limit.

1.2.2 Thermal

Thermal transducers perform simple microcalorimetry as they respond to heat generated by chemical reactions. The typical sensors that are available based on thermal transducers incorporate a catalytic enzyme reaction [17]. The heat evolved from this highly specific reaction is used as the initial signal indicating the presence of the target species. The transducer itself is usually a thermistor. These are chemically inert, inexpensive, small and very stable [18]. The sensors developed based on thermistors, however, have limited sensitivity. They can detect around 3mM concentrations of the target species. A more promising thermal transducer is the pyroelectric crystal [19][20]. These are crystals that develop opposite charges between two faces of the crystal as a result of changes in temperature. They are similar to piezoelectric crystals except the potential difference occurs as a result of a temperature change rather than a physical stress. Pyroelectric sensors developed in the research laboratory had a sensitivity of approximately 10 μW [21]. A consequence of this is that the direct measurement of the heat of desorption of less than one monolayer of gas is possible [22].

A third sensor based on a thermal transducer is the catalytic gas sensor [23]. These were primarily developed to monitor the concentrations of flammable gases in

mining safety and are often called pellistors. Structurally these sensors are very simple. They consist of a platinum wire passed through a pellet of ThO_2 / Al_2O_3. The pellet is coated with a porous catalytic metal. As gases react at the catalytic layer they increase the temperature of the pellet and so increase the resistance of the platinum coil. The detection limit for these devices is around 0.5 % v/v in air well below the lower explosion limit, (LEL) for most flammable gases. The LEL for methane for example is 5%. This made them ideal for applications as warning devices in the mining industry for concentrations of methane and other flammable gases.

1.2.3 Optical

Optical transducers are devices that can be used for the detection and determination of physical or chemical changes by the change in the optical properties of the sample. The optical properties that can be measured are absorbance, reflectance and luminescence. The technologies available are the same as those found in larger scale optical spectrometers such as FTIR, UV-Vis, and fluorescence as well as other optical instruments such as light scattering and refractive index devices. The improvements in optical fibre technology and advancement with light-emitting diodes, LEDs [24], and the miniaturisation of the laser [25] have all had a pronounced effect in the field of optical chemical sensors. These provide essential components in miniature spectroscopic instruments and light scattering devices. The lasers and LEDs provide the small, compact and high intensity light sources while the fibre optics provide the means of transporting and trapping both the incident and the transmitted or reflected radiation. These devices, however, have their limitations. The fibre optic cable limits the region of the electromagnetic spectrum that can be transmitted. In the case of silica fibres this extends down from about 60000 cm^{-1} to only 5555 cm^{-1} [26]. The region used to identify organic species in infra-red spectroscopy is 4000 cm^{-1} to 600 cm^{-1}, well below the range available in fibre optic technology. One possible solution to this is to use the organic molecules overtone absorbance [27]. These often occur between 8000 cm^{-1} and 6000 cm^{-1}; however, the overtone absorbance is very low in intensity. An example of a chemical sensor employing such technology is the methane gas sensor [28]. The lower explosion limit for methane is 5 % and the higher explosion limit is 15 %. The sensor could

detect methane concentrations at 0.8 % of the lower explosion limit via its overtone absorbance. Other sensors developed based on optical techniques include a light scattering device for the determination of oil pollution in effluent water [29], a reflectance pH sensor based on immobilised bromothymol blue [30] and an ammonia sensor based on the changes in absorbance of *p*-nitrophenol [31].

1.2.4 Piezoelectric

Piezoelectric transducers are devices that respond to mass or viscoelastic changes. These changes can occur in either the transducer itself, on the surface of the transducer or in the medium that the transducer is operating. The historical applications of such devices in chemical analysis are as either surface mass detectors or strain indicators. However, work carried out over the past decade has shown the great potential for these devices to operate as selective chemical sensors. The application of piezoelectric transducers towards chemical sensing is a new and exciting area and has seen great advances in the last few years. This is best illustrated by a quote taken from G. J. Bastiaans of Integrated Chemical Sensors, Newton, Massachusetts, 1988 [32].

"Piezoelectric devices today play a relatively small role in chemical sensing, but there are indications that their use may expand greatly in the future"

To date chemical sensors based on piezoelectric resonators have been developed that respond to virtually any chemical species from gases [33], organic vapours [34], metal ions [35], proteins [36], organic molecules [37] or inorganic molecules [38][39]. The main topic of this thesis is the application of piezoelectric transducers towards selective chemical sensors and as such a more extensive review chapter follows this brief proem.

1.3 Piezoelectric Transducers

The first observations of an electrical effect associated with a crystalline structure can be traced back to the beginning of history itself. The ancient Greeks knew of the mysterious attractive power of rubbed amber [40] and the Ceylonese and Indian people observed that tourmaline crystals, when placed in hot ashes, first attract and then repel the ashes. Europe, however, was a little behind. It was not until 1703 when tourmalines were first imported from Ceylon that this effect was observed and documented.

These observations were all manifestations of the pyroelectric effect, that is, the development of charges at the ends of certain hemihedral crystals, such as tourmaline, as a result of a change in temperature [41], a phenomenon introduced previously. It was the investigation of this pyroelectric effect by Pierre and Jacques Curie in 1880 that led directly to the discovery of the piezoelectric effect [42]. The scientific discussions concerning the possibility of a piezoelectric phenomenon can be traced back to Coulomb (1736-1806), he is reputed to be the first person to suggest the possibility of generating electricity by the application of pressure to the surface of a suitable material [43]. Around 1820 Hauy [44] and Becquerel [45] performed some experiments in which certain crystals showed electrical effects when compressed. Their work was merely an observation of the effect, it was not until 1880 that this effect was systematically studied.

The two brothers, Pierre and Jacques Curie, had been investigating the relationship between pyroelectricity and crystal symmetry, their work had predicted the occurrence of electrical polarisation due to the application of mechanical stress. They developed a theory explaining the effect that could also be used to predict the direction of the applied pressure and to which crystal classes the material exhibiting the effect would belong. In later work they supported these predictions with experimental data showing the piezoelectric effect in several crystals; zinc blende, sodium chlorate, boracite, tourmaline, quartz, calamine, topaz, tartaric acid, cane sugar and Rochelle salt.

The piezoelectric effect, however, remained only a scientific curiosity for several decades. It was the outbreak of the First World War that saw a flurry in activity in the field of piezoelectricity. Langevin applied the principles of

piezoelectricity and developed quartz plates to be used as emitters and receivers of high frequency sound waves underwater, this led to the creation of sonar and the science of ultrasonics [46]. Around the same period it was also realised that the piezoelectric crystals could be employed as electrical resonators. If an alternating potential is applied across a quartz plate mechanical oscillations occur with in the crystal lattice, these oscillations are only stable at the natural resonance frequency of the crystal. Pierce [47] and Cady [48] produced crystal controlled oscillators of high stability for use as frequency filters and tuning devices in the radio and communications industry.

As one might expect the technology associated with these applications has developed over the years. Principally it was the demand from the communications and radio industries that led to the ready availability of cheap, reliable, high quality crystal resonators which are employed for the analytical and scientific research applications. The piezoelectric effect has found extensive applications in a variety of forms and functions [49], pressure and force sensors, accelerometers, microphones, gas lighters, wave filters, ink jet printers, sonar, timing devices, and "smart materials" i.e. active shape, active vibration and active noise control. More recently research has focused on the development of novel chemical sensors based on piezoelectric devices. It is the chemical sensor application that is the main focus for the remainder of this thesis.

1.3.1 Piezoelectric Quartz Crystal Resonators

The crystal structures that will possess the property of piezoelectricity can be predicted from crystallographic studies [50][51]. Although a large number of solids satisfy the conditions required for only a handful of materials are actually used [52]. The material employed for specific applications depends on several physical considerations such as temperature coefficients, magnitude of the piezoelectric potential, mechanical-electrical coupling constants, the direction and size of the piezoelectric displacement etc. In order to develop and enhance these properties research into piezoelectric materials has now been extended from ionic crystalline solids to include ceramics, polymers and composites [53]. These "new" piezoelectric materials have some remarkable properties and as the research continues they will,

with out doubt, replace the current systems. The quartz crystal resonator is, however, the most widely used and most extensively investigated of all the piezoelectric devices [53].

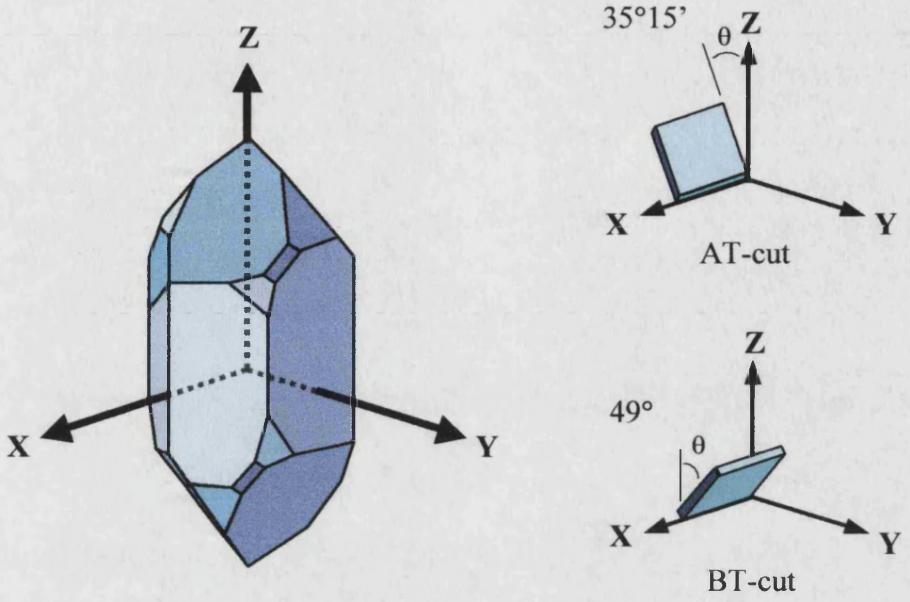

***Figure 1.1**: The assignment of axis to a quartz crystal and the two crystal cuts AT and BT.*

A piezoelectric quartz resonator is a precisely cut slab of a single crystal of quartz. These can be shorn from either natural or synthetic crystals. The application of an external pressure across two faces of the slab results in the formation of internal mechanical stress and produces an electrical potential across the two faces. This is referred to as the direct piezoelectric effect [41]. The reverse effect also applies, that is the application of external electrical potential results in the production of internal mechanical stress, this is known as the converse effect [41]. Thus, when electrodes are attached to the quartz crystal unit and connected to an alternating voltage the quartz unit will oscillate at the frequency of the exciting voltage. If the frequency of the driving voltage is very close to the natural mechanical resonant frequency of the crystal unit then the amplitude of the vibration will reach a maximum. This also results in the electrical impedance of the crystal oscillator to an AC-current becoming resistive only. These two phenomena enable the quartz resonator to be placed in a positive feedback loop of an oscillating circuit. The circuit will then operate at the resonance frequency of the crystal, resulting in an extremely stable frequency generator.

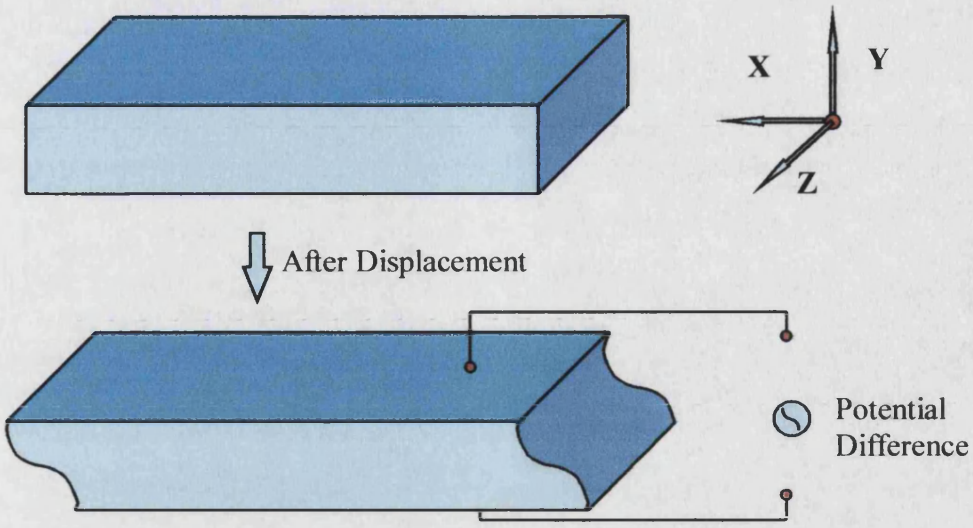

***Figure 1.2**: A quartz slab oscillating in the thickness shear mode. As the acoustic wave propagates it causes displacement in the X-direction on the axis defined in the diagram.*

At its fundamental resonance frequency the piezoelectric quartz resonator can possess several modes of vibrations. A rectangular solid bar for example may have three different vibrational modes; longitudinal (extensional), lateral (shear), and torsional (twist) on all three of the dimensional axes. In addition to the fundamental modes of vibration the system can also oscillate at the overtones of each mode. Further, more complicated modes of vibration can be formed by the coupling of several individual modes, resulting in a set of vibrations that occur in all three-dimensions. By cutting the quartz slab from the main crystal in a specific crystallographic orientation it is possible to enhance one particular mode of vibration and suppress all others. This orientation of the cut also has a marked effect on the temperature dependence of the resonance frequency.

The mode of vibration that is most sensitive to mass changes is the thickness-shear mode. In this mode of vibration the two major surfaces vibrate antiparallel with each other and are always antinodal, see Figure 1.2. In order to maximise a particular mode and suppress all others the slab must be cut from the mother crystal in a exact three dimensional orientation. For a thickness-shear mode resonator these cuts belong to the rotated Y-cut family, the AT-cut and BT-cut crystals are the most extensively used from this group. Over the temperature range of -20 °C to 60 °C the

AT-cut crystals has been found to have the least temperature dependence on their fundamental oscillating frequency [54]. For applications in ranges other than those around room temperature different crystal cuts can provide different temperature stability.

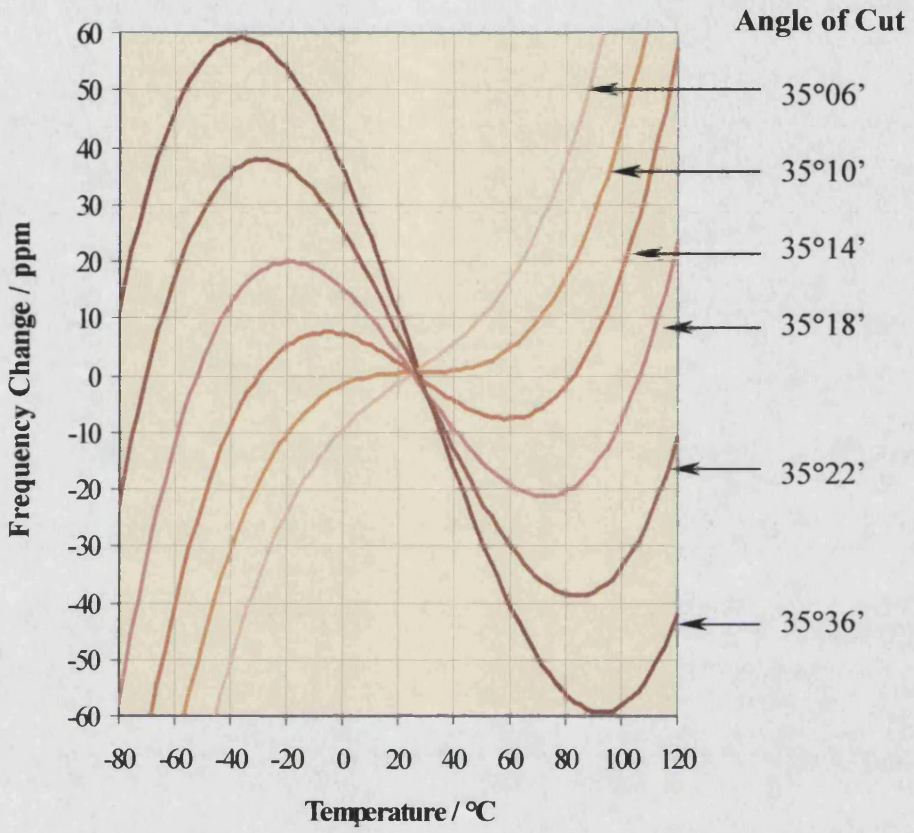

***Figure 1.3**: The dependence of the cutting angle on the frequency-temperature curves for AT-cut quartz crystal resonators.*

1.4 The Quartz Crystal Microbalance

The frequency stability of the quartz resonator is extremely high, typically parts-per-billion, consequently they found extensive use in the communications and electronics industry. This coupled with the accuracy of simple frequency determination measurements, typically part-per-trillion, meant that the quartz crystal resonator became a very reliable highly sensitive device. One of the advantages of the quartz crystal resonator was its fine tuning capabilities. It was soon observed that by simply placing a pencil line on the surface of resonator the frequency of

oscillation could be lowered. Similarly removing the pencil mark via a pencil eraser would restore the initial frequency [55]. The manufacturers produced resonators at a frequency slightly higher than that required, allowing the operator to fine-tune them to their own standards. This frequency shift phenomenon was not investigated systematically for several decades. Sauerbrey [56] was the first to undertake such an investigation in the late 1950's and concluded that there was a simple mass-frequency relationship [57]. This relationship was later used as the fundamental principle behind the quartz crystal microbalance, a device employed to determine film thickness and minute mass changes at the surface of a quartz resonator.

The development of a theoretical model for the quartz crystal microbalance can be traced back to Lord Rayleigh [58] and his work on the propagation of sound waves and addition of mass to a vibrational body. This laid the foundations for the development of a theory relating mass changes on the surface of an acoustic oscillator to the shift in the fundamental resonance frequency of that oscillator. Onoe [59] applied these theories to the quartz resonator to investigate the general case of a quartz plate loaded with a surface film. It was Sauerbrey, however, who suggested using a quartz resonator as a sensor to measure film thickness. He showed experimentally that, under certain conditions, the frequency shift induced by the addition of material to the surface of the resonator was proportional to the mass of the added material to within ± 2%. Later work extended the theoretical understanding and confirmed the experimental data. This was performed by several different groups including, Oberg and Lingensjo in 1959 [60], Behrndt and Love 1962 [61], Warner and Stockbridge 1962 [62][63], EerNisse 1967 [64], Miller and Bolef 1968 [65], and Lu and Lewis 1972 [66][67].

1.4.1 Development of the Sauerbrey Equation

The quartz crystal microbalance, (QCM), as described by Sauerbrey [56][57] can be thought of as a simple piezoelectric resonator coupled to an oscillating circuit. The electronic circuit allows for both the driving of the resonator and the determination of the fundamental oscillating frequency. An idealised physical model of the resonator can be seen in Figure 1.4.

i/

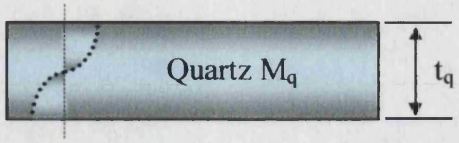

i/ At the fundamental resonance frequency the acoustic wavelength is equal to twice the thickness of the quartz plate.

ii/

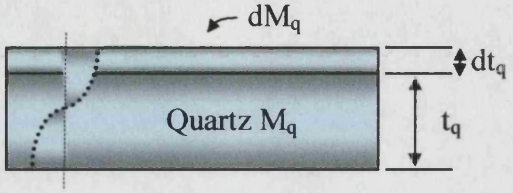

ii/ An increase in the plate thickness results in an increase in the wavelength of the fundamental frequency.

iii/

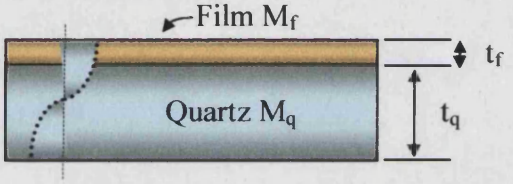

iii/ An addition of a deposited film is treated as the addition of the equivalent thickness of quartz.

***Figure 1.4**: A simplified model of a QCM resonator*

For a quartz plate oscillating in the thickness-shear mode at its fundamental resonance frequency the following equation must be satisfied.

$$t_q = \gamma_q / 2 \qquad (1)$$

Where t_q is the thickness of the quartz plate and γ_q is the wavelength of the shear wave propagating in the thickness direction. The effects of the electrodes are neglected in this simplified case. Equation (1) can be rewritten in terms of the frequency f_q and the velocity v_q of the shear wave.

$$f_q t_q = v_q / 2 \qquad (2)$$

From equation (2) the resonance frequency shift df_q induced by an infinitesimal change in the crystal thickness dt_q can be expressed as;

$$df_q / f_q = - dt_q / t_q \qquad (3)$$

The negative sign indicates that an increase in thickness results in a decrease in frequency.

Equation (3) can also be expressed in terms of the mass of the crystal M_q and its mass change dM_q, thus:

$$df_q / f_q = - dM_q / M_q \qquad (4)$$

Sauerbrey made the assumption that for a small mass change the addition of foreign material can be treated as an equivalent mass change of the quartz crystal itself. This assumption modifies equation (4) to the more general form below.

$$df_q / f_q = - dM / M_q \qquad (5)$$

Where dM is an infinitesimal amount of foreign mass uniformly distributed over the surface of the crystal. Again this equation can be extended to a more general form for an arbitrary addition of foreign mass such as a thin film M_f.

$$(f_c - f_q) / f_q = - M_f / M_q \qquad (6)$$

Where f_c is the resonance frequency of the quartz crystal with the deposited material.

If the mass per unit area of the deposited film and the quartz crystal are equal to m_f and m_q respectively, then for materials with a spatially uniform density m_f and m_q are equal to the product of thickness and density.

$$m_f = t_f \rho_f \qquad (7)$$

$$m_q = t_q \rho_q \qquad (8)$$

Where ρ_f and ρ_q are the densities of the film and the quartz crystal respectively and t_f and t_q are the thickness of the film and the quartz.

By assuming that $- M_f / M_q = m_f / m_q$ and substituting equations (2) and (8) into equation (6) then:

$$m_f = -(f_c - f_q) \rho_q v_q / 2 f_q^2 \qquad (9)$$

It is more satisfactory to use the term m_f, the mass per unit area, rather than the absolute mass, M_f, as the resonators do not have a very well defined area. Also the piezoelectrically active area has a spatial dependence on the frequency response [68][69]. If the film density is known then equation (9) can be used to calculate the film thickness by substituting equation (7) into equation (9).

Equation (9) has become known as the Sauerbrey equation and is often expressed simply by:

$$\Delta f = - C_f m_f \qquad (10)$$

Where Δf is the frequency shift, $\Delta f = f_c - f_q$, and C_f is a constant for a particular cut of quartz.

$$C_f = 2 f_q^2 / (\rho_q v_q) \qquad (11)$$

C_f is used as the mass sensitivity or calibration constant for a QCM.

For an AT-cut quartz crystal $\rho_q = 2650$ kg m^{-3} [70] and $v_q = 3750$ m s^{-1} [71]. This gives a mass sensitivity, for a 10 MHz resonator, of 20.13 M Hz m^2 kg^{-1}. This means that the addition of material equivalent to 4.97 ng cm^{-2} will induce a frequency shift in the resonator of 1 Hz. The resolution of a number of frequency-determining techniques is several orders of magnitude better than 1 Hz.

The derivation performed by Sauerbrey resulted in a simple frequency to mass relationship and leads to several important points. Firstly the QCM monitors the mass per unit area or areal density of the deposited film. The area is that covered

by the overlap of the two electrodes [72]. This is referred to as the piezoelectrically active area and is difficult to calculate experimentally. Consequently any attempt to estimate the mass of a film that does not have a complete uniform coverage will result in the introduction of large experimental uncertainties. Secondly, and more beneficially, the mass sensitivity of the QCM is dependent only on the physical properties of the quartz, so as long as the deposited material covers the active surface completely with an even film then no individual calibration procedure is required. The mass sensitivity is also independent of the physical properties of the deposited film so the nature of deposition should have no effect on the final outcome. The equation was supported by experimental evidence obtained with a calibrated electromechanical microbalance and a QCM operating with 14 MHz AT-cut resonators [57]. The two microbalances gave values that fell within 2% of each other for deposited films over the range 0 – 20 $\mu g\ cm^{-2}$. Several other workers investigated the validity of Sauerbrey's equation by calculating the mass sensitivity C_f of QCMs operating with crystals of various resonance frequencies and a variety of deposited materials [73]. These results confirm that within the range of mass loads investigated C_f is independent of the physical properties of the deposited materials. They also show that the Sauerbrey equation only holds for thin rigid films of mass loads (m_f / m_q), of less than 2 %.

Although the Sauerbrey equation was supported by extensive experimental evidence, the assumptions made during its derivation needed sounder justification; the main criticism being the equivalence drawn between the deposition of a quartz film, effectively extending the bulk material, and the deposition of a foreign material. Sauerbrey assumed that the foreign material acted in identical fashion to the quartz itself, it had the same physical and acoustic properties. The only justification for this assumption was the fact that the theory fitted extremely well to the experimental evidence. In order to support the work by Sauerbrey, Stockbridge [63] applied the perturbation analysis developed by Rayleigh [58] to describe the effect of added mass to a vibrating entity. He assumed that the mass added to an antinode of a vibrating system, such as that at the surface of a quartz crystal resonator oscillating in the thickness shear mode, does not store any potential energy. This implies that the acoustic wave does not propagate into the deposited film. The result of this analysis for a one-dimensional vibrating system with an added mass

uniformly distributed over the entire surface is a power series, which, neglecting the second order and higher terms can be shown to equate to:

$$(f_c - f_q) / f_q = M_f / M_q \qquad (12)$$

This is the same as equation (6) and the Sauerbrey equation.

The two approaches produced identical results, however, the interpretation given by Stockbridge still involved assumptions that were difficult to defend. The assumption that the deposited material did not propagate the acoustic wave can be justified for thin films if one considers the surface roughness. Typically for a QCM resonator this is in the order of 10-100 nm [74]. For a deposited film with thickness less than one micron the acoustic wave interaction will be minimal. The experimental studies design to test the validity of equation 6 employed much thicker films often up to 1.5 mg cm^{-2}. This argument is also contrary to the fact that an even uniform film is required for accurate mass determination. Another problem associated with the Stockbridge equation was the dependence of the higher order terms in the power series on experimentally measured constants that had no physical interpretation [75]. The two theories did however result in the same conclusion, approaching the problem from different angles they both produced the same final equation.

1.4.2 The Period Technique

The Sauerbrey equation was used extensively to monitor thin film deposition and a range of thin film monitors became commercially available. These devices were, however, limited in their practical use due to the break down in the accuracy of the Sauerbrey equation for mass loads greater than 2 %. Despite this these devices proved to be extremely useful. Their commercial success increased interest in the work initiated by Onoe [59] and Sauerbrey [57] with research focusing on overcoming the limitation on the mass load. In 1962 Behrnt and Love [61] extended this mass load to 10 % by replacing f_q, the resonance frequency of the uncoated QCM, with f_Q, the resonance frequency of the QCM prior to deposition. This change

was introduced because of a common operating practice employed by QCM technicians. Material was often deposited onto a resonator that already had a number of layers deposited on it. Thus, using the resonance frequency of the uncoated crystal introduced a progressive error that could be minimised by employing f_Q in place of f_q. They also suggested that the whole equation should be expressed in terms of the change in vibrational period, $\Delta\tau$, where $\tau = 1/f$ and $\Delta\tau = (1/f_c - 1/f_Q)$.

$$m_f / m_q = \Delta\tau / \tau_q \qquad (13)$$

These simple adaptations resulted in a greater correlation between the experimentally deposited mass and that estimated by the QCM. One of the reasons for this is in a mathematical approximation present in the original Sauerbrey equation. The transformation from frequency, f, to period, τ, eliminated this approximation [74]. QCM manufacturers adopted the theory put forward by Berhnt and Love, which became known as the "period technique".

1.4.3 The Z-Match Technique

In 1968 Miller and Bolef [65] addressed the problems associated with the derivations put forward by Sauerbrey and Stockbridge. For the first time the QCM resonator was treated as a composite, with both the film and the bulk quartz interacting with the acoustic wave independently. Both Miller and Bolef had worked on the propagation of continuous acoustic waves through composite resonators systems [76] and developed a strategy for determining the resonance frequencies of the systems. These strategies are too complex to be easily analysed, however, a brief attempt will be made to summarise their work. They considered the acoustic losses and interface reflections associated with a composite resonator and showed that for small mass loads their complex equation approximated to the Sauerbrey form. The work of Miller and Bolef was extended by Lu and Lewis [66] in 1972. They introduced the terms Z_q and Z_f to represent the acoustic impedance of the quartz and the film respectively. The final form of the Lu and Lewis equation is as follows.

$$\frac{m_f}{m_q} = -\frac{z_f f_q}{z_q \pi f_f} \arctan\left(\frac{z_q}{z_f} \tan\frac{\pi f_f}{f_q}\right) \qquad (14)$$

Where Z_f and Z_q are the acoustic impedance of the film and the quartz resonator, f_f and f_q are the resonance frequencies of the QCM with the deposited film present and the prior to deposition respectively.

This equation was employed by the third generation film-thickness monitors and became known as the Z-Match [77] technique. The first and second generation devices were based on the Sauerbrey and Behrnt theories respectively. The Z-Match technique extended the usable mass load of the resonator to well above 60 %. It can be shown that the Z-Match technique encompasses all the previous theories as equation (6) and (13) can be developed from equation (14) by successive approximations [75]. This is presently the most accurate description of the heavily loaded crystal oscillator. The equation indicates that materials with different acoustic properties will obey different mass sensitivity on the resonator. Many independent authors have substantiated the accuracy of the Z-Match technique [78], however, the model is by no means complete. For certain materials a slight deviation is observed at mass loads, greater than 40%, these deviations are most likely caused by tensile stress in the deposited film. The model also breaks down when the deposited film is a viscoelastic material or fluid. This is thought to be as a result of several related and unrelated problems for example; the damping of the mechanical wave by the liquid or viscoelastic film, trapping of the liquid in surface cavities on the crystal and the trapping of tiny microbubbles at the film surface interface. Several later models have attempted to address these problems, most noteworthy are those by Benes [75] and Mecea *et al.* [79].

1.4.4 The Energy Transfer Model

In 1979 Mecea and Bucur introduced the Energy Transfer Model (ETM). The ETM describes the quartz crystal resonator and the deposited film as one entity. The quartz resonator passes vibrational energy to the deposited film that in turn causes the film

to resonate, some of the transferred energy is stored in the film and the rest dissipated to the surroundings. This differs from the Sauerbrey and Berhnt models that viewed the over-layer as an extension to the main resonator, and the Z-Match technique that modelled the acoustic wave rather than the acoustic energy coupling. For a metallic film the ETM equation can be represented as follows:

$$f_q^2 / f_c^2 = 1 + (2\, m_f / m_q) \qquad (15)$$

1.4.5 Implications

Of all the theories describing the mass loaded QCM resonator only the Z-Match technique takes into account the acoustic properties of the over-layer. The nature of the material deposited has a greater effect on the resonance frequency as the mass load increases, Figure 1.5 below illustrates this fact.

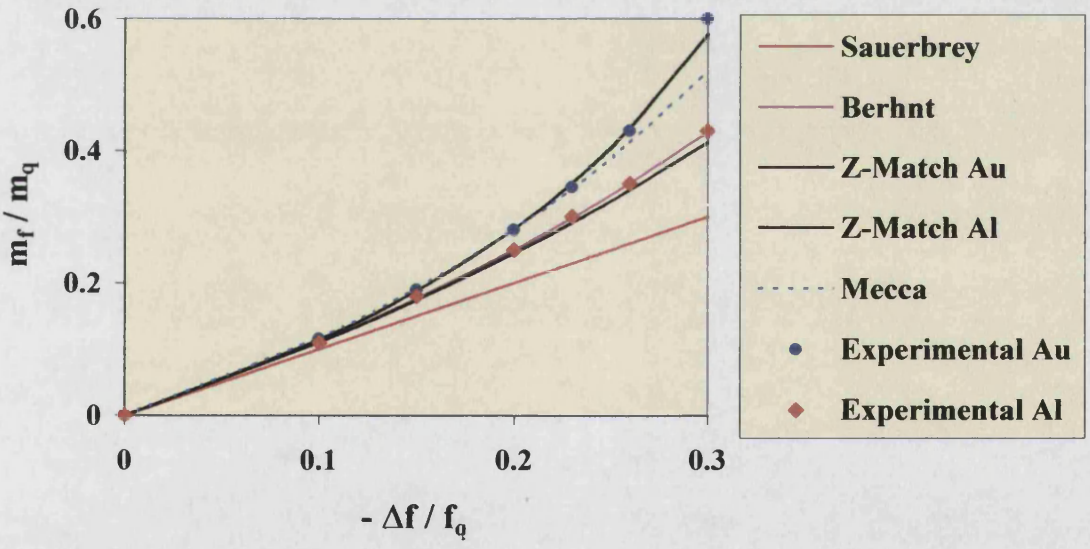

***Figure 1.5**: A graphical representation of the reduced mass, m_f / m_q, against reduced frequency, $\Delta f / f_q$, for different theoretical equations; Sauerbrey equation (9), Berhnt equation (13), Mecea equation (15), Z-Match Au and Al equation (14) Z = 0.381 and Z = 1.077 respectively, and two experimental sets of data for the deposition of Au and Al.*

The two materials, Au and Al have acoustic impedance ratio Z equal to 0.381 and 1.077 respectively, (where $Z = Z_f / Z_q$ the acoustic impedance of the film over the acoustic impedance of the bulk quartz) [80]. These two different materials follow different mass-frequency curves. The systematic error incorporated into the Sauerbrey equation, Berhnt's period technique and Mecea's ETM which do not include a function to account for different acoustic properties, increases dramatically with higher mass loads. This error can be seen graphically in Figure 1.5. When the acoustic impedance ratio equals 1 the Z-Match technique approximates to Behrnt period technique, so for Al equation (13) is an accurate model, however for Au the model would break down. The same applies to Mecea's ETM model, for Au the model works well, however, for Al the model fails after a mass-load of around 20 %.

A linear mass-frequency relationship is assumed throughout the experimental work conducted and the data presented within this thesis. The justification for this is that the frequency changes induced on the QCM resonators are well below 10 kHz. On the graph plotted in Figure 1.5 this corresponds to the frequency-mass region below 0.001 $\Delta f/f_q$. In this region all the theories discussed can be approximated to the Sauerbrey equation with the change in frequency proportional to the change in mass.

1.5 Liquid Phase Application of the QCM

The successful application of the QCM and the development of a fundamental understanding of the oscillating crystal when operated in air or *in vacuo* encouraged the rapid proliferation of the microbalance into the wider scientific community. The absolute sensitivity of the QCM to small mass changes on the surface of the crystal was soon realised and attempts were made to utilise this inherent sensitivity in a variety of different applications. The first application of the QCM resonator other than as a film thickness monitor was by Slutsky and Wade [81]. They performed limited experiments on the adsorption of gases at the surface of quartz crystal resonators with a view to examine the possibility of utilising the resonator as a detector for gas chromatography. King [82] later extended Slutsky's work and looked at crystals coated with gas chromatography stationary phases in an attempt to

introduce selectivity to the frequency response. His approach and results led to some interesting conclusions, mainly that the QCM can be successfully applied as a selective and sensitive chemical sensor. This was the first application of the QCM as a chemical sensor, and as such the subject receives a more extensive review in section 1.6.1.

By the early 1980's the use of the QCM had extended from that of a simple thin film monitor to a huge array of both physical and chemical applications [83]. These include, sorption detectors [82], particulate and aerosol analysis [84][85], trace metal analysis [86][87], the analysis of polymer-solvent interaction [88][89], the quartz crystal pressure gauge [90], and the quartz crystal thermocouple [91].

An interesting finding made by workers applying the QCM in novel systems was the discovery that stable oscillation of the resonator can be obtained in a liquid phase environment. This was initially thought to be impossible due to the increased damping of the liquid at the surface of the resonator preventing adequate energy conservation. This realisation led workers to investigate the use of a QCM chemical sensor based in a liquid environment. Following the success of King *et al.* in the development of the QCM as a detector for gas chromatography, Bastiaans and Konash [92] investigated the potential of the QCM as a detector for liquid chromatography. It had been demonstrated by Nomura that, with an appropriate oscillating circuit, a quartz crystal resonator can be successfully brought to resonate with either one [93], or both [94], of its faces in contact with a viscoeleastic fluid. It soon became apparent, however, that the Sauerbrey equation [56] and other models [60][65][78] describing the oscillation of a quartz crystal resonator in the gas phase or *in vacuo* were severely deficient when applied to the QCM in contact with a liquid. This deficiency was a major issue in the understanding of the QCM frequency response in a liquid environment. However, the great potential associated with the application of a liquid phase QCM device encouraged several workers to investigate the problem. Attempts were made to establish the factors affecting the oscillation of the QCM, and to develop a fundamental theory describing its application in contact with viscoeleastic fluids.

The following sections describe in detail the physical parameters of the oscillating medium that effect the fundamental frequency of a QCM resonator operating in a liquid environment. These include density, viscosity, temperature and conductivity.

1.5.1 Density and Viscosity Effects

Nomura *et al.* [93][94] was the first to investigate the oscillation of a QCM resonator in aqueous solution. Their work involved examining the factors that influence the fundamental oscillating frequency of the resonator. The results showed that the frequency was dependent on the density, viscosity and conductivity of the solutions [93]. They then extended the investigation to encompass organic liquids and found that for a non-electrolyte only the density and viscosity of the solvent influence the frequency of the immersed crystal [94]. The experimental procedure involved recording the oscillating frequency of the resonator in air then immersing it into the appropriate solvent. After a given time interval to allow for stabilisation of the oscillating resonator in the new environment, the fundamental frequency was again recorded. The value of Δf was obtained by subtracting the resonance frequency in the solvent from that of the crystal in air. The data was fitted mathematically and no physical model was presented to describe this dependence. Their equation took the following form;

$$\Delta f = a\,\rho^{1/2} + b\,\eta^{1/2} + c \qquad (16)$$

Where Δf is the frequency change with respect to air, ρ is the density and η the viscosity of the solvent, a, b and c are constants depending on the crystal.

Nomura *et al.* [95][96][97] demonstrated that with suitable calibration techniques, this lack of theoretical understanding can be negated and the QCM used in a variety of liquid phase analytical applications, for example metal ion assay [98][99] and iodide determination [100]. The dependence of the oscillating frequency on the density and viscosity of the oscillating solution was also

demonstrated by Bastiaans and Konash [92] in their work on QCMs as liquid chromatography detectors.

The development of a relationship based on a purely theoretical model that successfully described this frequency dependency was achieved by Kanazawa *et al.* [101]. He predicted that as the density and viscosity of water increased, the frequency of an oscillating crystal with only one face exposed to the solution would change according to the following equation.

$$\Delta f = - f_o^{3/2} (\rho_L \eta_L / \pi \rho \mu)^{1/2} \qquad (17)$$

Where Δf is equal to the frequency change with respect to air, f_o the resonance frequency of the unloaded crystal, ρ_L the fluid density, η_L the absolute viscosity of the fluid, $\pi = 3.142$, ρ is the density of the quartz and μ is the shear modulus of the quartz crystal.

The model was based upon the analysis of a damped shear wave propagating into the bulk solution that is coupled to the shear motion at the surface of a resonating crystal. The theoretical derivation of the equation is too complex to reproduce here and equation (17) is the 'linear liquid limit' applicable only when $(\rho_L \eta_L)^{1/2}$ is less than 20 [102]. The theory was, however, substantiated by two sets of experimental data. Kanazawa used aqueous solutions of glucose and ethanol to produce density and viscosity variations in a series of solutions and then compared the frequency change of a QCM resonator immersed in the solutions with those predicted from equation (17) [101].

Around the same time Bruckenstein and Shay [103] predicted a similar relationship between the resonance frequency and the density and viscosity of the oscillating fluid.

$$\Delta f = - 2.3 \times 10^{-6} n f_q^{3/2} (\eta_L \rho_L)^{1/2} \qquad (18)$$

Where Δf is the frequency change with respect to air as the crystal is immersed in solution L, n is the number of faces exposed to the solution (either one or two), f_q is the fundamental oscillating frequency in air, η_L and ρ_L are the dynamic viscosity and density of the solution respectively.

They also demonstrated that during electrochemical experiments where the density, viscosity, specific conductivity and temperature of the oscillating solution were maintained the mass sensitivity of the QCM was as predicted by the Sauerbrey equation. This was achieved by investigating the electrodeposition of silver and comparing the data from the QCM frequency drop with the galvanostatic and potentiostatic methods. The technique employed by Bruckenstein *et al.* became known as the electrochemical quartz crystal microbalance (EQCM) and is now a well-defined electrochemical tool. The device operates with the QCM acting as a working electrode in a conventional three electrode experiment and allows for the quantitative analysis of the electrical double layer structure and any deposited mass that may occur during electrochemical experiments. The EQCM has also been used to monitor mass transport processes that accompany redox reactions in thin films deposited on the QCM surface. EQCM applications have been extensively reviewed elsewhere and as such will not receive close attention in this thesis. For more detailed reviews see [104][105][106].

The work of Bruckenstein and Shay on the mass sensitivity of the QCM operating in the liquid phase led to another important application of the device as a thin-film dissolution rate monitor. Hinsberg, Willson and Kanazawa [107] were the first to propose the use of the QCM in such away. They studied the influence of the photoproducts on the dissolution kinetics of photoresists by monitoring the rate of loss of an unexposed and exposed film from the surface of a QCM resonator rinsed in a developing solvent. The results showed the QCM to be a general and convenient tool for the determination of thin film dissolution rates and that it can be applied to a large range of materials including polymers and metals. Today many examples can be found in the literature where the QCM has been employed as a thin film dissolution monitor [108][109].

1.5.2 Conductivity Effects

The observation made by Nomura *et al.* [93] that the conductivity of the solution had an effect on the oscillating frequency of the QCM was much more difficult to quantify. Unlike the density and viscosity dependence the conductivity dependence could not be fitted to an empirical mathematical formula similarly reproducible results were difficult to obtain. They found that with the QCM operating in water or an electrolyte solution the fundamental resonance frequency was influenced by temperature and electrical fields to a greater extent than when it was operated in a non-electrolyte. The frequency of oscillation was not only dependent on the temperature of the solution but also on the temperature of the oscillating circuit. Similarly, different designs and types of oscillating circuit had different temperature dependence. The variation between the frequency response of different oscillators was most apparent in the frequency versus conductivity profiles for the QCM operating in aqueous solutions of different salts [100]. For the application of the QCM in solutions these differences can be eliminated by careful calibration, however, the dependency of the oscillating crystal on solution conductivity is still unanswered and posses a major problem for any theoretical interpretation. As Kanazawa and Melroy [106] pointed out " this conductivity effect would be a very serious additional contribution to the frequency shift; it would have to be understood in order to preserve the quantitative interpretation of frequency shift data ".

Kurosawa *et al.* [110] undertook an extensive investigation of the dependence of the liquid phase QCM and confirmed that for non-electrolytes the density and viscosity were the only influencing factors. They also showed that for aqueous salt solutions and viscous polymer solutions the simple density-viscosity relationship broke down. In recent years this conductivity dependence has become know as an acoustoelectric effect [111] and has been described as arising from the fringe field effects associated with the oscillating electrodes [112][113].

In conductive liquids the operation of the QCM appears to be influenced by the electrical properties of the solution. It is believed that the acoustic wave interacts with the ions and dipoles of the solution through the induced electrical potential on the resonator surface. It is known that an acoustic plate mode (APM) device operating in solution will interact with ions and dipoles close to the plate-liquid

interface as the acoustic wave propagates along the plate surface. APMs are piezoelectric resonators that operate with both electrodes on the same surface of a piezoelectric plate. The acoustic wave is stimulated via the initial electrode and received by the second. As the wave propagates between the two electrodes its influence can be observed on the opposites face of the plate. Induced dipoles created from the piezoelectric displacement of the crystal lattice develop on the opposite face to the electrodes, these dipoles propagate with the acoustic wave and interact with the medium that the surface of the plate is exposed to. For electrolyte solutions the velocity shift and attenuation of the APM can be related to the conductivity of this medium [114], a series of equations and a sound theoretical description can be applied to account for these interactions [115]. However, this interaction is minimised for the thickness-shear wave devices employed with the QCM as the oscillating plate has electrodes on both faces, the surface dipoles induced by the acoustic vibration are essentially masked by the potential applied to the plate surface. However, at the edge of the electrodes there is a region where the acoustic wave propagates with no electrode masking. This region is very small as the amplitude of the acoustic displacement decays exponentially from the edge of the electrode [116], however, sufficient electrical fields can be established to couple with fields in the electrolyte solution encouraging energy dissipation to the medium. This acoustoelectric coupling can dominate the energy losses of the oscillating QCM and lower the resonance frequency [117].

The effect of conducting solutions on the liquid phase application of the QCM is still not clearly understood. Not only are there no suitable theories describing the dependence, but the origin of the frequency shift is also unclear. Nomura [93] and Yao [118] observed that the temperature and electrical environment of the oscillating circuit as well as the resonator itself effect the fundamental frequency. These suggest that the origin may be unrelated to any physical characteristics of the piezoelectric resonator and rather a consequence of the means of oscillation and frequency determination. These observations are supported by the lack of reproducible data in the literature. Rodahl [113] claims that only the parallel resonance frequency of the QCM is influenced by the conductivity of the liquid, and that the series resonance is unaffected. However, the QCM utilised by the author operates at the series resonance and can be shown to have marked

conductivity dependence. Other workers have also presented data showing the dependence of the series resonance on solution conductivity [111][118][119]. On a more positive note the acoustoelectric response can be utilised for sensor applications. In liquid phase chemical sensing applications the acoustoelectric response of the QCM can be removed by simple calibration procedures and in some cases may even be used as the major influence on the frequency shift to create a conductivity or particular ion concentration sensor [118]. The uncertainty surrounding the effect will however continue to limit the quantitative interpretation of frequency shift data connected to the application of the QCM in electrolyte solutions.

1.5.3 Conclusion

It has been shown that QCM resonator can be successfully operated with either one or both of the resonator faces exposed to a viscoelastic fluid. The fundamental oscillating frequency of the resonator is dependent on the density, viscosity and electrical conductivity of the oscillating medium, as well as the viscoelastic properties of any over-layer on the surface of the resonator. The temperature dependence of the fundamental frequency is a lot greater than that of the same resonator operating *in vacuo*. Not only does the temperature effect the quartz resonator directly through the crystal lattice, but also indirectly by the temperature dependence of the density, viscosity and conductivity of the oscillating medium.

As with the gas phase application, the inherent sensitivity of the QCM and the accuracy of the frequency determining elements make the liquid phase application an extremely sensitive and versatile device. The very fact that the final oscillating frequency is coupled to the trio of physical parameters described above has hindered the development of a sound theoretical understanding, however, this dependence will also increase the potential application of the oscillating resonator. With careful calibration procedures and the use of multiple resonator arrays it should be possible to monitor and to remove these influences selectively. The overall mass sensitivity of the resonator has been shown to be the same as that predicted by Sauerbrey or more completely by the Z-Match technique. However, with the

exception of an acoustically thin rigid over-layer such as that obtained with the electrical deposition of a metal, the viscoelastic properties of the surface layer have a much greater contribution to the fundamental oscillating frequency than the surface mass. Again with careful calibration and well-defined surface structures this dependence can be utilised to form a sensitive chemical or physical sensor.

Overall the potential application of the liquid phase QCM is as great, if not greater, than the application of the gas phase counterpart. At present the theoretical understanding is incomplete, however, the practical research and analytical applications are proving to be very rewarding.

With regards the applications developed throughout the work presented in this thesis the extra response associated with the viscoelastic properties of the over-layer will be utilised to enhance the response of the aqueous $K^{+}_{(aq)}$ sensor. The conductivity changes associated with the cations in solution will also contribute to the overall response. Two reference systems are used, a blank resonator with no coating and a resonator coating containing no crown-ether groups. In the solutions used the frequency of these two reference systems and that of the developed sensor are dominated by the conductivity of the solution. The responses of the two references are therefore utilised to interpret the response of the final sensor.

1.6 QCM based Chemical Sensors

The application of the QCM as a transducer for chemical sensors has received considerable attention in recent years. The sensitivity of the device to mass or viscoeleastic changes at the surface of the QCM resonator has long been appreciated. Typically, for a 10 MHz resonator operating in the gas phase, frequency measurements can be recorded with a sensitivity of approximately ± 0.01Hz [120]. Given an overall response for the QCM of 4.97 ng cm^{-2} Hz^{-1} this frequency sensitivity corresponds to the detection of less than 10 % of a H_2 monolayer on the surface of the resonator. This clearly illustrates the great potential of the QCM to act as a transducer for chemical sensors.

QCMs are well established in the field of thin film monitoring [121][122]. They have also found other applications as detection devices for atmospheric particulates and aerosols [123][124]. More recently, work has been carried out to develop specific chemical sensors based on the QCM [125][126][127]. These function on the principle that the QCM monitors small changes in mass. By modifying the surface of a resonator with a film that will selectively bind a particular species a sensor can be developed for that species. The majority of sensors reported are designed to operate in the gas phase, for example organic vapour detection [128][129] and electronic nose systems [130]. The nature of the selective coating employed covers a whole range of chemical and physical properties, examples include metals [131], metal oxides [132], metal-complexs [133], polymers [134][135], and host compounds such as porphyrins [136], cryptands [137], crown ethers [138] and cavitands [139].

The study of liquid phase systems has been more limited due to the difficulties in maintaining satisfactory operation of the QCM resonators in a highly damping, viscous fluid. These problems have been largely overcome by the design of suitable electronic circuits [140] and the application of sensor systems where only one face of the resonator is exposed to the viscous fluid. The majority of liquid phase sensors involve the use of biological recognition species such as lectin-sugar [141] and avidin-biotin [142] interactions. Such devices fall under the general heading of biosensors [143]. Man-made recognition species such as calixarenes [144][145], crown ethers [146], a variety of polymers [147] and molecularly imprinted polymers [148] have also been employed as recognition membranes for aqueous QCM sensors.

This chapter reviews briefly the historical development of QCM based chemical sensors. The major steps in the design and application of the devices and the evolution of the sensor system from a simple gas phase microbalance to a highly sensitivity and selective chemical sensor, for use in both the gas phase and in solution. The compounds used as selective coatings and the relative success of different approaches will be discussed, as well as some indication of the lower detection limits and overall sensitivity of the developed sensors.

1.6.1 Gas Phase Chemical Sensors

As mentioned previously the first application of the QCM as a chemical detector rather than a thin film monitor was in 1962 by Slutsky and Wade [149]. They conducted several experiments on the adsorption of gases onto the surface of a QCM resonator and fitted the accompanying frequency changes with simple isotherms. The results showed the QCM resonator to be sensitivity to surface adsorption phenomena. King [150][151] initiated the concept of applying such adsorption studies to the QCM coated with a selective binding layer. He used piezoelectric resonators coated with different gas chromatography stationary phases. Since these phases had proved to be useful in partitioning various gases on a column King proposed that they would be capable of interacting with the same components of a gas stream while on the surface of the resonator. The frequency of the resonator would then depend on the interaction parameters of the coating and the target species in the gas stream. A selection of coating materials employed, and the species they responded to can be seen in Table 1.1 below.

Resonator Coating	Response and Selectivity
Squalene, Silicone oil	Hydrocarbons non-selective
Polyethylene glycol and Dinonyl phthalate	Selective for aromatic, oxygenated or unsaturated polar molecules
Silica-gel, Zeolites and Hydroscopic polymers	Selective for water vapour

Table 1.1: *Resonator coatings used by King for the application of the QCM as a gas chromatography sorption detector [151].*

As the species pass over the resonator both adsorption and absorption would occur and increase the mass of the coating. This in turn changes the fundamental resonance frequency of the oscillator. The QCM proved to be a useful detector. They could be operated in a range of temperatures from around 0 °C to 200 °C, with a variety of carrier gas systems including helium, nitrogen and air. Another advantage was their extremely long operating lifetimes. QCM water-analysers have regularly

been in service for more than 5-years without fouling or poisoning, the detector lifetime does not become an important issue in the instrument performance [152].

Several workers followed up this initial investigation and developed systems to calculate interaction and partition parameters for the response of the QCM detectors [153][154][155]. Karasek *et al.* [153] reported the performance characteristics of a coated resonator and minimum detectable concentrations of a number of materials. These included alkanes, aromatic hydrocarbons, simple ketones and esters, over the range 2×10^{-8} g to 8×10^{-6} g. He also described the response of the coated resonator to a compound eluted from a gas chromatography column by the following equation [156]:

$$A = C\,M / \gamma\,P^{\circ}\,F \qquad (19)$$

Were A is the area under the response curve, M is the total weight of the eluent, γ is the activity coefficient of the eluent in the coating, P° is the vapour pressure of the eluent at the operating temperature, F is the carrier gas flow rate, and C is a constant characteristic of the detector temperature, piezoelectric resonator and resonator coating. The equation highlights some of the problems associated with QCM gas chromatography detectors. The sensitivity of the detector decreases with increasing temperature whereas retention times for gas chromatography columns increase with a decrease in temperature. This means that a compromise must be reached between retention time and sensitivity. Another consequence is the dependence on vapour pressure, as the vapour pressure of the eluted compound decreases the detector sensitivity increases, however, a suitably high vapour pressure is a prerequisite for gas chromatography.

Janaghorbani *et al.* [154] described the response of a coated resonator in terms of the partition constant of the coatings to vapours dissolved in a gas flow. The authors assume the detector is connected to the outlet of a gas chromatography column and that the peak response is related to an imaginary plug of the sample-gas mixture. The equation they derived describes the behaviour of the resonator employed in gas or liquid chromatography under conditions that approximate to equilibrium:

$$A_y = - C_f K_{yx} V_x M_t / F \qquad (20)$$

Where A_y is the area under the peak due to component y, C_f is the constant describing the frequency change (Δf) of the resonator due to the addition of mass (ΔM) to the surface ($\Delta f = - C_f \Delta M$) [56], (see the development of the Sauerbrey equation section 1.4.1, page 13) and K_{yx} is the partition coefficient of the gas y in a stationary phase x, described by the ratio:

$$M_{yx} / M_y = K_{yx} \qquad (21)$$

Where M_{yx} is the mass of gas y in a unit volume of the resonator coating, x, at equilibrium, and M_y is the mass of gas y in a unit volume of the gas phase. V_x is the volume of the coating x present on the sensitive area of the resonator. M_t is the mass of the gas contained within the detector volume when it is at equilibrium with the coating and F is the flow rate of the gas stream. Excellent linear relationships between A_y and an injected volume of an organic solvent were obtained for several solvent-solute systems, for example octane, heptane, hexane and pentane with a squalene-coated resonator. Other theoretical predictions presented include response times and the effect of temperature on the sensitivity of the detector.

1.6.2 Liquid Phase Chemical Sensors

The application of the QCM in liquid phase systems is more complicated than the gas phase application. Damping of the piezoelectric oscillation and propagation of the acoustic wave into the surrounding medium causes instability in the fundamental frequency (see section 1.5 for a more detailed discussion). Initial liquid chromatography detectors based on the QCM avoided this problem by spraying samples of the liquid chromatography eluent directly onto the surface of a QCM resonator [157]. The solvent evaporates rapidly leaving any residual low vapour pressure solute on the surface. The mass deposited can then be calculated and used to determine the relative concentrations. The complete sampling time for one cycle was approximately 60 seconds and the method was unsuitable for many applications.

Bastiaans and Konash [158] developed a simpler liquid chromatography detector. They incorporated a piezoelectric resonator directly in the outlet flow of a liquid chromatography column. The detector responded to density and viscosity gradients associated with the presence of a solute in a solvent system. As the solute passes over the surface of the resonator these gradients induce a frequency shift in the resonator. These non-specific interactions can be used as the bases of a detector; however, a much more useful and versatile device would be a sensor that responds selectively to a specific species. An attempt was made by Bastiaans and Konash [158] to introduce this selectivity. They employed a reference resonator in the same sampling procedure and subtracted the response of the working resonator from that of the reference, in this way the density and temperature effects could be removed from the resonator response. Coating the working resonators with a compound that possessed a specific binding potential then controlled the surface adsorption properties of the solute targeted. The system employed by Bastiaans *et al.* was designed to detect small nonpolar organic molecules in an aqueous flow. By coating the reference resonator with long chain hydrocarbons a sensor system was developed. The small nonpolar molecules partition from the aqueous flow and penetrated the organic coating inducing a frequency response. All responses associated with density and viscosity gradients in the eluent flow were removed and the frequency response induced solely by the surface interaction of the target species.

Overall it was concluded that piezoelectric sorption detectors offer efficient, sensitive, cheap and reliable sensor systems for analytes in both gas phase and the liquid phase applications. The foundations laid by the work of Slutsky [149], King [150], Karasek [153], and Edmonds [155] showed the versatility of the QCM detector. Over the next few decades a variety of different coatings were used to introduce greater selectivity and enhance sensitivity of the detector response. In the following sections the relative successes of these approaches are reviewed as well as the type and design of the selective coatings employed.

1.7 Polymer Coated QCM Sensors

Polymer coatings have been used extensively in conjunction with QCM resonators to produce chemical sensors. The polymers form an interface between the surface of the resonator and the external medium, and offer a versatile method for controlling the partitioning and binding of molecules from the external source to the surface of the resonator. Generally the polymer coating has one of three functions:

I. Non-selective adsorption membranes

This involves the polymer coating interacting with species such as volatile organic compounds (VOCs) either in the vapour phase or in solution. The VOCs partition onto the surface of the resonator and induce mass and viscoeleastic changes in the polymer layer. These changes in the polymer membrane induce a shift in the resonance frequency of the QCM.

II. Matrix or encapsulation membranes

This involves the polymer coating forming a stable and inert matrix for encapsulating a host compound. The host selectively binds a target species from the external medium. The polymer matrix is simply an anchor to hold the host compound in position, preventing dissolution or evaporation. The membrane is not directly involved in the sensing mechanism.

III. Selective adsorption membranes

The polymer coating can also be used directly as the host species. By developing polymer chemistry and structural composition that impart selective binding potentials to the coating.

The range of polymers and copolymers available for such applications is extensive. Their variety in structure, chemistry, solubility and reactivity leads to a huge array of potential systems. Examples of these three applications and the polymer systems employed are presented in the following paragraphs.

1.7.1 Non-selective Adsorption Membranes

The most common use of polymer coatings with QCM based chemical sensors is a non-selective adsorption membrane. The resonator is typically coated by dissolving the polymer or copolymer in a volatile solvent and depositing a known quantity onto the surface either by dip-coating [159], spin-coating [160], air brush or by placing a drop of the solvent polymer mixture directly onto the QCM surface [161][162]. The solvent evaporates leaving a known quantity of the polymer coating on the resonator. The system is very simple and easy to perform; however, the deposited film is very heterogeneous in nature and has a problem with reproducibility. The process involves many variables such as evaporation rate, film thickness, solution concentration etc. These all affect the final sensor response. However, the procedure is routinely used and is effective as an initial investigation of a sensor response.

The sensors can potentially be operated in both the gas phase and in solution phase, but the polymer must be insoluble for solution phase application. This requirement limits the use of such sensors in solution phase systems; however, the solubility limitation can be avoided by either cross-linking of the polymer or by the covalent attachment of the polymer to the QCM surface. These are the two methods chosen to coat the $K^{+}_{(aq)}$ sensor discussed in Chapter Three of this thesis. Table 1.2 summarises the use of polymer coatings with QCM resonators and lists the species analysed by the final sensors.

The different recognition sites available in the polymer chains lead to different adsorption equilibrium between different types of analytes. As an example aromatic and aliphatic compounds can be differentiated using polymers with phenylated groups. The aromatic molecules interact strongly with the arene groups present in the polymer coating and induce a larger frequency response compared to the aliphatic molecules. The sensors tend to have a detection limit in the area of 10-100 part per million (where 1 ppm is equal to 1 $\mu g\ cm^{-3}$), however some researchers reported detection limits as low as 1 $\mu g\ dm^{-3}$ for the vapour phase systems [135]. The characterisation of a sample, either vapour or solution can be achieved with a sensor array consisting of several individual sensors coated with different polymer

systems. For every sample mixture an individual response pattern for the whole array is recorded [162]. This can then be fed into a pattern recognition program and used to analyse more complex mixtures [163]. In such away the identification of complex vapour mixtures has been achieved with QCM based chemical sensors, for example the identification of spice aromas [164].

Target Compounds	Polymer Coating	Reference
VOCs gas phase	Poly(3-hydroxybutyric acid) Poly(dimethylsiloxane) Poly(phenylmethylsiloxane) Poly(aminopropylmethylsiloxane)	[160] [165] [166] [126]
Phenols gas phase	Poly(vinyl pyrrolidone)	[135]
VOCs in water	Poly(ethyl acrylate) Poly(epichlorohydrin) Poly(trimethyloxyproylsilane-octadecyltrimethoxysilane) Poly(octadecyl methacrylate) *cis*-1,4-Polybutadiene Poly(ethylene-propylene-styrene) Poly(styrene) Silicone OV225 Poly(triethoxyhydroxysilane) Polyimide	[167] [165] [165] [168] [145] [145] [145] [145] [169] [166]
Alcohol vapour	Poly(methyltrimethoxysilane)	[170]

***Table 1.2**: Non-selective polymer coatings used to produce chemical sensors.*

1.7.2 Matrix Encapsulation Membranes

One of the potential applications of host-guest chemistry is in the development of selective chemical sensors [171]. The incorporation of a host species into a transducer capable of converting signals from the host to a signal that can be easily recorded or interpreted by a human operator would lead to an effective sensor. As the guest interacts with the host the signal is produced, indicating the presence of the guest species and its relative concentration.

One of the major obstacles limiting sensor production is the lifetime of the selective coating [172]. Simple films of the host species can rapidly deteriorate. If

the molecules have limited adhesion to the surface of the transducers, the thin films can erode with only mild abrasion. A useful way to ameliorate film lifetime is to incorporate the host species into a polymer layer [173]. This encapsulation improves film-transducer adhesion and protects the host from physical erosion and chemical attack.

Eamples of host species encapsulated in such a way are the cyclodextrins [126], for more details on cyclodextrin compounds see section 1.8.6. Wessa *et al.* [126] used 50 % w/w of a modified γ-cyclodextrin embedded in a polysiloxane backbone containing phenyl, vinyl, and methyl groups. A QCM resonator was coated with the polymer-host mixture using the spray technique mentioned earlier. The cyclodextrin used had been extensively studied using conventional gas chromatography (GC). When employed in a GC stationary phase the cyclodextrin could separate three chiral anaesthetics, (deflurane, isoflurane and enflurane) from their biologically inactive isomers. The response of the QCM sensor was in excellent agreement with the data obtained from the GC system. The encapsulation of the cyclodextrin molecules in the polymer matrix led to only a minor loss in the sensor response but greatly improved the sensor and film lifetime.

1.7.3 Selective adsorption membranes

The process of encapsulating host compounds in a polymer matrix has been shown to improve the long-term stability of the host-guest sensor. The method does, however, have its limitations. Although the film lifetime is increased, leaching of the host and other low molecular weight materials from within the polymer film can still occur. This leads to deterioration in the porosity of the film and the overall sensitivity of the sensor. Also for liquid phase applications of the sensor the host compound still suffers severe dissolution if used in a highly solvating medium. By attaching the host species directly to the polymer backbone via a covalent link the lifetime of the selective membrane will be increased greatly. The host may also act as a plasticiser increasing the free volume of the polymer chains and so improving the porosity of the film. This also increases the host's availability for binding [174][175].

Dickert *et al.* [176] covalently attached cyclodextrin macrocycles to a polyurethane backbone and used the polymer as a selective interface on the surface of a 10 MHz QCM resonator. The sensor had enhanced selectivity for gaseous xylene isomers with full reversibility and response times of less than 5 minutes. They also attached *p-tetra*-butylcalix[6]arene (see section 1.8.1) in a similar system. Again the selectivity induced into the sensor response by the presence of the calixarene were probed with the *o*-, *m*- and *p*-xylene isomers. The embedding of the larger macrocycles into the polymer matrix opened channels within the network increasing the specific surface area and acting as a porogen. The two sensors had detection limits of about 50 ppm.

Another method used for the production of chemical sensors utilising polymer coatings with specific binding potentials is the application of molecularly imprinted polymers, MIPs [176][177]. Molecular imprinting [178][179] is a technique used to create polymer networks that have cavities of precise size and shape to complement a target molecule. The cavities can also have functional groups arranged in a 3-dimentional (3-D) orientation to interact with complementary functional groups on the target molecule. Due to the size, shape and 3-D interactions the cavities selectively rebind the target species from either the gas phase or in solution.

The most favourable transducers for use in association with MIPs are the piezoelectric based devices such as the surface acoustic wave (SAW) and the QCM. These transducers are sensitive to mass or viscoelastic changes on the resonator surface and the binding of a target compound into the MIP cavity can be monitored by the associated mass change. The MIP polymers are readily synthesised on the surface of the resonator, and by their very nature afford a chemically inert, rigid system, insoluble in any solvent or environment. These properties make the MIP-QCM combination an ideal system for the preparation of simple hand-held chemical sensors [177]. QCM resonators coated with polyurethane imprinted with THF have been shown to have a selective response for THF vapours over other solvents [180]. Changing the solvent used during the polymerisation process can alter the selectivity of the MIP. If the polyurethane is imprinted with ethanol or ethyl acetate then the coated QCM sensor responds selectively for ethanol and ethyl acetate respectively [180].

The simplicity, versatility and compatibility of the MIP technique with the QCM transducer make the two an ideal match. The non-covalent imprinted polymers now offer a universal solution for sensor technology as well as in their main application of chromatography. MIP based sensors have not yet made their way into the commercial market but the result obtained from the current research efforts suggest that these polymers have a bright future [181].

1.8 Selective Host Compounds

The selectivity of any QCM based sensor is achieved by placing an interface between the surface of the QCM resonator and the oscillating environment. The interface is designed to possess a selective binding property and interacts with only one component of the sensor's external environment. This introduces selectivity to the sensor as a whole as a signal is only recorded as a consequence of the interaction of the interface with the target species.

Host-guest chemistry is an ideal mechanism for introducing this selective binding affinity. The variety of compounds available and the range of target species are constantly increasing, with a huge amount of research being involved in the general field of molecular recognition. In theory any one of the host-guest systems available can be readily incorporated within a QCM based chemical sensor.

This section takes a brief look at the types of host compounds used to date. The recognition mechanism involved in the binding process and their suitability to QCM sensor technology. The discussion opens with a look at calixarene based systems. These compounds have been extensively employed in conjunction with the QCM transducer. The work covered progresses from the simple gas phase sensors to more sophisticated liquid phase sensors and the use of self assembled ordered monolayers. This is particularly relevant to the cyclodextrin sensor system under investigation in Chapter 4 of this thesis and as such receives greater attention. However, due to the nature of the experimental conditions it was not possible to compare the response of a sensor operating in both environments.

1.8.1 Calixarenes

Calixarenes [182][183] are cyclic organic molecules. Named from the Greek, *Calix-*, meaning a cup, they are composed of aryloxide repeat units connected to form a macrocyclic structure. In most cases the ring has between 4 and 8 aryl units. At the centre of the ring is the cavity that gives these molecules their molecular recognition capabilities and selective chemistry. By controlling the number of aryloxide repeat units the dimensions of the internal cavity can be varied. The chemistry and the chemical environment of the cavity is dominated by the aromatic systems of the repeat units but can also be mediated by changing the functional groups on the rim and on the base of the calixarene molecule, see R and R′ respectively in Figure 1.6. The naming of calixarenes follow the general form of R-calix[n]arene-R′, where R is the functional group at the open end of the cavity, these vary considerably but some standard examples are *t*-butyl and *t*-amyl. R′ is the group at the base of the cavity attached to the arene ring via the phenolate linkage for example methylether (-OMe). The [n] refers to the number of aryloxide repeat units and is usually between 4 and 8.

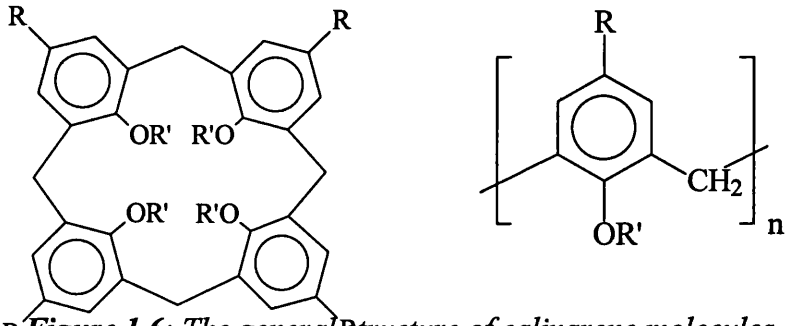

***Figure 1.6**: The general structure of calixarene molecules.*

The cavity can be both hydrophilic and hydrophobic depending on the nature of the phenoxide protons. This gives the molecule the ability to bind small organic compounds or transport metal ions through a hydrophobic interface [184].

Calixarenes have been extensively employed in the field of chemical sensors [185][186][187]. Their applications are in the general field of organic vapour detection although some work has also been published concerning their metal-ion complexing ability [188][189]. The transducers utilised include optical devices [189][190] as well as QCM based systems [144][145].

1.8.2 Calixarene Vapour Phase Systems

Hartmann *et al.* [191] coated a 10 MHz QCM resonator with the calixarene *t*-butylcalix[4]arene-*tetra*methylether and compared the frequency response of the resonator with that of a similar resonators coated with poly(3-hydroxy-butyric acid) or *n*-pentadecyl-thioglycolate. The resonators were mounted in a gas flow system of 2000 ml/h and exposed to five different organic vapours; methanol, acetonitrile, chloroform, benzene and styrene. The results presented were very limited and allowed only qualitative analysis. The calixarene coating had an increased sensitivity towards all five of the analytes when compared to the other organic coatings, and had a response five times greater for acetonitrile. This apparent selectivity for acetonitrile is consistent with the organic vapours binding within the cavity of the calixarene molecule. The X-ray crystal structure of the solid calixarene-acetonitrile complex [192] shows the linear CH_3CN molecule bound perpendicular in the cavity with its CN group extending down towards the phenlate calixarene groups. The profile of the frequency shifts was also markedly different for the calixarene system compared to the others. The peaks obtained had an extended desorption phase of up to 600 seconds whereas for the polymer system and the thioglycolate system the desorption phase was completed by approximately 100 seconds. This suggests the analyte binds to the calixarene film in a manner unavailable in the polymer and the thioglycolate films.

The results of the work carried out by Hartmann *et al.* showed the potential of the calixarene systems to function as a binding interface on the surface of the QCM resonator and illustrates their improved sensitivity and selectivity compared to other non-specific interfaces such as polymer coatings. The specific binding of the organic vapours had a marked effect on the frequency profile of the resonator during exposure to the vapours; the slow desorption and the total peak height being the main examples.

1.8.3 Calixarene Liquid Phase System

Following the success of the vapour phase system Lucklum *et al.* extended Hartmann's work to examine the liquid phase application of QCM-calixarene based

sensors [145][193]. They tested a variety of calixarenes with a selection of organic analytes to investigate the response of a QCM coated resonator to trace amounts of the analytes in seawater. The experimental procedure was very simple. The calixarenes were coated onto the resonators by airbrush. A known volume of a predetermined concentration of the calixarene dissolved in chloroform, trichloroethanol or methanol was sprayed onto the surface of the resonator. After evaporation of the solvent a thin film of calixarenes remain on the resonator. The calixarenes used, and the analytes tested can be seen in Table 1.3.

Calixarenes Selected
t-Butylcalix[6]arene, *t*-Butylcalix[8]arene, *t*-Amylcalix[8]aren-acetate, *t*-Butylcalix[8]arene-octaacetate, *t*-Butylcalix[8]arene-aceticmethylate, *t*-Butylcalix[8]arene-dibenzylether
Target Analytes Investigated
Trichloroethylene, Dichloroethylene, Chloroform, Dichloropropane, Trichloropropane, Benzene, Toluene, Pyridine, Octane, Methanol

***Table 1.3**: List of calixarenes studied and target analytes selected as potential water pollutants [193].*

After coating, the resonators were mounted in a flow cell though which seawater was pumped. A premixed solution of seawater and the analyte investigated was intermittently blended with the seawater flow. As with the vapour phase system the presence of the target species in the flow induced a frequency shift in the QCM resonator. The detection limit of a selection of the calixarenes to the target analytes can be seen in Table 1.4.

Target Analyte	Calixarene Coated		
	i-nonyl calix[8]arene	*t*-amyl calix[8]arene	*t*-butyl calix[8]arene
Trichloroethylene	0.8 ppm	0.3 ppm	0.2 ppm
Tetrachloroethylene	0.1 ppm	0.06 ppm	0.1 ppm
Chloroform	1.9 ppm	0.5 ppm	0.6 ppm
Benzene	2.8 ppm	0.8 ppm	0.6 ppm
Toluene	1.0 ppm	0.4 ppm	0.5 ppm
Dichloromethane	3.7 ppm	1.0 ppm	1.1 ppm
1,2-Dichloroethane	2.2 ppm	0.6 ppm	0.5 ppm
1,2-Dichloropropane	2.3 ppm	0.6 ppm	0.5 ppm

***Table 1.4**: Detection limits of 10 MHz QCM resonator coated with calixarenes, to aqueous solutions of the target analyte [193].*

The detection limits quoted by Lucklum *et al.* are comparable, and in some cases better than, the current detection limits of other sensors developed to detect hydrocarbon pollutants in aqueous solutions [194]. However no comparison was made between the liquid and vapour systems and so it was unclear whether the sensitivity of a calixarene system to specific organic compounds is independent of the local environment.

1.8.4 Ordered Monolayers of Calixarenes

An improvement on the coating technique employed by Lucklum *et al.* is the so-called self assembled monolayer (SAM) approach utilised by Cygan *et al.* [144]. SAMs form spontaneously on gold surfaces when exposed to several thiol containing molecules [195]. They offer a general mechanism for the production of highly ordered pseudo-crystalline monolayers of compounds on the surface of gold electrodes. The surfaces of the gold electrodes on QCM resonators offer an ideal

application for SAMs and an opportunity to incorporated the highly ordered structures within a chemical sensor device.

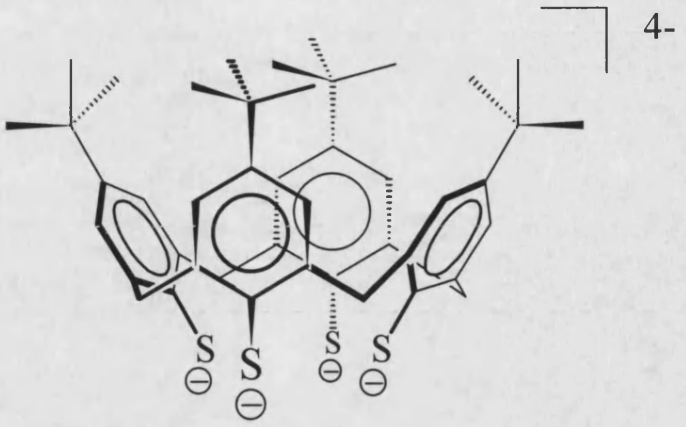

***Figure 1.7**: The t-butylcalix[4]arene-tetrathiolate synthesised by Cygan et al. [144].*

Cygan synthesised *t*-butylcalix[4]arene-*tetra*thiolate, see Figure 1.7, and used this compound to form a SAM on the surface of a QCM resonator. Infrared external reflection spectra, IRS, single wavelength ellipsometry and contact angle measurements were used to investigate the SAM structure. These all confirmed the ordered crystalline nature of the film and the orientation of the calixarene molecules. The arene ring is parallel to the surface with the *t*-butyl groups extended away from the gold as illustrated crudely in Figure 1.8. A similar sensor was prepared with the standard phenolate calixarene, *t*-butylcalix[4]arene. This is incapable of forming a SAM and instead forms a randomly oriented surface layer. The two sensors were employed in a flow cell similar to that described previously, and exposed to aqueous solutions of several organic molecules. The concentration of the aqueous solutions was in the part-per-million range.

The results demonstrated the effect of the orientation of the calixarene cavity on the sensor selectivity and overall sensitivity. The SAM sensor had an increased response for the alkylbenzenes; *o*-xylene, *m*-xylene, *p*-xylene, and toluene. Typically a response of 1-3 Hz was obtained for the sensor on exposure to 0.5 mmol dm^{-3} aqueous solutions of non-alkylbenzenes compared to a response of 10-15 Hz on exposure to 0.5 mmol dm^{-3} aqueous solutions of the alkylbenzenes mentioned. Using

the Sauerbrey equation [57] the frequency response was converted to the moles of the analyte bound, this was found to yield a 1:1 binding ratio between the calixarene cavity and the alkylbenzenes. In contrast the *t*-butylcalix[4]arene film had a response of 2-6 Hz for all the anayltes and a maximum binding ratio of anaylte : calixarene of 1:2.

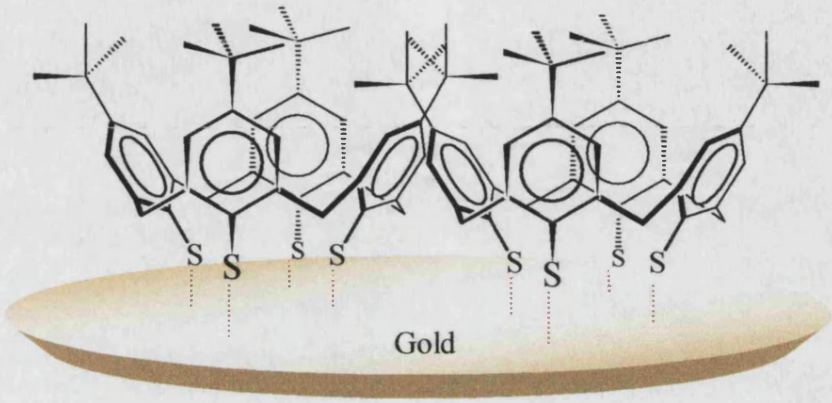

***Figure 1.8**: A representation of an ordered self-assembled-monolayer of the calixarene-tetrathiolate.*

1.8.5 Cavitands

Cavitands are another class of synthetic organic molecules with enforced concave surfaces, or cavities. The cavities of these species can be used as interesting and versatile molecular receptors. The compounds are capable of forming host-guest type complexes with an array of aliphatic or aromatic species in the gas phase, solution phase or solid phase [196][197]. The main interaction parameters are hydrophobic van der Waals forces, dipole-dipole interactions and the CH$\cdots\pi$ interactions. As with the calixarenes by modifying the chemical functionality around the cavity rim the molecular recognition capabilities of the cavitand can be tailored to selectively bind target analytes. These modifications can take place on both the upper and low rims, see Figure 1.9.

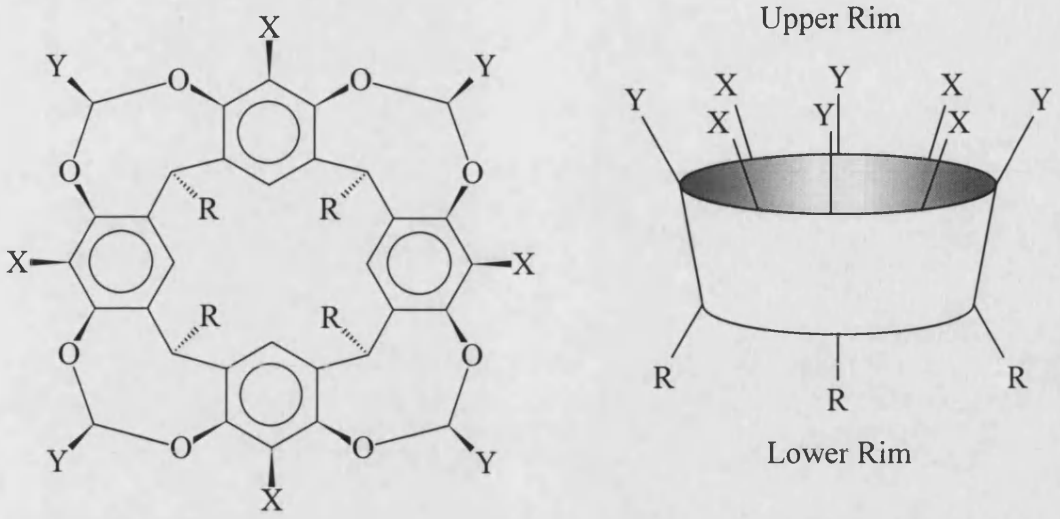

***Figure 1.9**: The general chemical structure of cavitands and a representation of their shape, cavity and functional group orientation.*

Because of their selective binding properties towards organic solvents cavitands have been applied in chemical sensor membranes [198][199][200]. Dalcanale *et al.* [201] first investigated the potential for cavitand coated QCM sensors for the detection of volatile organic compounds. Their initial study yielded promising results [139]. Modifying the functional groups on the cavitand surface had a marked effect on the frequency response of the coated sensor. Comparing the sensor response of the modified cavitands to organic vapours these effects were systematically studied. The cavitand they utilised can be seen in Figure 1.10.

The paper first investigated the effect of deepening the cavity of the basic cavitand shown in Figure 1.9. This was achieved by adding the four diaza-naphthalene units to the upper rim. The organic vapours used to probe the cavitand coated sensor were; hexane, ethanol, acetonitrile, chloroform, tetrachloromethane, nitromethane, THF, benzene, cyclohexane, butanone and ethyl acetate. They showed that reducing the number of diazanaphthalene bridging units (from four to three, two, one and finally zero) had only a minor effect on the sensor response to chlorinated and aromatic compounds. Typically a reduction of about 3 % of the sensor response was observed for each bridge unit removed, the total frequency response was around 100 Hz for a 200 ppm solvent vapour concentration. A significant change in the frequency response pattern was only observed for the organic solvents that could not

contribute a CH···π interaction, namely nitromethane, ethyl acetate and acetonitrile. These compounds doubled their frequency response on removal of all the bridge units.

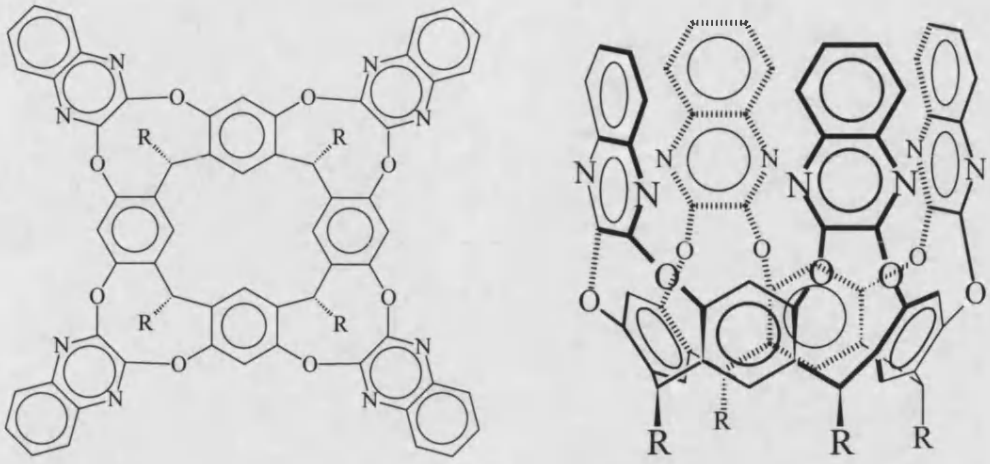

***Figure 1.10**: The chemical structure and shape of the cavitands use by Dalcanale [139].*

The second investigation looked at the effect of changing the substituents on the lower rim of the cavitand. The lower rim of the *tetra*-diazanaphthalene cavitand was modified with R = methyl, R = hexyl, R = phenyl and R = phenoxybutyl. These modifications were found to have a much more pronounced effect on the sensor response. The phenyl derivatised cavitand had virtually no response to any of the vapours. The frequency shift was below 20 Hz in all cases compared to frequency shifts of between 100-200 Hz for the *tetra*-hexyl cavitand. The *tetra*-methyl cavitand also had a very minor response to all the probes, less than 60 Hz. In all cases the *tetra*-hexyl or the *tetra*-phenoxybutyl cavitands had the largest response, typical values were greater than 100 Hz. In general the changing of the hexyl groups to methyl groups reduced the sensitivity to most analyte vapours. The same trend could be seen in the changing of the phenyl groups to phenoxybutyl groups.

Both experiments indicated that it is the chemical nature of the lower rim that has the greatest influence on the interaction of the cavitand with organic vapours. However it is worth mentioning that the deposition of the cavitand film was carried

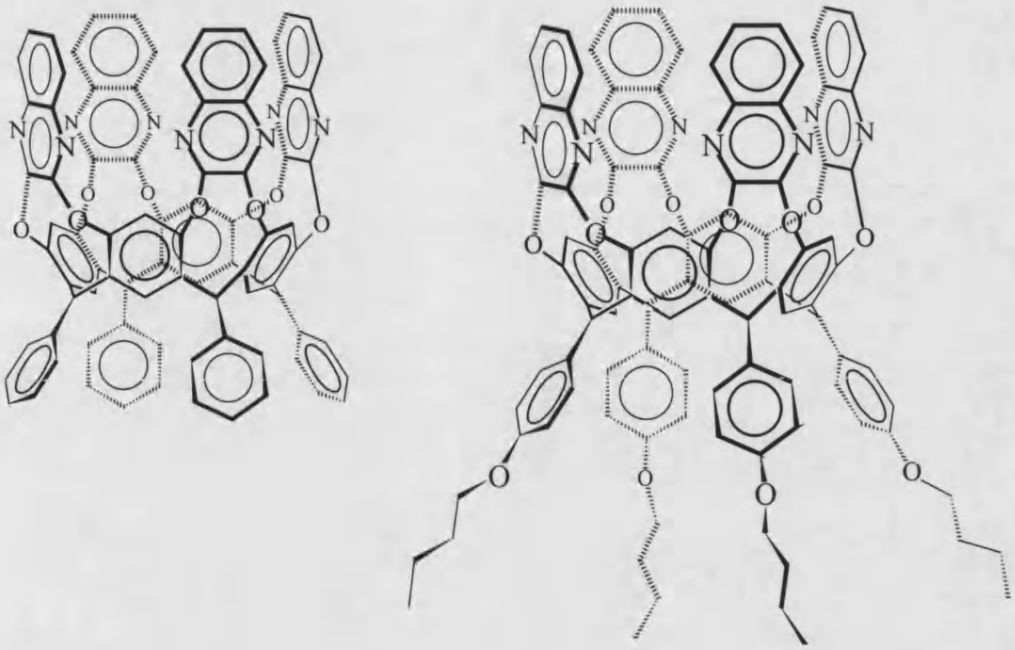

***Figure 1.11**: An illustration of the tetra-phenyl and tetra-phenoxybutyl derivitised cavitands*

out with the evaporation method. This involves the application of a solution of the cavitand in a suitable solvent to the surface of the QCM resonator via an airbrush, followed by simple solvent evaporation. This method results in a film with no directional order, a random orientation of the cavitands. Although some self-assembly may occur it is unlikely that the cavitand will be placed on the QCM surface orientated as shown in the diagrams, so the labelling of the upper and lower rims is arbitrary. Only the chemical modifications on the lower rim of the cavitand induced a variation in the selectivity profile of the coated sensor, it can therefore be assumed that only this region is involved in the vapour binding. This is supported by previous work. In several systems guest molecules have been observed residing in sites other than the central cavity of host molecules [202]. X-ray crystal structures of cavitands with pendant alkyl chains have found molecules such as acetone and dichloromethane bound within the chains as opposed to the cavity [203][204].

Pinalli *et al.* adapted the basic cavitand shown in Figure 1.9 to develop a chemical sensor for the detection of C_1-C_5 alcohols [205]. They introduced a hydrogen-bond donor group, P=O, to interact with the alcohol –OH group forming

the P=O···H–O–R hydrogen bond. The orientation of the arene cavity, the CH···π interaction and the traditional hydrogen-bond system all combined to increase the binding potential of these cavitands to small alcohol molecules.

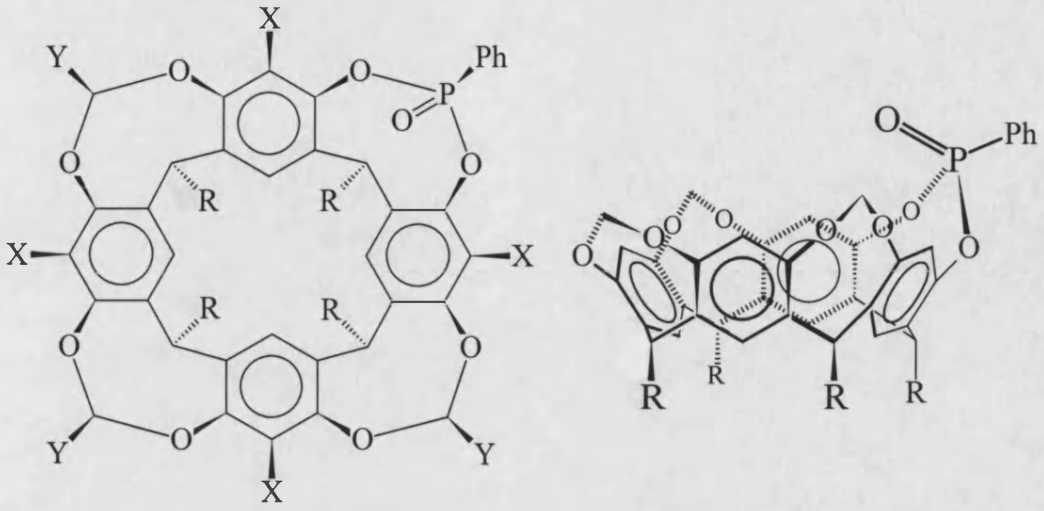

Figure 1.12: *The modified cavitand employed by Pinalli [205] showing the presence of the P=O group and its orientation.*

The contribution to the binding potential that arose from the pre-organised cavity and spatial functionality was investigated by the structural isomers of the cavitand. The hydrogen-bond donor was orientated towards the cavity and away from the cavity. This simple shift in geometry of the P=O donor resulted in a five-fold drop in sensitivity for all the alcohols investigated. The sensor response to each alcohol increase slowly with the addition of more $–CH_2–$ units, methanol had the lowest sensitivity and 1-pentanol had the highest sensitivity. The typical response, to 3000 ppm alcohol vapour, of a sensor coated with the cavitand shown in Figure 1.12, were 60 Hz, 80 Hz, 110 Hz, 150 Hz and 400 Hz for methanol to pentanol respectively. The structural isomer with the P=O facing away from the cavity had typical responses of 2 Hz, 3 Hz, 5 Hz, 20 Hz and 80 Hz respectively. They concluded that the response of the two diastereomeric-cavitands clearly showed the simultaneous presence of the two binding interactions, and that these combined to give a remarkable increase in the response of the sensor to linear alcohols. Their strategy of 'focusing' interactions, so those molecules located in a molecular receptor can be suitably entrapped, can be utilised to produce highly selective supramolecular mass sensors.

1.8.6 Cyclodextrins

Another group of molecules with a well-documented cavity is the cyclodextrins [206]. These are cyclic amylose structures that usually containing 6, 7 or 8 glucose units, as shown in Figure 1.13. The three common cyclodextrin molecules are α-, β-, and γ-cyclodextrin and consist of 6, 7 and 8 member rings respectively. The cavity ranges in size from about 0.4 nm diameter in the case of the α-cyclodextrin to 0.8 nm in the γ-cyclodextrin. The depth of the cavity is the same for all three, approximately 0.8 nm.

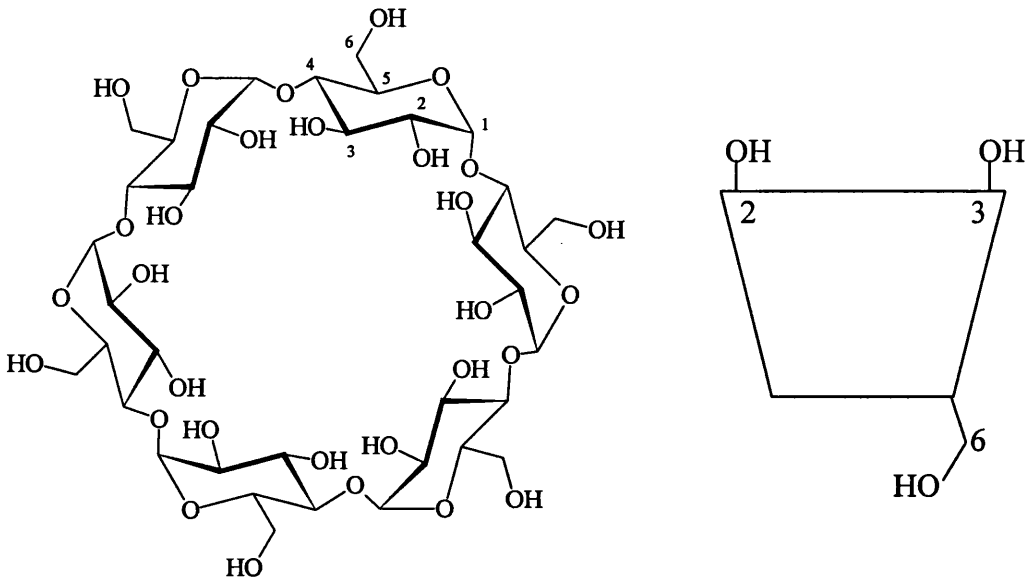

***Figure 1.13**: Molecular structure of α-cyclodextrin and a schematic representation of the shape of the molecule with the primary and secondary hydroxyl groups shown.*

The upper rim of the cavity has two slightly different orientated secondary hydroxyl groups, one attached to the glucose carbon numbered 2 angled inwards and one on carbon number 3 angled outwards. The lower narrower rim has the primary hydroxyl groups projecting outwards. These functional groups allow various chemical modifications to be made to the basic cyclodextrin molecules via simple primary and secondary hydroxyl chemistry. The cyclodextrins are well known for their complexes in solution, especially aqueous medium. They form simple 1:1 cage type complexes with a variety of species ranging from the noble gases to large organic molecules [207]. The exact nature of the complex varies from molecule to molecule. Stable complexes are known with large species that have one end of the guest

molecule protruding out of the cavity, similarly, smaller species such as methanol form complexes containing one or more water molecules co-complexed. Cyclodextrin derivatives have been used to separate organic vapours with gas chromatography columns, enantiomers have also been successfully resolved in such a way [208].

The variety of ring sizes and functional group modifications available offer great scope for developing host-guest interactions and creating highly specific systems. For these reasons cyclodextrins have been studied for a whole range of potential applications such as enzyme mimics, drug delivery [209] and chemical sensors [210][211]. Their application in combination with a QCM, however, seems slightly limited. Ide *et al.* [212] successfully used a QCM resonator coated with cyclodextrin to discriminate between two optical isomers in the gas phase. It was shown that a sensor produced using a phospholipid layer or a cellulose film in place of the cyclodextrin film had no difference in response to the two isomers. The results confirm the molecular recognition capabilities of the cyclodextrin cavity and the chiral nature of the compound.

Dickert *et al.* [213] utilised the cyclodextrin to monitor the formation of Grignard reagents. The cyclodextrin was attached to a polymer support coated onto a QCM resonator. The resonator was placed in a reaction mixture and used to detect the reactant chlorobenzene. The sensor response was linear in the range 10-500 ppm with respect to chlorobenzene and could determine the end point of the Grignard reaction to within 2 %. Another advantage of the sensor over other devices was its on-line capabilities, the ability to supply a real-time read-out for the analyte concentration. The problem of coating selectivity was negated in this instance, as only one potential analyte would interact with the cyclodextrin in the reaction mixture.

More recently several works have used SAW devices coated with modified cyclodextrins to examine volatile organic species (VOCs) [214][215]. Yang *et al.* [215] used SAMs of β-cyclodextrin on SAW surfaces and exposed these surfaces to a selection of VOCs. In general the sensor could detect vapours down to 100 ppm concentrations. The largest response was for the perchloroethylene and toluene with the smaller molecules such as methanol and acetone having the lower responses. They concluded that by incorporating molecular recognition reagents such as

cyclodextrins and their derivatives into sensing layers SAW sensors with high sensitivity and selectivity can be obtained.

The lack of work published on QCM based sensors coated with cyclodextrin material is surprising. Considering the success of SAW coated devises and other chemical sensing applications of cyclodextrins as well as the potential for chiral recognition, cyclodextrins should offer ideal solutions for QCM based chemical sensors. For this reason the response of α-cyclodextrin and β-cyclodextrin coated resonators to VOCs, and more specifically alcohol vapours will be explored in chapter 3. This is with a view to establishing the groundwork for a more extensive investigation utilising derivatised cyclodextin compounds in both gas phase and liquid phase sensor applications.

The results of several QCM sensor experiments involving the binding and molecular recognition potential of cavitands, calixarenes and cyclodextrins were the subject of a published correspondence [216]. In the article Grates *et al.* point to the lack of a control in most of the QCM sensor reports. They present data to suggest that the interaction and selectivity profiles observed are in some cases due to general dispersion interactions of the vapour with the sensor-vapour interface and are therefore not true cases of molecular recognition. A fundamental difficulty in attempting to use host-guest or lock and key interactions to obtain selective gas phase sensors is that the main interaction between the host and the guest molecules is driven by solvating parameters and partition coefficients. These interactions take place between the guest and any part of the host interface; they do not depend on the nature of the pre-organised cavity. For example, the interactions available between a solvent molecule and the cavitand surface will be the same as those available between a solvent molecule and a non-cyclic polymer or oligomer of similar chemical functionality. Such polymers could be used as control membranes demonstrating whether the presence of the pre-organised cavity increases the binding potential of such molecules to these surfaces. These conclusions do not exclude the possibility that the presence of a pre-organised cavity may perturb the selectivity patterns expected solely on the grounds of dispersion interactions. The total binding potential will be the sum of all interactions, of which dispersion interactions may well be the dominant factor. In some cases these may prove to be useful in sensor development. A trend has developed in recent years to move away from the

investigations of single sensor device with highly selective binding potentials and to focus instead on the development of sensor arrays. The arrays consist of a number of individual sensors each coated with different absorbing membranes such as polymers, dendrimers and sol-gels. These membranes are non-selective and absorb or adsorb many different chemical species indiscriminately, however, the response pattern of the whole array will be indicative of a particular analyte. The response of the whole array to a given analyte or analyte mixture is then recorded and processes by a pattern recognition program or artificial neural network. These systems recognise 'smells' in a similar way to the human olfactory system and are proving to be of great potential in the field of chemical sensors, electronic nose and electronic tongue devices.

1.8.7 Clathrates and Inclusion Complexes

In the previous examples of QCM based selective chemical sensors the molecular recognition was achieved within a cavity. The cavity was present in a larger macromolecule and supplied both size and shape selectivity as well as functional group orientation. Another potential source of species recognition are clathrate compounds [217] and both organic and inorganic inclusion complexes.

Clathrates are compounds in which a guest molecule is physically trapped in the crystal lattice of the host species. The interaction between host and guest is often limited to van der Waals forces. Other more energetic interactions such as hydrogen bonding and dipole-dipole interactions can also occur between the host and the guest species. Reinbold *et al.* [218] used the clathrate structure of bis-fluorenyl derivatives and lactic acid as selective vapour sorption membranes on QCM resonators. The QCM was used to determine the host-guest ratio of the clathrate-vapour complex, and to examine the internal phase transitions that occur during formation and decay of the clathrate-vapour complex. The clathrate coated resonator was also employed as a chemical sensor responsive to the organic vapours that form complexes with the compounds used. The sensitivity and selectivity of the sensors was not quoted but the frequency changes in the resonator on exposure to the analytes were fast and reproducible. A further investigation involved modifying the clathrate host in such away as to induce greater selectivity in the vapour uptake. This was achieved by the

addition of bulky *t*-butyl groups distorting the crystal lattice and limiting clathrate formation. A system was developed that could selectively uptake cyclohexanone or dioxane in the presence of methanol, ethanol, 1-butanol, acetone, THF and trichloromethane. Reinbold *et al.* also claimed some chiral separation when single enantiomers of the host were employed to form the clathrate lattice [219]. A minor drawback to the systems studied by Reinbold *et al.* was the observation that quantities of the clathrate host were lost from the crystal lattice during exposure of the crystal interface to the organic vapours. This is a consequence of using relatively small molecules with an appreciable vapour pressure, and one reason why sensor coatings tend to consist of larger macromolecules such as calixarenes and cavitands. This loss of material resulted in the occasional random frequency shift and would be a major concern for the sensor lifetime. However the chiral recognition potential of clathrates crystal lattice could prove to be extremely useful in the field of chemical sensors.

1.8.8 Transition Metal Complexes

The selective chemistry of transition metal complexes has also been employed as the basis for a QCM chemical sensor. Several inorganic compounds have the desired properties for application as selective binding membranes, fast, reversible and selective interactions. Current work concerning the fixation of atmospheric CO_2 for organic synthesis has involved the development of transition metal complexes that react reversibly with CO_2 gas. The *trans*-[carbonylhydroxy-*bis*(triphenylphosphine)-rhodium(I)] species is stable under standard atmospheric conditions [220]. The interaction between CO_2 and this rhodium complex can be considered to be molecular recognition due to the highly selective nature of the binding. Li *et al.* [221][222] coated the complex onto the surface of a QCM resonator via the standard dip technique using dichloromethane as the solvent. The resulting sensor had a pronounced frequency response to CO_2 gas but only a limited sensitivity. The lower detection limit was approximately 500 ppm. The sensor was also influenced by the presence of atmospheric impurities such as water, SO_2 and NH_3. The author suggested that the sensor head could be manufactured under a dry atmosphere, packaged and sealed before storage, and unsealed by the end user. This is a rather complex procedure and economically unsound. In general the use of inorganic metal

complexes for either gas phase or liquid phase selective QCM based chemical sensors has be largely unexplored. The selective and reversible binding potential of these metal centres should in theory be ideally suited to chemical sensor applications. As with most chemical systems a comparison can be drawn with nature, all of the natural processes that involve the recognition and use of gases such as O_2 and CO_2 have transition metal complexes at the heart of the chemistry. Without a doubt the use of such complexes in man-made chemical sensors will increase rapidly over the coming years.

1.8.9 Crown Ethers

The crown ether compounds are well known for their metal ion chelating ability. They have found a variety of applications mainly as phase transfer catalysts [223] and extraction reagents [224] but also in more elaborate areas such as membranes for ion-selective electrodes [225]. However, their use as selective host material in QCM based sensors have been limited to vapour phase VOC detection [226][227].

As with the majority of the work discussed so far the crown ether host compounds were deposited using the dropping technique and the sensor response determined by the exposure of the coated resonator to a mixture of the VOCs in an air stream. The results obtained were similar to those reported for the other host VOC systems and so will not be discussed al length here. Battenberg *et al.* developed an interesting variation of the system [228]. They compared the response of the standard crown ether polymer coatings with that of the metal loaded crown ether polymer. The results shown a 1000 times increase in the sensor response to alcohol vapours in the presence of the metal loading. They also employed porphyrin based coatings in a similar fashion.

As with cyclodextrin based sensors the lack of published data on crown ether systems is surprising. They are known for their Group I cation binding ability and yet have only been employed as vapour phase VOC detectors. For this reason the subject of QCM based, Group I metal ion sensors, utilising crown ether systems is the main topic of this thesis. Chapter Three describes the sensor systems developed. The binding ability of the crown ethers and the factors influencing this are discussed, followed by a detailed account of the fabrication of the sensor and the response studies undertaken.

1.9 Conclusion

The papers discussed in this section illustrate the binding and molecular recognition capability of a range of host molecules. These have been successful translated into selective chemical sensors via the QCM transducer. The development of the QCM calixarene systems is representative of the general trend; firstly the application of a vapour phase system followed by the progression to the liquid phase and subsequent fine tuning of the chemistry to produce an acceptable chemical sensors. The initial development of a vapour phase system is probably as a result of the improved stability and greater fundamental understanding associated with the vapour phase application of QCM transducers. This reinforces the observation that a greater understanding of the liquid phase QCM transducer is a prerequisite to any sound commercial development. Improved theoretical description and greater stability will lead to more versatile and more selective liquid phase sensors.

The variations of the response of the host-coated sensors and their correlation with the chemical modification of the molecules confirm that the frequency response is associated with the binding of target species within or around the central cavity. It is clear that the host-guest interactions relate to the frequency change of the resonator and that the use of selective binding is an excellent way of introducing selectivity to the QCM response for both liquid phase and vapour phase systems. The selective binding can be used as a simple mass change, as in the case of MIP coated sensors, or as a means of inducing a viscoelastic change in the coating, as in the case of the phase transitions associated with clathrates.

The work presented and discussed in the following chapters is concerned with the development of both vapour and liquid phase QCM chemical sensors. The sensors make use of the host guest relationships associated with the crown ether compounds and cyclodextrin compounds as well as ordered Langmuir-Blodgett (LB) layers of smaller organic molecules. The crown ether based systems were developed as selective aqueous metal ion sensors, the LB coated systems as selective gas phase sensors and the cyclodextrin based systems as general VOC sensors. Each system will be discussed in turn with the relevant background and experimental detail after discussion of the general principles of the set up used.

EXPERIMENTAL

CHAPTER TWO

2.1 Introduction

The research carried out during the project involved a variety of different areas. These include copolymer syntheses, uptake studies, the sensor fabrication and response studies both in the gas phase and in the liquid phase. The experimental details of the main points common to these studies are presented here. A more detailed discussion on the methodology used for the individual studies is presented at the relevant points in the specific chapters that follow.

The section opens with the details of the quartz crystal microbalance employed. The operating conditions and frequency stability are discussed. This is followed by a general account of the other analytical equipment utilised, chemicals purchased and synthetic procedures that were followed.

2.2 The Quartz Crystal Microbalance

The QCMs were built 'in house' by Dr Mike Bailes. They are based on the standard transistor oscillator circuit shown in Figure 2.1. The design incorporated two individual resonators, these being the reference and the working with the difference between the two being the frequency output. The QCM functions with 10 MHz resonators as this is the region the oscillating circuit operates.

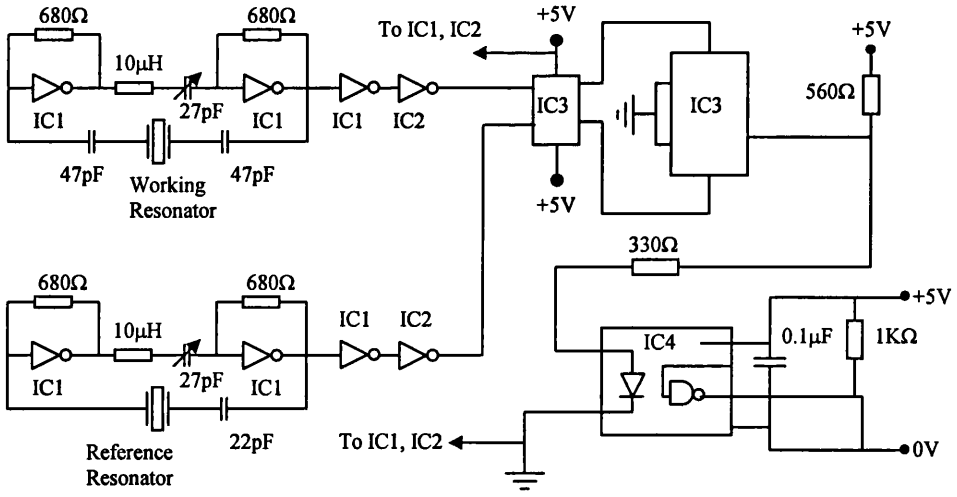

Figure 2.1: Shows a diagram of the electrical circuit used in the QCM.

The resonators are placed in a positive feedback loop and oscillate at the frequency of lowest impedance. This is often referred to as the series resonance. The frequency output from the QCM was recorded on a desktop PC running QBasic and fitted with a Metrabyte IEEE analogue-to-digital interface card. 10MHz, AT-Cut, thickness shear, quartz resonators were used as purchased from International Crystal Manufacturing Co, Inc, Oklahoma City, Oklahoma. These consisted of a 15.0 mm diameter quartz disc coated on either side by a 4.5 mm diameter circular electrode. The electrodes had a 50 Å Cr under-layer on the quartz surface and a 1000 Å Au top-layer. The Cr interface improved adhesion of the gold to the resonator surface. Figure 2.2 shows the general appearance of the resonators.

The connections to the oscillating circuit were made via two screw adapters joining the QCM to the two base pins; these pins were connected to either electrode. The active piezoelectric area is that covered by the overlap of the two electrodes and only mass changes in this region effect the QCM frequency. The mass sensitivity decays rapidly at the edge of the electrodes [229].

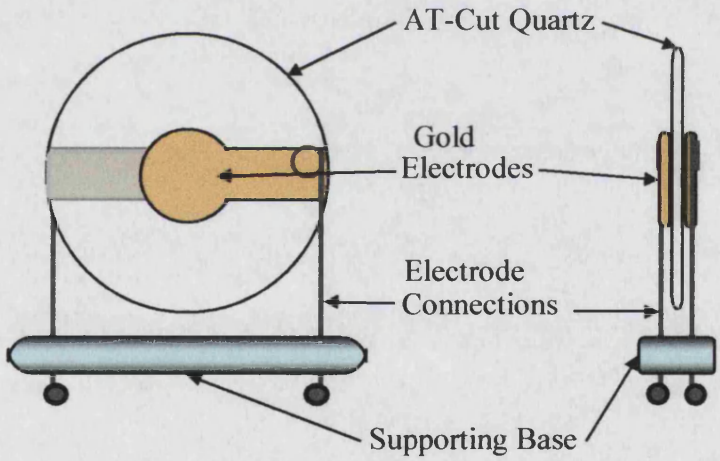

***Figure 2.2**: A schematic representation of the QCM resonators.*

Once connected the resonators were mounted in individual flow cells and placed within a Faraday cage along with the oscillating circuit. Three different flow cells were utilised throughout the QCM response experiments. These are illustrated in the appropriate sections later in the thesis. Briefly two liquid phase systems (the batch chamber and a flow injection analysis cell) and one gas flow cell were utilised. The QCM set up and the Faraday cage can be seen in Figure 2.3. The dual resonator

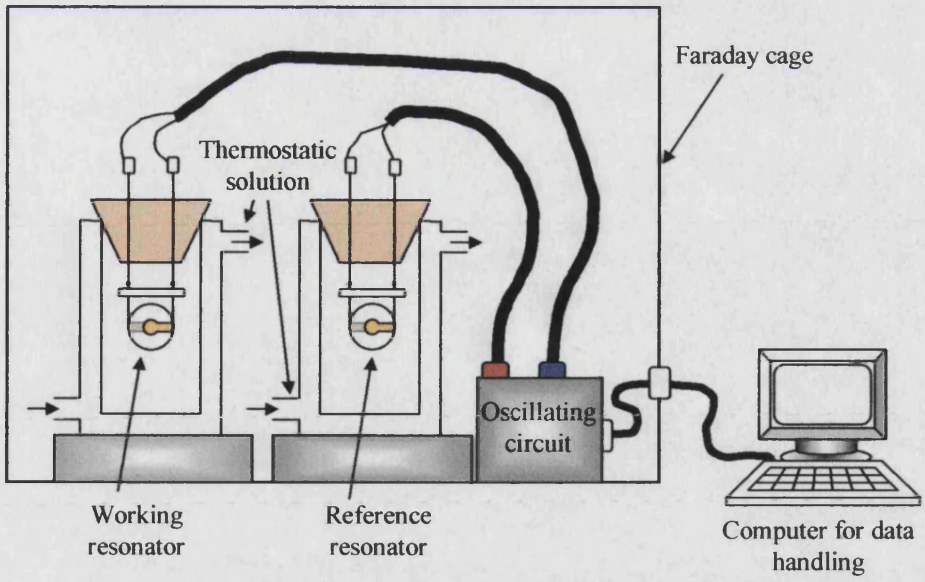

***Figure 2.3**: The QCM set up for the batch method*

system increases the overall stability of the recorded frequency by eliminating the changes associated with external conditions such as temperature. The reference is generally exposed to the same operating environment as the working resonator with the difference between the two being the recorded frequency. Not only does this eliminate unwanted frequency shifts but it also reduces the recorded frequency from 10MHz down to the kHz region. As the frequency change of interest is typically below 1kHz this facilitates data manipulation. The stability of the QCM frequency output can be seen in Figure 2.4. This was typically ± 0.2 Hz in the gas phase with a baseline drift of approximately 0.5 mHz sec^{-1} and ± 5 Hz with a drift of 20 mHz sec^{-1} in liquid phase systems.

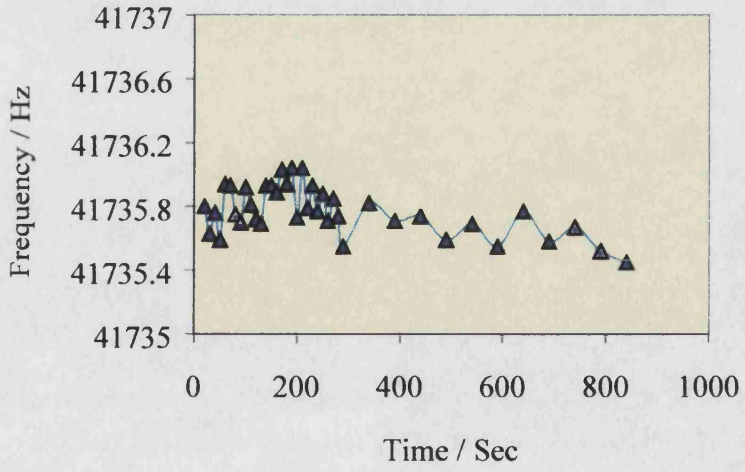

***Figure 2.4**: The stability of the QCM frequency output for a resonator oscillating in air.*

2.3 Analytical Instrumentation

^{1}H- and ^{13}C-NMR NMR spectra were recorded in $CDCl_3$ or C_5D_5N on a Varian 400 mercury system spectrometer using TMS as the reference.

Mass spectroscopy Mass-spectrometry was conducted on a Micromass VG autospec. Typically both EI and FAB+ ionisation were used.

CHN Elemental analysis was conducted on a CarloErba 1106.

SEM and X-PES SEM images and X-PES data were obtained on a JEOL 6310 scanning electron microscope.

AES Aqueous metal ion concentrations were determined using atomic emission spectroscopy (AES) on a Varian AA275 instrument using standard calibration techniques.

GPC GPC analysis was carried out by RAPRA on a polymer laboratories GPC-210 using DMF as the solvent and poly(methylmethacrylate) as the standard.

DSC Differential Scanning Calorimetry was carried out on a TA instruments 2910 DSC. Aluminium pans were employed with the lids crimped. An empty pan of equal mass was used as the reference.

FTIR FTIR was carried out on a Perkin Elmer spectrometer.

2.4 Syntheses

Except where indicated all solvents were purchased from Aldrich as HPLC grade reagents and used without further purification. AIBN was purchased from BDH Chemicals Ltd. α-Cyclodextrin and β-cyclodextrin were purchased from Fluka. All chemicals were used without further purification. Milli-Q_{plus} 185 water was used throughout for the production of aqueous stock solutions and the sensor response.

2.4.1 Crown Ether Monomer Synthesis

Acryloyl chloride, 96% purity, was purchased from Aldrich and used with no further purification. 2-(Aminomethyl)-15-crown-5 and 2-(aminomethyl)-18-crown-6 were also purchased from Aldrich with 97% and 95% chemical purity respectively. Sodium carbonate was purchased from Fisons Laboratory Reagents and dried in an oven at 120 °C prior to use.

Synthesis of acrylamidomethyl 18-crown-6, 1

Dried Na_2CO_3 (approximately 5 g) was added under N_2 to dry 1,4-dioxane (25 cm^3). The solution was allowed to stand with stirring for a 10 minutes before the addition of 2-(aminomethyl)-18-crown-6 (1 g). This was followed by the addition of acryloyl chloride (1 cm^3) in three equal aliquots over a period of 2 hours. This solution was left, with stirring, at room temperature, under N_2 for a further 3 hours before being filtered. The Na_2CO_3 was washed with chloroform before being discarded and the chloroform added to the reaction mixture. The reaction mixture was then reduced via vacuum distillation to constant mass. The product was viscous yellow oil with a 96% yield.

- **^{1}H NMR** [6.2, 6.2, 5.5 ppm alkene protons, 2.7 integration. Multiplet 3.2-3.8 ppm, ring protons, integration 25].
- **^{13}C NMR** [165 ppm C carbonyl, 130 ppm CH alkene, 125 ppm CH_2 alkene, 70-65 ppm CH_2 ring, 40 ppm CH_2 amine].
- **FAB Mass Spec $(M+H)^+$** = 348.2 [calculated = 348.4].
- **CHN**: 55.2C, 8.3H, 3.9N [calculated 55.3C, 8.3H, 4.0N].

Synthesis of acrylamidomethyl 15-crown-5, 2

The same procedure was repeated substituting 2-(aminomethyl)-15-crown-5 for 2-(aminomethyl)-18-crown-6 using identical mass ratios. The product was very similar in appearance with a yield of 80%.

- **^{1}H NMR** [NH proton, integration 1, 6.8 ppm. Alkene protons, integration 3, 6.1, 6.2, 5.6 ppm mutliplet. Ring protons, integration 19, multiplet, 3.4-3.8 ppm].
- **^{13}C NMR** [166 ppm C carbonyl, 132 ppm CH alkene, 126 ppm CH_2 alkene, 72-66 ppm CH_2 ring, 42 ppm CH_2 amine].
- **FAB Mass Spec $(M+H)^+$** = 304.2 [calculated = 304.2].
- **CHN**: 53.0C, 7.6H, 3.6N [calculated 53.1C, 7.9H, 4.4N].

2.4.2 Cross-linked Crown ether Copolymer Resin

In a typical procedure the crown ether monomer 1 (0.9g), ethylene-glycol-dimethacrylate, EGDMA, (7g), acrylic acid (2g) and AIBN (0.1g) were dissolved in 200 cm^3 acetonitrile under N_2. The solution was heated to 65 °C with stirring for 24 hours. During the polymerisation the solution went from a clear colourless liquid to opaque white colloidal suspension. After 24 hours 50 cm^3 of ice cold methanol were added and the resulting precipitate recovered via filtration. The polymer was washed separately with methanol, diethyl ether, chloroform and water in a Soxhlet apparatus for 12 hours, 12 hours, 24 hours and 24 hours respectively. The polymer was recovered and dried in the oven at 80°C with an average yield of 95%. The same procedure was employed to produce the equivalent 15-crown-5 cross-linked copolymer, using monomer 2 in place of monomer 1.

The recovered material was analysed by CHN elemental analysis, FTIR spectroscopy, SEM and differential scanning calorimeter (DSC). See Appendix 1 for further details and the results of the analysis.

2.4.3 Crown Ether Acrylic Acid Copolymer

Synthesis of poly(acrylamido-18-crown-6)-(acrylic acid), 3

AIBN (0.07 g) was dissolved in a solution of dry DMF (20 cm^3) and acrylic acid (3.2 g) at 0 °C under N_2. The 18-crown-6 monomer **1** (0.90 g) was also dissolved in DMF (5 cm^3) and the two solutions combined. The reaction mixture was then heated to 60 °C for 2.5 hours. After this time the heat source was removed and ice cold methanol (40 cm^3) was added to quench the reaction. The copolymer was recovered via precipitation into diethyl ether and subsequent filtration. The total yield of the copolymer was 72 % with 2 % of the crown ether remaining unreacted.

- **^{1}H NMR** [4-3 ppm multiplet integration 1.28 crown ether ring protons, 3.8-1.8 ppm multiplet integration 1 copolymer backbone protons].
- **^{13}C NMR** [180 ppm C carboxylic acid, 70 ppm CH_2 crown ether ring, 43 ppm CH copolymer backbone, 35 ppm CH_2 copolymer backbone].
- **CHN**: 49.9C, 6.3H, 1.9N [calculated 51.5C, 6.7H, 2.0N].
- **FTIR** [3800-2800 cm^{-1} OH (carboxylic acid), 1876-1700 cm^{-1} C=O (carboxylic acid), 1700 cm^{-1} C=O (amide), 1642 cm^{-1} N-H bend, 1500-1200 C-H bend, 1104 cm^{-1} C-O str, 951 cm^{-1} C-N str].
- **GPC** [M_w 801000, M_n 37500, polydispersity 23].

Synthesis of poly(acrylamido-15-crown-5)-(acrylic acid), 4

The same procedure was repeated substituting the **2** for **1**. The synthesis proceeded as before with the copolymer recovered in a 70 % yield.

- **^{1}H NMR** [3.8-3 ppm multiplet integration 5 crown ether ring protons, 3.8-1.8 ppm multiplet integration 4 copolymer backbone protons].
- **^{13}C NMR** [180 ppm C carboxylic acid, 70 ppm CH_2 crown ether ring, 42 ppm CH copolymer backbone, 35 ppm CH_2 copolymer backbone].
- **GPC** [M_w 1040000, M_n 31500, polydispersity 32].

2.5 Uptake Experiments

For this section all glassware was carefully washed with 2M sulphuric acid and rinsed using Milli-Q_{plus} 185 water, 18.2 MΩcm resistance. This water was also used to make up all aqueous stock solutions.

Batch Uptake

The resins were dried in a vacuum oven at 30 °C then a pre-weighed amount added to a precise volume of the aqueous metal ion solutions. The concentration of the solutions was determined via AES. Several stock solutions of the metal ions were prepared containing between 10 and 200 ppm with respect to the metal cation. Before weighing the metal salts were dried in an oven at 120 °C for several hours then allowed to cool in a desiccator. Two types of stock solutions were produced. The individual stocks made as indicated and a series of mixed stocks containing $Li^+_{(aq)}$, $Na^+_{(aq)}$ and $K^+_{(aq)}$ were prepared. These mixed stock solutions were used to investigate the competitive binding properties of the resins.

Uptake Kinetics

The experimental method consisted of pre-soaking the resin (1.343 g) in 53 cm^3 of Milli-Q_{plus} 185 water, 3 cm^3 of the water were then removed and saved for analysis. To the remaining solution 50 cm^3 of a 100 ppm $K^+_{(aq)}$ stock solution were added. These were mixed rapidly by vigorous shaking before a 1 cm^3 sample was removed. At three minute intervals further samples were removed until a total reaction time of 40 minutes had elapsed. After removal the samples were instantly filtered to separate the copolymer resin from the metal ion solution. On shaking the mixture of the resin and the stock solution an even suspension of the solid resin was produced throughout the stock. Removing 1 cm^3 of this suspension effectively removed a constant ratio of resin and stock solution from the total mixture. The procedure was such that the ratio of resin to stock solution was maintained throughout. The results of this study can be seen in Table A2.5.

2.6 Resonator Preparation

The resonators were cleaned prior to use with piranha solution [230], (a 1:1 ratio of 98% sulphuric acid and 40% H_2O_2), and rinsed with Milli-Q_{plus} 185, 18.2 MΩcm, water. They were then soaked in methanol and chloroform and dried under an air stream at room temperature. This procedure was repeated several times until a constant dry frequency was obtained (± 25Hz). After drying the resonance frequency was recorded and this used as the 'clean' frequency. In order to maintain satisfactory oscillation of the resonators in the aqueous solutions the resonators were capped [231]. This involved the placement of a glass cover over the gold electrode on one side of a resonator, preventing the contact of this electrode with the oscillating solution. The glass cover was held in place by a polysiloxane resin. The reference was maintained in air as the placement of both the working and the reference resonators in a liquid environment resulted in unstable oscillation.

2.6.1 Cross-linked Resin Coating

A solution of the individual monomers was prepared by dissolving the 18-crown-6 monomer **1** (0.0636 g), acrylic acid (0.2283 g), EGDMA (0.1575 g) and AIBN (0.0060 g) in acetonitrile (100 cm^3). The resonators were coated by placing 0.5 cm^3 of the monomer mixture in a 0.5 cm^3 reaction well on the QCM resonator. The monomer ratios were the same as those used to prepare the cross-linked resins. The solution was then heated to 75 °C for several hours to polymerise. After cooling the coated resonators were rinsed with hot acetonitrile followed by hot methanol. The frequency was recorded after drying and this used as the 'coated frequency'.

2.6.2 Cyclodextrin and Copolymer Coating

The cyclodextrin and crown ether-acrylic acid copolymer were coated onto the resonator using the drop technique [232]. This involves placing a drop of solution of the material dissolved in an appropriate solvent onto the surface. In the case of the cyclodextrins water was used as the solvent and for the copolymer DMF was used. The drop is then left to evaporate in air, depositing the material and coating the resonator.

2.6.3 Self-Assembled Monolayer of 2-Aminoethanethiol

The resonators were placed into 30 cm^3 of ethanol, removed, rinsed with ethanol, acetone and chloroform respectively, and then dried in air. This procedure was repeated and a reproducible dry resonance frequency was obtained. This shows that the exposure of the resonator to ethanol produced no frequency change in the resonator. The data from these runs were used as a blank control experiment. A second clean resonator was then placed into 30 cm^3 of a 2-aminoethanethiol solution. All thiol solutions were 5 x 10^{-3} mol dm^{-3} of the appropriate thiol in ethanol. After several hours the resonator was removed, rinsed with ethanol, acetone and chloroform respectively, then dried. The resonance frequency was again recorded.

2.7 Liquid Phase Resonator Response

The responses of the coated resonators were monitored in two ways, a batch method and an FIA method. As described previously the resonators utilised in the liquid phase were capped prior to use. The reference was maintained in the gas phase.

Batch Response

The sensor was placed in a volume of pure water (30 cm^3) and allowed to stabilise. After stabilisation metal cations were added to the water via the injection of a metal sulphate stock solution (0.230 mol dm^{-3}). The $M^+_{(aq)}$ concentration was steadily increased by successive injections. This process is referred to the batch method and was used to investigate the response of the coated sensors to $Li^+_{(aq)}$, $Na^+_{(aq)}$ and $K^+_{(aq)}$. The metal stock solutions were added in 10-100 µl injections.

FIA Response

The FIA system involved the injection of the metal sulphate solutions into an eluent flow that carried the cations through a flow cell containing the coated resonator. The same stock solutions were used as before. The flow of water across the resonator surface was started and the resonator frequency allowed to stabilise. Injections in the range of 5-40 µL of the stock solution were then added into the eluent flow and the

frequency response of the sensor monitored. The FIA system had a flow rate of 1.66 $cm^3\ s^{-1}$ and tube diameter of 5 mm. Milli-Q_{plus} 185, 18.2 MΩcm water was employed as the eluent.

2.8 Gas Phase Sensor Response

Once coated the resonators were mounted in a PTFE flow cell. The flow cell contained two resonators. These were the reference resonator and the working resonator, the working resonator being the sensor employed. The actual frequency recorded was that of the reference minus the working resonator. N_2 was used as the carrier gas. This was first passed through a zeolite-containing purification tube and a silica-gel moisture indicator before reaching the injection point. The VOC vapour was introduced by the injection of approximately 1 μl of the liquid solvent into the N_2 flow. The distance from the injection point and the flow cell was 70 cm with a tube diameter of about 4 mm. The flow rate employed was 40 $cm^3\ min^{-1}$.

CROWN ETHER BASED $K^+_{(aq)}$ SENSORS

CHAPTER THREE

3.1 Introduction

The chapter describes the development of an aqueous metal ion sensor based on a QCM resonator coated with a copolymer layer. The copolymer forms a selective adsorption interface between the transducer, the QCM, and the sensing medium, the aqueous solution. On exposure to a solution containing the target ion the copolymer chelates the ion at the interface. This induces a mass change and a viscoelastic change in the copolymer layer and subsequently a frequency change in the QCM resonator. This process is depicted schematically in Figure 3.1 where the QCM is coated with a 'virtual' layer designed to chelate spheres over triangles. In theory a sensor can be developed that will respond selectively for any given target species provided that a suitable selective adsorption interface could be created.

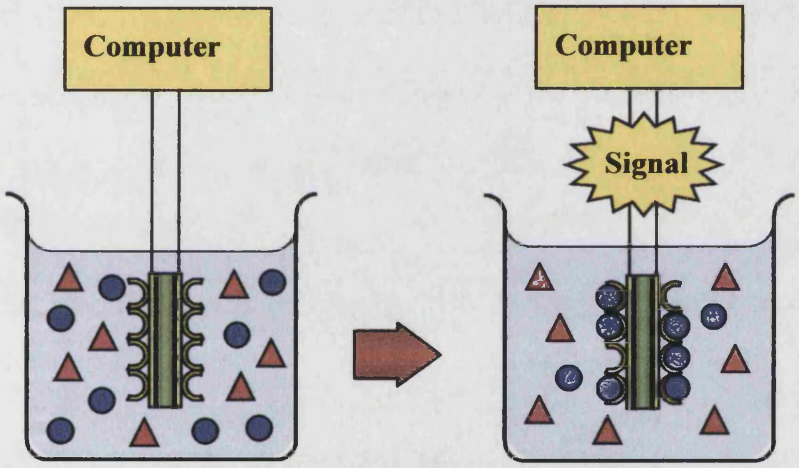

***Figure 3.1**: A schematic representation of the sensing mechanism. The sensor designed to respond to spheres over triangles is immersed in a solution of both species. The spheres bind to the selective coating and produce a signal proportional to their concentration.*

The technique of coating a QCM with a selective adsorbing copolymer has been shown to be a useful approach to developing QCM based aqueous metal ion sensors. Previous work by Hunter *et al.* [233] led to the successful coating of a QCM resonator with a copolymer designed to chelate $Cu^{2+}_{(aq)}$ [234]. The coated resonator responded to the presence of $Cu^{2+}_{(aq)}$ with a detection limit of ~0.1 ppm. However, the resonator also responded to a variety of other metal ions, particularly $Ni^{2+}_{(aq)}$, and to a lesser extent $Co^{2+}_{(aq)}$, $Zn^{2+}_{(aq)}$ and $Fe^{2+}_{(aq)}$. In order to develop systems for the

analysis of Group I metal ions and introduce a higher degree of metal ion selectivity it was decided to investigate sensors based on crown ether [235] containing copolymers.

The polymer coating on the resonator is a water compatible copolymer containing crown ether substituents. The metal ion binding properties of a number of crown ether copolymers have been investigated by Kimura *et al.* [236] who showed that the copolymers reflect, and in some cases enhance, the binding properties of the free crown ether rings. For this reason the polymers used in this work were based on those employed by Kimura *et al.* The crown ether moieties selectively chelate the metal ion with an ionic radius compatible with the diameter of the crown ether ring [237][238]. This selective chelating potential has been well documented ever since the initial work carried out by Pedersen [235] in the mid 1960's.

In the following section the composition of the copolymer coating and the properties associated with their individual components are discussed. Two sections covering the synthesis of the crown ether monomer and the synthesis of a cross-linked resin follow. The uptake properties of the resin are then examined and discussed before the final sections concerning the fabrication and response of the $K^+_{(aq)}$ sensor developed.

3.1.1 The Crown Ether Copolymer

The crown ether copolymer forms the basis of the adsorption interface. This imparts the selectivity on the QCM sensor. Its chemical composition and overall binding potential are crucial factors influencing the sensor response. It was our intention to develop a coating that fulfilled two initial requirements; firstly possessing some selective adsorption property, and secondly, to be water compatible. The first of these requirements was realised by incorporating crown ether groups which selectively bind Group I ions. This is discussed in section 3.1.2. The second requirement was achieved by incorporating poly(acrylic acid). This is necessary so as to increase the interaction between the aqueous phase and the adsorption interface. Poly(acrylic acid) is a highly water-soluble polymer containing carboxylic acid side groups. Apart from the water solubility the poly(acrylic acid) has two other major contributions to both the synthesis and overall performance of the copolymer layer:

The monomers can be readily derivatised via simple amide or ester chemistry, the derivatives of which can be included in the polymerisation process. This aids the synthesis and incorporation of the crown ether groups. The carboxylic acid side groups can also facilitate metal ion adsorption by providing added donor sites and charge neutralisation.

The final property of the copolymer not yet discussed is its anchoring to the surface of the QCM resonator. Previous sensors based on crown ether polymer systems use the simple dropping technique to coat the resonator [239][240]. This involves dissolving a known mass of the coating material in a suitable volatile solvent. Applying a small drop of this solution to the surface of the resonator and subsequently evaporating the solvent produces a thin film of the coating material. However, the sensors are of no practical use in liquid applications as the films simply dissolute from the surface. Two approaches were taken to anchor the copolymer coating to the surface of the resonator. The first was to attach the copolymer directly to an amine functional self-assembled monolayer [241] providing a covalent link between the copolymer and the surface of the resonator. The second was to cross-link the copolymer with ethylene-glycol-dimethacrylate, EGDMA. With a high cross-linker percentage present during the polymerisation a solid material is formed. This material is insoluble and is permanently adhered to the QCM surface in a similar fashion to epoxy-resins and other copolymer based glues. The solid resin is porous and water can penetrate the inner network of the copolymer layer allowing the metal cation access to the crown ether rings. This also swells the resin although with the high cross-linker ratio this swelling is expected to be minimal. The choice of cross-linker has a pronounced effect on the porosity, EGDMA was chosen as the cross-linker is a diester and as such aids the water compatibility of the final copolymer resin.

3.1.2 Crown Ether Complexes

Ever since their discovery by Charles Pedersen [242] the ability of the crown ethers to form stable complexes with metal cations has been well documented. The award of the 1987 Nobel Prize in chemistry to Charles Pedersen, Donald Cram and Jean-Marie Lehn emphasises the importance of their work on the crown ethers, binaphthocrown ethers [243][244] and cryptands [245][246] respectively. In the case

of crown ethers the stability of such complexes varies with the size of the crown ether ring and the metal cation involved. At a basic level this variation in complex stability is rationalised by size exclusion and compatibility concepts. These concepts are adequate for a general discussion, however, they are not the only factor involved. The following paragraphs attempt to introduce some of the other factors and place them in context with the crown ether copolymer system employed for the final chemical sensor.

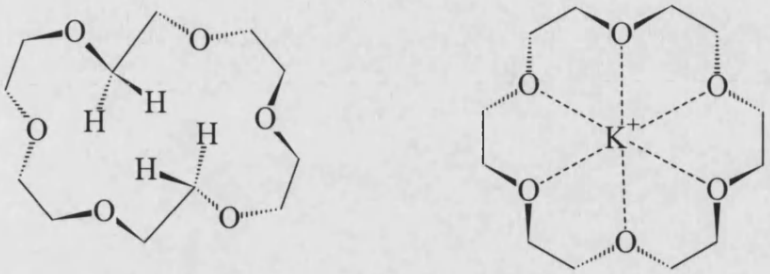

Uncomplexed 18-crown-6 **K^+ Complexed 18-crown-6**

***Figure 3.2**: The conformational shape of complexed and uncomplexed 18-crown-6.*

The basic structure of the free 18-crown-6 ring is a useful starting point to begin this discussion. The ring is in a different conformation to the ring involved in the metal complex. The central 'cavity' occupied by the metal cation represents a destabilising void when unoccupied. This destabilisation is minimised by the inward rotation of two opposite methylene groups, see Figure 3.2. The structural shape of the free crown ether that represents the most energetically favourable configuration is therefore a distorted ring [247].

The complex formed between 18-crown-6 and K^+ is a much more symmetrical structure. The K^+ ion is situated at the centre of the crown ether ring with approximately equal bond lengths to all six oxygen donors, see Figure 3.2. The average $K^+ - O$ bond length is 2.8 Å [247] with the hetroatoms adopting the energetically favourable *gauche* configuration. The structure is difficult to depict in a 2D-diagram but can be imagined with the oxygen atoms in Figure 3.2 alternating between pointing up and pointing down with respect to the plane of the paper. Another aspect of the ring structure, which has a major contribution to the overall complex stability, is the co-ordination number of the metal cation. In this case the

central K^+ is in its preferred site, hexa co-ordinate, however, this is not always the case.

The ability of the crown ethers to form stabile complexes with the Group I cations is not related to size compatibility alone, 12-crown-4 can complex Na^+ and 30-crown-10 can complex K^+. These clearly do not represent ideal ion-cavity size ratios. However the Na^+ complex of 12-crown-4 is not a simple 1:1 structure but a sandwich type structure with a stoichiometric ratio of crown ether to Na^+ of 2:1. This stoichiometry is induced not only by the size difference between the ring and the ion but also by the co-ordination requirements of the Na^+ cation. The 12-crown-4 ring can only provide 4 donor groups and Na^+ prefers a solvation number of six. A similar 2:1 structure exists between 15-crown-5 and K^+ for the same reasons; the 15-crown-5 ring can only provide five donor groups not enough to stabilise the K^+ cation. The donor group stabilises the metal cation by donating electron density. The closer they are to the cation the stronger their electron donation and the greater their stabilising effect. The stable complex formed between 15-crown-5 and Na^+, and 18-crown-6 and K^+, is a trade-off between preferred co-ordination number and M^+-O bond lengths. With the 18-crown-6 Na^+ complex the co-ordination number of Na^+ is satisfied but the Na^+-O bond lengths enforced by the crown ether ring are too great to stabilise the Na^+ cation. For the crown ether metal cation complex where the metal cation occupies the central cavity the bond lengths are fixed to those available by conformational changes in the crown ether ring. For example the cavity size of the 18-crown-6 ring can vary between 2.6 Å and 3.2 Å [248] and so the M^+-O bond lengths must fit within these dimensions. The preferred bond lengths vary for each metal cation and increase with co-ordination number.

If the co-ordination number of the M^+ cation is too low then extra ligands can help stabilise the ion. These extra ligands are often the anion associated with the metal cation but can also come from other sources such water or from structural donors incorporated into the crown ether macrocycle. In the case of the copolymers used the crown ether rings will be in close proximity to –COOH side groups. These form suitable ligands to help complex the Group I cations, stabilising the complex formed with the cations too large to bond entirely within the cavity of the crown ether ring, for example the 15-crown-5 K^+ complex. The ready availability of these extra ligands will render the crown ether rings more susceptible to forming

complexes with metal cations larger than the ring. However cations too small for the ring will still be uncomplexed as these can not gain enough electron donation from the extra ligands to fully stabilise the central ion.

The final contribution to the complex stability discussed here arises from the macrocyclic effect [247]. One of the key factors involving the stability of the crown ether metal cation complex is the preorganisation of the crown ether ring. This can best be imagined by considering the enthalpy and entropy contributions in the complex formation. For six free ligands to come together and form a 3D structure there is an enthalpy and entropy barrier to be overcome. With the pre-organised macrocycle these barriers have already been overcome and the energy contributed to the stability of the overall complex. The close proximity of the crown ether rings to the extra carboxylic acid groups will add to this pre-organisation and again add an extra stabilising effect.

3.2 Synthesis of Crown Ether Monomers

In order to incorporate the crown ether rings into the copolymer network via a covalent linkage the crown ethers themselves must first be derivatised to contain a polymerisable functional group. This section details the chemical synthesis of the crown ether monomers 1 and 2 below. It details their design and intended properties, as well as their structure as determined by a variety of spectroscopic and analytical techniques.

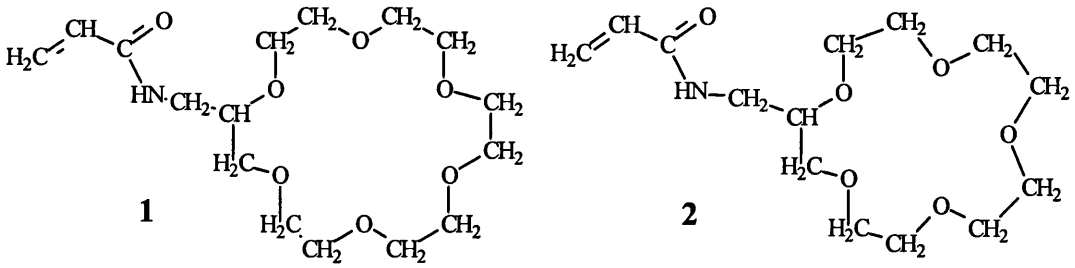

***Figure 3.3**: The crown ether monomers synthesised*

The two monomers utilised can be seen in Figure 3.3 above. They comprise of an arcylamino functional group attached directly to the crown ether ring via a methyl

chain. The vinyl bond in the acrylamino group is open to polymerisation through the standard free radical addition mechanism. This has been confirmed by previous work undertaken by Kimura *et al.* [236] and Yagci *et al.* [249]. See Chapter Two section 2.4.1 for the experimental procedure.

3.2.1 Analysis

The synthesis of the 18-crown-6 monomer was accomplished via a simple coupling reaction between acryloyl chloride and the amine functionalised crown ether as shown in scheme 3.1 below.

Aminomethyl-18-Crown-6 **18-Crown-6 monomer**

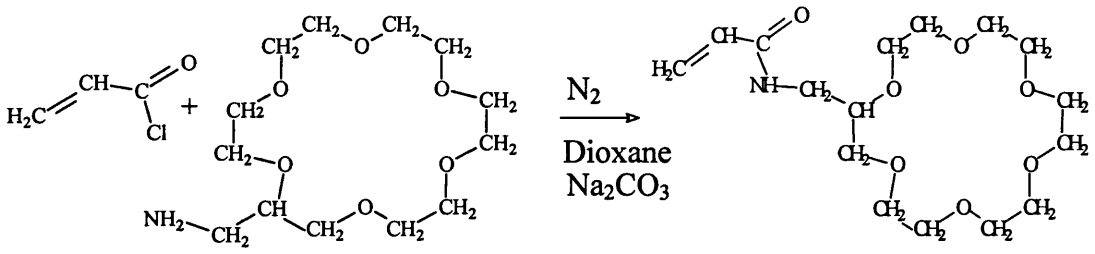

***Scheme 3.1**: The chemical reaction used to form the 18-crown-6 monomer*

The reaction was performed at room temperature and under a nitrogen atmosphere. The total yield of the acrylaminocrown ether was around 96%. The product was not subjected to any further purification and collected simply by vacuum distillation of the reaction mixture. The NMR, Mass Spectrum, FTIR and CHN analysis carried out on the product confirmed its structure and showed it to be that illustrated in Scheme 3.1. They also showed the product to be uncontaminated. The results of the analysis are discussed in the following pages.

^{13}C-NMR

The ^{13}C-NMR of the vinyl crown ether prepared in scheme 3.1 can be seen in Figure 3.4. This shows the presence of all the carbon nuclei at their expected chemical shift (the reference was TMS). The spectrum compares well with the predicted spectrum obtain from the Spec-Info Chemical Database Service, Daresbury Lab.

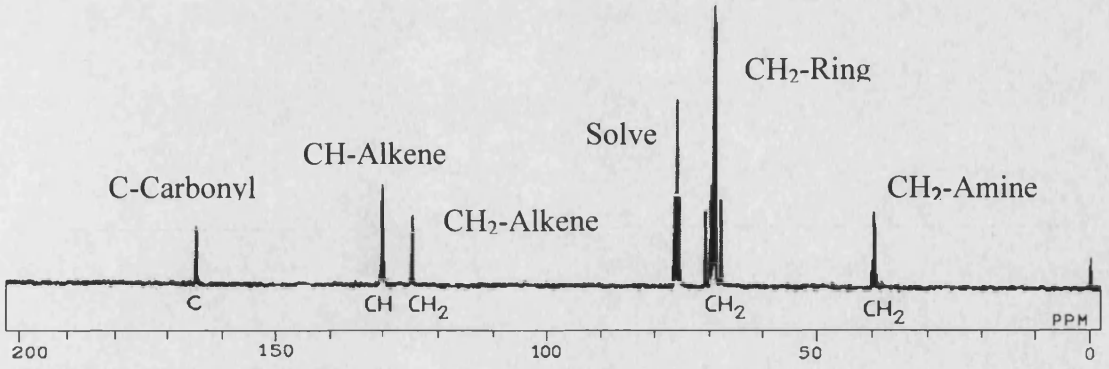

***Figure 3.4**: The ^{13}C-NMR of the 18-crown-6 monomer*

^{1}H-NMR

The ^{1}H-NMR below shows the three alkene protons, H_x at 5.5 ppm, H_a and H_b at 6.2 ppm (where $RH_aC{=}CH_xH_b$). The crown ether ring protons appear between 3.2 ppm and 3.8 ppm as a multiplet unresolved by the spectrometer. The integration ratio for the multiplet and the alkene protons is 2.7:23; this is in good agreement with the expected 3:23 ratio. The alkene protons H_x, H_a and H_b have an integration ratio of 2:1 ($H_a + H_b : H_x$), and coupling constants, J_{xb} =2.6 Hz, J_{xa} =9.7 Hz, J_{ab} =17.0 Hz.

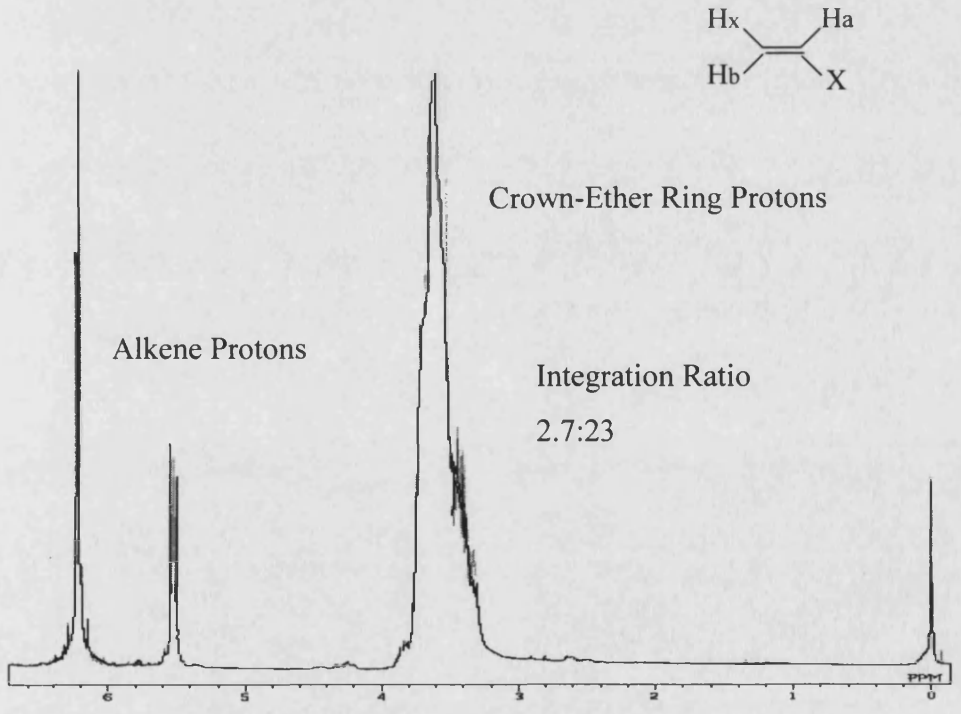

***Figure 3.5**: The ^{1}H-NMR of the 18-crown-6 monomer*

FAB^+ Mass Spectra

Experimental m/z = **348.2** Calculated m/z $(M+H)^+$ = **348.4**

Experimental m/z = **370.2** Calculated m/z $(M+Na)^+$ = **370.2**

The FAB^+ mass spectra showed two dominant peaks. Peak one at m/z 348.2 with 92% intensity and peak two at m/z 370.2 with 99% intensity. There was no significant fragmentation and all other peak appeared below 6% intensity. The peak at m/z 348.2 is attributed to the molecular ion plus a proton, $(M+H)^+$. The peak at m/z 370.2 has been assigned to the ($M+Na^+$) species. The reaction of the crown ether was carried out in the presence of sodium carbonate and so some Na^+ ions will have been extracted into the dioxane phase in the form of the crown ether Na^+ complex.

Elemental Analysis

Calculated 4.0 % **N**, 55.3 % **C**, 8.4 % **H** ⇒ $\mathbf{C}_{16}\mathbf{H}_{29}\mathbf{N}_{1}$

Experimental 3.9 % **N**, 55.2 % **C**, 8.3 % **H** ⇒ $\mathbf{C}_{16.0}\mathbf{H}_{28.9}\mathbf{N}_{1.0}$

The carbon, hydrogen and nitrogen content of the acrylamino-18-crown-6 monomer were identical to the calculated value. The percentages above lead to a C:H:N atomic ratio of $C_{16.0}H_{28.9}N_{1.0}$ compared to the vinyl 18-crown-6 monomer that has a C:H:N atomic ratio of $C_{16}H_{29}N_{1}$.

Infrared Analysis

The infrared (IR) spectrum of the crown ether monomer is consistent with the product's structure and functional groups. Comparison of the IR with that of the reactant, aminomethyl-18-crown-6, confirms the functional group transformations. The large broad peak associated with N-H stretching in the primary NH_2R functional group, (3360 cm^{-1}), reduces in intensity on transformation to the secondary NHRX amide group. The C-N stretching of the primary amine shifts from 944.59 cm^{-1} to

958.93 cm^{-1} in the secondary amide and a C=O stretching peak appears at 1716.48 cm^{-1}. These observations all confirm the transformation of a primary amine to a secondary amide. The reaction is further confirmed by the appearance of a new peak at 1553.38 cm^{-1} assigned to the H_2C=CHCONHR double bond. This is in the expected region for an α,β-unsaturated amide C=C stretching frequency.

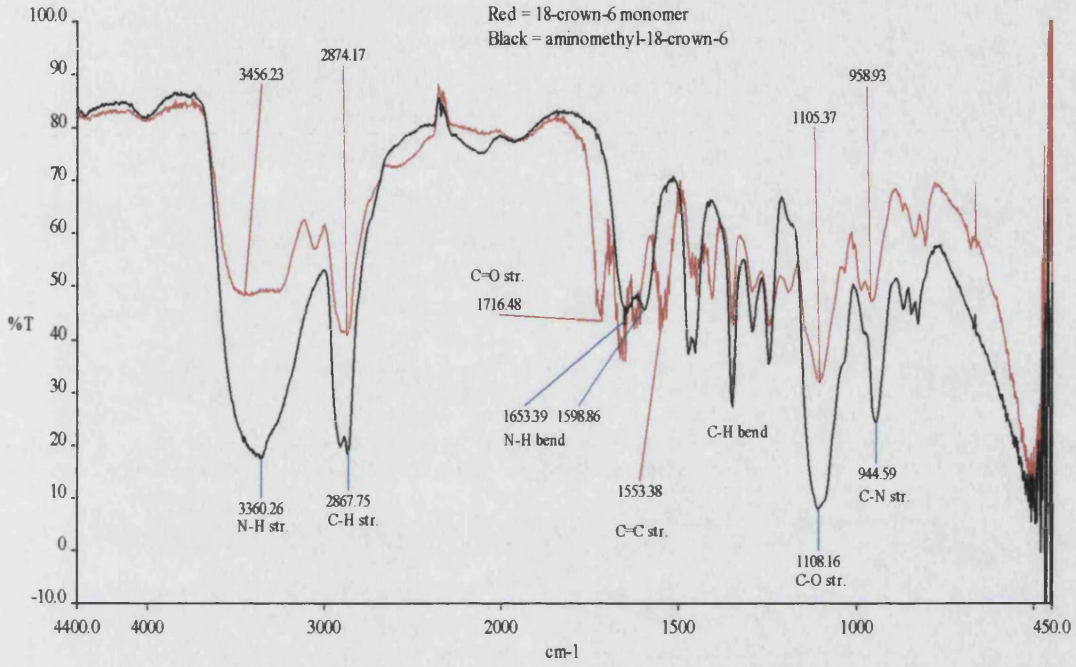

***Figure 3.6**: The FTIR of the 18-crown-6 monomer and the starting material aminomethyl-18-crown-6.*

3.2.2 Conclusion

The analysis performed confirms the structure of the product to be that of the 18-crown-6 monomer depicted in Scheme 3.1. The synthesis is straightforward with a high percentage yield, typically above 90 %. The product must be refrigerated and stored under nitrogen. Under these conditions the monomer has a shelf life of approximately 2 weeks after which time some precipitate is formed that is assumed to be from the autoinitiated polymerisation of the product.

3.3 Absorption Properties of the Copolymer Coating

The crown ether monomers synthesised in the previous section are included in the formation of the copolymer coating and responsible for its inherent adsorption properties. The sensor is dependent on these properties for its overall response and selectivity. For this reason the binding properties of the acrylic acid crown ether copolymers were investigated.

The standard approach to study the binding properties of crown ether systems is to extract the metal ions from the aqueous phase to the organic phase via the crown ether metal ion complex. An alternative method is to monitor the concentration of the crown ether metal complex directly via spectroscopic techniques, usually UV-Vis spectroscopy. Determination of the concentration of this metal ion crown ether complex in the organic phase, and comparison with the concentration of free crown ether leads to the stability constant log K, were K is the equilibrium constant described in equation 22 page 97.

These two systems can not be achieved with the acrylic acid crown ether copolymers employed directly on the sensor as the copolymers are solid resins formed *in situ* on the QCM surface. However, it is possible to synthesise a solid powder of the same composition as the sensor coating. This powder can be used to examine the binding potential of the crown ether acrylic acid copolymer system and a valuable insight into the metal ion binding interactions can be obtained. This is the chosen route to investigate the binding potential of the selective coating.

The resins synthesised were insoluble and so easily separated via decanting the liquid or filtering the solid. They were designed to be hydrophilic in nature and compatible with aqueous phase systems. This maximises the solid-liquid interaction and results in the surface crown ether groups being available to chelate aqueous metal ions. The interaction leads to the binding of the target ions and a concentration drop for these specific metal ions in the bulk solution. From the concentration drop the binding properties of the resins, their uptake and overall selectivity can be compared. This method also allows for the calculation of the selectivity constant for each crown ether system. The concentration drop of the aqueous metal ions could be monitored by atomic emission spectroscopy, AES.

The synthesis of the cross-linked resins has a second major function. Not only can the resins be used to gain an insight into the binding properties of the film but they can also be used to investigate the polymerisation mechanism induced on the surface of the QCM sensor. The nature of the thin film can be related to the bulk properties of the resin, the monomer composition and the nature of the cross-linked network. Secondly the concentration drop of the aqueous metal ions associated with the bulk material compared to that of the sensor film will be much larger. This allows the possibility of monitoring these changes via different mechanisms and obtaining some kinetic data on the binding mechanism. In turn this data can be used to support any data obtained directly from the sensor response.

3.3.1 Experimental

The following resins were synthesised using the experimental procedure described in Chapter Two section 2.4.2.

Resin	% Monomer Mixture		Resin C H N		
	Crown Ether	Cross-linker	%C	%H	%N
15c5/70	10 % 15-5	70 % EGDMA	54.05	6.82	0.46
15c5/30	10 % 15-5	30 % EGDMA	48.35	6.35	0.61
15c5/2	10 % 15-5	2 % EGDMA	46.75	6.07	0.62
18c6/70	10 % 18-6	70 % EGDMA	54.10	6.83	0.52
18c6/30	10 % 18-6	30 % EGDMA	50.25	6.40	0.62
18c6/2	10 % 18-6	2 % EGDMA	49.10	6.33	0.54
EG/70	00 % crown ether	70 % EGDMA	54.97	7.14	0.08

***Table 3.1**: The composition of the cross-linked resins synthesised. All percentages are based on w/w values. The monomer mixture was made up to 100 % with acrylic acid. The CHN data is that obtained experimentally from the final resins.*

3.3.2 Analysis of the Resin

For each sample the recovered resin was in the form of a white powder, all seven of the resins looked visually similar. After filtering, washing and drying the percentage yield based on the mass of the monomers used was typically between 84 % and 99 %. Also, no unreacted crown ether monomer could be recovered from the reaction mixture.

The SEM data was obtained for the three 70 % EGDMA samples, resins 15c5/70, 18C6/70 and the blank resin EG/70. They showed the resins to comprise of spheres approximately 300 nm to 1000 nm in diameter. Resin EG/70 was the most monodispersed sample with spheres evenly distributed between 0.38 μm and 0.45 μm a few larger spheres were found up to 0.67 μm. This narrow size distribution led to evenly packed spheres forming compact macroscopic particles, see Figure 3.7. The two crown ether containing resins were more polydisperse. Resin 15c5/70 consisted of particles mainly in the range 0.26 μm to 0.57 μm but with some larger particles present in the range 1.19 μm to 1.33 μm. Resin 18c6/70 consisted of particles in the range 0.23 μm to 0.66 μm but no larger spheres. Their larger size distribution led to less compact macroscopic particles with a more globular shape compared to the angular structures of the blank resin particles.

The DSC studies were conducted on resin 18c6/70. The primary objective of this was to simply investigate the composition of the recovered powder. The percentage yield for the polymerisation based on the concentration of monomers indicated that >90% of the monomers were incorporated into the growing network. Using DSC it is possible to establish that the resin consists of a single cross-linked network rather than an agglomeration of individual polymer chains. This is an important issue as the stability of the resin and their chelating properties depend on their composition. If any of the components are free to migrate compositional changes may occur within the network, also components can be leached out on exposure to particular solvents. These compositional changes may have a detrimental effect on the chelating potential of the resin and the overall sensor response. The DSC trace showed no evidence of glass transitions or any other phase transition within the temperature range of –10 °C to 200 °C. This is consistent with

the view that the resins comprise of a single cross-linked copolymer network. See Appendix 1 for the DSC trace and FTIR spectra of the resin 18c6/70.

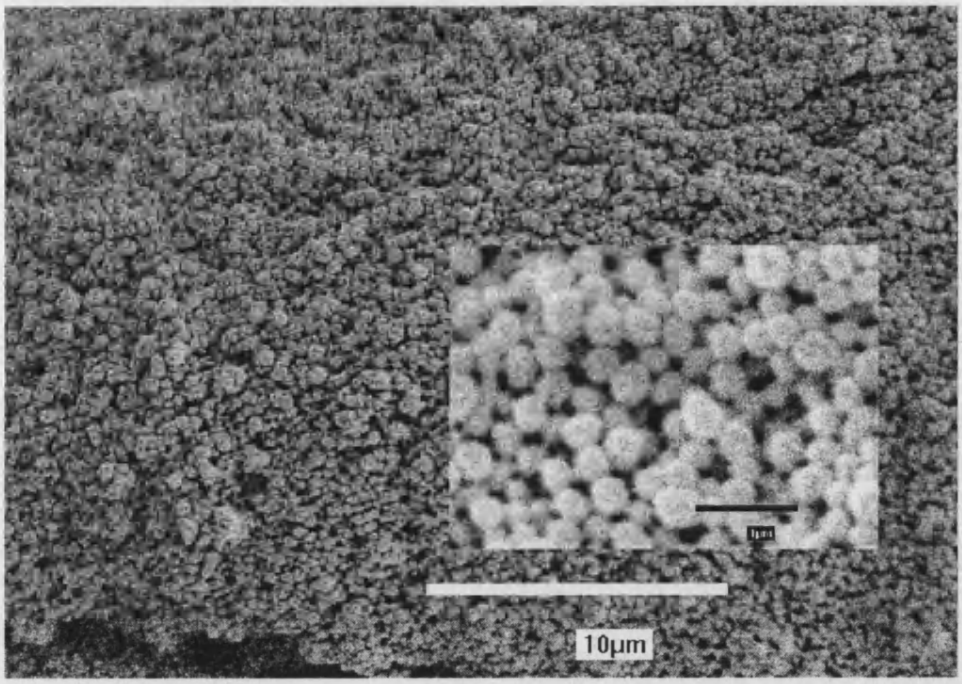

***Figure 3.7**: SEM images of resin* EG/70, *the black bar in the smaller inset picture represents 1 µm.*

Crown Ether Content

The percentage crown ether in each resin was estimated from their CHN elemental analysis. The nitrogen content of the resins can be directly associated with the crown ether content of the resin as the acrylaminomethylcrown ether monomers are the only major source. A second minor source of nitrogen arises from the initiator AIBN. This contributes the NC-C(Me)$_2$- group to the copolymer network. The initiator is normally assumed to have a negligible contribution to the nitrogen content of the copolymer as this is only present in trace amounts, less than 1%. However, the blank resin EG/70 was shown from its CHN to have nitrogen present. This indicates that the initiator contributes an appreciable nitrogen response. The content in resin EG/70 was therefore taken as a measure of the uncertainties in the CHN analysis and the contribution to the overall nitrogen content due to the initiator AIBN. This value was subtracted from the other readings prior to any calculation of

the percentage crown ether. The error in the crown ether content was estimated at ± 2 %. This was calculated from the theoretical nitrogen content with 100 % monomer conversion both neglecting the AIBN contribution and including it in the calculation.

Resin	% Yield	% Crown Ether
15c5/70	84 %	8.12 %
15c5/30	99 %	11.36 %
15c5/2	82 %	13.31 %
18c6/70	74 %	10.78 %
18c6/30	69 %	13.38 %
18c6/2	83 %	11.40 %
EG/70	94 %	Not Applicable

***Table 3.2**: The percentage yield from the polymerisation and the crown ether content of the resins. All values are weight percent. The error associated with the crown ether content is estimated at ± 2 %*

3.3.3 Conclusion

The experimental procedure describing the synthesis of the crown ether resins produces a highly cross-linked copolymer network. This network contains all three of the monomers. No information was obtained on the spatial distribution of the individual monomers within the network, however, this is assumed to take a random statistical form with an even distribution. The appearance and macroscopic structure of the resins are that of a white powder consisting of spheres approximately 300 nm to 1000 nm in diameter. The crown ether content calculated from the CHN elemental analysis varied from around 8 % w/w to 13 % w/w

3.4 Uptake Experiments

As discussed earlier the change in concentration associated with the aqueous metal ions solutions were used to investigate the uptake properties of the resins. The experimental procedure involved placing a known mass of the specific resin into a volumetric flask containing the aqueous solution. The concentrations of the aqueous metal ions were determined both before and after the addition of the resin by atomic emission spectroscopy, AES.

The initial investigations involved the chelating potential of the resins towards the different Group I ions $Na^{+}_{(aq)}$, $Li^{+}_{(aq)}$ and $K^{+}_{(aq)}$. Further investigations concentrated on the variation of the metal ion resin ratio. This allowed for the determination of the number of crown ether rings within the copolymer that are accessible to the metal ions and the equilibrium constant for the metal ion crown ether complex. A second investigation looked at the uptake of several 2+ metal cations, namely $Co^{2+}_{(aq)}$, $Ni^{2+}_{(aq)}$, $Zn^{2+}_{(aq)}$ and $Ca^{2+}_{(aq)}$. For the experimental detail see section 2.5.

3.4.1 Results and Discussion

The tables of results are listed in Appendix 2 and the uptake values plotted in Figure 3.8. It is clear that all of the resins absorbed $K^{+}_{(aq)}$ as the concentration fell by more than 6 ppm g^{-1}. The $Na^{+}_{(aq)}$ and $Li^{+}_{(aq)}$ concentrations fell by a lower extent, typically below 2 ppm g^{-1}. This larger fall in the $K^{+}_{(aq)}$ concentration is expected as K has an atomic mass of 39.1 compared to Na and Li with atomic masses of 22.9 and 6.9 respectively. As 1 ppm is equivalent to 1 $\mu g\ cm^{-3}$ any uptake measured in ppm will be five and a half times larger for $K^{+}_{(aq)}$ than $Li^{+}_{(aq)}$. Since the crown ether rings chelate the ions in a 1:1 ratio (2:1 in the case of 15-crown-5 to K^{+}) the results should be represented in terms of a molar uptake, $molg^{-1}$.

Uptake of the 18-crown-6 Copolymers

Figure 3.10 shows the molar uptake of the resins with respect to $Li^{+}_{(aq)}$, $Na^{+}_{(aq)}$ and $K^{+}_{(aq)}$. It can be seen that the resins containing 18-crown-6, i.e. resins D, E and F have an uptake of about 25 μmoles of $K^{+}_{(aq)}$ ions per gram of copolymer and a high degree of selectivity for $K^{+}_{(aq)}$ over the other two ions. These observations can be attributed to the crown ether ring. 18-Crown-6 has a ring diameter of 2.6-3.2 Å [247]

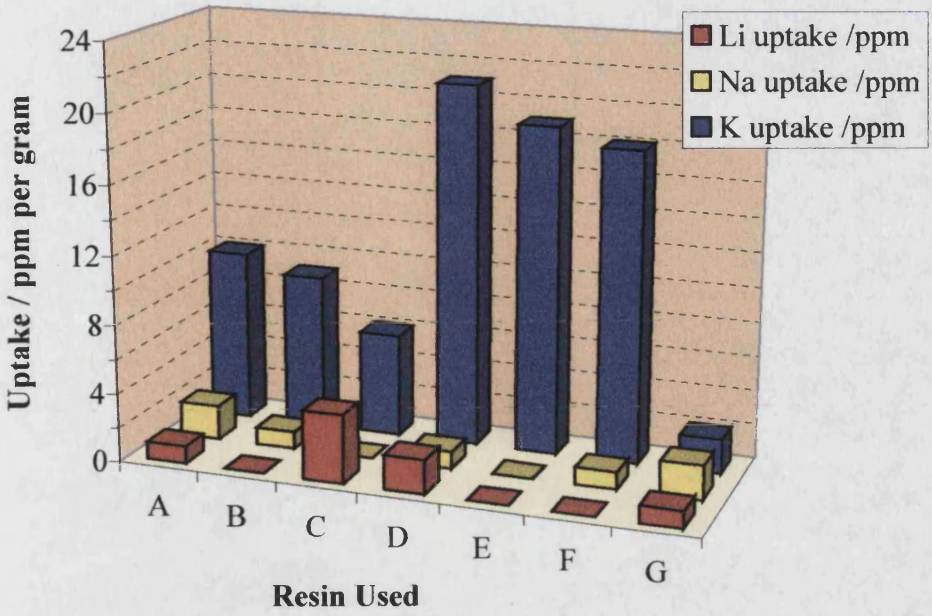

***Figure 3.8**: The uptake of aqueous metal ions by the resins synthesised.*

A=15c5/70 B=15c5/30 C=15c5/2 D=18c6/70 E=18c6/30 F=18c6/2 G=EG/70

Only one metal ion was present in each run. The experimental procedure involved a 50 cm^3 volume of a 50 ppm stock solution and 1 g of resin.

and K^+ a diameter of 2.7 Å [247]. Because of this size comparability the K^+ ions bind strongly to the crown ether ring and they are retained in the copolymer network. Na^+ by comparison has a diameter of 1.9 Å [247] and Li^+ a diameter of 1.2 Å [247], therefore these ions are not held as strongly by the crown ether groups and remain mobile passing in and out of the copolymer network and the solvent. The stability constants, $\log_{10}K$ (see equation 26 on page 98), for the 18-crown-6-metal ion complex in water are 0.8 and 2.03 for $Na^+_{(aq)}$ and $K^+_{(aq)}$ respectively [247]. The value calculated for $\log_{10}K$ for the 18-crown-6 $K^+_{(aq)}$ complex in the copolymer is 3.20 (see section 3.5.2). The data indicates that the copolymer resin has an increased affinity for $K^+_{(aq)}$ as compared to the free crown ether compounds.

The uptake of $Li^+_{(aq)}$ by the copolymer appears to be approximately half that of the $K^+_{(aq)}$ uptake for resin D and zero for resins E and F. This large fluctuation in values is associated with the mass of the metal. Li^+ is five and a half times lighter than K^+ consequently when the data is transformed from a mass change to a molar

change a large experimental error is introduced; the readings are either 0 or 7 μmolg^{-1}. For this reason the molar uptakes of Li^+ shall be treated with great care and used only as an indication of any trend.

The calculated K^+ / Na^+ selectivity based on the molar uptakes for the 18-crown-6 containing resins are 18c6/70=13.01, 18c6/30=13.01 18c6/2=13.76. For comparison the selectivity for the blank resin EG/70=2.14.

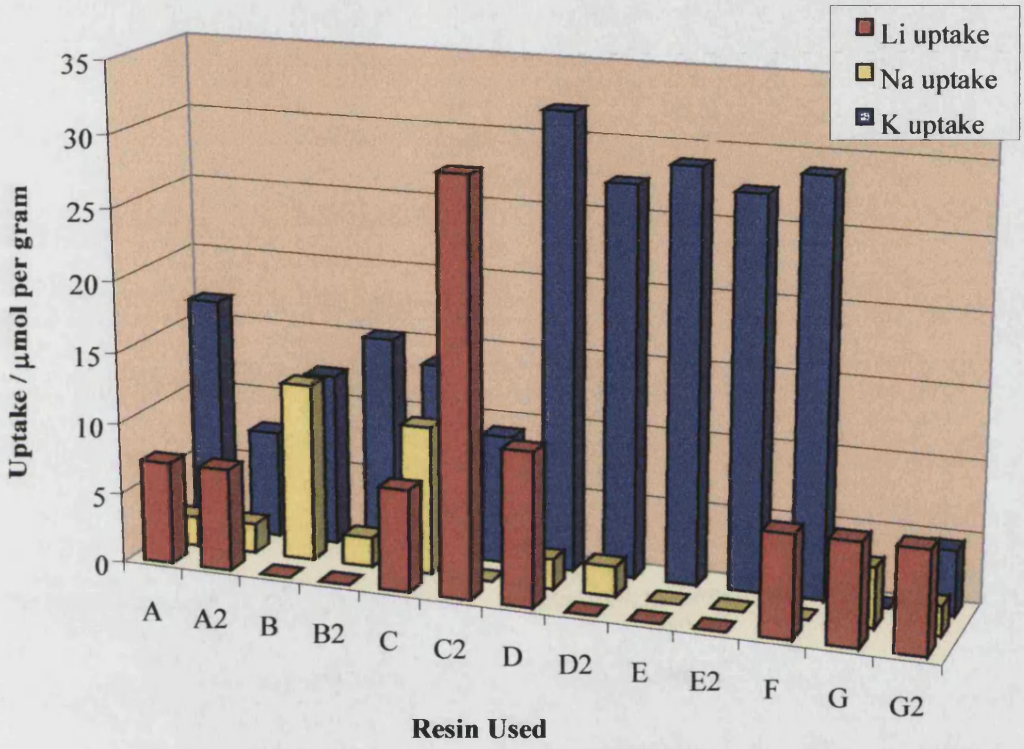

***Figure 3.9**: The results of all the uptake experiments.*

A=15c5/70 B=15c5/30 C=15c5/2 D=18c6/70 E=18c6/30 F=18c6/2 G=EG/70

Resins marked with a 2 indicate that all three metal ion were present in each stock. Other resins used separate stock solutions. The experimental procedure involved a 50 cm^3 volume of a 50 ppm stock solution and 1 g of resin.

Uptake of the 15-Crown-5 Copolymers

The resins containing 15-crown-5 have a much lower uptake of $K^+_{(aq)}$ compared with the equivalent 18-crown-6 resin, 34-50% lower, and a much larger $Na^+_{(aq)}$ uptake. This is as expected. The cavity size of the 15-crown-5 ring is 1.7-2.2 Å, too small for

the $K^+_{(aq)}$ ion to form a strong stable complex. The free 15-crown-5 compound forms a 2:1 crown ether-metal ion complex with $K^+_{(aq)}$ ion [247], so the K^+ uptake could be expected to drop by 50%. However, these complex have a stability constant in water of 0.74 compared to the 18-crown-6 K^+ stability constant of 2.03 [248], this would lower the expected uptake to below 50 %. The Na^+ ion has an ionic radius of 0.8 Å [248], comparable to the 15-crown-5 cavity diameter of 1.7-2.2 Å. This leads to an increase in the $Na^+_{(aq)}$ uptake of the resin from 2.5 μmoles per gram in the case of the 18-crown-6 resins, to more than 10 μmoles per gram for resins B and C.

The calculated K^+ / Na^+ selectivity based on the molar uptakes for the 15-crown-5 containing resins are 15c5/70=3.62, 15c5/30=7.23 15c5/2=4.33.

The blank copolymer

Looking at the blank resins G, it can be seen that they have only limited uptake ability (below 3 μmol per gram) and no selectivity. The acrylic-acid EGDMA copolymer is not capable of chelating the metal ions and so there is only a very small drop in the concentrations of the ions in the solution presumably from non-specific ion exchange. These two blank resins enable us to estimate the experimental uncertainty of ± 1 ppm in the concentration changes. This is in good agreement with the values obtained for the concentration readings of the same sample over an extended period of time. As discussed previously, this estimation when converted to an error in the mole changes reveals a large uncertainty in the uptake of Li^+ ions.

The calculated K^+ / Na^+ selectivity based on the molar uptake of the blank resin EG/70=2.14.

The Competitive Uptake Studies

In order to study the selective uptake of each resin it is necessary to have both $Na^+_{(aq)}$ and $K^+_{(aq)}$ ions present in the same solvent. Although it is possible for each resin to uptake both metal ions it is more important for the resins to selectively uptake one of the metals when both metal ions are present in the same solution. Figure 3.10 shows the results. Resins B and C were placed separately into solutions of 50 ppm $Na^+_{(aq)}$ and 50 ppm $K^+_{(aq)}$, while resins B2 and C2 were placed in solutions containing both

C uptake $Na^{+}_{(aq)}$ and $K^{+}_{(aq)}$ in equal amounts, however, when both $Na^{+}_{(aq)}$ and $K^{+}_{(aq)}$ are available for chelating only $K^{+}_{(aq)}$ is taken up. This reveals the selectivity of the resins for $K^{+}_{(aq)}$ over $Na^{+}_{(aq)}$.

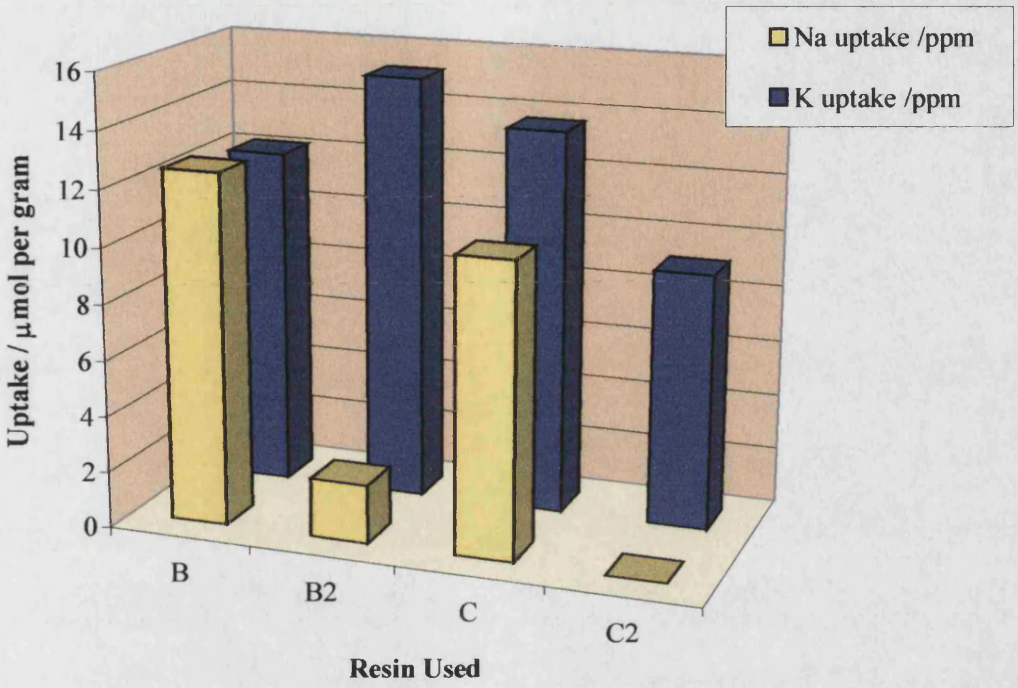

***Figure 3.10**: Highlighting the difference between the competitive and non-competitive uptake of the resins. Resins B=15c5/30 C=15c5/2. Runs B and C were conducted with separate metal-ion stock solutions and runs B2 and C2 used a stock solution containing all three of the metal ions.*

3.4.2 Uptake Kinetics

The result of the kinetics experiment can be seen in Figure 3.12. The data indicate that 90 % of the total metal ion uptake by resin 18c6/70 (D) is completed within the first 2 minutes of contact. The expected time scale for the uptake mechanism was in the order of hours and days rather than seconds, so the experimental procedure used to follow the reaction is not considered adequate for such a rate.

The kinetics of the binding processes were investigated by recording the concentration change associated with the addition of the resins to the stock solutions as a function of time. This was achieved by filtering a sample of the resin-stock mixture after a given time interval, effectively separating the copolymer and metal ions after a certain contact time. There were several difficulties with the procedure.

Firstly the powdered resin in the dry state required approximately twelve hours to fully immerse in an aqueous solution. On initial contact the powder appeared to be hydrophobic and simply float on the solution in a similar fashion to that of powdered poly(styrene). After a short time particles of the resin would begin to sink until eventually all the resin had fully immersed in the solution. These observations were presumed to be due to the slow incorporation of water into the porous network of the copolymers. As the water is drawn into the network the density of the particles increases until they eventually sink. The time scale of this process is such that without pre-soaking the resins in clean water any uptake of the metal ions can not be measured for the first twelve hours of exposure. Secondly and more importantly the removal of samples of the stock solution and resin from the total mixture will alter the crown ether metal ion ratio and change the equilibrium conditions. However no alternative method could be perceived and the procedure followed was considered suitable for an initial investigation of the time scale involved in the adsorption process.

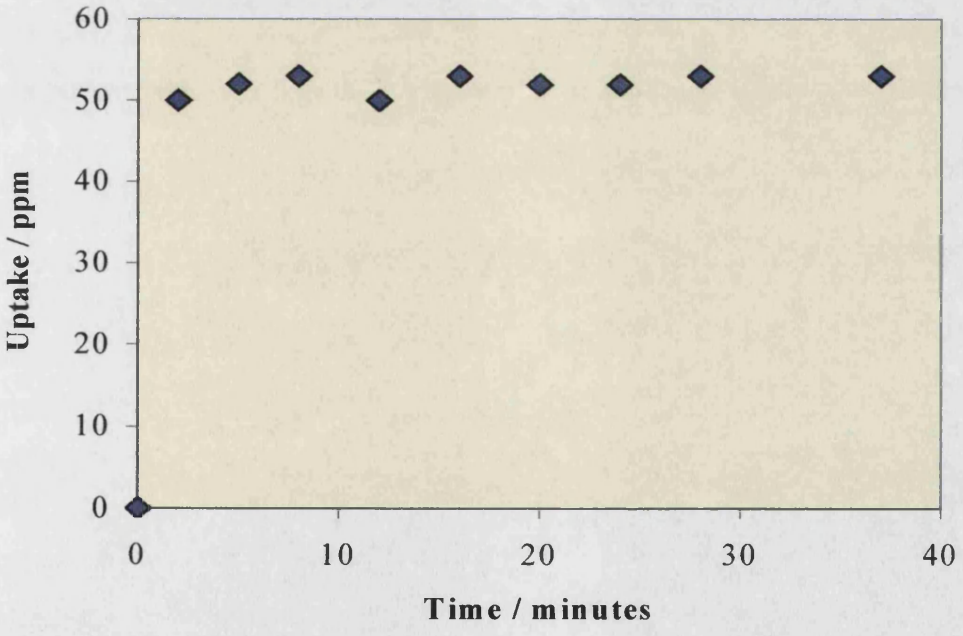

***Figure 3.11**: The results of the kinetic uptake experiment. The data refers to the uptake of $K^{+}_{(aq)}$ by 1.343 g of resin 18c6/70 in a 70 ppm stock solution.*

3.4.3 Initial Conclusion

Overall the resins behave as expected. The 18-crown-6 resins, D, E and F, uptake about 25 $\mu molg^{-1}$ of $K^+_{(aq)}$ and only trace amounts of $Na^+_{(aq)}$ or $Li^+_{(aq)}$, less than 3 $\mu molg^{-1}$. The percentage of cross-linker has very little effect, although the high cross-linker ratios do tend to have a slightly increased uptake of about 10 %. The 15-crown-5 resins, A, B and C, uptake Na^+ and K^+ equally, around 11 $\mu molg^{-1}$ but selectively bind $K^+_{(aq)}$ over $Na^+_{(aq)}$ when both ions are in the same solution. In the case of resins A, B and C the % cross-linker appears to have a slight effect. The 70% EGDMA resin, A, has a 60% drop in $Na^+_{(aq)}$ uptake compared to the 30% EGDMA, resin B, and the 2% EGDMA, resin C. This may be due to the smaller Na^+ ion penetrating deeper into the resins with low cross-linker ratios and so increasing the availability of binding sites. The $K^+_{(aq)}$ uptake is constant for all three of the resins suggesting that the larger $K^+_{(aq)}$ ion binds at sites around the surface of the resin particles and has limited penetration into the inner copolymer network.

The data collected shows that the resins successfully chelate $Na^+_{(aq)}$ and $K^+_{(aq)}$ and that the 18-crown-6 or 15-crown-5 moieties impart a high degree of selectivity to the copolymers. They also show that the percentage cross-linker has only a minor effect on the uptake abilities.

3.5 Further Investigation

The graph in Figure 3.12 shows the uptake of $Li^+_{(aq)}$, $Na^+_{(aq)}$, and $K^+_{(aq)}$ for resin 18c6/70 as a function of the mass of the resin. The results confirm the selectivity towards $K^+_{(aq)}$ over the other Group I ions, $Li^+_{(aq)}$ and $Na^+_{(aq)}$. These ions showed no uptake by the resin. The uptake was a competitive process with $Li^+_{(aq)}$, $Na^+_{(aq)}$ and $K^+_{(aq)}$ present in the same stock solution. These data confirms the conclusions discussed previously, that the resin selectively binds $K^+_{(aq)}$ in the presence of $Li^+_{(aq)}$ and $Na^+_{(aq)}$. The resin was washed and recycled after each run. This cleaning was performed by simply washing the resin in a Soxhlet thimble with warm Milli-Q_{plus} 185, 18.2 MΩ cm water. Previous experiments had confirmed that this washing procedure fully recharged the resin ready for another uptake run. EDTA was also

employed in the washing rinse, however, this was found to be unnecessary as no discernible difference could be observed between the uptake of the resin rinsed with EDTA solution or that rinsed with pure water.

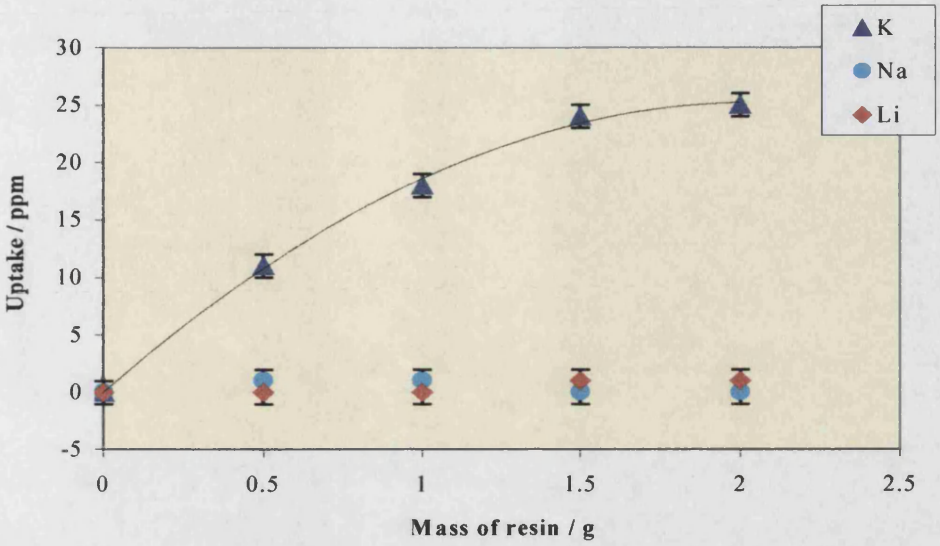

***Figure 3.12**: The competitive uptake of Resin 18c6/70 as a function of the mass of the resin. The concentration of the metal stock solution was 50 ppm, the precise values can be seen in Table A2.4, Appendix 2. Uptake values were recorded after 24 hours of exposure.*

The uptake of 0.5 g of resin 18c6/70 as a function of metal ion concentration can be seen in Figure 3.13. The profile of the curve associated with the uptake of $K^+_{(aq)}$ indicates that the adsorption of the ions by the resin is an equilibrium characterised by the concentration ratio of the $K^+_{(aq)}$ and resin used. The theoretical prediction plotted on the graph was calculated by applying a Langmuir type isotherm to the adsorption mechanism. The derivation of this isotherm is discussed in the following section. Values can be calculated from the model for the equilibrium constant involved and the total number of binding sites available to the $K^+_{(aq)}$. This later value can be related directly to the percentage of the crown ether groups available at the surface of the resin.

The data relating to similar experiments with resin 15c5/70 can be seen in Figures 3.14 and 3.15. They show similar trends as those observed for resin 18c6/70 but with a much lower uptake of the metal ions. The phenomenon of the 15-crown-5 resin chelating $K^+_{(aq)}$ to a larger degree than $Na^+_{(aq)}$ is once again observed. The results confirm that this is not an experimental error and that the resin does indeed have a preference to absorb $K^+_{(aq)}$ over both $Na^+_{(aq)}$ and $Li^+_{(aq)}$. The two extra points

in the $K^{+}_{(aq)}$ plot, the white triangles, are estimates (taken from Table A2.4) on the values expected in this region from other experiments. These are included as there was some doubt over the validity of the points obtained from the 150 ppm and 200 ppm stock solutions.

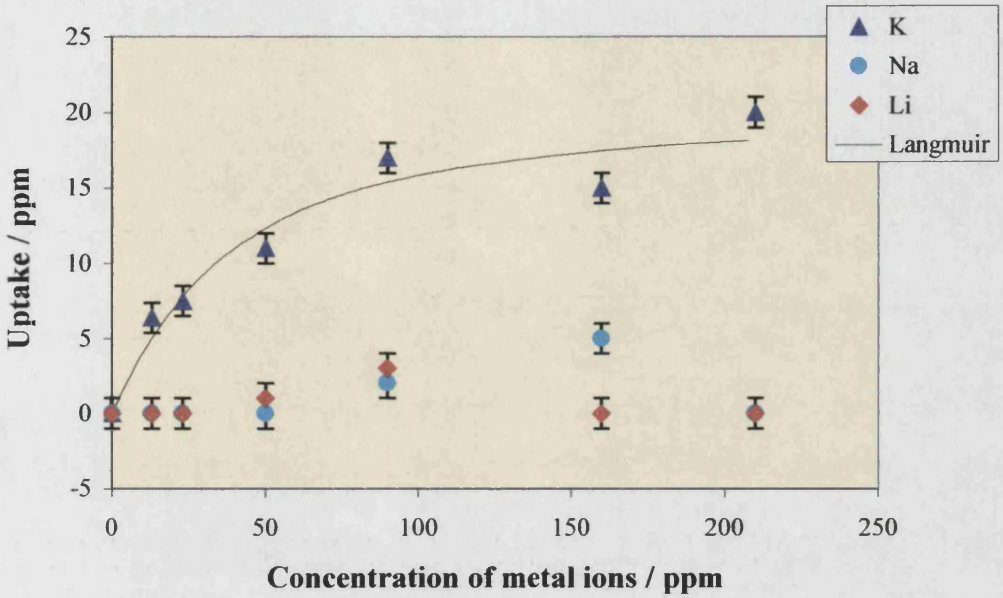

***Figure 3.13**: The uptake of 0.5 g of resin 18c6/70 in various concentrations of metal ion stock solution. Uptake values were recorded after 24 hours of exposure. The data was taken from Table A2.3.*

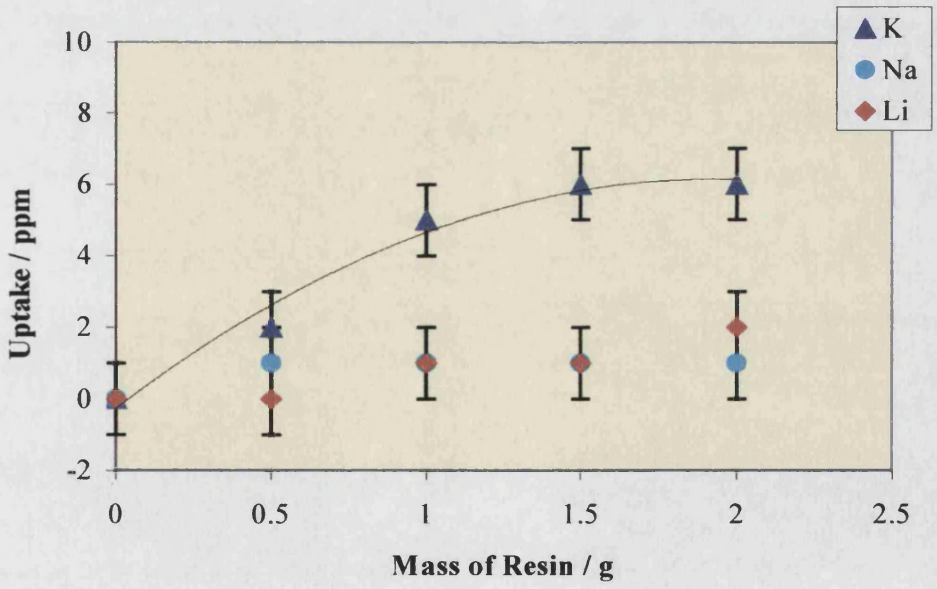

***Figure 3.14**: The uptake of Resin* 15c5/70 *as a function of the mass of the resin. The concentration of the metal stock solution was around 50 ppm, the precise values can be seen in Table A2.4.*

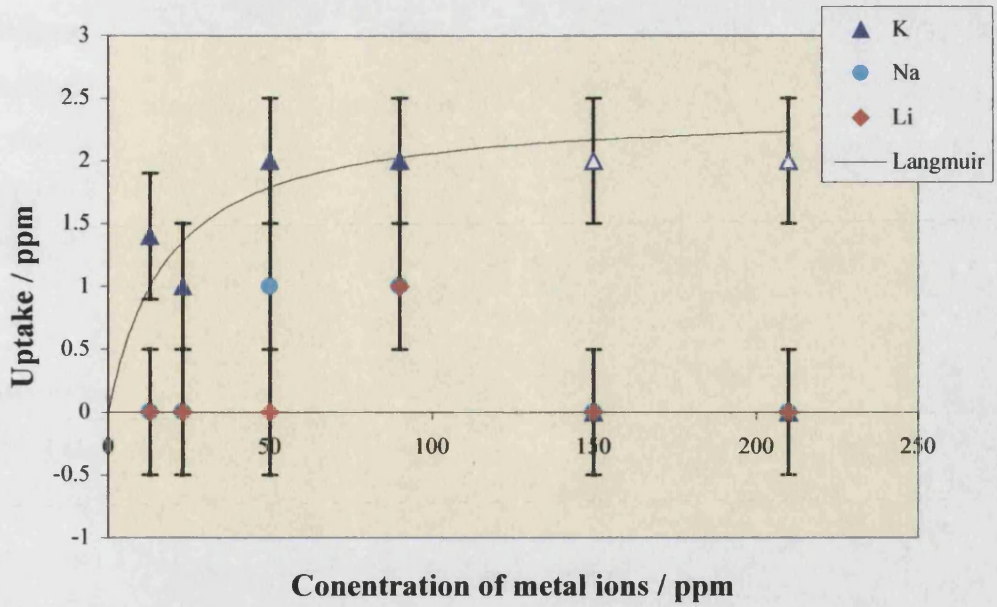

***Figure 3.15**: The uptake of 0.5 g of resin 15c5/70 in various concentrations of metal ion stock solution. The data was taken from Table A2.3. The two extra points were values estimated from previous experiments taken from Table A2.4. Uptake values were recorded after 24 hours of exposure.*

3.5.1 Langmuir Isotherm

From the data collected it is possible to obtain information on the availability of the crown ether groups within the copolymer network. It is also possible to calculate a value for the equilibrium constant, K, for the formation of the complex between the metal ions and the crown ether rings. This is achieved by applying a Langmuir type adsorption profile.

The uptake of the metal ions by the crown ether resins can be equated to the surface adsorption of molecules at solid-fluid interfaces. The crown ether groups at the solid surface provide the binding sites for the ions that adsorb from the solution. The Langmuir isotherm [250] and the assumptions made during its derivation are ideally suited to the adsorption mechanism involved in this system. The isotherm assumes that every adsorption site is equivalent and that the ability of a species to bind is independent of any occupancy of a surrounding site. In the system used the binding sites are the crown ether rings so all binding sites can be assumed to be equivalent. Also the interaction of a crown ether group with a metal ion will be

independent of the chemical state of any neighbouring crown ether group so all the binding sites are independent of the occupancy of a surrounding site. The Langmuir isotherm can be derived in several way, however the derivation that applies most suitably to the surface reactions involved here can be obtained from the application of simple equilibrium theory.

The following section derives the Langmuir based absorption profile from basic principles and applies the theory developed to the surface interaction of the crown ether groups with the aqueous metal ions. Values are calculated from the data for the equilibrium constant K and the total number of binding sites L_t available. L_t is then related to the crown ether content and compared to the values obtained from other sources such as CHN elemental analysis.

3.5.2 Derivation of the Langmuir Isotherm

The Langmuir isotherm is applied to the adsorption of gases at solid surfaces. It is assumed that the free gas and the adsorbed gas are in dynamic equilibrium and that the fractional coverage, θ, depends on the pressure of the gas at the surface. The dependence of the fractional coverage on the pressure for a set temperature is described by the adsorption isotherm. In our system the binding of the metal ions by the crown ether groups is assumed to be in a similar dynamic equilibrium. The number of crown ether metal ion complexes compared to the number of free crown ether groups i.e. the fractional coverage θ, is dependent on the concentration of the metal ions in the solution and the total available crown ether groups.

The dynamic equilibrium is described by the following equation;

$$[L_{(s)}] + [M^{+}_{(aq)}] \underset{k_d}{\overset{k_a}{\rightleftharpoons}} [LM^{+}_{(s)}] \qquad (22)$$

Where $[L_{(s)}]$ is the concentration of the uncomplexed crown ether rings, $[M^{+}_{(aq)}]$ is the concentration of the aqueous metal ions, $[LM^{+}_{(s)}]$ is the concentration of crown ether metal ion complex and k_a and k_d are the rate constants for the adsorption and desorption steps respectively. Because of the difficulty in relating the concentration of the crown ether groups $[L_{(s)}]$ and the concentration of the free metal ions $[M^{+}_{(aq)}]$

these terms are replaced by the total 'amount' present, moles instead of moles per dm^3.

If the total crown ether content is equal to L_t then;

$$[L_t] = [L_{(s)}] + [LM^+_{(s)}] \qquad (23)$$

and the fractional coverage θ equals;

$$\theta = [LM^+_{(s)}] / [L_t] \qquad (24)$$

then by combining equations (23) and (24);

$$\theta / (1-\theta) = [LM^+_{(s)}] / [L_{(s)}] \qquad (25)$$

Since the equilibrium constant K equals;

$$K = [LM^+_{(s)}] / [L_{(s)}][M^+_{(aq)}] \qquad (26)$$

then

$$[LM^+_{(s)}] / [L_{(s)}] = K\,[M^+_{(aq)}] \qquad (27)$$

and so combining equations (25) and (27);

$$\theta / (1-\theta) = K\,[M^+_{(aq)}] \qquad (28)$$

rearranging equation (28) and substituting in equation (24) for θ gives;

$$\frac{K\,[M^+_{(aq)}][LM^+_{(s)}]}{[L_t]} + \frac{[LM^+_{(s)}]}{[L_t]} = K\,[M^+_{(aq)}] \qquad (29)$$

This rearranges to the final useful equation;

$$\frac{[M^+_{(aq)}]}{[L_t]} + \frac{1}{K[L_t]} = \frac{[M^+_{(aq)}]}{[LM^+_{(s)}]} \qquad (30)$$

Hence, plotting $[M^+_{(aq)}] / [LM^+_{(s)}]$ verses $[M^+_{(aq)}]$ will give a straight-line graph of gradient $1 / [L_t]$ and intercept $1 / K\,[L_t]$.

The plot of equation 30 for resin 15c5/70 and 18c6/70 can be seen in Figure 3.16 and 3.17 respectively. The two extra points plotted for resin 15c5/70 were estimated from previous experiments and are only displayed for reference. The points were not included in the calculation of the gradient or intercept. From the two graphs the following values were calculated.

Resin	$[L_t]$ / moles	Percentage of Total	K / $dm^3\ mol^{-1}$
15c5/70	$1.947 \times 10^{-6} \pm 0.421 \times 10^{-6}$	2.77	2187.6 ± 866.6
18c6/70	$1.597 \times 10^{-5} \pm 0.186 \times 10^{-5}$	10.14	1554.1 ± 616.9

***Table 3.3**: Values for $[L_t]$ and the equilibrium constant K calculated from equation 30 for the binding of K^+ to the crown ether groups. The percentage of total in column 3 is the percentage of crown ether groups available for binding compared to the total amount included in the resin synthesis.*

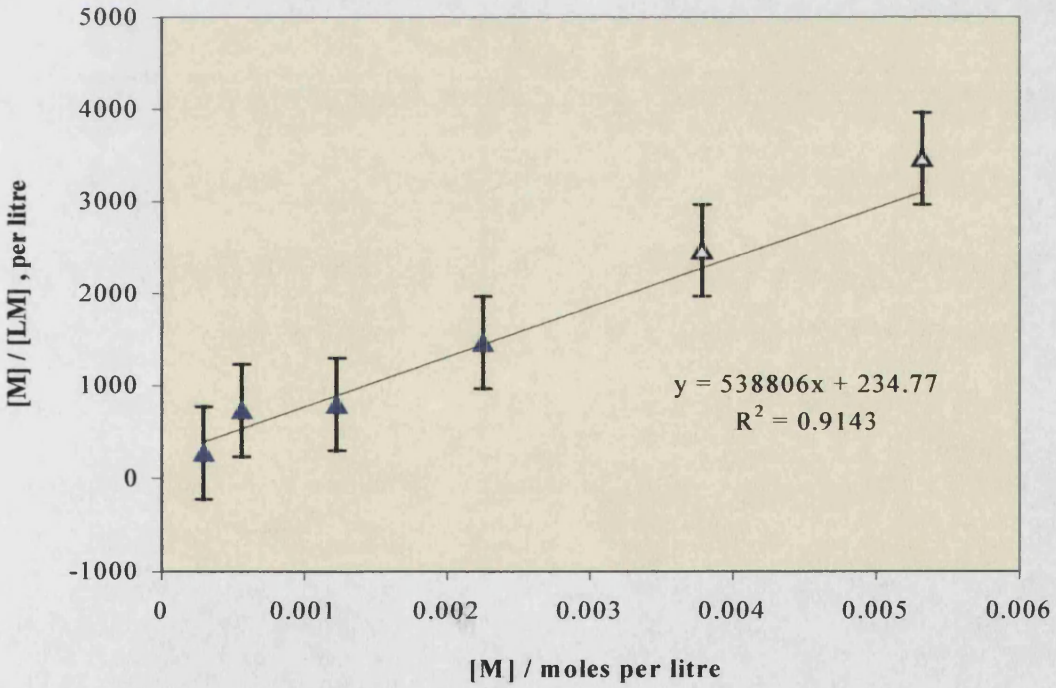

***Figure 3.16**: A plot of equation 30 for the uptake of $K^+_{(aq)}$ by resin 15c5/70. The data is displayed in Table A2.3. The extra two points shown, the light blue triangles, are those values estimated from other experiments and are included purely for reference purposes. The points were not used in the calculation of the gradient or intercept quoted.*

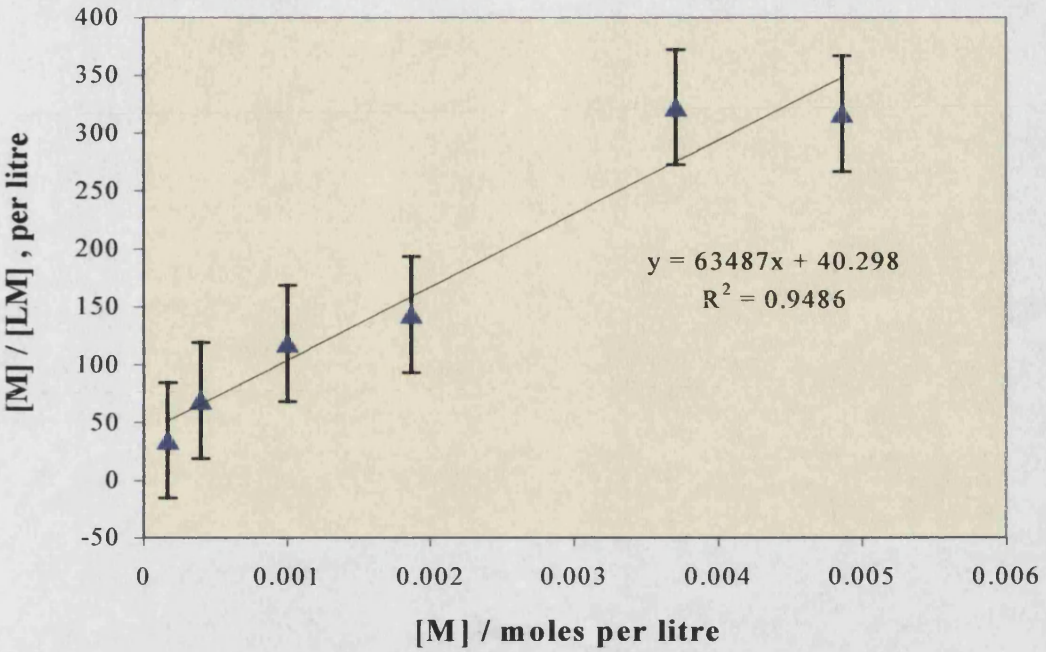

***Figure 3.17**: A plot of equation 30 for the uptake of K by resin 18c6/70. The data used can be seen in Table A2.3.*

The values obtained for the equilibrium constants suggest that the 15-crown-5 copolymer, resin 15c5/70, has binding sites with a greater affinity for $K^+_{(aq)}$ than the equivalent 18-crown-6 copolymer. However, the values are calculated from the Langmuir isotherm which assumes all binding sites within a sample are equal. This is not necessarily the case, as the surface binding sites will vary considerably in their chemical environment, accessibility and surface distribution. From the calculated values it can be concluded that the binding sites available to $K^+_{(aq)}$ in resin 15c5/70 are on average of greater affinity than those available in resin 18c6/70. However, the sites in resin 15c5/70 are present in a much lower concentration as shown by the $[L_t]$ values. These sites may simply exist as a result of the random formation of sites with abnormally high $K^+_{(aq)}$ affinity, for example the close proximity of two 15-crown-5 rings capable of mutually binding $K^+_{(aq)}$ in a 2:1 ratio. Sites with an equally high affinity for $K^+_{(aq)}$ could exist in the 18-crown-6 resin, however the greater distribution of sites with lower affinity reduce the average binding potential. The values of the equilibrium constants are comparable with those quoted for other crown-ether systems [247][248]. Typically values for $\log_{10}K$ are 3.24 and 3.43 in the

case of 15-crown-5 and 4.35 and 6.08 for 18-crown-6 binding $Na^{+}_{(aq)}$ or $K^{+}_{(aq)}$ respectively. The values that were calculated here are 3.34 and 3.19 for the 15-crown-5 and 18-crown-6 copolymers binding $K^{+}_{(aq)}$.

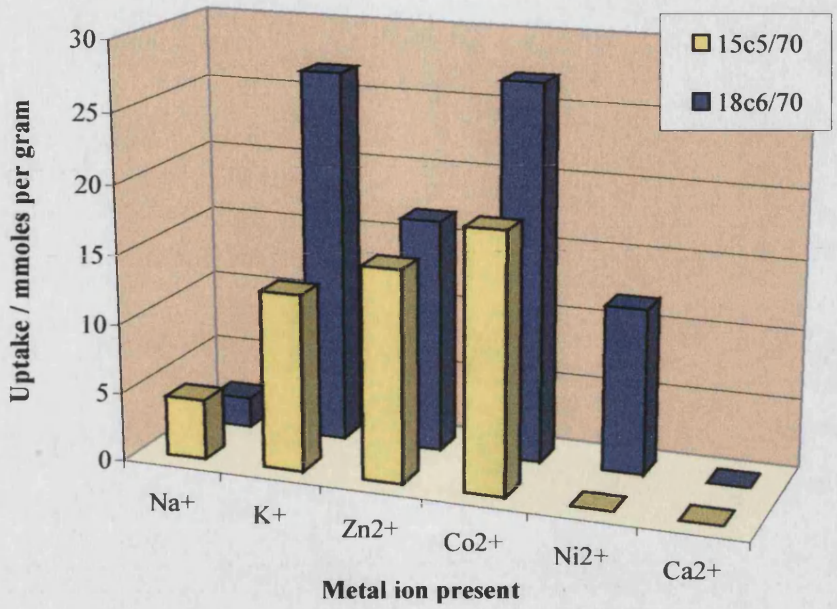

***Figure 3.18**: The uptake of various metal ions by resins 15c5/70 and 18c6/70. The metal ion stock solutions were 50 ppm, with only one ion present. 0.5 g of each resin was used and the uptake values calculated after 24 hours exposure.*

The uptake of the two resins for other metal ions can be seen in Figure 3.19. The results do not correlate with the expected uptake based on the ionic radii of the ions, these can be seen in the table below.

Ion	$Li^{+}_{(aq)}$	$Ni^{2+}_{(aq)}$	$Co^{2+}_{(aq)}$	$Zn^{2+}_{(aq)}$	$Na^{+}_{(aq)}$	$Ca^{2+}_{(aq)}$	$K^{+}_{(aq)}$
r / pm	68	69	72	74	97	99	133

***Table 3.4**: Ionic radii, r, for the metal ions used in uptake studies. The values quoted are for the maximum coordination number of the ion [251].*

Resin 15c5/70 binds the ions in the following order, with the highest uptake first;

$$Co^{2+}_{(aq)} > Zn^{2+}_{(aq)} > K^{+}_{(aq)} > Na^{+}_{(aq)} > Ni^{2+}_{(aq)} = Ca^{2+}_{(aq)}$$

In contrast resin 18c6/70 binds the ions in the following order;

$$K^{+}_{(aq)} = Co^{2+}_{(aq)} > Zn^{2+}_{(aq)} > Ni^{2+}_{(aq)} > Na^{+}_{(aq)} > Ca^{2+}_{(aq)}$$

If the Group I ions are disregarded then the uptake affinity is in the same order for both resins. This is in agreement with the expected result, that the crown ethers have an unusually large complexity constants for the Group I ions [252] compared to other ions. The relative effects of altering the crown ether ring size only influence the order of the uptake of $K^{+}_{(aq)}$, $Na^{+}_{(aq)}$, and $Li^{+}_{(aq)}$. The results suggest that trace amounts of other metal ions may have a pronounced effect on the sensor developed from the copolymer system. This observation warrants further investigation, a more extensive study including a greater distribution of aqueous metal ions. Further work with the uptake of the resins should also included the variation in crown ether content, both increasing and decreasing the crown ether percentage in the final resins. In conclusion, the data collected shows that the resins successfully bind $K^{+}_{(aq)}$. Resin 18c6/70 and the other 18-crown-6 copolymers have a high degree of selectivity for $K^{+}_{(aq)}$ over the other Group I ions with the percentage cross-linker having only a minor effect on the uptake. The synthesis was straightforward and the analysis shows the resin to be a highly cross-linked network with an even distribution of all the components. Overall the copolymers should form an ideal binding interface on the surface of a QCM resonator designed to selectively respond to $K^{+}_{(aq)}$ over $Na^{+}_{(aq)}$ and $Li^{+}_{(aq)}$.

3.6 The $K^{+}_{(aq)}$ Sensor: System One

Following the work described in section 3.4 and 3.5 on the uptake properties of a series of crown ether copolymers a suitable system was selected for coating onto a QCM resonator. The 18-crown-6 copolymer systems provided the highest degree of selectivity for one particular Group I cation, in this case $K^{+}_{(aq)}$. The copolymer displays a high affinity as well as a high degree of selectivity for $K^{+}_{(aq)}$, with a response time of less than 60 seconds. The results of the uptake studies demonstrate the potential of the resins to act as an ion-selective membrane in conjunction with a QCM resonator.

3.6.1 Introduction

The copolymer described in the previous sections consisted of crown ether rings covalently attached to a highly cross-linked network of EGDMA and acrylic acid. This cross-linked network can be assumed to have a semi-rigid structure with very limited volume changes associated with solvent uptake. Similarly the potential of the cross-linked network to undergo viscoelastic changes are limited. An improvement in sensor response could be achieved with a copolymer coating that can undergo greater structural changes during the metal-ion binding process. For example increased swelling and inter-chain cross-linking. In such a case the response of the QCM sensor to the binding of the target species would be governed not only by the mass change but also to a greater extent the viscoelastic changes associated with the binding mechanism. These extra contributions would add to the overall response of the sensor and increase the sensitivity.

To this end a non cross-linked crown ether containing copolymer was synthesised and employed as a selective membrane on the surface of a QCM. The response was investigated in via the batch method described in section 2.5. The coated sensor was stabilised in a set volume of pure water and metal sulphate solutions injected into the system, progressively increasing the metal ion concentration.

This section describes in detail the copolymer synthesis and the fabrication of the final sensors. The results from the investigation of the sensor response to $K^+_{(aq)}$, $Na^+_{(aq)}$ and $Li^+_{(aq)}$ are presented and a model put forward to account for these responses.

3.6.2 Sensor Design

The copolymer employed is an acrylic acid backbone substituted with crown ether pendent groups, see Scheme 3.2. The copolymer is hydrophilic in nature and swells considerably when exposed to water. This swelling increases the copolymer water interaction and hence the crown ether metal-ion interaction. The swollen copolymer

is more susceptible to the viscoelastic changes that accompany the metal ion binding and these in turn contribute to the overall sensor response. In order to prevent copolymer dissolution the copolymer was attached covalently to the resonator surface. This was achieved via a self-assembled monolayer, (SAM) [253]. SAMs form spontaneously between gold surfaces exposed to solutions of many sulphides, disulphides and thiol containing species. The structure of the SAMs is that of a pseudo-crystalline monolayer on the gold surface with close packing of the molecules. The Au-S bond dissociation energy is 418 $kJmol^{-1}$ [254] this is the driving force behind the SAM formation and provides a covalent link between the sulphur containing species and the gold surface [255].

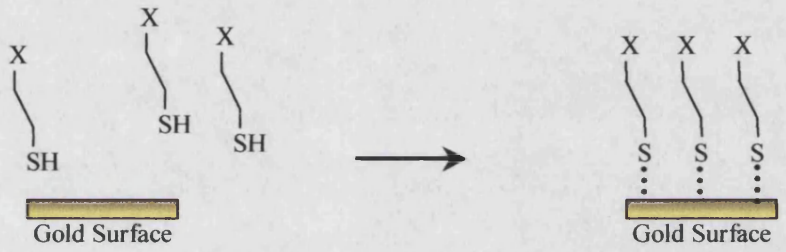

***Figure 3.19**: A schematic representation of the formation of a SAM*

By selecting an appropriate thiol species a surface monolayer of differing chemical functionality can be established. In this case 2-aminoethanethiol was used. This forms a SAM with an amine functional surface, see Figure 3.19, $X=NH_2$ [256]. The amine groups are used to anchor the copolymer to the SAM via an amide link with the carboxylic acid groups present in the copolymer backbone.

The formation of the SAM proved to be a very difficult process to observe and only limited evidence could be produced to support the assumptions made concerning the structure. The standard techniques employed are; contact angle measurements [257], infrared grazing angle reflectance spectroscopy (FTIR-RAS) [258], surface plasmon resonance [253], X-ray photoelectron emission spectroscopy (X-PES) [257] and X-ray diffraction [259]. However the orientation and structure of the QCM resonator and the availability of the analytical instruments limited the application of such techniques. The QCM itself can be used to monitor the formation of a SAM [260][261], by stabilising the resonator in an appropriate solvent and

monitoring the frequency change associated with the addition of a thiol species. The frequency change is instigated by the build-up of the SAM and is generally of the order of 100 Hz, although values from 10-900 Hz have been quoted [260][261]. The time scale for the SAM formation varies considerably depending on the solvent-thiol combination employed and can be anywhere from a few seconds to several hours [261].

Once the SAM has formed the copolymer can be chemically attached by the reaction of the amine functional groups present on the SAMs surface and the carboxylic acid groups present in the copolymer backbone. Two approaches were used to attempt this coupling reaction. Firstly a SAM coated resonator was placed in a DMF solution of the copolymer along with a suitable catalysts. The catalyst is an amino acid coupling agent, dicyclohexylcarbodiimide (DCC) [262]. This encourages the formation of the amide link. The second approach simply involved the placing of a copolymer layer onto the surface of a pre-formed SAM and heating the coated resonator to 130 °C. The combination of a carboxylic acid group and a primary amine results in the formation of a salt. These salts can be converted to amides by simple heating of the sample [263]. The reaction is not often used for preparative methods, however, the amide linkages formed should be sufficient to anchor the copolymer to the QCM surface.

The first of these methods is considered to be more elegant but initial attempts proved to be unsuccessful. A precipitate formed which covered the resonator. The precipitate was not as a result of the copolymer coupling and could be removed by rinsing of the resonator with various solvents, for example methanol and ethanol. The second approach of heating the copolymer layer in the presence of the SAM was successful and it is this method that is utilised to fabricate the sensor described in section 3.9.

3.7 Synthesis of the Copolymer

Acrylic acid was polymerised in the presence of the acrylamidocrown ether monomers synthesised in section 3.2. The polymerisation followed standard free radical conditions. Scheme 3.2 below illustrates the process and the final copolymer produced. The reaction was initiated with AIBN by heating the monomer solution to above 60 °C. The ratio w/w of the acrylic acid to crown ether monomers in the initial reaction mixture was about 3.5:1 (acrylic acid = 3.5). See section 2.3 for more detail on the experimental procedure.

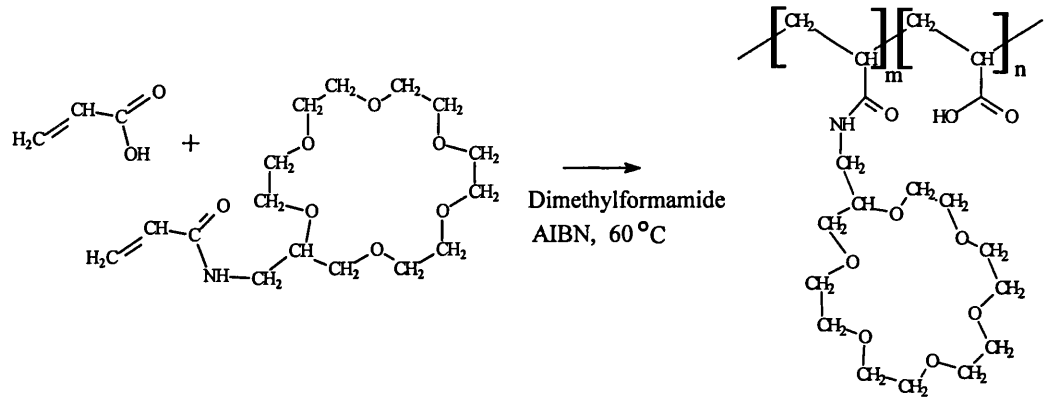

Scheme 3.2: Formation of the crown ether copolymer

3.7.1 Analysis

The copolymers were recovered with 70 % and 72 % yield with respect to the 15-crown-5 and 18-crown-6 copolymers. They both displayed the same solubility; of the common solvents tested they were only soluble in DMF, pyridine and DMSO although both copolymers swelled in water and methanol. This lack of solubility hampered the analysis, however ^{13}C-NMR, ^{1}H-NMR, CHN, FTIR and GPC were performed on the 18-crown-6 copolymer and confirmed the structure to be that illustrated in Scheme 3.2. NMR and GPC analyses were conducted on the 15-crown-5 copolymer and confirmed the structure to be the same as the equivalent 18-crown-6 copolymer with identical m:n ratio. The results of the 18-crown-6 analyses are discussed in the following pages.

^{13}C-NMR

The ^{13}C-NMR, Figure 3.20, shows three carbon nuclei, C-triplet at 70 ppm, C-doublet at 43 ppm and C-triplet at 35 ppm. The NMR also revealed a C-singlet nuclei at 180 ppm, however, for ease of presentation the entire spectra is not shown. The spectrum is consistent with the copolymer structure shown in Scheme 3.2. The C-singlet nuclei can be assigned to the carboxylic acid. The C-doublet and C-triplet nuclei at 43 and 35 ppm respectively can be assigned to the copolymer backbone carbon atoms and the C-triplet at 70 ppm to the crown ether ring CH_2 carbon atoms.

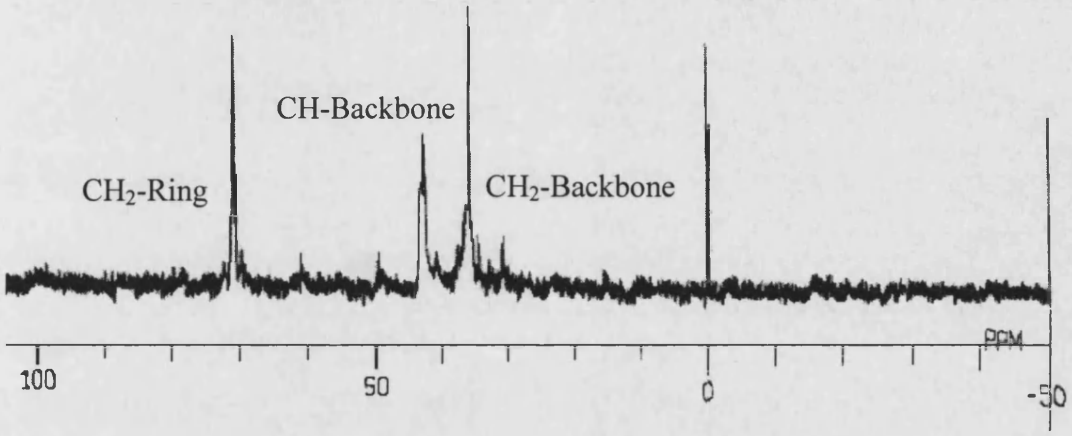

***Figure 3.20**: The ^{13}C-NMR of the 18-crown-6 copolymer.*

^{1}H-NMR

The ^{1}H-NMR of the crown ether copolymer can be seen in Figure 3.21. This shows poor peak resolution, which can be attributed to the slow molecular motion associated with polymer chains as well as chemical and magnetic inequivalence of the proton chemical environments. This, combined with the viscosity of the copolymer-C_5D_5N solution limits the structural information available from the ^{1}H-NMR. The multiplets associated with the crown ether ring protons and the copolymer backbone protons, however, can be isolated. These appear between 3-4 ppm and 2-3 ppm respectively. The integration ratio of these two regions can be used to calculate the percentage crown ether present in the copolymer. The spectrum showed the crown ether loading to be 16.7 % i.e. the m:n ratio in Scheme 3.2 to be 1:5.

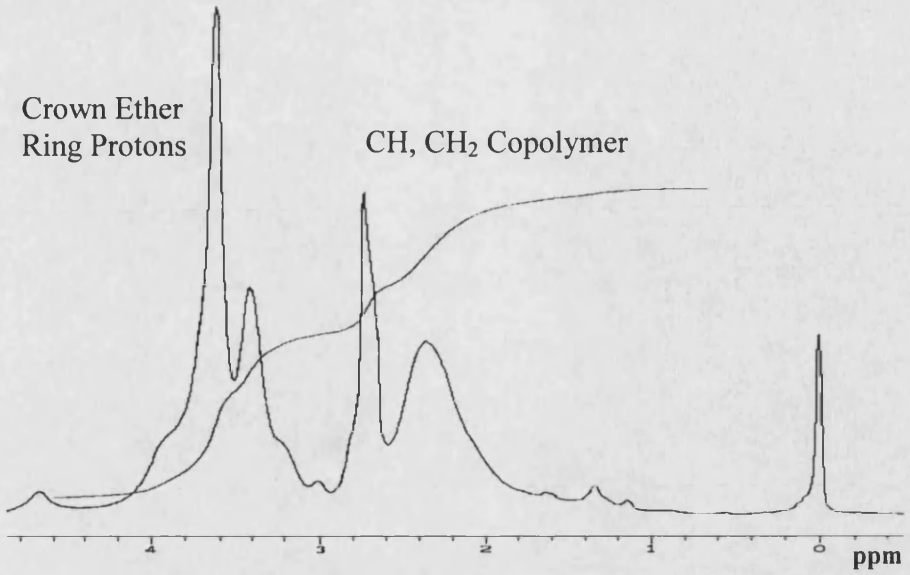

***Figure 3.21**: The ^{1}H-NMR of the 18-crown-6 copolymer.*

Elemental Analysis

Experimental	1.9 % **N**, 49.9 % **C**, 6.3 % **H**	$\Rightarrow$	$\mathbf{C}_{30.6}\mathbf{H}_{46.5}\mathbf{N}_{1.0}$
Calculated	2.0 % **N**, 51.5 % **C**, 6.7 % **H**	$\Rightarrow$	$\mathbf{C}_{30.7}\mathbf{H}_{48.6}\mathbf{N}_{1.0}$

The elemental analysis of the copolymer revealed the nitrogen content to be 1.9 % assuming this arises only from the amide linkage the CHN data can be utilised to calculate the crown ether loading of the copolymer. This worked out to be 17 % of the carboxylic acid groups and agreed well with the 16.7 % predicted from the ^{1}H-NMR. The calculated values for the CHN data above were based on the crown ether loading value obtained from the ^{1}H-NMR.

Infrared Analysis

The infrared (IR) spectrum of the poly(18-crown-6)-(acrylic acid) copolymer can be seen in Figure 3.22. The spectrum indicates the removal of the C=C stretching frequency at 1546.59 cm^{-1}. It also shows the large broad absorption between 3800 cm^{-1} and 2800 cm^{-1} indicative of the carboxylic acid O-H group. The

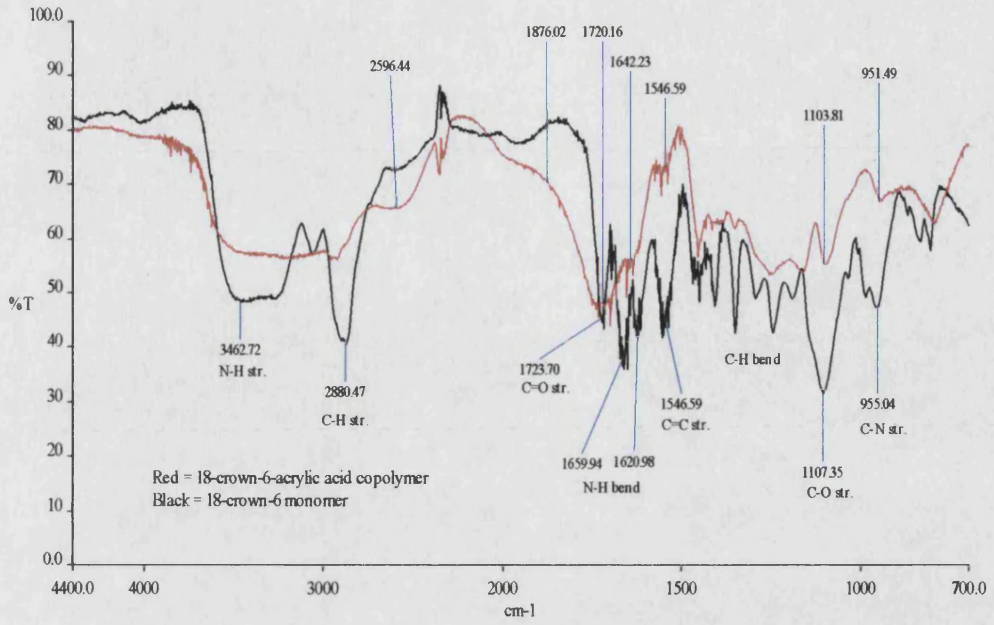

***Figure 3.22**: The FTIR of both the 18-crown-6 monomer and the 18-crown-6 copolymer.*

region extending from 1880 cm^{-1} to 1700 cm^{-1} shows a large broad peak. This is consistent with the expected C=O stretching frequency of poly(acrylic acid). The shoulder on this peak below 1700 cm^{-1} can be assigned to the C=O amide stretching frequency and the N-H bending frequency. Both these will be expected in the copolymer but with a decreased intensity compared to the bulk poly(acrylic acid) absorption.

GPC

The GPC trace of the two crown ether containing copolymers can be seen in Figure 3.23. A standard poly(acrylic acid) sample synthesised by the identical experimental procedures excluding the crown ether monomer can also be seen. The results of the data analysis performed on the samples are shown in Table 3.5. The GPC system was calibrated with poly(methylmethacrylate) standards and so the values for the molecular weights are PMMA equivalent molecular weights and not the absolute values.

Sample	M_w.	M_n.	Polydispersity
PDAA1	37100	8360	4.4
PDAA2	36100	8340	4.3
PD15P1	1000000	31500	32
PD15P2	1040000	27700	37
PD18P1	801000	37500	21
PD18P2	840000	36300	23

***Table 3.5**: Poly(methylmethacrylate) equivalent molecular weights and the polydispersity for the two crown ether copolymers and the standard poly(acrylic acid) samples synthesised in section 2.4.3.*

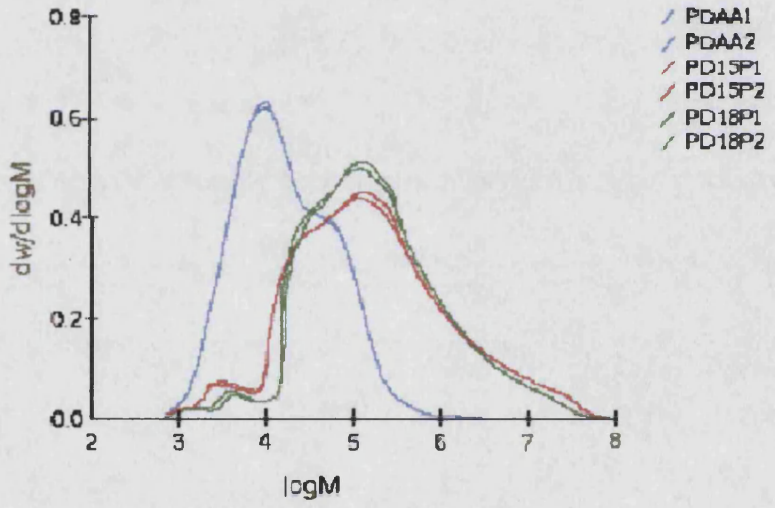

***Figure 3.23**: Molecular weight distributions for the three copolymers synthesised. PDAA is the standard poly(acrylic acid), PD15P is the 15-crown-5 containing copolymer and PD18P is the 18-crown-6 copolymer.*

3.7.2 Conclusion

The spectroscopic and elemental analysis of the poly(18-crown-6)-(acrylic acid) copolymer confirm the proposed structures. The ^{1}H-NMR and CHN analysis of the copolymer reveals the ratio of crown ether pendent groups to carboxylic acid groups to be 1:4.96 and 1:4.88 respectively. Both calculations are in good agreement and the ratio m:n can assumed to be 1:5. This shows a large crown ether content. The carboxylic acid groups are present to induce the hydrophilic nature of the copolymer. If they are reduced in population the copolymer may not interact with the aqueous solutions. The copolymer, however, still swells in the presence of water so the high crown ether content does not have an overwhelming effect on the hydrophilic nature of the copolymer. The carboxylic acid groups are present in a high enough ratio and so anchoring of the copolymer to the sensor surface via an ester or amide linkage should be easily achieved.

These three properties, high crown ether content, hydrophilic nature and free carboxylic acid groups were the main targets for the synthesis. The copolymer developed has been shown to meet these requirements and should form a suitable cation selective membrane when incorporated in a QCM based chemical sensor.

3.8 Self-Assembled Monolayers

Several methods were utilised in the formation of the self-assembled monolayers. A variety of thiol compounds, different solvent systems and a range of surface pre-treatments. The results from these studies will be discussed in this section. The experimental detail presented in section 2.4.3 is that used to fabricate the SAM employed in the final sensor. The experimental details of the previous attempts are neglected for ease of presentation, however details of the attempts are discussed and the conclusions presented.

3.8.1 Results

Two resonators were employed to investigate the SAM formation. Both were subjected to the same cleaning procedure. Resonator 1 was placed in pure dry ethanol while resonator 2 was placed in a 5 mmoldm^{-3} ethanol solution of aminoethanethiol. The frequency change associated with the exposure of resonator 1 to pure ethanol was consistently below 20 Hz. By contrast Resonator 2 had an increase in resonance frequency of 119 Hz. Using equation 10 and a value of 0.70 Hz ng^{-1} for the calibration constant this is equivalent to the addition of 83 ng of material. Assuming a value of 25 Å^2 for the area of one molecule and a 0.16 cm^2 geometric area for the gold electrode, monolayer coverage would be expected to be approximately 8 ng.

Unsuccessful Methods

Other thiol species employed were 3-mercapto-1,2-propandiol and thioctic acid. The mercaptopropandiol species was found to undergo a chemical reaction. When the QCM resonator was placed in an ethanol solution of the mercaptopropandiol a precipitate was formed. Interestingly this precipitate only formed when the QCM resonator was oscillating. A solution of the thiol in ethanol remained clear and free from precipitate for several weeks. All early attempts to from the SAM failed. The frequency change of the resonator on exposure to the thiol compounds was inconsistent and less than 50 Hz. This was attributed to the nature of the gold surface. The formation of an ordered SAM is very dependent on the structure and composition of the gold surface [264]. Several methods exist for the pre-treatment of the gold surface in preparation for the SAM these include physical polishing with alumina slurry [265] and electrochemical cleaning [266]. Due to the delicate nature of the gold electrode on the resonator surface the polishing procedure was not suitable, the electrode simply eroded away. The electrochemical cleaning process was effective and is the cleaning procedure recommended for further work. However, with appropriate QCM resonators these steps are not required. The work conducted with the QCM resonators in this thesis utilised two different 'batches' of the same specification resonators. Batch one failed to form SAMs even after

extensive cleaning, whereas batch two resonators responded well to the formation of SAMs. The X-PES a spectrum of the gold electrodes on a batch one resonator was dominated by a silicon peak. By contrast the expected Au peak dominated the X-PES spectra of the gold electrode in the second batch. It is therefore highly probably that the Si contamination on the Au surface was responsible for inability of these electrodes to form SAMs. It is recommended that future resonators be subjected to X-PES analysis on receipt simply to confirm the chemical nature of the gold surface. See Appendix 3 for the X-PES spectra.

3.9 Fabrication of the Sensor

The final sensor was fabricated by taking a resonator with a pre-formed SAM of aminoethanethiol and placing a layer of the acrlyamido-18-crown-6 copolymer over the surface. The coated resonator was then heated to 130 °C with the intention of promoting the formation of an amide link between the amine functional SAM and the copolymer [263]. The response of the coated resonator to $K^+_{(aq)}$, $Na^+_{(aq)}$ and $Li^+_{(aq)}$ were then investigated using the batch method described in section 2.7. The following pages discuss the results from the fabrication of the sensor and the sensor response

3.9.1 Results for the Fabrication of the Sensor

Table 3.6 lists the frequency changes associated with the fabrication of the sensor. On formation of the SAM layer the resonance frequency of the crystal dropped by 119 Hz. This is as expected for the formation of a monolayer of the thiol species on the surface of the resonator. The copolymer coating induced a frequency shift of around 2200 Hz indicating a mass of approximately 1.59 μg. On heating to 130 °C and subsequent rinsing with warm DMF this mass reduced to 1.41 μg.

	ΔF / Hz	Mass / μg
Thiol Layer	119	0.08
Copolymer Coating After heating	2021	1.41
Copolymer Coating After soaking in water and drying in air	2599	1.81

***Table 3.6**: The frequency changes associated with the sensor fabrication.*

Previous attempts to coat the resonator with the copolymer produced similar results. However, on soaking the coated resonator in water for several hours and after several injection runs, the frequency returned to that of the clean resonator. Using this SAM methodology the frequency of the coated resonator remained constant throughout the sensor response studies.

The change of resonance frequency of the dry film on exposure to water is believed to be due to the hydrophilic character of the copolymer layer. Differential scanning calorimetry (DSC) studies conducted on the copolymer show that it has a 5 % by weight moisture content when exposed to the atmosphere. After soaking in water and simply drying in an air stream at room temperature this moisture content would be expected to increase substantially. The QCM data above suggest that the moisture content of the copolymer film after soaking in water and drying is 28 % by weight.

The heating to 130 °C was intended to promote the formation of the amide link between the copolymer acrylic acid groups and the SAM amine groups, effectively dehydrating the copolymer layer. Once heated the copolymer shows no physical change that may be associated with thermal decomposition, and a thin film can be seen on the surface of the resonator. All attempts to remove the copolymer film failed, these included washing with warm solvent, 1M sulphuric acid, 1M NaOH and gentle rubbing. The gold electrodes on the surface of the resonator are very thin and any vigorous cleaning techniques such as polishing and ultrasonic

etching damage the electrodes rendering the resonator inoperative. We are therefore confident that the polymer film is present and adhered to the resonator surface.

3.9.2 Response Studies

The response of the sensor was monitored in a batch process (see Chapter Two section 2.7). This involved the injection of 10 µl, 50 µl and 100 µl of a 0.68 mol dm^{-3} $[M]^{+}_{(aq)}$ concentration. After each injection the resonant frequency was allowed to stabilise before any subsequent injections. This was about 10 minutes for the coated sensor. The frequency was considered 'stabilised' when the value was ± 5Hz for a period of 2 minutes. After this time the resonant frequency was recorded for 30 to 40 seconds prior to the next injection. Typically a total of 800 µl of the metal ion stock solution were injected for each run.

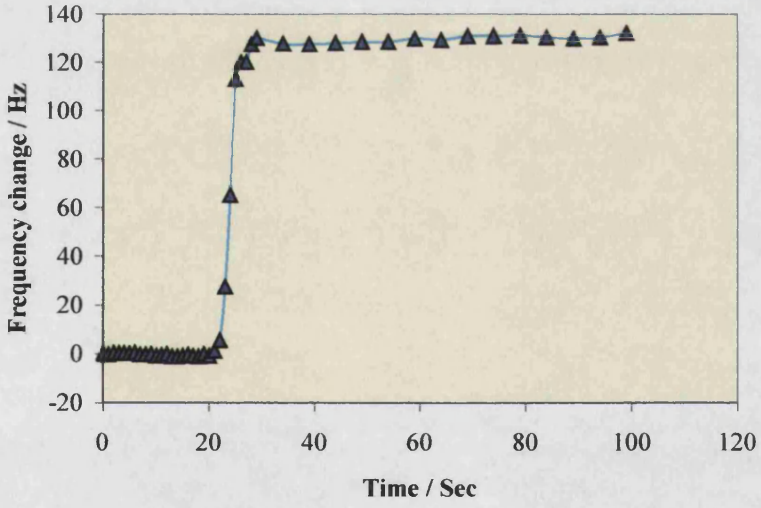

***Figure 3.24**: The response of the coated resonator to the injection of 100 µl aliquot of 0.68 mol dm^{-3} $K^{+}_{(aq)}$ solution.*

The response of the coated QCM to the injection of the metal sulphates followed a similar trend for all the sensor system, see Figure 3.24. This was an

almost instantaneous shift in the resonant frequency that occurred within 1 or 2 seconds of the injection time. In some cases the shift would level off as much as 50 seconds after the injection. This was only in the first few runs and can be attributed to the flux of the solvent molecules in the region close to the resonator surface. Initially the resonator is operating in an ion free solvent environment. The addition of the Group I sulphates therefore has an immediate effect on the resonator oscillation. This effect takes several seconds to reach an equilibrium condition. Later injections simply add more ions into the system so the overall flux of water molecules and metal ions near the surface of the electrodes is greatly reduced. Once the initial shift has occurred the resonant frequency remains stable. Further experiments on the stability of the QCM have shown that the base line drift in water is in the region of 0.03 Hz Sec^{-1} and can be maintained for a period of several hours.

The response of the copolymer coated resonator to the injections of $K^{+}_{(aq)}$, $Na^{+}_{(aq)}$, and $Li^{+}_{(aq)}$ can be seen in Figure 3.25. The resonator displayed a similar trend for all three of the metal ions. Both in the magnitude and in the time period of the frequency shifts. After each cleaning run the fundamental oscillating frequency of the copolymer coated sensor returned to a value representative of the resonator after the initial copolymer layer was deposited.

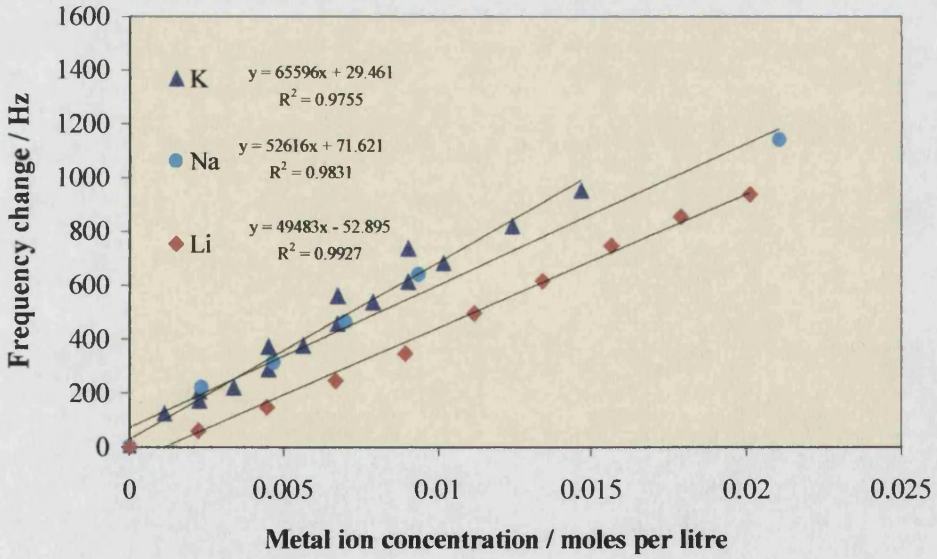

***Figure 3.25**: The response of the 18-crown-6 copolymer coated sensor to the injection of metal stock solutions*

The response ratio of the three metal cations (the ratio of the three gradients in Figure 3.25) is 1.32:1.06:1.0 for $K^+_{(aq)}$:$Na^+_{(aq)}$:$Li^+_{(aq)}$. This is the ratio predicted from the simple conductivity changes associated with the metal cation concentrations and indicates that the sensor has no selective response to $K^+_{(aq)}$. The following section accounts for these observed ratios and shows that no frequency change associated with the uptake of any of the Group I ions occurred.

Frequency Response Interpretation

The frequency change of the non-functionalised resonators is believed to be associated with changes in the conductivity and viscoelastic properties of the oscillating medium. The resonant frequency of an oscillator operating in a liquid environment is related to the density, viscosity and ionic concentration of the solution [267]. The relationship between these three physical properties and the resonance frequency of the QCM are discussed in length in section 1.4 of this thesis and are not wholly understood at the present time.

The response observed in this case can be accounted for by considering only the changes in conductivity of the oscillating medium. The ratios developed from experimental observations can be predicted by applying Kohlrausch's law [268], or more completely by the Debye-Hückel-Onsager theory [269] to the metal sulphate solutions. These two theories relate the conductivity of a solution to the concentration of the electrolyte.

The Debye-Hückel-Onsager theory states that;

$$\Lambda_m = \Lambda^\circ_m - (A + B\,\Lambda^\circ_m)\,c^{1/2} \qquad (31)$$

where Λ_m is the molar conductivity of the solution, Λ°_m is the limiting molar conductivity of the electrolyte, c is the molar concentration of the added electrolyte and A and B are constants related to the stoichiometry of the electrolyte.

For the metal sulphates used $\Lambda°_m$ equals [270];

Li_2SO_4 $\Lambda°_m = 237.32$ S cm^2 mol^{-1}

Na_2SO_4 $\Lambda°_m = 260.16$ S cm^2 mol^{-1}

K_2SO_4 $\Lambda°_m = 306.96$ S cm^2 mol^{-1}

The concentration, c, of the metal sulphates after injection was less than 1 mmol dm^{-3} in all cases and the values of A and B are constant for all three sulphates. For these reasons the values of A, B and $c^{1/2}$ can be neglected when calculating the ratio of the conductivity ratios and Λ_m assumed to be equal to $\Lambda°_m$.

For equally concentrated solutions this leads to a conductivity ratio of;

$$[K_2SO_4]\,\Lambda_m / [Li_2SO_4]\,\Lambda_m = 1.29 \qquad (32)$$

$$[Na_2SO_4]\,\Lambda_m / [Li_2SO_4]\,\Lambda_m = 1.10 \qquad (33)$$

$$[Li_2SO_4]\,\Lambda_m / [Li_2SO_4]\,\Lambda_m = 1.00 \qquad (34)$$

These values are close to the response ratios developed experimentally for the uncoated resonators. This suggests that the initial response observed for the resonators are related to the conductivity of the oscillating solution. The change in viscoelastic properties were also plotted using Kanazawa's equation (17), however these were insignificant in comparison frequency change associated with the conductivity and are therefore neglected.

For these reasons the response of $Li^+_{(aq)}$ by the resonators was used as a calibration response. From this the predicted response of an uncoated resonator to the other cations $Na^+_{(aq)}$ and $K^+_{(aq)}$ could be calculated by the application of the simple ratio quoted. The predicted response calculated in this way was subtracted from the actual response. This revealed the response associated with the crown ether containing copolymer coating. The process can be expressed mathematically by the following equations. The predicted response for a resonator operating with no metal adsorption taking place i.e. an uncoated resonator or a resonator coated with a non-chelating copolymer was found to follow these ratios;

$$P_K / A_{Li} = 1.44 \quad (35)$$

$$P_{Na} / A_{Li} = 1.06 \quad (36)$$

$$P_{Li} / A_{Li} = 1.00 \quad (37)$$

Where P_K is the gradient of the predicted $K^+_{(aq)}$ response, P_{Na} is the gradient of the predicted $Na^+_{(aq)}$ response and P_{Li} is the gradient of the predicted $Li^+_{(aq)}$ response and A_{Li} is the actual experimental $Li^+_{(aq)}$ response. These ratios were obtained experimentally by observing the response of several uncoated resonators using the batch method described in section 2.7.

The 'normalised' frequency response is calculated from the predicted response minus actual the response:

$$N_K = P_K - A_K \quad (38)$$

$$N_{Na} = P_{Na} - A_{Na} \quad (39)$$

$$N_{Li} = P_{Li} - A_{Li} \quad (40)$$

Where N_K is the gradient of the 'normalised' $K^+_{(aq)}$ response, N_{Na} is the gradient of the 'normalised' $Na^+_{(aq)}$ response and N_{Li} is the gradient of the 'normalised' $Li^+_{(aq)}$ response.

From these equations it follows that for a resonator response identical to the uncoated resonator the 'normalised' gradient will equal zero, and for a resonator with modified response the gradient will not equal zero.

The normalised response graph is not plotted for the current sensor system shown in Figure 3.25 as the ratios indicated that no absorption was occurring and so no reference data from a blank poly(acrylic acid) system was obtained. However the $K^+_{(aq)}$ sensor developed in system two section 3.12 was shown to respond as predicted and this normalisation process used to plot the data.

3.9.3 Conclusion

The coating of the sensor was apparently successful. The frequency changes associated with the SAM formation and subsequent copolymer coating followed those expected. After careful cleaning and throughout the sensor application the copolymer remained intact on the sensor surface. This is evident by the dry oscillating frequency of the sensor. Previous coating attempts resulted in the gradual depletion of the copolymer layer, with the dry frequency returning to that of the clean resonator prior to the coating procedure. These observations support the assumption that the copolymer layer is covalently attached to the SAM and permanently adhered to the resonator surface.

The response of the coated sensor to aqueous metal ions was disappointing. The sensor displayed no response associated with the selective binding of $K^+_{(aq)}$, $Na^+_{(aq)}$ or $Li^+_{(aq)}$ and only responded to the conductivity changes of the solution induced by the metal ion concentration. This was surprising as the crown ether moieties were shown to be present in the copolymer prior to coating and the equivalent cross-linked copolymer displayed definite uptake properties towards $K^+_{(aq)}$. This suggests that the copolymer coating in the present system has in some way lost its uptake. The two most likely explanations for this are that the copolymer synthesised has no potential for uptake or that the copolymer under went some kind of structural change during the coating procedure. The analytical evidence obtained on the copolymer prior to coating indicates that the crown ether groups are present and intact, this includes ^{13}C-NMR, ^{1}H-NMR and FTIR. The only process involved in the copolymer coating that may have a detrimental effect on the copolymers chemical composition was the heating procedure. It is possible that the heating of the copolymer layer may induce structural changes with in the copolymer, destroying the crown ether groups or hindering their binding mechanism.

The following section describes the DSC studies undertaken to investigate the chemical and physical changes induced in the copolymer layer upon heating.

3.10 Copolymer Thermal-Stability

The DSC investigation on the thermal stability of the 18-crown-6 copolymer and the 18-crown-6 resin will reveal any chemical or physical change in the two polymers under the conditions employed to coat the resonator.

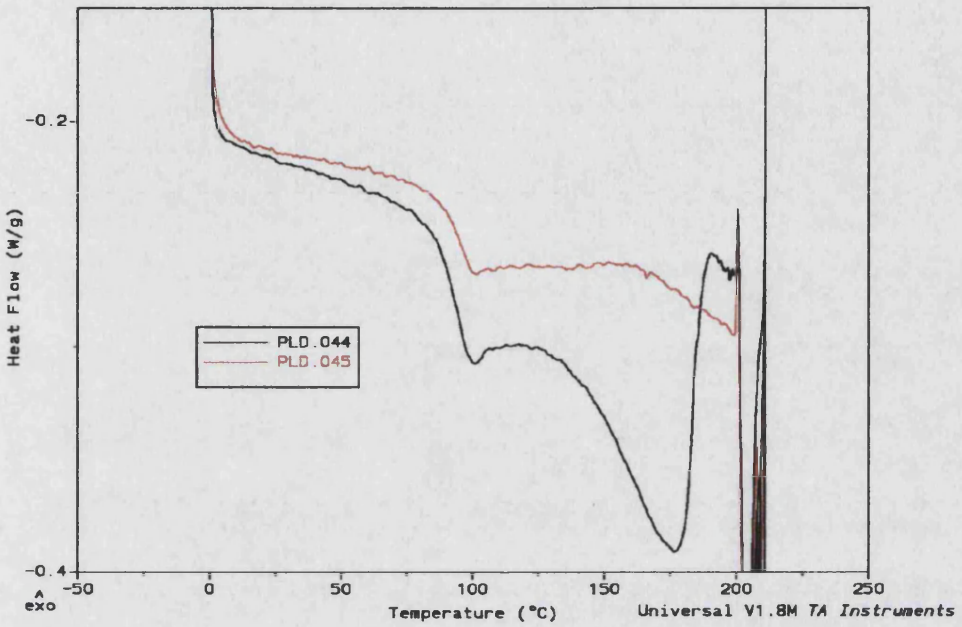

***Figure 3.26**: The DSC trace obtained for the 18-crown-6 copolymer. PLD.044 was the first heating cycle followed by PLD.045.*

The 18-crown-6 copolymer synthesised in section 3.7 was heated from 25 °C to 200 °C with a rate of 5 °C min^{-1}. The copolymer was dried prior to the run by cycling from 20 °C to 60 °C. This removes any moisture from the system. The results showed the glass transition temperature, T_g, to be 94.96 °C. This is consistent with the expected T_g given the T_g of poly(acrylic acid) is 106 °C [271]. A second thermal process was initiated at a temperature of about 130 °C. This appeared as an endothermic peak in the DSC trace and suggests a decomposition reaction. The DSC trace can be seen in Figure 3.26.

On repeating the heating cycle this second peak reduced considerably in intensity and the T_g increased to a higher temperature, 97.08 °C. With continued heating from 25 °C to 150 °C the T_g increases further. The process was repeated with a second sample the results of which can be seen in Figure 3.27, Table 3.7 shows the T_g values.

Number of heating cycles	T_g / °C	Mass of the sample / mg
0	-	11.544
1	94.96	11.216
2	97.08	11.044
3	104.13	10.874
4	110.13	10.804
Heated to 200 °C for 48 hours	132.91	10.370

Table 3.7: *The change in T_g and mass of the sample that accompanied the heating cycles. These are for the 18-crown-6 copolymer.*

The shift in the T_g value and the loss of mass in the copolymer sample both suggest that a thermal degradation of the copolymer is occurring. The mass change is not related to the evaporation of moisture from the copolymer as this was removed prior to the experiments. After drying and prior to the heating process cycling up to 70 °C produced no mass change in the copolymer or shift in the T_g. The total mass change was 10 %, this compares well with the 11 % mass change associated with the heating of the copolymer layer on the surface of the sensor during the sensor fabrication.

The increase in the T_g value indicates a reduction in the free-volume of the copolymer chains. This can be associated with the removal of a plasticiser, such as water molecules, or large spacer groups preventing the close contact of the copolymer backbones. As the copolymer was already dried and all moisture had been removed one possible explanation for this shift would be the decomposition of the crown ether rings. These form large bulky pendent groups attached to the copolymer backbone and act as internal plasticisers. As the rings decompose the copolymer chains have less free-volume and the T_g shift to a higher value. FTIR and CHN analysis were used in an attempt to confirm this hypothesis however the results were inconclusive. No obvious difference could be determined between the heated

copolymer and the original copolymer. ^{13}C-NMR or ^{1}H-NMR was not possible, as the heated copolymer was no longer soluble in the solvents available.

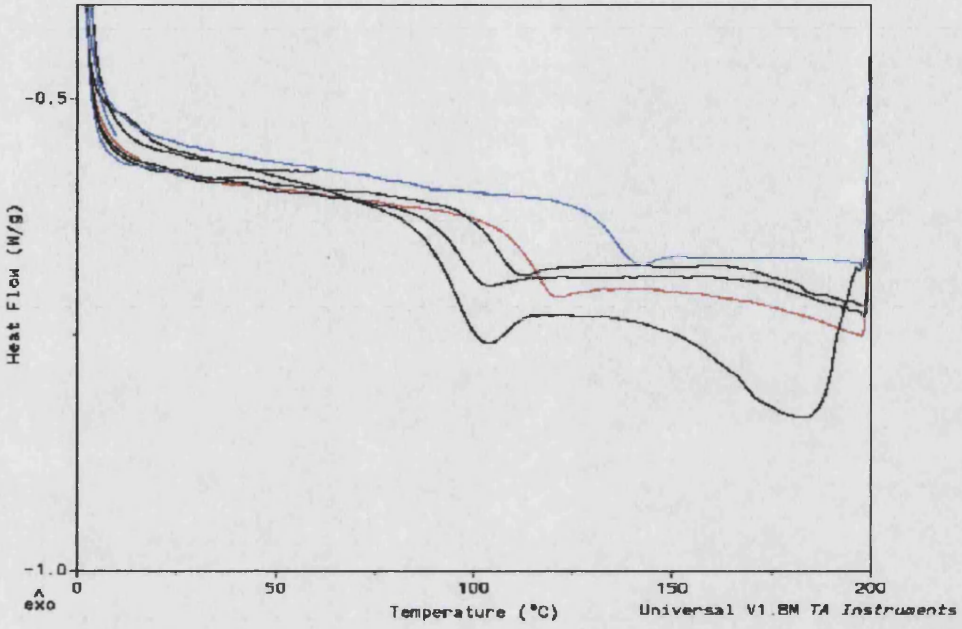

***Figure 3.27**: The shift in T_g and the initial first order endothermic decomposition peak associated with the heating of the 18-crown-6 copolymer 130 °C.*

3.11 Cross-linked Resin Thermal Stability

The uptake properties of the heated copolymers were investigated with the cross-linked resins synthesised in section 3.3. The chemical environment of the crown ether groups in the cross-liked resins are very similar to those in the copolymer. Any thermal degradation of these groups will be comparable in both the cross-linked resins and the copolymer system. As the uptake properties of the resins can be readily investigated using aqueous solutions of Group I ions, the uptake properties of the heated resins can be equally investigated.

The study was conducted in two parts. The first section used the DSC to investigate the thermal properties of the resins. The second section looks at the uptake properties of the heated resins.

3.11.1 DSC Investigation

A sample of the 18-crown-6 cross-linked resin 18c6/70 [272] was dried in the DSC chamber by cycling from 10 °C to 80 °C. The cycling was conducted in an air atmosphere. This resulted in a reproducible trace after approximately four cycles and a mass change from 5.05 mg to 4.79 mg. This is consistent with the drying of the resin by the evaporation of the excess moisture. The reproducible DSC trace indicates that no irreversible thermal processes are taking place during this drying step. The DSC trace can be seen in Figure 3.28.

Once dried the resin was heated to 190 °C. As with the copolymer this saw the emergence of an endothermic peak at about 140 °C see Figure 3.29. The peak was not reversible and later cycles displayed a reduction in the peak to a constant base line. This suggests the occurrence of a thermal oxidation or degradation process taking place with in the cross-linked resin. The process was repeated with two new samples with identical results.

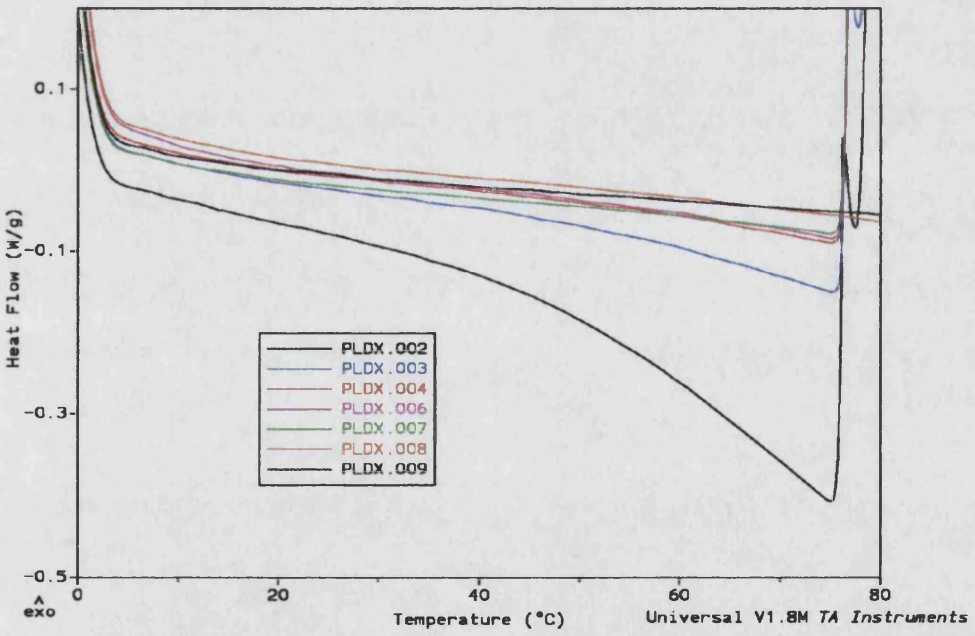

***Figure 3.28**: The DSC trace showing the drying of resin D. The mass of the sample was initially 5.05 mg and reduced to 4.79 mg. The process was conducted in an air atmosphere.*

Again as with the copolymer the resin had identical FTIR spectra both before and after heating. However due to the low concentration of the crown ether groups the degradation of these moieties would not be expected to show an obvious change in the FTIR spectra. See Appendix 4 for the FTIR spectra.

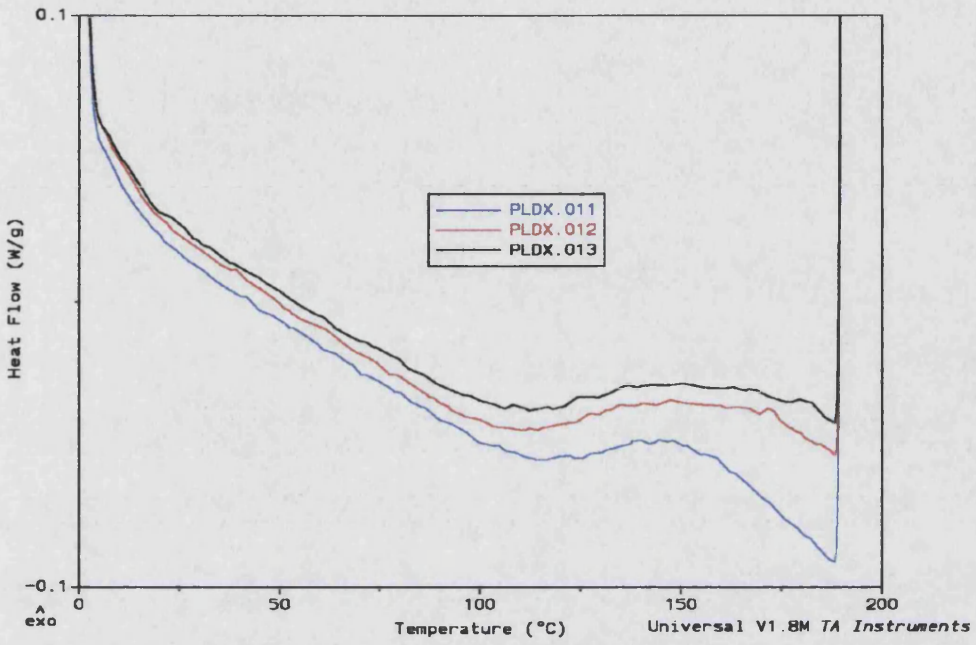

***Figure 3.29**: The DSC trace showing the thermal degradation of resin D.*

3.11.2 Uptake Investigation

The uptake properties of the heated resin were determined in an identical fashion to that of the original sample [273]. The resin was heated for 48 hours in a fan-assisted oven at 180 °C. The resin was subjected to occasional stirring to ensure an even heating. This resulted in no obvious degradation, the resin appeared the same before and after the heating with no charring or colour change, however, the uptake of the resin was effected. This can be clearly seen in Figure 3.30. The original resin had an uptake of 53 ppm with respect to $K^{+}_{(aq)}$. This was for a 1.3 g sample in 100 cm^3 of a 69 ppm stock solution. By comparison the heated resin had an uptake of only 41 ppm under similar conditions.

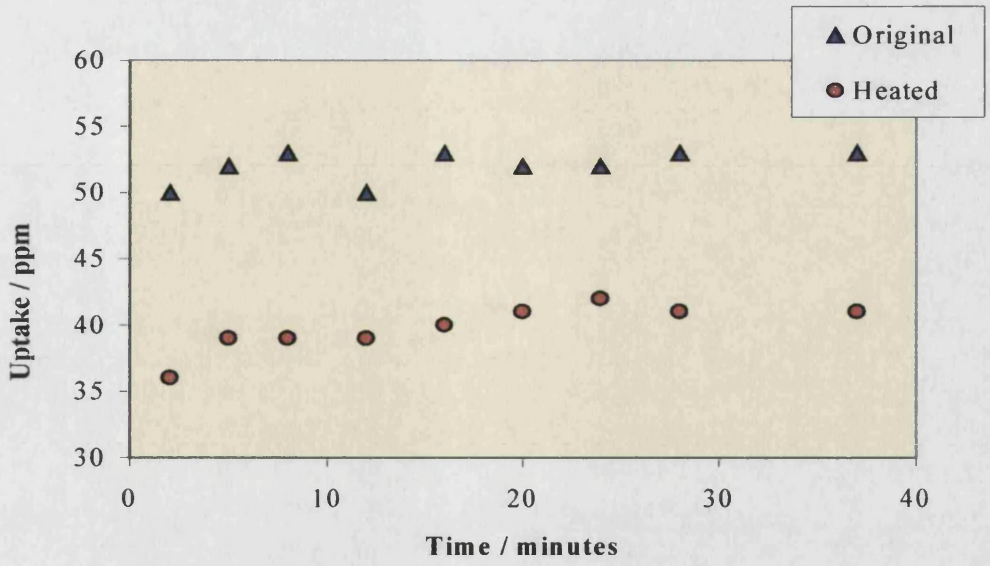

***Figure 3.30**: The uptake properties of both the original and a heated sample of resin D. The sample consisted of 1.3 g of the resin in 100 cm^3 of 69 ppm $K^+_{(aq)}$.*

The results confirm that the uptake of the cross-linked resin is reduced considerably after heating. Since this property is directly related to the crown ether content it leads to the conclusion that the heating of the resin in some way limits the binding of the metal cations to the crown ether rings, either by the degradation of the rings or by hindering the accessibility of the rings. The resin is synthesised with 70 % cross-linker and so it is very unlikely that the heating of the resin could limit the accessibility of the crown ether rings by further cross-linking. For this reason it is believed that the crown ether groups are either chemically or thermally degraded.

3.12 The $K^+_{(aq)}$ Sensor: System Two

The copolymer coated sensor displayed no uptake of any of the Group I ions. This was attributed to the thermal degradation of the crown ether groups during the sensor fabrication. An alternative method for coating the sensor would be to form the cross-linked copolymer resin utilised in sections 3.3 and 3.4 directly on the resonator surface. The conditions required would be identical to those used to synthesise the bulk powdered resin, which are known to selectively uptake $K^+_{(aq)}$.

3.12.1 Introduction

The experimental procedure applied to create the powdered copolymer resins synthesised in section 3.3 was readily modified to produce a cross-linked copolymer film on the surface of the QCM resonator. The three individual monomers, (acrylamidomethyl-18-crown-6, acrylic acid and EGDMA) were combined with a suitable solvent, (acetonitrile) and initiator (AIBN) in a small reaction well, the base of which was formed by the QCM resonator. By slowly heating the mixture the copolymerisation was initiated. The end result was a solid film permanently adhered to the resonator surface. On the bases of the monomer ratios employed it is assumed that this film possesses a similar composition to that of the powdered resin described previously. The coated resonator was then employed as a $K^{+}_{(aq)}$ sensor in two different applications, a batch system and a flow injection analysis (FIA) system.

The following sections describe the coating procedure and the response of the developed sensor. The analytical results used to confirm the presence of the coating layer and its chemical composition will be presented and discussed. The sensor response will also be investigated by the application of the Langmuir isotherm derived in section 3.5.2.

3.12.2 Fabrication of the Sensor

Two copolymer coatings were investigated; an 18-crown-6 copolymer based on the composition of resin 18c6/30 and a blank copolymer containing no crown ether based on resin EG/70. The monomer mixtures were prepared in a solution of acetonitrile using the ratios shown in Table 3.8. The concentrations were limited so that the mass of the final film would be around 1μg. This was based on the assumption that thinner films have greater response times and that the oscillation of the resonator is impaired as the thickness of any coating increases. Experimental details can be found in section 2.6.

Solution	18-Crown-6 monomer / g	Acrylic Acid / g	EGDMA / g	AIBN / g	Acetonitrile / cm^3
1	0.0636	0.2283	0.1575	0.0060	100
2	None	0.2848	0.1651	0.0063	100

***Table 3.8**: The monomer ratios in the solutions used to coat the QCM resonator.*

3.12.3 Results and Discussion

To investigate the response of the final sensor three resonators were prepared. The first one coated with the 18-crown-6 containing copolymer using solution 1. The second coated with solution 2, the "blank" resin containing no chelating groups and the third simply an uncoated resonator with no copolymer layers. The frequency changes associated with the coating of the resonator can be seen in Table 3.9.

Resonator	Coating Solution	Functionality	Δf / Hz	Mass / ng
A	1	18-crown-6	1593 ± 50	1111 ± 35
B	2	None	1011 ± 50	705 ± 35
C	None	None	None	None

***Table 3.9**: The three resonators prepared. Δf is the frequency difference between the coated and uncoated resonator measured in air. The coating solutions are those described in Table 3.8.*

The coating process resulted in a visible film that was unaffected by the usual cleaning methods, for example rinsing with hot solvents and gentle swabbing with cottonwool soaked in a suitable solvent. The chemical nature of the film was difficult to determine *in situ* via any analytical techniques. This was due to the shape of the resonator and the thin film thickness estimated at about 70 nm (assuming a density of 1 g cm^{-3}). However, X-ray photoelectron emission spectroscopy, X-PES, showed the expected carbon and oxygen peaks as well as the silicon, gold and oxygen peaks associated with the uncoated QCM resonator surface. These confirm the presence of

the carbon based coating but can not be utilised to calculate the carbon : oxygen ratio confirming the copolymer elemental ratios, see Appendix 3.

Sensor Response in the Batch Process

The response of the individual resonators, A, B and C were very similar. On injection of the metal stock solution the resonance frequency increased by about 10 Hz for a 10 µl injection of the 0.230 mol dm^{-3} stock solution. An example of the frequency response can be seen in Figure 3.31.

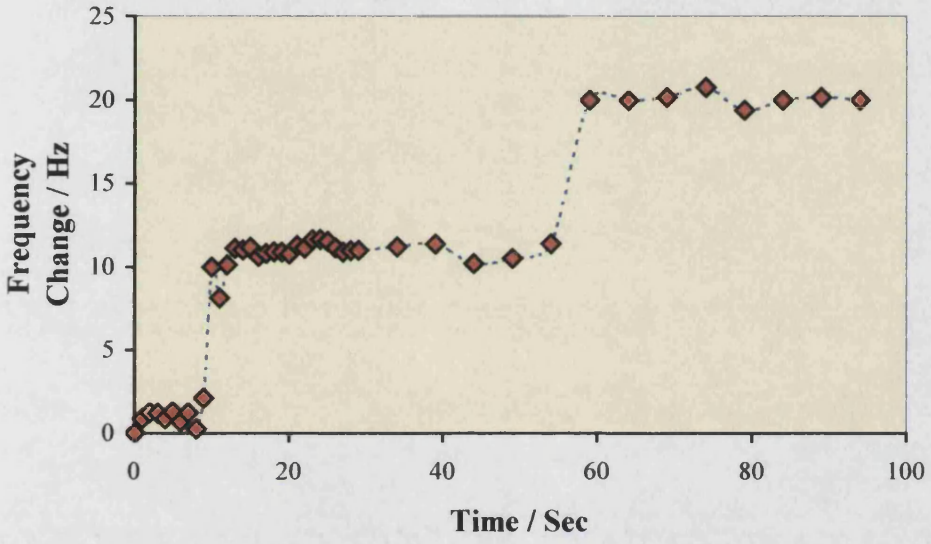

***Figure 3.31**: The response of resonator A to the injection of two successive 10 µl aliquots of 0.230 mol dm^{-3} $K^{+}_{(aq)}$ stock solution. The injections were on 10 seconds and 58 seconds.*

The frequency response occurred instantaneously as the injections were made. The profile shown in Figure 3.31 was observed for all resonators and is considered to be representative of the general trend. However, a tail-off of the frequency response was occasionally observed. This tail-off could be minimised with the inclusion of a magnetic stirrer in the reaction vessel. The stirrer speed had no effect on the value or stability of the resonance frequency. As before the frequency increase for all three resonators was found to have a linear relationship when plotted against the injected volume. The graphs can be seen in Figure 3.32, 3.33 and 3.34. The R^2 values obtained from the linear regression analysis for all three resonators to $Na^{+}_{(aq)}$, $Li^{+}_{(aq)}$, and $K^{+}_{(aq)}$ were all greater than 0.996.

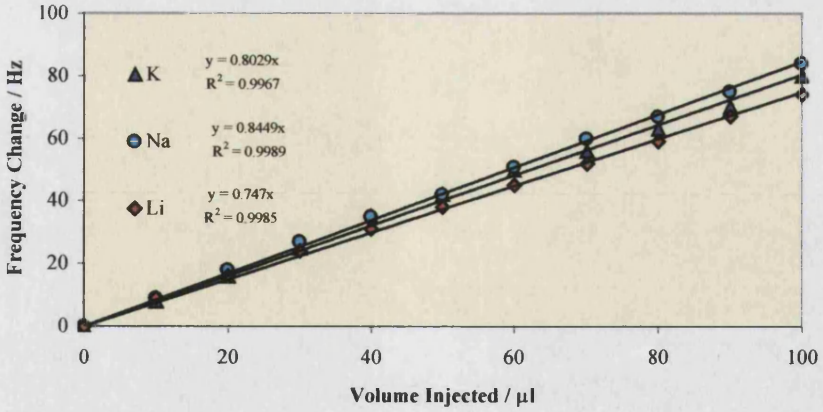

***Figure 3.32**: The response of resonator A to the injection of 0.230 mol dm^{-3} metal cation stock solutions.*

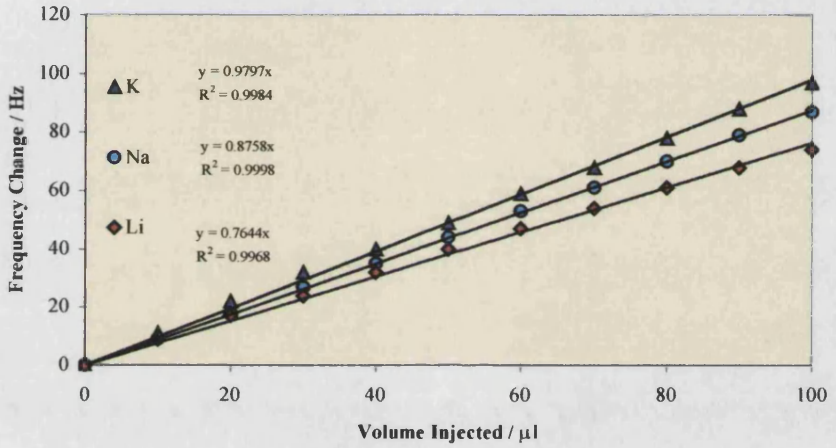

***Figure 3.33**: The response of resonator B to the injection of 0.230 mol dm^{-3} metal cation stock solutions.*

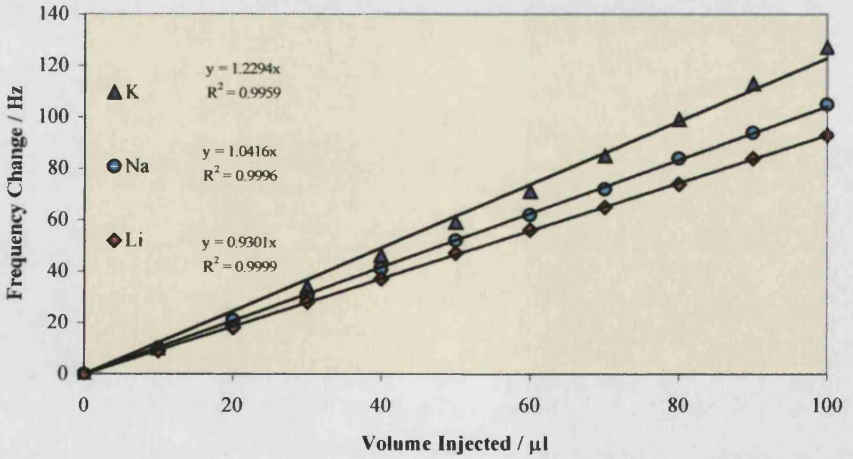

***Figure 3.34**: The response of resonator C to the injection of 0.230 mol dm^{-3} metal cation stock solutions.*

Frequency Response Interpretation

The initial frequency responses of the resonators, i.e. the gradients in Figures 3.32, 3.33 and 3.34, were found to follow the simple ratios quoted Table 3.10. It was the consistency of the response for the uncoated resonator C and the blank copolymer coated resonator B that led to the observation of the shift in the $K^+_{(aq)}$ response associated with the coated resonator A. The response was normalised following the procedure described in section 3.9.2.

	Ratio of Response Gradients		
Resonator	K^+ / Li^+	Na^+ / Li^+	Li^+ / Li^+
A 18c6/30 coated	1.07	1.13	1.00
B EG/30 coated	1.28	1.14	1.00
C no coating	1.32	1.12	1.00

***Table 3.10**: The ratio of the gradient for the response of resonator A, B and C taken from Figures 3.32, 3.33, 3.34.*

The normalised frequency response graphs can be seen in Figures 3.35 and 3.36. These clearly show the response of the crown ether coated resonator and are discussed in the following paragraphs.

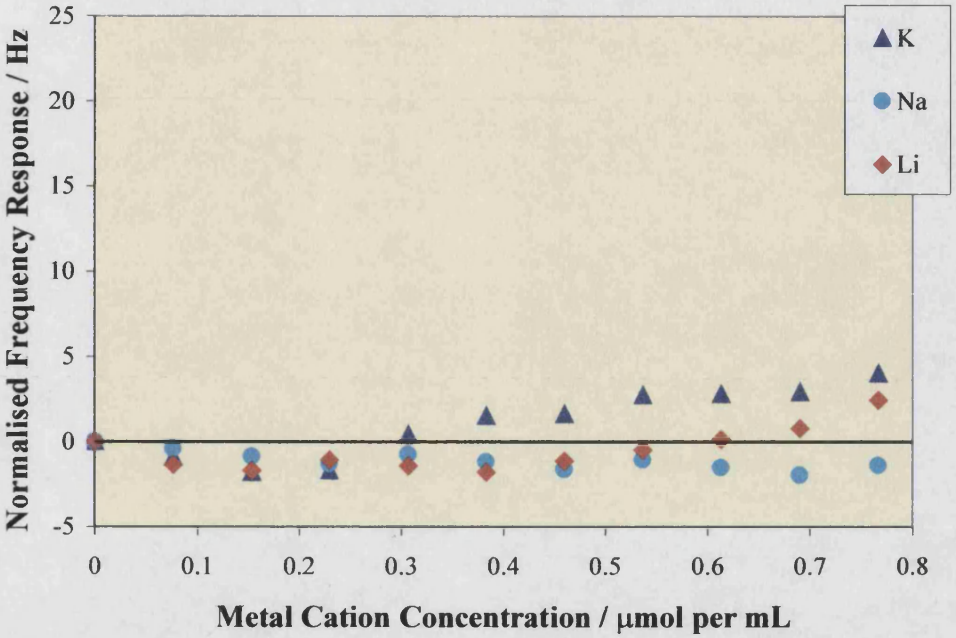

***Figure 3.35**: The normalised frequency response of resonator B (no crown ether) to the addition of metal cations. The experimental procedure involved the injection of 10 μl of a 0.230 moldm^{-3} stock solution into a 30 cm^3 sample of pure water.*

From the graph in Figure 3.35 it can be seen that resonator B, coated with the copolymer containing no crown ether, had no extra response to the addition of the metal cations. The normalised response profiles of the resonator to $Li^+_{(aq)}$, $Na^+_{(aq)}$ and $K^+_{(aq)}$ were obtained and the resonator showed no affinity for any of the ions investigated. The response was the same as that predicted for the uncoated resonator. This is the expected result; the equivalent bulk copolymer (resin EG/70) showed no uptake in the previous section. With no adsorption of the metal cations the copolymers mass and viscoelastic properties remain constant, independent of the metal cation concentration. The resonator is the control for the response experiments. It is worth pointing out however that the linear regression for the $Li^+_{(aq)}$ data by definition has a gradient equal to zero. This is a prerequisite for the data transformation performed and means the response plotted is with respect to any $Li^+_{(aq)}$ uptake

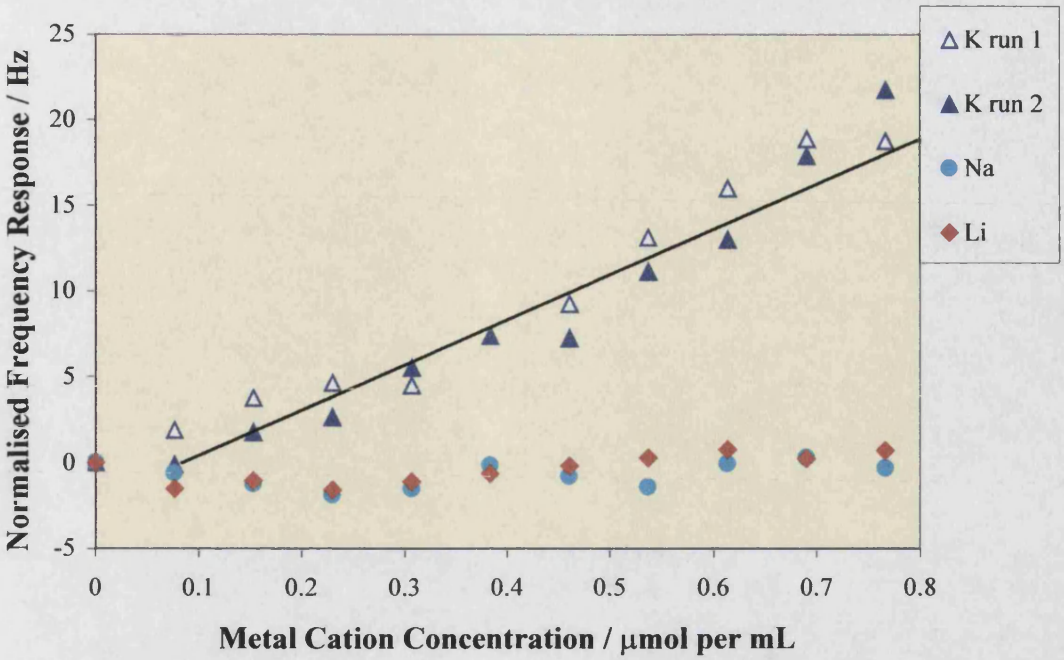

***Figure 3.36**: The normalised frequency response of resonator A to the addition of metal cations. The experimental procedure involved the injection of 10 μl of a 0.230 mol dm^{-3} stock solution into a 30 cm^3 sample of pure water.*

The response of resonator A coated with the 18-crown-6 copolymer can be seen in Figure 3.36. It can clearly be seen that the resonator has a pronounced response to $K^+_{(aq)}$ over the other two Group I ions $Na^+_{(aq)}$ and $Li^+_{(aq)}$. The results of run 1 were confirmed by the second set of data for run 2. This was collected for the same resonator after a light rinse with pure water. The second run also illustrates the mild cleaning conditions required between each exposure of the resonator. As with the powdered copolymer a simple rinse with pure water appears to fully reactivate the resonator. From the slope of the plot, a response factor of 0.68 Hz ppm^{-1} can be calculated. Assuming a frequency stability of ± 0.10 Hz this gives an estimated sensitivity of 0.15 ppm for the current system. This value is well within the sensitivity required for environmental and clinical applications of commercial K^+ sensors. The concentration of K^+ in tap-water is typically in the range of 1-80 ppm [274]. In the human body the concentration of K^+ in blood serum is around 140 ppm [275] and bile around 500 ppm [274]

3.12.4 Initial Conclusion

The results of the two resonators strongly indicate that the binding properties of the copolymer resin synthesised in section 3.3 have successfully been transposed to the QCM chemical sensor. The resonance frequency of the sensor displays concentration dependence with respect to $K^{+}_{(aq)}$, induced by the chelating potential of the copolymer interface. This dependence is masked by the general response of the QCM resonator to the electrical and viscoelastic changes associated with the addition of Group I sulphates to pure water. These non-specific changes can be predicted and removed from the overall response.

The profile of the dependence does not follow that predicted by the Sauerbrey equation [276]. This is not surprising as the relationship between frequency change and absorbed mass will not be straightforward and will not be given to any degree of accuracy by the Sauerbrey equation. However, for the purpose of the work carried out in this area the precise origin of the frequency response is of limited interest. The important observation is that a response exists and that this response is associated with the presence of the functionalised polymer. The system is easily calibrated by measuring the response to solutions of known concentration and can be applied to very dilute solutions.

3.12.5 Sensor Saturation

The normalised response of the sensor has so far been displayed as a straight-line graph of the type $y = mx + c$. However, intuitively this relationship can not hold over an infinite concentration range. At some point the sensor response has got to tail-off. This section describes the experiment undertaken to discover this saturation point.

The experimental procedure was the same as that followed for the batch sensor response. Sensor A was placed in 30 cm^3 of pure water and allowed to stabilise. Volumes of a Group I metal sulphate solution were then injected into the system gradually increasing the metal cation concentration. The stock solution used can be seen in Table 3.11.

Group I Metal Sulphate	Mass / g	Volume / cm^3	Concentration / $moldm^{-3}$
$Li_2SO_4 \cdot H_2O$	2.9535	100	0.461
Na_2SO_4	3.2655	100	0.460
K_2SO_4	4.0191	100	0.461

***Table 3.11**: The metal ion stock solutions used for the saturation study of sensors A and B.*

The volumes of the stock solutions added to the reaction chamber were such that it was necessary to remove a sample of solution before adding an equal volume of the stock. Accordingly, 500 µl of the stock solution was added initially, followed by the removal of 500 µl of the solution from the reaction chamber. This process was repeated 11 times each consisting of the addition of a 500 µl aliquot of the stock solution followed by the removal of 500 µl of the solution. The initial response of the two sensors A and B can be seen in Figures 3.37 and 3.38. It can be seen that the frequency response follows a curve gradually tailing off as the concentration of the metal cations increases.

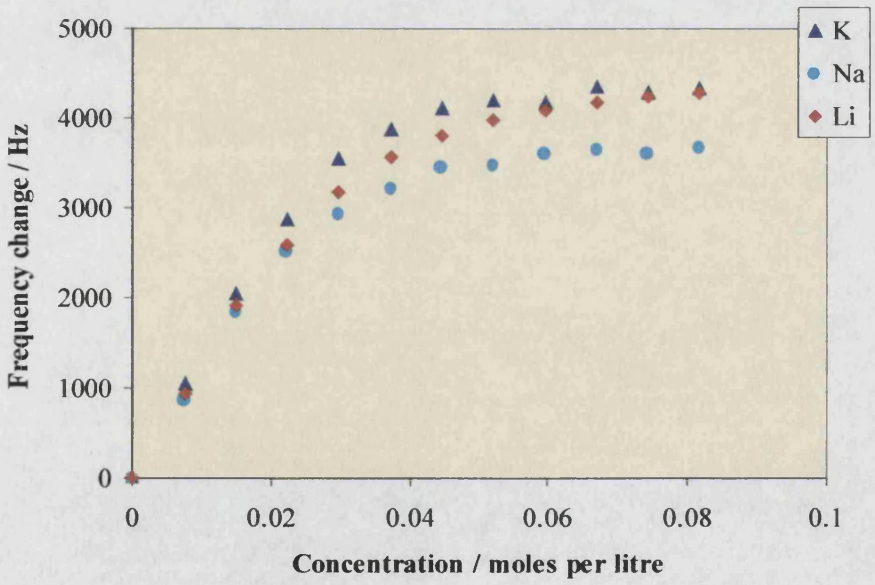

***Figure 3.37**: The response of sensor A (crown ether coated) to the injection of the metal stock solution*

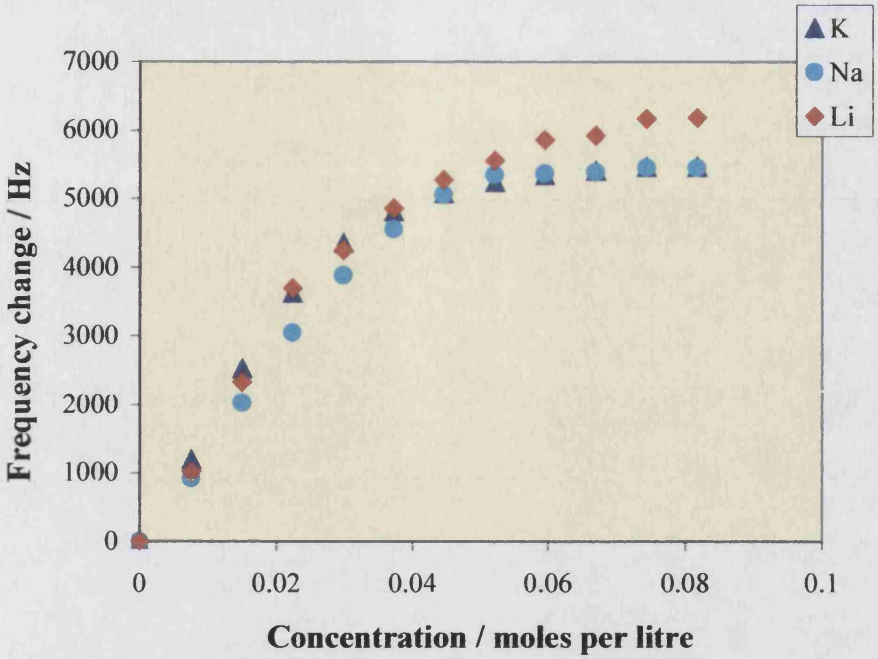

***Figure 3.38**: The response of sensor B (EGDMA coated) to the injection of the metal stock solution*

The initial frequency response was normalised following the same principle as before. The $K^+_{(aq)}$ and $Na^+_{(aq)}$ response were predicted from the $Li^+_{(aq)}$ response of sensor A based on sensor B. The normalised frequency graph for sensor A can be seen in Figures 3.39. This is the sensor coated with the 18-crown-6 containing copolymer. The error bars were calculated by assuming an uncertainty in the frequency response of ± 20 Hz estimated by observing the frequency fluctuations of the sensor immersed in the metal cation solution.

It can be seen from the graph that the $K^+_{(aq)}$ response rises to a plateau and levels off, the $Na^+_{(aq)}$ response tends to fluctuate around zero with no positive trend. Again, by definition the $Li^+_{(aq)}$ response is zero. Assuming that the plateau represents the saturated sensor response, from the data the fractional coverage θ can be calculated. By applying the Langmuir type isotherm derived in section 3.5.2 the fractional coverage can then be used to estimate the equilibrium constant for the metal ion adsorption process. The plot of equation 28 can be seen in Figure 3.40.

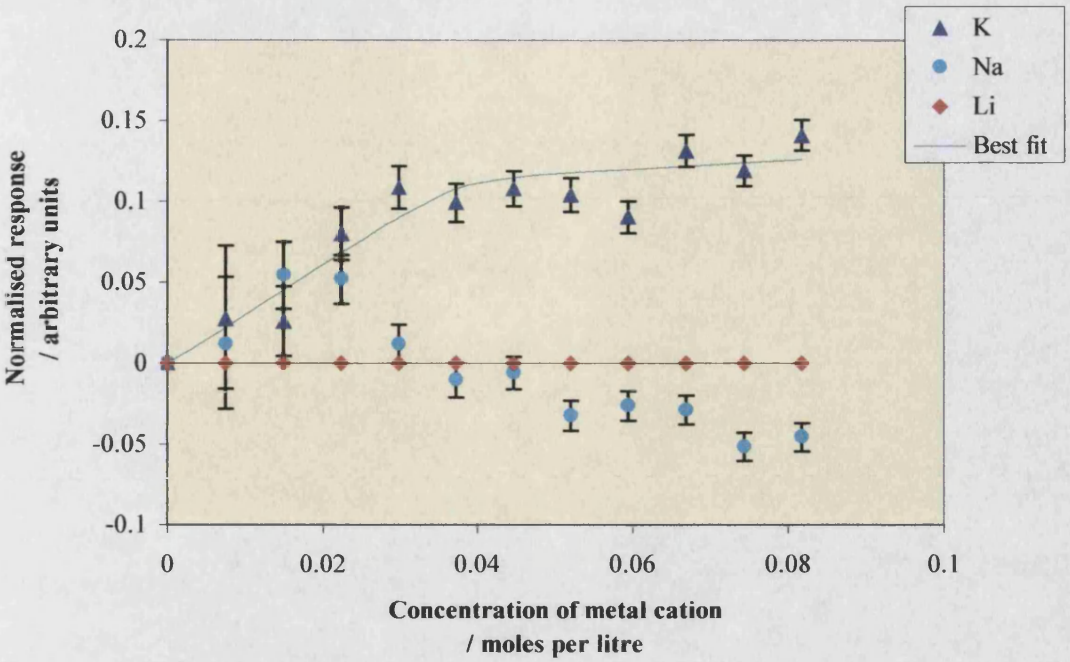

***Figure 3.39**: The normalised frequency response of sensor A to the injection of metal cation solutions.*

The Langmuir plot showed poor linear correlation. The expected fit should produce a straight-line graph with a zero intercept. The deviation from the Langmuir isotherm can usually be attributed to a failure in the assumption of equivalent, independent binding sites. The binding energy of each site increases or decreases with the fractional coverage. In this case the deviation suggests that the equilibrium constant K for the binding process is lower than expected at coverage with $\theta < 0.73$ and higher than expected at coverage with $q > 0.97$. From a mechanistic point of view this could be explained if the cation penetration and binding to the copolymer coating proceeds slowly at first but increases with time as more and more ions penetrate the network; effectively acting in a co-operative nature to encourage ion binding.

Different isotherms such as the Temkin [277] and Freunlich [278] isotherms show a much greater linear correlation with R^2 greater then 0.97, however, these offer no benefit in terms or calculating thermodynamic values for the binding process as they are empirical models only. For a more in-depth study it is suggested that that these isotherms are used to model the sensor response.

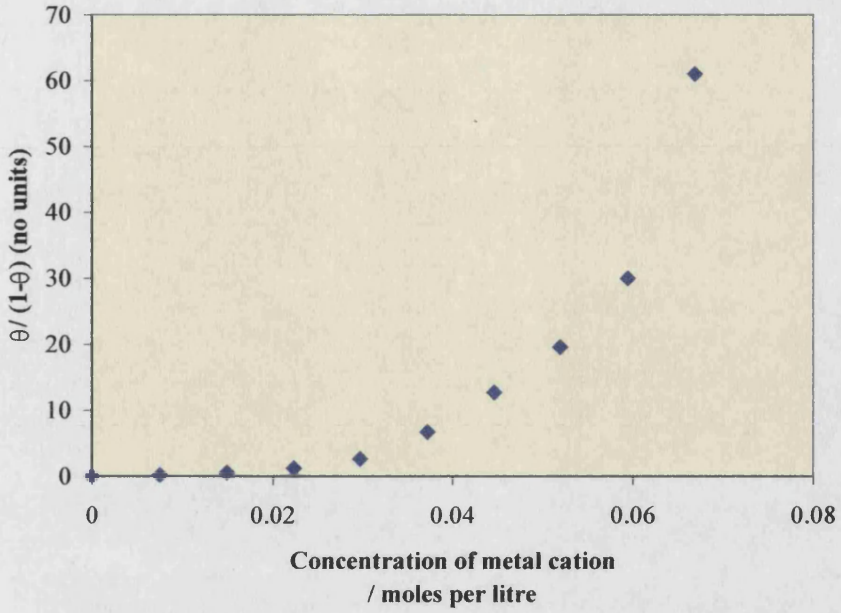

***Figure 3.40**: The plot of equation 28 for the saturation study of sensor A.*

Given the overall profile of the Langmuir plot shown in Figure 3.40 it was decided to approximate the isotherm to only include the values for $\theta/(1-\theta)$ greater than 5 and less than 40. The reason for this was the increased uncertainty outside this range. The plot of this region can be seen in Figure 3.41 and corresponded to the best linear approximation for the isotherm.

The gradient of the graph is equal to the equilibrium constant for the metal ion absorption process. Given the fact that equilibrium constants cover a larger numerical range this compares well with the same value calculated from the bulk resin in section 3.5.2. For reference the two values are shown in Table 3.16. The consistency in the value of K obtained supports the mechanism put forward for the sensor response based on the adsorption of K^+ ions by the crown ether macrocycles. They also show the chemical similarities between the bulk resin synthesised and the copolymer coating assumed to be on the sensor surface.

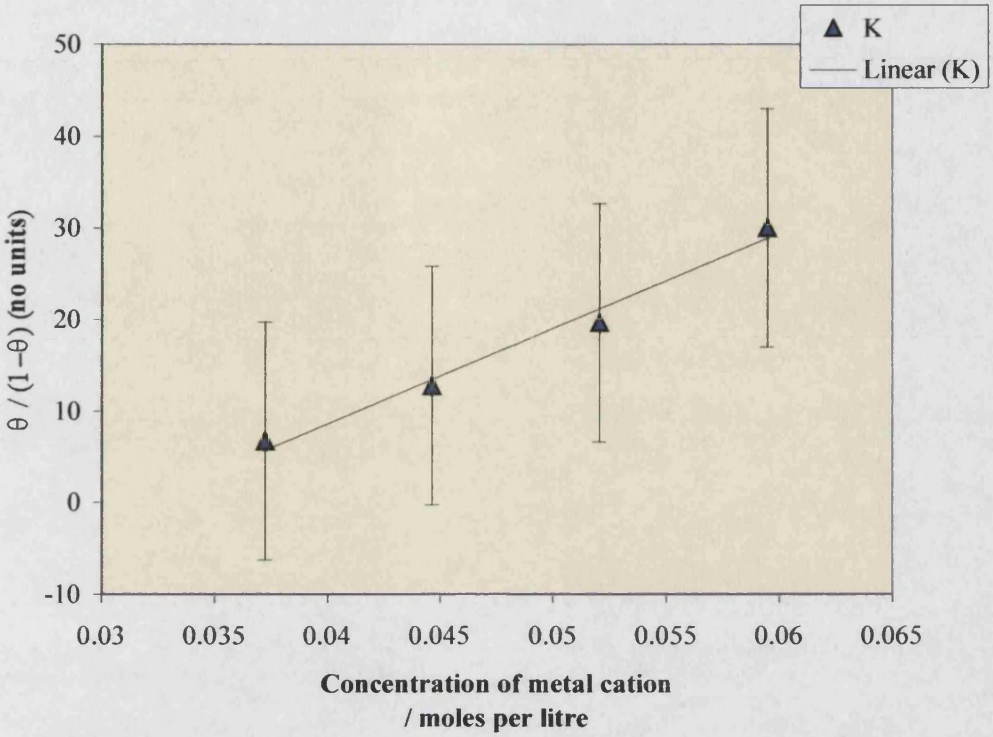

***Figure 3.41**: A plot of θ/(1- θ) against [$M^{+}_{(aq)}$] calculated from the data plotted in Figure 3.39. The gradient of the fitted line is 1033 $dm^3 mol^{-1}$.*

Method	K	Units
1, the bulk resin	1554 ± 617	$dm^3\ mol^{-1}$
2, response of sensor A	1033 ± 299	$dm^3\ mol^{-1}$

***Table 3.16**: Comparing the two values of the equilibrium constant K (from equation 26) calculated via two different experimental methods.*

3.12.6 Sensor lifetime

Experiments conducted on the bulk resin showed no significant loss in the uptake potential as a function of lifetime. The uptake conducted two years after the resin was first synthesised was the same as that of freshly prepared samples. Also repeated uptake experiments on the same sample of resin showed no loss in resin activity provided the resin was rinsed with pure water. However the response of the copolymer coated sensor showed a marked loss in activity after repeated exposure to $K^+_{(aq)}$ salts. This was most apparent after the saturation studies discussed in the previous section. All attempts to employ the sensor for further investigation resulted in a zero response after normalisation. A second copolymer coating was added to the sensor following identical procedures to those used in section 3.12.2, and the sensor response determined. The results can be seen in Figure 3.42.

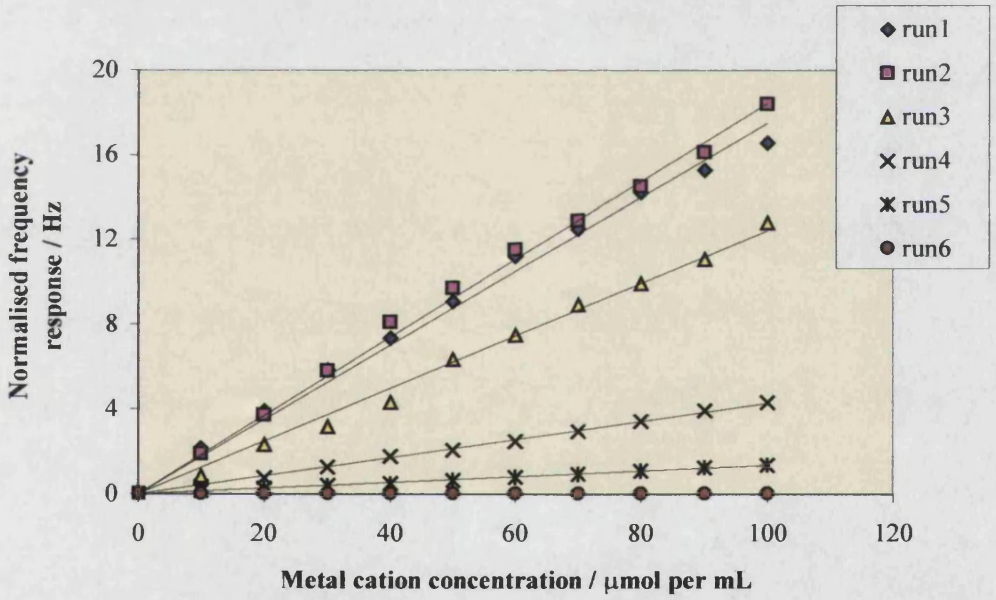

***Figure 3.42**: The response of sensor A after repeated exposure to $K^+_{(aq)}$ solution. Runs 1 and 2 were for the first coating. Runs 3, 4, 5 and 6 were conducted with the second coating.*

The first run with the second coating, run 3, followed the normal procedure. After this the sensor was soaked in a saturated $K^+_{(aq)}$ solution over night prior to the next run. This procedure was repeated for the subsequent runs and resulted in a zero response after three overnight soakings.

The loss in activity of the sensor was attributed to the permanent chelation of K^+ ions in the crown ether moieties of the copolymer layer. No conclusive evidence to support this could be obtained. The dry resonance frequency of the sensor in air shown no loss in mass of the sensor coating but could not be used to determine any increase in mass associated with the incorporated K^+. This was due to the small mass changes involved and the random fluctuation in the dry frequency. X-PES was used in an attempt to perform elemental mapping on the QCM surface. Although the technique could clearly show the presence of a carbon-based coating it was inconclusive as regards the potassium. Small peaks in the correct region of the spectra for K were present, however, these were very low in intensity, (see Appendix 5 for the spectra) and by no means definitive. The only conclusion that could be reached was that the copolymer coating was still intact and present on the sensor surface.

3.13 FIA Sensor Response

The FIA system was the second method employed to investigate the response of the sensor. The method differs from the batch studies in that the metal ion concentration is not progressively increased by successive injections of the stock solution. Rather a set volume of the stock solution is injected into a flow cell and exposed to the sensor. The time interval and maximum concentration for the exposure are determined by the flow speed and injection conditions of the system. The advantages of the flow system are that the injection process and the sensor exposure occur at different times allowing for a more detailed investigation of the early stages of the sensor response. This eliminates any perturbation to the resonance frequency by the injection mechanism itself. The method also allows the desorption process to be examined confirming the 'initial state' of the copolymer layer, whether loaded or unloaded.

A schematic representation of the FIA set-up can be seen in Figure 3.43. The metal cations are injected up stream of the sensor and carried down by the eluent flow. The eluent in this case was pure water. As the ions pass the QCM sensor a frequency shift occurs and is recorded by the data analysis system. Assuming no

metal ions are permanently adsorbed by the copolymer coating, once all the ions have passed the sensor the frequency of the QCM resonator returns to its initial state.

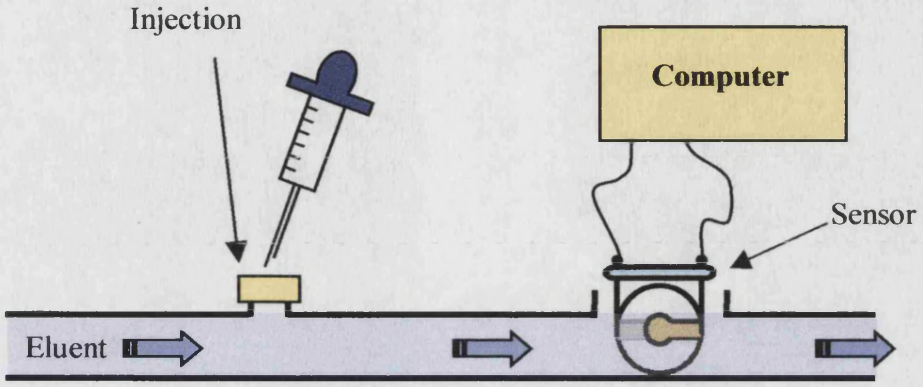

***Figure 3.43**: A schematic representation of the FIA system.*

Sensor Response

Sensors A, B and C were investigated by the FIA system with identical experimental procedures. After stabilisation of the sensor frequency in the flow system, known volumes of the metal ion solutions were injected. The onset of frequency changes corresponded to the expected time for the sample to reach the crystal surface. Examples of the elution peaks obtained for injections of $K^{+}_{(aq)}$ can be seen in Figure 3.44. On initial inspection no appreciable difference could be observed between the response of the uncoated sensor C, the nonfunctionalised copolymer coating sensor B, and the crown ether copolymer coating sensor A. This is the same as with the batch method. However on closer inspection and after the effectively removing the nonspecific response associated with the QCM resonator a clear $K^{+}_{(aq)}$ response can be determined.

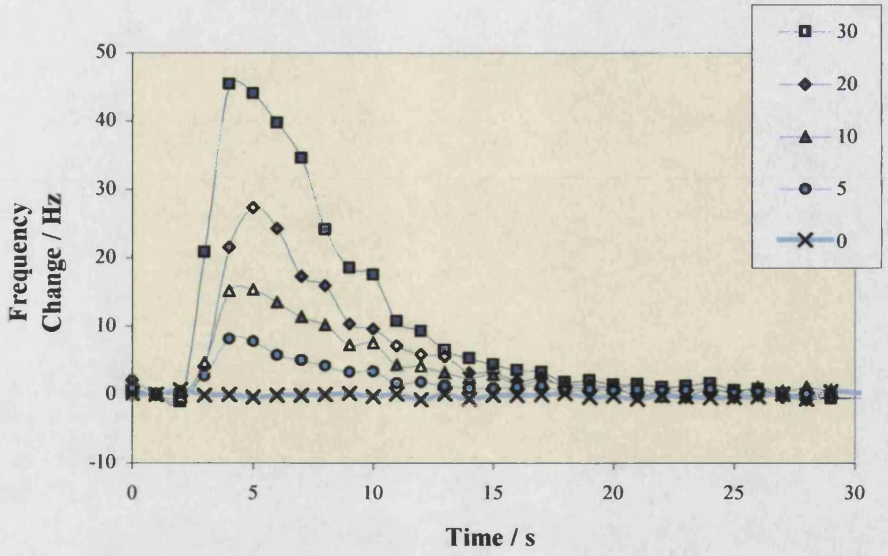

***Figure 3.44**: The response of sensor A to the injection of 0.230 moldm^{-3} $K^+_{(aq)}$ stock solutions. The numbers in the legend refer to μL volumes. The response profiles are representative for all three sensors responding to $Li^+_{(aq)}$, $Na^+_{(aq)}$, and $K^+_{(aq)}$.*

Again, as with the batch method a linear correlation was found between maximum peak height and the volume injected. The R^2 values for the linear regressions were 0.98-0.99 indicating an acceptable fit to the data. These can be seen in Figures 3.45, 3.46 and 3.47.

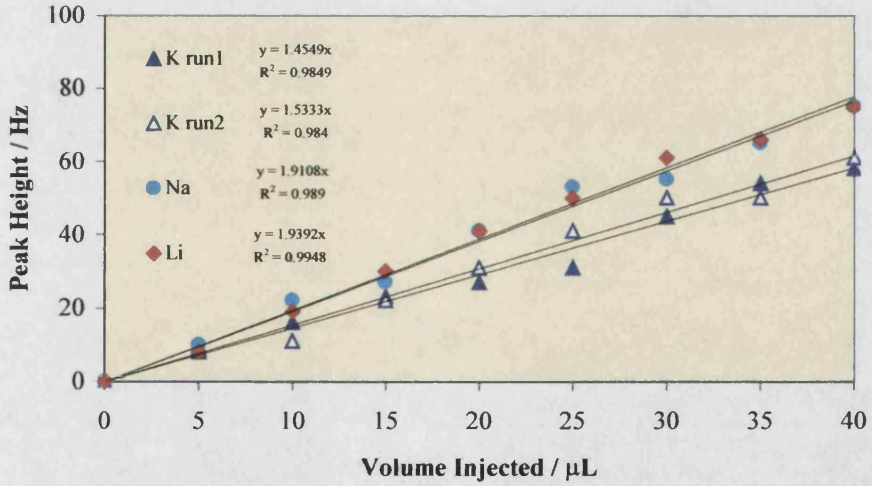

***Figure 3.45**: The response of sensor A to injection of 0.230 moldm^{-3} metal-cation stock solutions.*

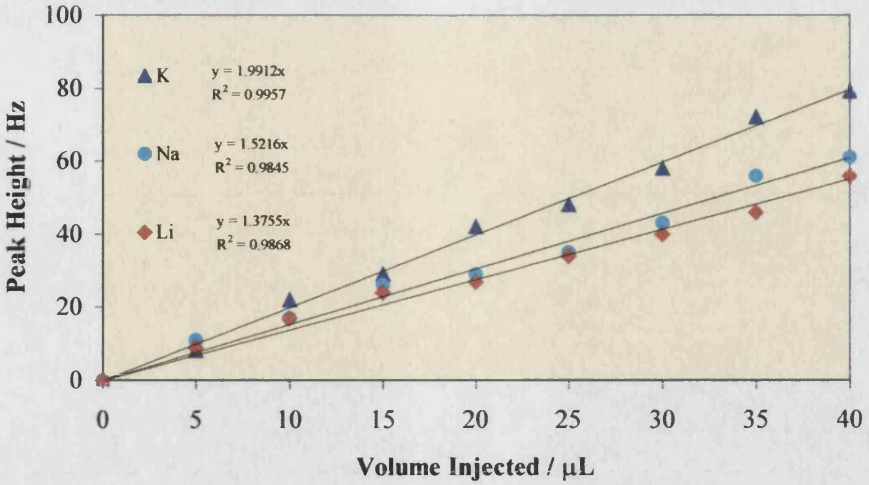

***Figure 3.46**: The response of sensor B to injection of 0.230 moldm^{-3} metal-cation stock solutions*

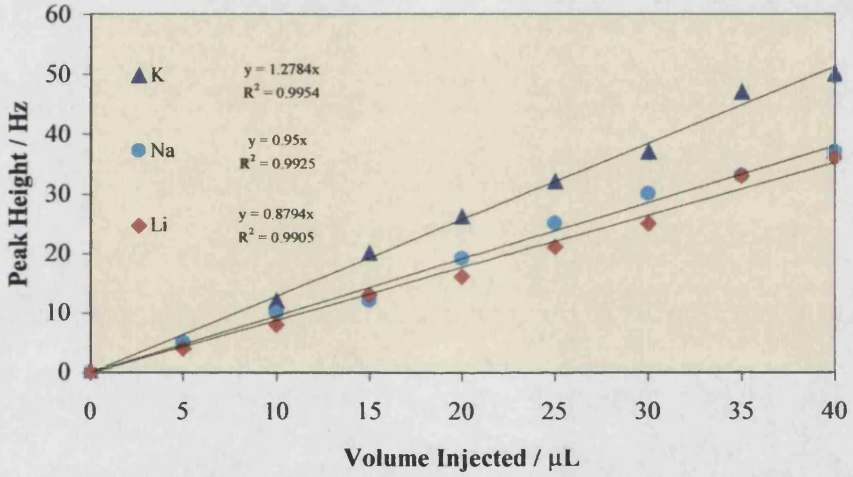

***Figure 3.47**: The response of sensor C to injection of 0.230 moldm^{-3} metal-cation stock solutions.*

The normalised results for the resonator coated with the copolymer containing no crown ether, (sensor B), are shown in Figure 3.48. The normalised response profiles of the crystal to $Li^+_{(aq)}$, $Na^+_{(aq)}$ and $K^+_{(aq)}$ were obtained and the crystal showed no uptake for any of the ions investigated. The same procedure was used to assess the response of the crown ether coated resonator (sensor A), the results being shown in Figure 3.49.

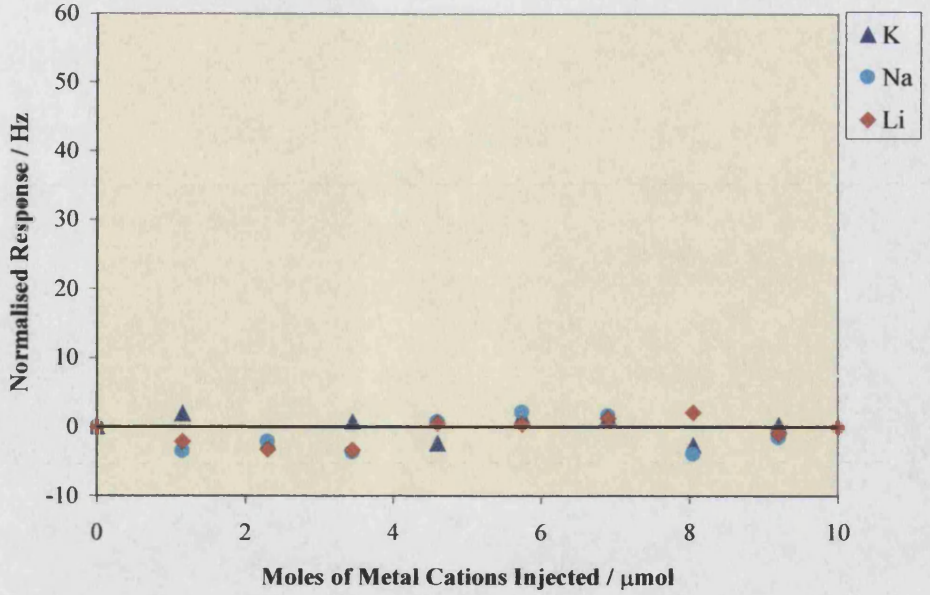

***Figure 3.48**: The normalised frequency response of sensor B to the injection of 0.230 moldm^{-3} metal ion stock solution into the FIA flow.*

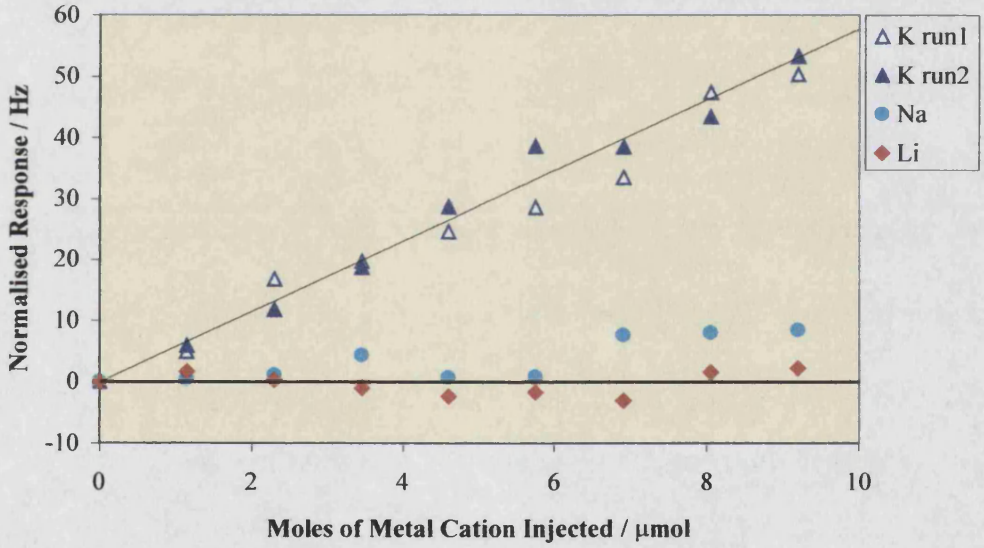

***Figure 3.49**: The normalised frequency response of sensor A to the injection of 0.230 moldm^{-3} metal ion stock solution into the FIA flow.*

It can been seen that the coating induced a small response to $Na^+_{(aq)}$ and a much larger response to $K^+_{(aq)}$ (with respect to $Li^+_{(aq)}$). This indicates a high degree of selectivity for $K^+_{(aq)}$. From the slope of the plot, a response factor of 5.77 Hz µmol^{-1} can be calculated. Taking into account the dilution in the FIA system, this gives an estimated sensitivity of 0.04 ppm for the current system.

3.14 Conclusion

3.14.1 Copolymer Synthesis

Two crown ether monomers were synthesised, acrylamidomethyl-18-crown-6 and acrylamidomethyl-15-crown-5. These monomers were utilised to produce a series of crown ether containing copolymers. This was achieved by the free-radical addition polymerisation of solutions containing acrylic acid, EGDMA and the crown ether monomers in acetontirile.

Two crown ether containing copolymers were synthesised. Poly(acrylic acid)-(arcylamidomethyl-15-crown-5) and poly(acrylic acid)-(acrylamidomethyl-18-crown-6). The copolymers were synthesised via free-radical addition polymerisation in DMF initiated by AIBN and subjected to ^{1}H-NMR, ^{13}C-NMR, FTIR, GPC and CHN elemental analysis. The crown ether loading was shown to be 18 % and 17 % respectively. The poly(methylmethacrylate) equivalent molecular weights were 1.04 x 10^{6} and 8.40 x 10^{5} g mol^{-1} respectively.

3.14.2 Copolymer Uptake Properties

The uptake properties of the copolymer system were determined via the EGDMA cross-linked resin. Both the 15-crown-5 and the 18-crown-6 resins selectively uptake $K^{+}_{(aq)}$ over the Group I metal ions $Li^{+}_{(aq)}$ and $Na^{+}_{(aq)}$. The crown ether content of the resins were calculated by CHN elemental analysis, these were found to vary between 8 % and 13 % w/w. The uptake of the resins for $K^{+}_{(aq)}$ was in the order of 1000 μg per gram of the resin and the response time was less than 60 seconds. The equilibrium constant for the crown ether complex formation with $K^{+}_{(aq)}$ was calculated by application of a Langmuir type isotherm, this was found to be 1554 ± 617 $dm^{3}mol^{-1}$.

3.14.3 Sensor Systems

System One: The Non Cross-linked Copolymer

The copolymer was chemically attached to the surface of the gold electrode on the QCM resonator via an amine functional SAM. This is apparent from the frequency changes associated with the various steps involved during the fabrication of the sensor. The film did not dissolve in water or DMF and remained intact throughout the experimental studies that followed. However, the coated resonator showed no response to any of the Group I ions. This is believed be as a result of the thermal degradation of the crown ether macrocycles during the sensor fabrication. The results of the DSC studies on both the copolymers and the 18c6/70 cross-linked resin confirm that the heating of the copolymers to temperatures above 130 °C induces a physical and chemical change within the copolymer network. The uptake studies performed on the heated resin 18c6/70 confirmed that this change reduces the binding potential of the copolymer towards $K^{+}_{(aq)}$.

The actual chemistry of this thermal degradation is difficult to investigate. The free crown ether rings are considered to be thermally stable at temperatures below 164 °C as the dibenzo-18-crown-6 compound has a melting point of 162-164 °C [279]. Any thermal degradation of the copolymer would be expected to involve the elimination of $CO_{2\,(g)}$ from the carboxylic acid groups. This would result in the reduction of the hydrophilic nature of the copolymer and so reduce the crown ether metal ion interaction. The heated resin did show evidence to support this; on immersion in water the resin at first repels the water with very limited resin-water interaction. However, after several hours the heated resin becomes fully immersed in the water in a similar fashion to the original 'unheated' resin. This hydrophobic effect would be greater in the copolymer system. The resin contains 70 % EGDMA which itself contributes substantial hydrophilic character. The presence of the T_g also indicates that the copolymer remains essentially uncross-linked. A fully cross-linked interconnected copolymer network displays no glass transition temperature, as can be seen in the DSC of the 18-crown-6 resin, Appendix 1 Figure A1.2.

Further work is required on this thermal degradation to establish the mechanism involved and the consequence of this on the coating process. A useful

investigation would be the mass spectroscopy or FTIR study of the vapour emitted during the DSC heating and the DSC of the aminomethylcrown ether starting material.

System Two: The Cross-linked Resin

The 18-crown-6 resin 18c6/30 was successfully synthesised on the surface of a QCM resonator with the selectivity over other Group I ions maintained. In this case the Langmuir based absorption isotherm utilised previously showed poor linear correlation, however, the equilibrium constant was calculated to be 1033 ± 299 dm^3mol^{-1}. An improved absorption model could be obtained using the Freundlich isotherm.

The resulting resonator was employed as a $K^+_{(aq)}$ chemical sensor. The lifetime of the sensor appeared to be limited when exposed to saturated salt solutions, however, when used to analysis solutions in the concentration range below 1000 ppm no loss in activity was observed. The sensitivity of the sensor was estimated to be 0.2 ppm over the concentration range of 0-2000 ppm. This should be considerably improved upon in future sensor fabrications. The sensor was also used in an FIA system to monitor the concentration of $K^+_{(aq)}$ injected into the flow.

The commercial implications of the sensitivity and operational range are discussed in the final conclusions at the end of this thesis.

GAS PHASE QCM-BASED

CHEMICAL SENSORS

CHAPTER FOUR

4.1 Introduction

Research conducted in the field of QCM based gas-phase chemical sensors is well established. For a review of the historical development in this area and some of the more recent applications see sections 1.6-1.9. The QCM affords a cheap reliable and sensitive transducer for such devices and has been successfully utilised to produce selective chemical sensors operating in the gas-phase. Unlike the liquid phase applications discussed in the previous chapter the theoretical understanding of the gas-phase oscillation of a QCM resonator is well understood. The reader is referred to Chapter One for a more detailed account of this theoretical understanding. The important point being that the gas-phase application of the QCM is more stable and more reliable than the equivalent liquid phase.

This chapter details two applications of the QCM operating as a gas-phase chemical sensor. These are as a general organic vapour sensor and as a specific gas sensor designed to respond selectively to a target species. The organic vapour sensor is based on the interaction of a cyclodextrin surface layer with a variety of organic vapours, specifically alcohols. The work focuses on the general response of α-cyclodextrin, β-cyclodextrin, and amylose coated resonators, the response characteristics imparted by the cyclodextrin structure and their potential in the field of selective chemical sensors. The final sensor envisaged would consist of an array of individual QCM resonators coated with different materials. The sensor would function as a general VOC sensor in both liquid and gas phases. For such devices the sensor coatings are required to respond to a variety of compounds with differing signals, the overall response of the array forming a finger print for a particular compound or mixture of compounds.

The specific gas sensor utilises an azobenzene dye developed primarily as a coating for optical NO_x gas sensors. The QCM is used as an alternative transducer for the material and looks at the binding kinetics and response factors of the QCM system.

4.2 Cyclodextrin Coated QCM Sensors

Cyclodextrins are amylose structures with well-documented host-guest interactions. The versatility of the macrocycle lies in the simple glucose repeat-unit. This forms the basic building block of all the cyclodextrin species. The chemistry of the glucose unit is has been extensively investigated and this can be easily translated to perform simple chemical modifications on the larger cyclodextrin molecules [280]. For example the three different hydroxyl groups on the rim of the cavity allow for the selective chemical transformation of both the upper and lower rims [281]. Such modifications alter the interaction parameters of the cyclodextrin cavity and can be used to tailor the response of the final sensor. The aim of the current work is to investigate the potential of the cyclodextrin-QCM system for application as both gas-phase sensors and liquid phase sensors. Previous work has been published on the application of several derivatised cyclodextrin-QCM sensors [282]. However, no published data could be found relating to similar systems utilising the underivatised macrocycle. Also the systems discussed in the literature are only applied to the gas-phase application and no record could be found for similar liquid phase systems. For these reasons the response of a QCM resonator coated with a surface layer of underivatised cyclodextrin molecules to volatile organic vapours was chosen as an initial study. This was with the view to developing more selective systems and applying these to both liquid and gas phase applications.

The response studies utilised four resonators. These were an α-cyclodextrin coated resonator, a β-cyclodextrin coated resonator, a resonator coated with a linear amylose and a blank resonator with no coating, resonators 1, 2, 3 and 4 respectively. The chemical structure of the three coatings can be seen in Figure 4.1. The solvents interact with the resonator surface via several mechanisms, for example van der Waals forces, dipole-dipole interactions and hydrogen bond interactions [283]. The pre-formed cyclodextrin cavity offers a binding site that can maximise these interactions and provide both hydrophobic and hydrophilic stabilisation. The inner cavity is predominantly hydrophobic and the outer rims hydrophilic. For compounds that are stabilised by the type of interactions available in the cyclodextrin molecule the pre-formed cavity offers improved binding sites. The orientation of the functional groups, focusing towards the central void and the three-dimensional encapsulation of

any molecule placed within the cavity enables a greater interaction to occur between the cyclodextrin surface and the passing VOC. Amylose is the linear equivalent of the cyclodextrin molecules and as such provides identical surface interaction with the solvent vapours, however, these exclude those interactions associated exclusively with the preformed cavity. For this reason an amylose coated resonator was employed as the experimental control. The response of this will be representative of the non-specific interactions associated with the VOCs and the glucose-type surface.

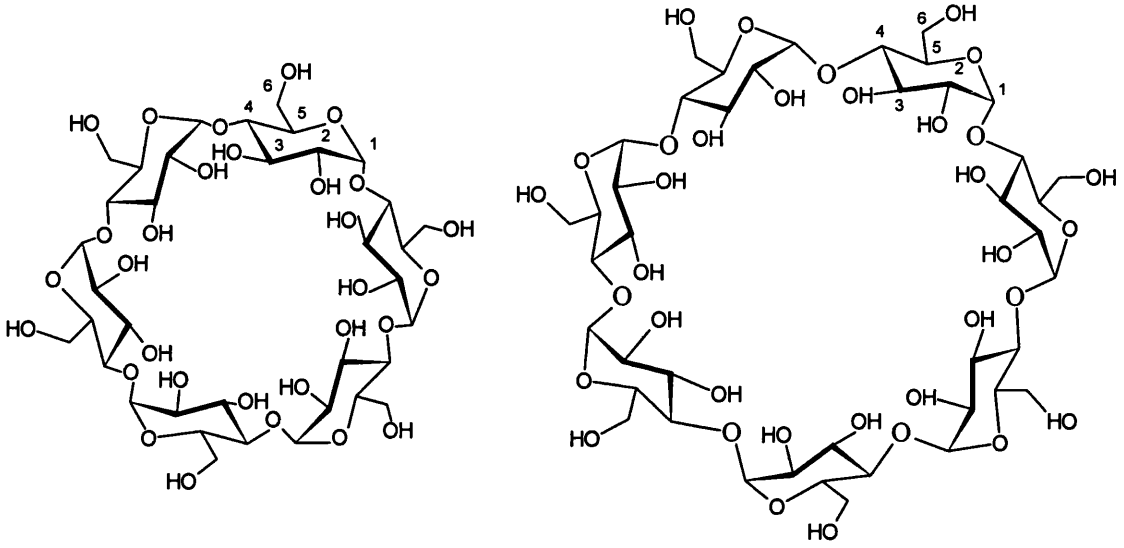

α-cyclodextrin

β-cyclodextrin

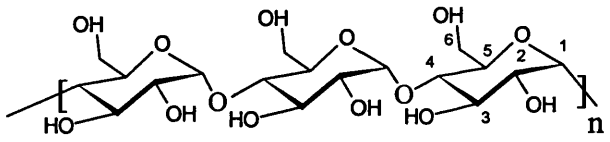

amylose

Figure 4.1: The structure of α-cyclodextrin, β-cyclodextrin and amylose.

4.2.1 Coating the Resonators

The resonators were coated by using the dropping technique [284]. 1 μl of a 1 mmol dm^{-3} aqueous solution of the cyclodextrin compound was placed onto the resonator surface. The drop was then allowed to evaporate in air, depositing the cyclodextrin and coating the resonator. The procedure was repeated twice, once on either face of

the resonator. The resonance frequency of the QCM could be used to monitor the deposition process. A typical frequency-time plot can be seen in Figure 4.2. The frequency of the resonator is recorded in air, after approximately 10000 seconds the copolymer solution is placed on the surface. This induces an instant frequency shift of about 6 kHz. As the solution dries the resonance frequency returns to a value greater than the initial frequency, approximately 3 kHz. This difference in the dry frequencies is proportional to the mass of the copolymer deposited.

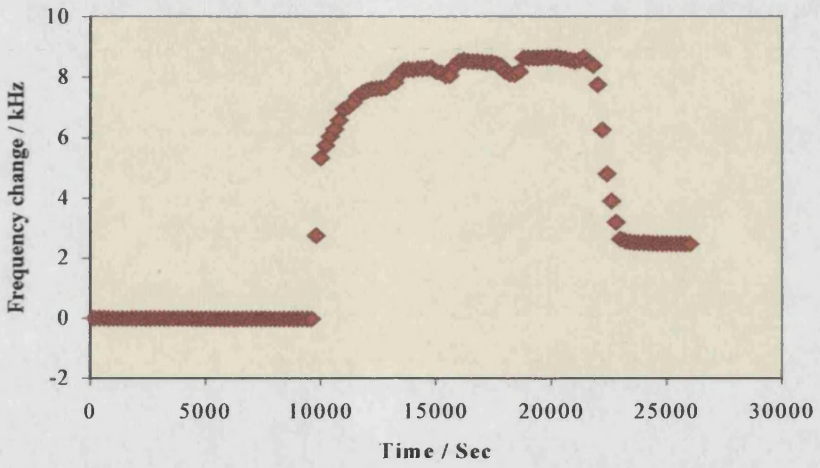

***Figure 4.2**: A typical frequency change profile for the deposition of a resonator coating using the dropping technique.*

It can be seen from the graph in Figure 4.2 that the deposition results in a permanent frequency change in the resonator. This frequency change can be used as an indication of the presence of the coating. Any change in the coating such as a loss of material will result in a change in this frequency.

The amylose coating was prepared from an aqueous solution of the same mass concentration as the β-cyclodextrin solution. The average molar mass of the amylose chain was unknown, however, by using the same mass of the dry amylose as the β-cyclodextrin the concentration of the glucose repeat units will be the maintained. The total frequency change and mass deposited for each resonator can be seen in Table 4.1.

Resonator	Coating	Frequency change / Hz	Mass / μg
1	α-cyclodextrin	3521 ± 60	2.46 ± 0.04
2	β-cyclodextrin	3799 ± 40	2.66 ± 0.03
3	amylose	1980 ± 60	1.39 ± 0.04
4	No coating	-	-

***Table 4.1**: The frequency change and mass deposited during the resonator coating. The mass was calculated from the Sauerbrey equation [285]*

The deposition resulted in a visible tarnish of the resonator surface. It was noted that the use of more concentrated solutions (effectively increasing the mass deposited) caused instabilities in the resonator oscillation. It also resulted in the formation of visible crystallites on the resonator surface. However with the concentrations used and the mass deposited the resonator oscillation was stable.

Once coated the resonators were mounted in a PTFE flow-cell. The flow-cell contained a reference and a working resonator with the difference between the two being the frequency measured. For more detail on the flow system see section 2.8.

4.3 Response to VOCs

The injection of the volatile organic compounds (VOCs) into the gas stream resulted in a frequency shift in the sensor. As the vapour passed through the flow-cell the frequency difference of the sensor compared to a reference increased. This difference returned to the original value after the vapour dissipated. An example of a frequency / time plot can be seen in Figure 4.3.

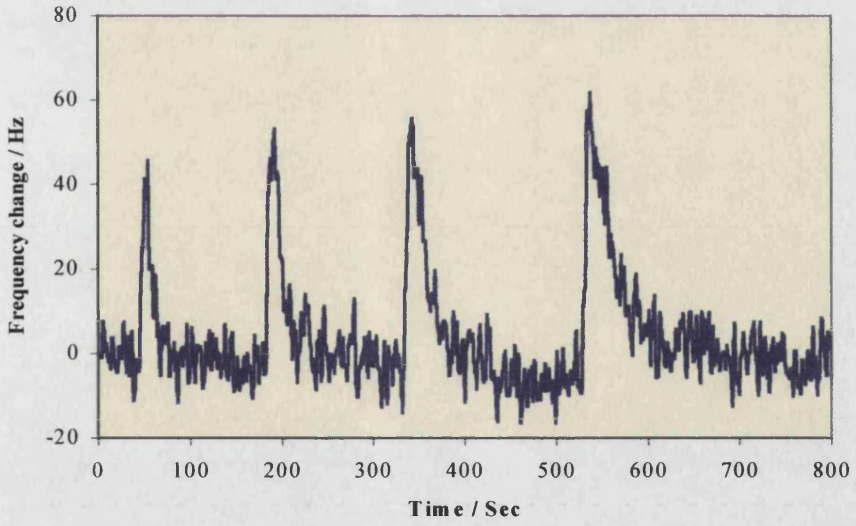

***Figure 4.3**: The response of resonator 2 to the injection of methanol. The injections were of 0.2, 0.4, 0.6 and 0.8 μl after about 30, 180, 300 and 510 seconds.*

A linear correlation was obtained between the peak area and the volume of methanol injected. The peak area was calculated using the trapezium rule [286]. This is considered appropriate as the peaks are composed of a series of frequency readings at one-second intervals. Consequently the peak-area is divided into roughly 40 segments. The trapezium rule gives a value of within 95 % for the peak area when the peak is segmented into 4 parts; this accuracy increases with further segmentation. Consequently the values obtained for the peak areas will be within in an acceptable uncertainty. The regression analysis results can be seen in Tables 4.2, 4.3 and 4.4. The response graphs can be seen in Figures 4.4, 4.5 and 4.6.

Resonator 1 α-cyclodextrin coated			
Solvent injected	**Regression analysis results**; Y = MX + C		
	M / Hz Sec μl^{-1}	**C / Hz Sec**	**R^2**
Methanol	4193.2	188.97	0.9832
Acetone	208.4	-0.80	0.9733
Chloroform	103.4	-16.23	0.9810
Hexane	142.3	-26.37	0.9806
Toluene	454.8	-47.58	0.9595

***Table 4.2**: The response factors of the resonator 1 to a series of volatile organic compounds.*

Resonator 2 β-cyclodextrin coated			
Solvent injected	**Regression analysis results**; Y = MX + C		
	M / Hz Sec μl^{-1}	**C / Hz Sec**	**R^2**
Methanol	2394.6	264.61	0.9954
Acetone	473.2	50.70	0.9832
Chloroform	706.3	-111.49	0.9814
Hexane	-64.7	42.47	0.354
Toluene	32.9	-23.92	0.0783

***Table 4.3**: The response factors of resonator 2 to a series of volatile organic compounds.*

Resonator 4 no coating			
Solvent injected	**Regression analysis results**; Y = MX + C		
	M / Hz Sec μl^{-1}	**C / Hz Sec**	**R^2**
Methanol	32.7	556.4	0.8448
Acetone	28.3	210.0	0.9087
Chloroform	19.6	-66.0	0.9724
Hexane	13.3	-38.7	0.9925
Toluene	82.7	-437.4	0.9863

***Table 4.4**: The response factors of resonator 4 to a series of volatile organic compounds.*

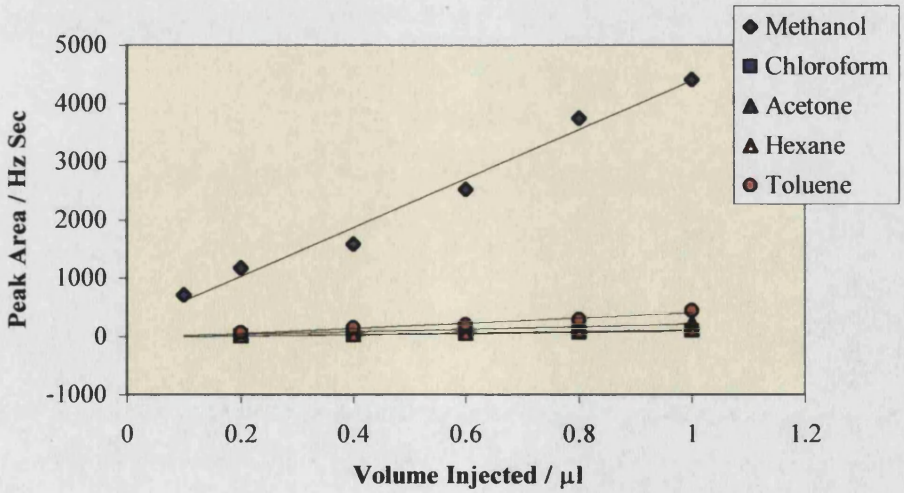

***Figure 4.4**: The response of α-CD coated resonator 1 to the injection of several volatile organic compounds.*

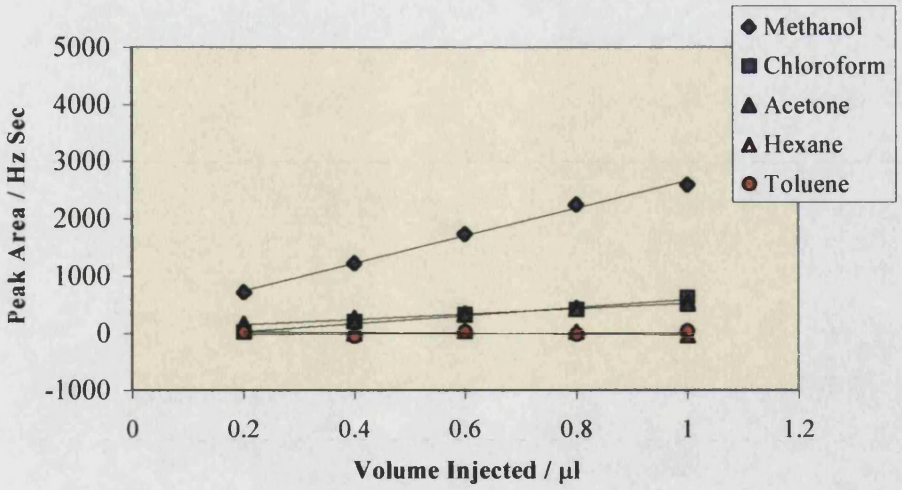

***Figure 4.5**: The response of β-CD coated resonator 2 to the injection of several volatile organic compounds.*

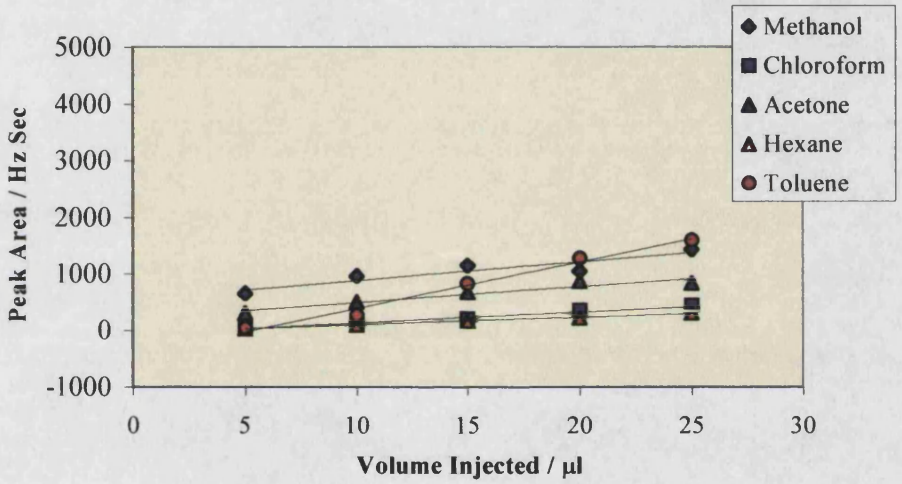

***Figure 4.6**: The response of the uncoated resonator 4 to the injection of several volatile organic compounds.*

The response of uncoated resonator 4 was too small to be determined with a volume range up to 1 µl so the injected range was increased to 25 µl. The gradients of the linear regression analysis are referred to as the response factors. These can be used to compare the response of each resonator to the particular VOC. However, for this comparison to be meaningful when compared to different VOCs the gradient must first be converted to a mass value, i.e. from Hz Sec μl^{-1} to Hz Sec μg^{-1}. The converted factors can be seen in Tables 4.5, 4.6, 4.7 and 4.8. The data can be seen plotted in Figures 4.7.

Resonator 1 α-cyclodextrin coated			
Solvent injected	**Regression analysis results; Y = MX + C**		
	M / Hz Sec μg^{-1}	**C / Hz Sec**	**R^2**
Methanol	5.30	188.97	0.9832
Acetone	0.26	-0.80	0.9733
Chloroform	0.07	-16.23	0.9810
Hexane	0.22	-26.37	0.9806
Toluene	0.52	-47.58	0.9595

***Table 4.5**: The response factors of resonator 1 to a series of volatile organic compounds. M expressed in terms of Hz Sec μg^{-1}.*

Resonator 2 β-cyclodextrin coated			
Solvent injected	**Regression analysis results; Y = MX + C**		
	M / Hz Sec μg^{-1}	**C / Hz Sec**	**R^2**
Methanol	3.03	264.61	0.9954
Acetone	0.60	50.70	0.9832
Chloroform	0.48	-111.49	0.9814
Hexane	-0.10	42.47	0.354
Toluene	0.04	-23.92	0.0783

***Table 4.6**: The response factors of resonator 2 to a series of volatile organic compounds. M expressed in terms of Hz Sec μg^{-1}.*

Resonator 3 amylose coated [287]			
Solvent injected	**Regression analysis results; Y = MX + C**		
	M / Hz Sec μg^{-1}	**C / Hz Sec**	**R^2**
Methanol	0.69	-746.5	0.9589
Acetone	0.23	-501.5	0.9843
Chloroform	0.05	188.55	0.9609
Hexane	0.09	0.343	0.9823
Toluene	0.25	-71.0	0.9378

***Table 4.7**: The response factors of resonator 3 to a series of volatile organic compounds. M expressed in terms of Hz Sec μg^{-1}.*

Resonator 4 no coating			
Solvent injected	**Regression analysis results; Y = MX + C**		
	M / Hz Sec μg^{-1}	**C / Hz Sec**	**R^2**
Methanol	0.04	556.4	0.8448
Acetone	0.04	210.0	0.9087
Chloroform	0.01	-66.0	0.9724
Hexane	0.02	-38.7	0.9925
Toluene	0.10	-437.4	0.9863

***Table 5.8**: The response factors of resonator 4 to a series of volatile organic compounds. M expressed in terms of Hz Sec μg^{-1}.*

4.3.1 Discussion

The response factor M represents the extent of the interaction of the resonator with the passing vapour. The higher the number the greater the interaction. It takes into account the molar mass of the passing eluent so that direct comparison can be drawn between its value and the extent of the solvent interaction with the amylose and cyclodextrin surface. The conversions from liquid volume to mass are necessary as the injection of the solvents with a constant liquid volume results in different molar quantities, and therefore a different concentration of the vaporised solvent in the gas streams. The QCM responds predominantly to mass changes. If the solvents were injected with a constant molar quantity then, assuming each solvent vapour interacts equally with the resonator, the response factor would be proportional to the molar mass, i.e. a greater response would be expected for a heavier species. By converting the response factor to a molar quantity and then dividing through by the molecular mass of each solvent the true interaction parameter can be found and these compared to develop an understanding of the effect each coating has on the overall resonator response. The data is displayed graphically in Figure 4.7.

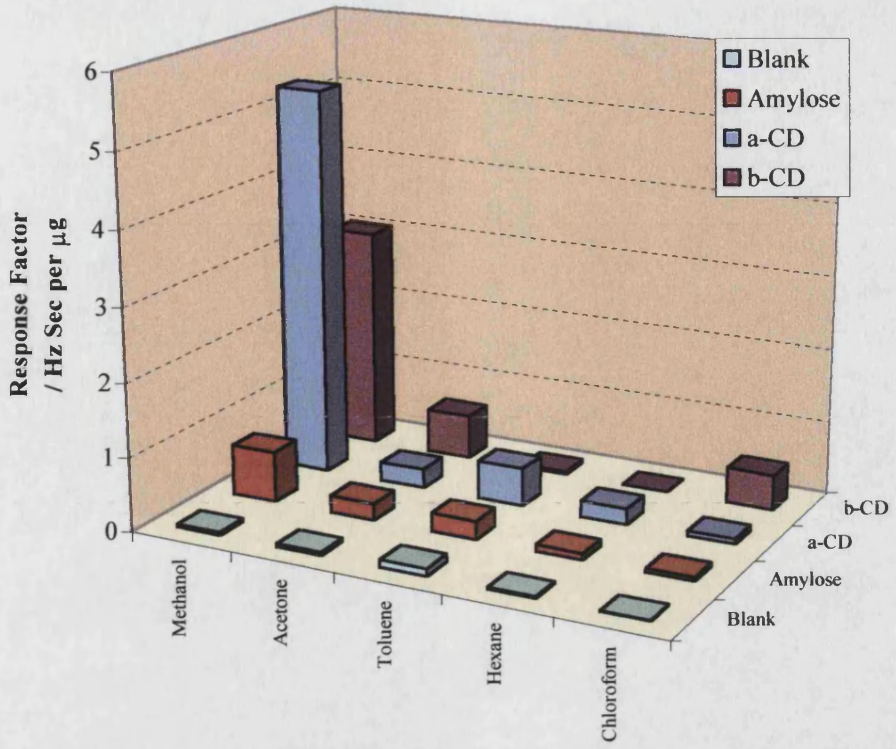

***Figure 4.7**: The response factors of the four resonators to VOCs. The data is shown in Tables 4.5, 4.6, 4.7 and 4.8.*

It can be seen in Figure 4.7 that the uncoated resonator 4 had no significant response to any of the VOCs used during these experiments. When the volume injected was increased by a factor of 25 some frequency shift in the resonator was observed, however, compared to the cyclodextrin-coated resonators this value was insignificant. The same results were obtained for the amylose-coated resonator 3. Simona Negro [287] obtained the data for the VOC response of this resonator. She also conducted similar experiments with the cyclodextrin-coated resonators, injecting volumes in the range 5-25 µl as opposed to the 1 µl range used previously. Her initial results reflected those presented here although the data have yet to be fully analysed

The two cyclodextrin-coated resonators 1 and 2 had a marked deviation in their response pattern. This change was dominated in both cases by the large methanol response. This response increase is related to the cyclodextrin cavity. The methanol can form hydrogen-bonds with the hydroxyl groups associated with the glucose repeat unit. However the same hydrogen-bonds can form with the amylose coating and in the case of the amylose resonator these interactions do not lead to such a high frequency shift. The cavity of the cyclodextrin ring adds a second factor

to the interaction potential. The hydrophobic cavity can stabilise the methyl group of the alcohol. This dual interaction and pre-formed binding site offer extra input to the overall stabilisation energy increasing the extent of the methanol interaction and so increasing the response of the resonator. The same arguments account for the slight loss in resonator response of the β-cyclodextrin coating compared to the α-cyclodextrin coating. The larger cavity offers less interaction parameters than the smaller cavity, lowering the methanol binding energy and lowering the resonator response. The volume of the cyclodextrin cavities are estimated at 174 $Å^3$ and 262 $Å^3$ for the α-cyclodextrin and β-cyclodextrin respectively [288].

The response factor associated with the cyclodextrin cavity can be represented by the overall response factor of resonators 1 and 2 minus the response of resonator 3. The amylose coating offers the VOC vapour the same binding sites and interaction energies as the cyclodextrin coating except with out those associated with the cyclodextrin cavity. The cavity response factors can be seen plotted in Figure 4.8.

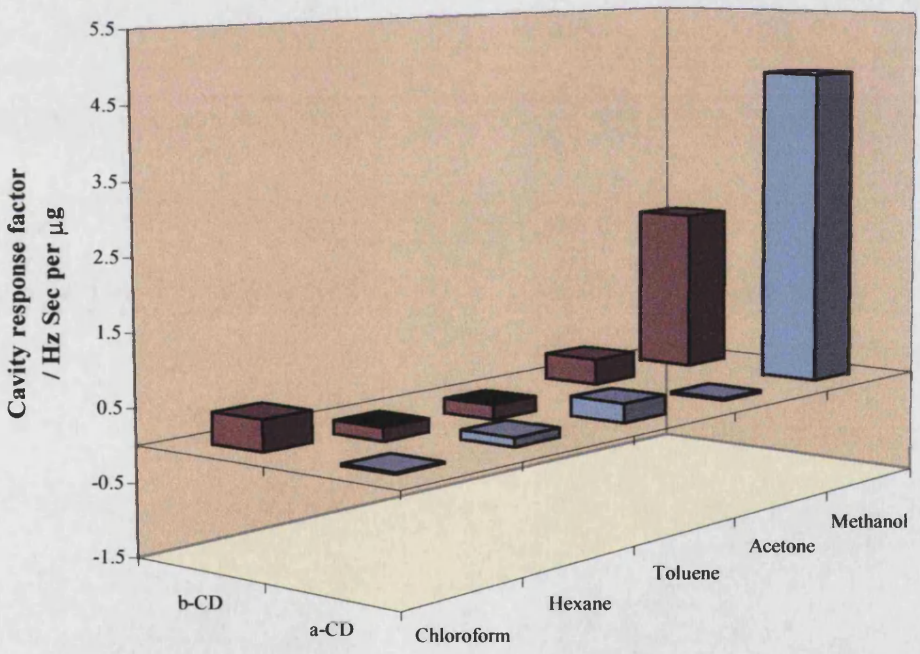

***Figure 4.8**: The response factors of the cyclodextrin cavities. The data is obtained from Table 4.5-4.8.*

Both the cyclodextrin-coated resonators respond selectively for methanol over the other VOCs studied. The response factors quoted neglect the effect of the solvent vapour pressure, however, the amylose-coated resonator had no response to any of the VOCs. This implies that the vapour pressure effects can be assumed to have only a minimal contribution to the overall resonator response.

4.4 Response to Alcohols

Following the observation that methanol interacts strongly with the cyclodextrin a more detailed investigation of a series of alcohols was conducted. The aim was to determine the effect of increasing the carbon chain and the overall size of the alcohol molecule, to observe any steric effect associated with increasing the molecular volume. The same experimental conditions were used as the previous section. The alcohols used were methanol, ethanol, propanol and butanol, as well as the branched isomers of propanol and two of the branched isomers of butanol.

Results

As with the previous study a linear correlation was found between the peak area and the volume injected. This can be seen in the three graphs plotted in Figures 4.9, 4.10 and 4.11. The results of the regression analysis can be seen in Tables 4.9, 4.10 and 4.11.

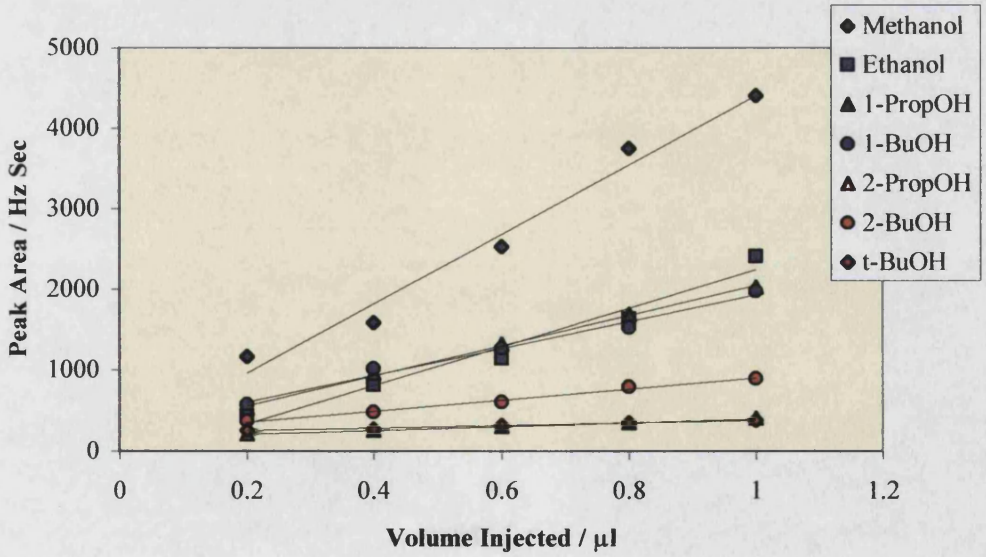

***Figure 4.9**: The response of resonator 1 to the injection of a series of alcohols.*

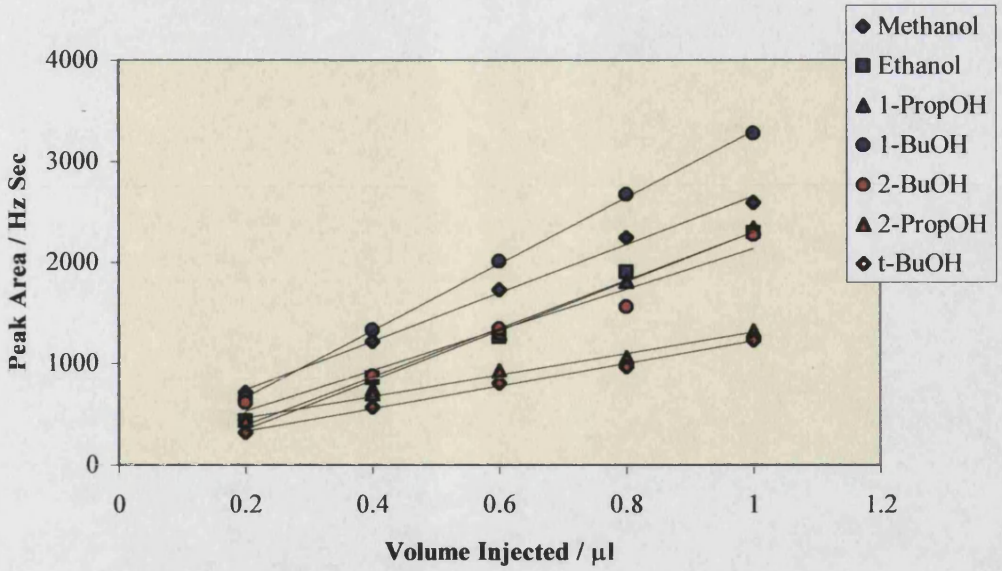

***Figure 4.10**: The response of resonator 2 to the injection of a series of alcohols.*

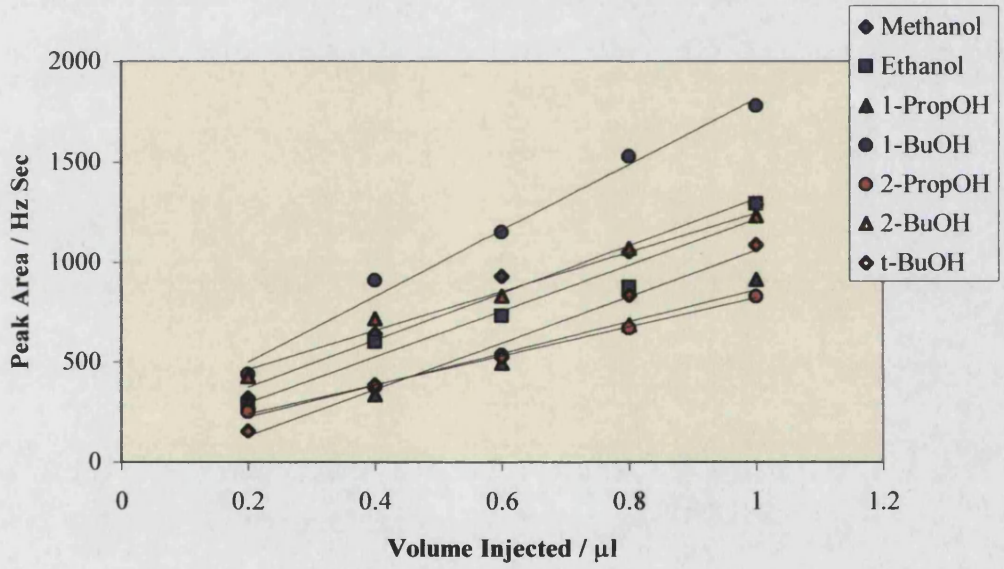

***Figure 4.11**: The response of resonator 3 to the injection of a series of alcohols.*

In order to compare the response of the resonators to each alcohol the response factors (the gradients of the graphs listed in Tables 4.9, 4.10 and 4.11), were again converted to mass values. The unconverted values are listed in Appendix 6, Tables A6.1, A6.2 and A6.3.

Resonator 1 α-cyclodextrin coated			
Solvent injected	**Regression analysis results; Y = MX + C**		
	M / Hz Sec μg^{-1}	**C / Hz Sec**	**R^2**
Methanol	5.45	98.3	0.9781
Ethanol	3.02	-141.8	0.9680
1-Propanol	2.31	189.7	0.9982
1-Butanol	2.04	279.6	0.9862
2-Propanol	0.31	160.8	0.9980
2-Butanol	0.84	224.2	0.9910
t-Butanol	0.18	221.8	0.9824

***Table 4.9**: The response factors for resonator 1 (in mass values) to a series of alcohols.*

Resonator 2 β-cyclodextrin coated			
Solvent injected	**Regression analysis results; Y = MX + C**		
	M / Hz Sec μg^{-1}	**C / Hz Sec**	**R^2**
Methanol	3.03	264.6	0.9954
Ethanol	3.02	-77.3	0.9930
1-Propanol	3.02	-131.0	0.9922
1-Butanol	4.07	12.2	0.9996
2-Propanol	1.34	258.7	0.9901
2-Butanol	2.47	138.1	0.9638
t-Butanol	1.24	116.0	0.9951

***Table 4.10**: The response factors for resonator 2 (in mass values) to a series of alcohols.*

Resonator 3 amylose coated			
Solvent injected	**Regression analysis results**; Y = MX + C		
	M / Hz Sec μg^{-1}	**C / Hz Sec**	**R^2**
Methanol	1.48	142.9	0.9776
Ethanol	1.45	71.2	0.9563
1-Propanol	0.99	69.8	0.9537
1-Butanol	2.03	171.7	0.9882
2-Propanol	0.92	98.5	0.9984
2-Butanol	1.21	267.1	0.9857
t-Butanol	1.29	-95.8	0.9876

***Table 4.11**: The response factors for resonator 2 (in mass values) to a series of alcohols.*

4.4.1 Discussion

It can be seen in Figure 4.12 that the control resonator 3, coated with amylose, displays no selectivity. The response factors are within ± 0.5 Hz Sec μg^{-1} for all seven alcohols. The interaction of the alcohol vapour would be predicted to vary slightly with vapour pressure and hydrogen-bonding capability. By contrast the two cyclodextrin coatings have very different response factors. The general trend is of an increase in the straight chain alcohols response and no change in the branched alcohol response. Also the larger β-cyclodextrin ring has an increased response compared to the α-cyclodextrin.

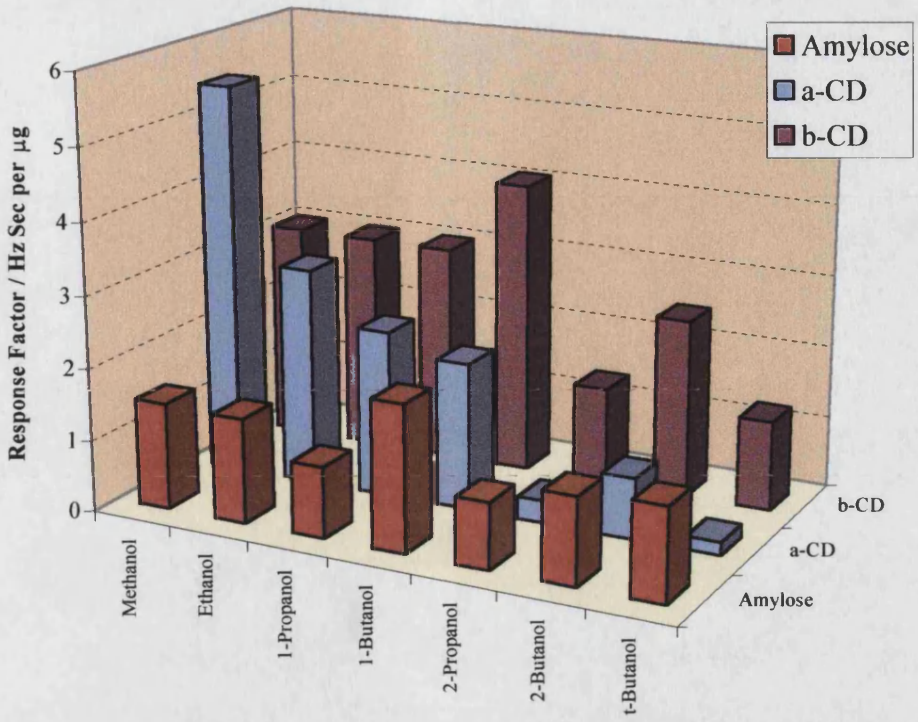

***Figure 4.12**: Comparison of the response factors for resonators 1, 2 and 3. The data are obtained from Tables 4.9-4.11.*

With respect to the straight chain alcohols the α-cyclodextrin resonator has an increase in response compared to the amylose coated resonator of 3.97, 1.57 and 1.32 Hz sec μg^{-1}. These values are for methanol, ethanol and propanol respectively. There was no difference in response to butanol. This suggests that the three shorter chain alcohols bind within the cavity of the cyclodextrin ring with a greater interaction for the smaller species. The enhanced methanol sensitivity can be attributed to the size compatibility of the methanol molecule with the cyclodextrin cavity. The zero response for the larger butanol molecule suggests that this interacts with the coating at sites external to the central cavity.

The α-cyclodextrin resonator displays an overall fall in response to the three branched isomers with the largest drop for the sterically hindered *t*-butanol molecule. This is consistent with the view that the branched molecules can not interact with the internal cavity and so the total available binding sites will be lower for the α-cyclodextrin coating compared to the linear amylose coating. The response factors associated with the cyclodextrin cavity can be seen in Figure 4.13.

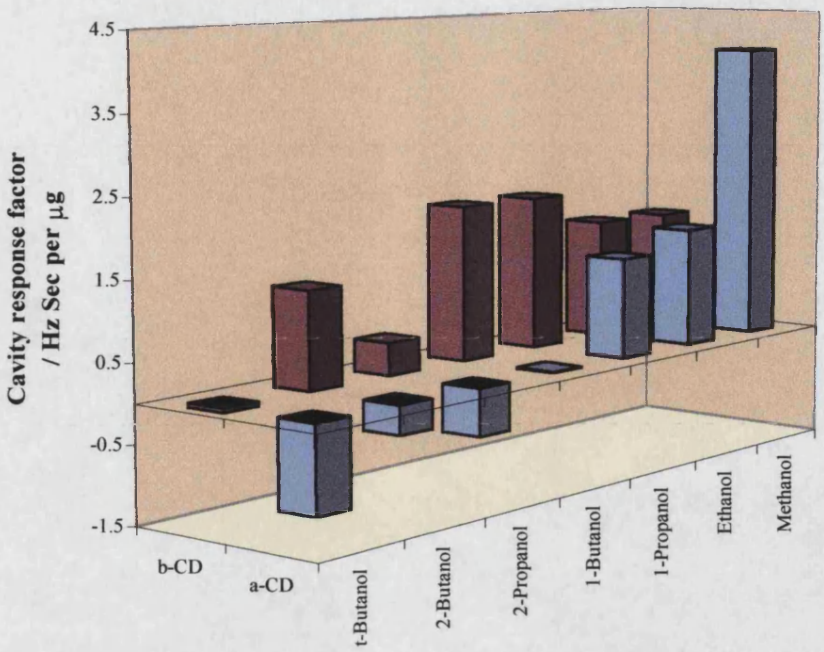

***Figure 4.13**: The response factors associated with cyclodextrin cavity. These are the M values obtained for the cyclodextrin resonators minus the values obtained for the amylose resonators. The data are obtained from Tables 4.9-4.11.*

The β-cyclodextrin resonator displays a similar increase in the response to the straight chain alcohols, however, the largest increase is associated with the longer chains, butanol and propanol. The values are 1.55, 1.57, 2.03 and 2.04 Hz sec μg^{-1} for methanol, ethanol, propanol and butanol respectively. The β-cyclodextrin resonator also has an increased response to the two secondary alcohols 2-propanol and 2-butanol compared to the linear amylose coating, suggesting that these two branched molecules can interact with the larger internal cavity of the β-cyclodextrin ring. The *t*-butanol response is identical to the amylose resonator but larger than the α-cyclodextrin coating. As before the similarity of the *t*-butanol response for the amylose and β-cyclodextrin resonators indicates that the *t*-butanol molecule interacts with sites external to the cyclodextrin cavity that are available in both the glucose based coatings.

4.5 Conclusion

Three AT-cut quartz resonators (10 MHz) were coated with 2.46 μg, 2.66 μg and 1.39 μg of α-cyclodextrin, β-cyclodextrin and amylose respectively. The response factor associated with the exposure of the sensor to VOCs were calculated. For α-cyclodextrin the methanol response factor was 5.30 Hz Sec μg^{-1} with all other non-alcoholic VOCs less than 0.50 Hz Sec μg^{-1}. For β-cyclodextrin the methanol response factor was 3.03 Hz Sec μg^{-1}, again with all other none alcoholic VOCs were less then 0.60 Hz Sec μg^{-1}. The amylose sensor had response factors less than 0.70 Hz Sec μg^{-1} for all VOCs. This revealed the selectivity of the cyclodextrin coating.

The second study utilised a series of alcohols. The results obtained show that the interaction of the resonator coating with the alcohols present in the gas stream is dominated by the structure and shape of the two cyclodextrin molecules. These impart selectivity to the response of the overall resonator. The response of the underivatised cyclodextrins are guided by hydrogen bond interactions with size exclusion adding greater detail. The cyclodextrin coated sensors generally showed signals ten times greater for the alcohols than the other VOCs investigated. These included an aromatic compound, a straight chain hydrocarbon and polar compounds incapable of acting as hydrogen-bond donors.

The smaller α-cyclodextrin cavity has a greater response for the smaller alcohol while the β-cyclodextrin cavity has a greater response for the larger alcohols. As the cavity size increased the response of the larger molecules increased and the response of the smaller molecules decreased. Similarly only the branched alcohols interact with the larger β-cyclodextrin cavity; they showed no response with the smaller α-cyclodextrin cavity.

The results illustrate the potential of the coatings to distinguish between different solvent vapours with such diverse properties as toluene and acetone or such similar properties as ethanol and methanol. By derivatising the parent cyclodextrins this selectivity could be directed and optimised for specific target vapours. The hydroxyl groups can be replaced with a variety of species offering different

interaction potentials, for example methyl-groups. Removing the hydrogen-bond donor and acceptor capabilities and adding dipole-dipole and van der Waals interacting groups should have a marked effect on the resonator response. This should switch from being alcohol dominated to other compounds such as the straight chain hydrocarbons and aromatic species. At the same time the size exclusion properties would be maintained, again provide the fine detail to the resonator response.

4.6 NO_x Gas Sensor

The work described in this section was carried out as part of a collaboration with the Centre for Molecular and Biomolecular Electronics, Coventry University.

4.6.1 Introduction

With an increase in environmental concern laws and legislation covering gaseous emissions and their permitted level of concentration are under review. NO_x is major component in combustion exhausts [289] and an important species in photochemical air pollution [290]. This pollution is a problem in all the major cities through out the world and is largely caused by the action of NO_x gas with atmospheric O_2 in the presence of sunlight [291]. For this reason there is great interest in developing NO_x sensors that can give rapid *in situ* readings for the concentration of the gas in a variety of environments. These sensors would find applications in environmental research and emission monitoring required for new legislation as well as devices for monitoring the operating conditions of the internal combustion engine.

The current EC legislation has a first safety limit for NO_2 of 200 $\mu g\ m^{-3}$ [292], this corresponds to about 100 ppb [293]. The 1996 threshold limits value for NO_2 and NO as set by the American Conference of Governmental Industrial Hygienist, ACGIG, is 3 and 25 ppm respectively [294]. The analytical methods currently employed for NO_x monitoring include chemiluminescence, infrared spectroscopy and UV-vis spectroscopy [295][296]. However these systems are often

impractical due to size and expense. Attention has therefore been applied to the development of cheaper and simpler sensor systems. These include solid state amperometric sensors [297][298] and optical gas sensors [299][300]. The current detection limits of these devices are around 1 ppb and 0.1 ppm respectively.

The work covered in this section discusses the use of a QCM resonator coated with an azobenzene dye. The coated resonator is employed as a specific chemical sensor for NO_x gas. The mass detection limit for the QCM utilised in this study is 4.97 ng Hz^{-1} cm^{-2}. This corresponds to a 10 % NO_2 monolayer on the surface of the resonator. It is clear from this sensitivity that the detection of low NO_x concentrations will be possible. The QCM resonator was coated with Langmuir Blodgett (LB) layers of the azobenzene dye, compound 5 Figure 4.14. Compounds based on this structure have been shown by Scheerder *et al.* [299] and Worsfold *et al.* [301] to bind $NO_{2\,(g)}$ in a reversible process. This reversible nature coupled with a strong binding energy suggests that the compound will be of great potential as a surface sensitive layer in a QCM sensor designed to respond to NO_2 gas.

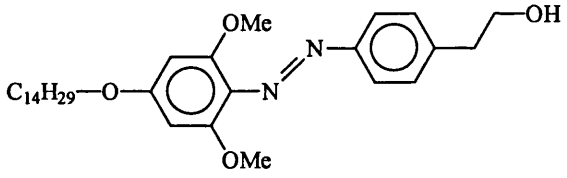

Compound 5

$M_w = 498$ g mol^{-1}

***Figure 4.14**: The azobenzene dye used as the sensitive coating.*

The azobenzene dye was synthesised by Worsfold *et al.* [301] at the Centre for Molecular and Biomolecular Electronics, Coventry University. The dye was employed as an optical sensing material for NO_2 and NO_x gas. The mechanism for the gas sensing is unclear at present but is believed to be centred on the N=N double bond [299][301]. This is highlighted by the UV-Vis spectra of the dye both before and after exposure to NO_x gas, see Figure 4.15.

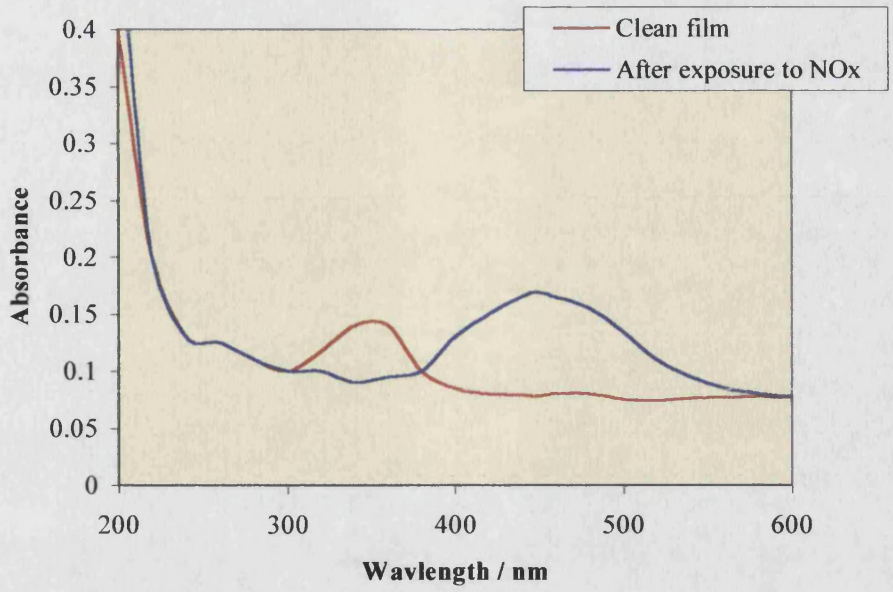

***Figure 4.15**: The change in the UV-Vis spectrum of compound 5 upon exposure to 100 ppm NO_x gas.*

4.6.2 Experimental

Langmuir-Blodgett film deposition was carried out at the Centre for Molecular and Biomolecular Electronics, Coventry University. The QCM resonators were dipped through a surface layer of the azobenzene dye. Once coated the resonators were dried in an air stream and stored in a dry atmosphere for 72 hours. The difference in the fundamental resonance frequency between the clean resonators and the coated resonators were used to estimate the mass of the deposited LB layers.

Gas Sensing

Two resonators were mounted in a flow cell, a reference and a working sensor. The QCM monitored the difference in resonance frequency between the two resonators. The working sensor was coated with the azobenzene dye and the reference resonator was uncoated. This set up allows for the subtraction of non-specific binding interactions between the NO_2 gas and the surface of the resonator.

The QCM was allowed to stabilise in airflow. Once stabilised the airflow was switched to a 100 ppm NO_2 in air. The frequency response was recorded until the frequency difference between the working sensor and the reference resonator remained constant. The exposed resonators were then removed and heated to 60 °C for about one hour to eliminate the bound NO_2 gas.

4.6.3 Langmuir-Blodgett Film Deposition

The quartz resonator resonators were coated with LB layers of the azobenzene dye. After the deposition a thin orange film could clearly be seen on the surface of the resonators. This is as expected for the addition of a small amount of the dye onto the resonators. The 10 monolayer sensor appeared from simple observation to have an uneven coating of the dye. The colour was patchy and irregular, however, the 20 and 30 monolayer sensors had what appeared to be uniform coatings. For this reason the frequency change associated with the deposition of the 10 monolayer LB films was assumed to be more susceptible to errors.

Number of LB layers	Frequency Change / Hz	Mass / μg
0	0	0
10	236	0.17
20	1382	0.97
30	2116	1.50

***Table 4.12**: The frequency change and deposited mass associated with the addition of the LB layers.*

The data in Table 4.12 above leads to the graph in Figure 4.16. As expected the mass associated with the 10 monolayer deposition is slightly lower than that predicted by extrapolation from the other data points. This point was therefore excluded from the linear regression.

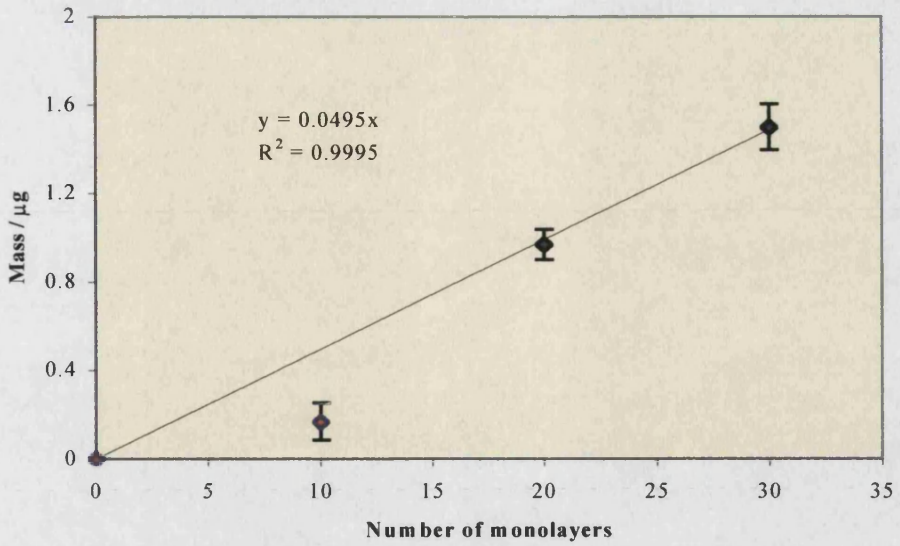

***Figure 4.16**: The increase in mass on the surface of the QCM resonator associated with the deposition of LB layers of compound 5.*

4.6.4 Sensor Response

Figure 4.17 shows the response of the 10 LB coated sensor to NO_2 gas. The frequency change plotted is the resonance frequency of the sensor minus the resonance frequency of the sensor in the initial airflow. The NO_2 flow was initiated at time zero and had a time delay of about 300 seconds before reaching the sensor flow cell. It can be seen from the graph that the resonance frequency dropped slowly after the NO_2 reached the sensor, finally levelling off at a value 20 to 25 Hz lower than the resonance frequency in air. Accompanying this shift was a colour change in the coating from orange to brown. This is the same colour change observed in the optical studies and the UV-Vis spectra of the dye exposed to NO_2. The colour change is attributed to the binding of the NO_2 gas to the azo-linkage in the dye. Simple heating of the sensor to a temperature of 60 °C is sufficient to return the film coating to its initial colour and hence remove the bound NO_2. The sensor was then used for runs 2 and 3, the results of which were slightly different from the first exposure.

All three runs provided a similar response, however, the second and third runs had an interesting frequency time relationship. A plateau appeared 20 seconds after the sensor frequency shift was initiated. This levelled of at 5 Hz below the resonance frequency in air. The frequency remained constant for a further 100

seconds, then proceeded to drop to the final value with an overall time period the same as the first run.

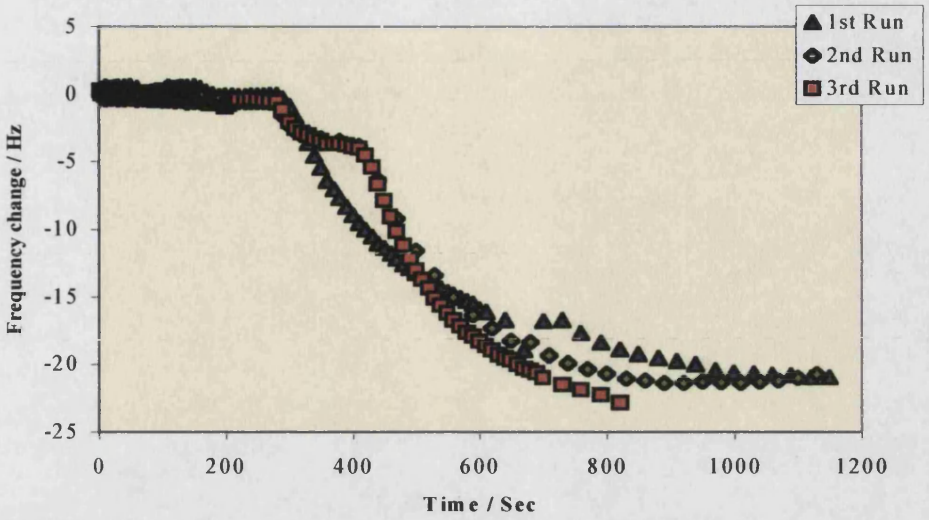

***Figure 4.17**: The response of the sensor coated with 10LB layers to 100 ppm NO_x.*

As both the second and third runs displayed identical frequency-time responses this initial plateau can not simply be due to experimental error. The mostly likely explanations is of a reorganisation in film morphology that occurred upon heating the coated sensor to 60 °C. This may result in the formation of heterogeneous binding sites within the film. It is also interesting to note the absence of this binding phenomenon with the higher LB film sensors. This suggests that it may be a consequence of the uneven coating of the 10 LB sensor rather than a consequence of the chemical binding interactions. Further study of the frequency-time response will reveal more information on the nature of this plateau. It may also go some way to answering the questions on the macroscopic morphology of the LB coatings and the mechanism for the NO_2 binding.

Figure 4.18 shows the response of the 20 LB layer sensors. The frequency change on exposure to 100 ppm NO_2 gas is approximately twice that of the 10 LB layer sensor. The colour change in the film was the same as that experienced for the 10 LB sensor and previous studies on the exposure of the azobenzene dye to NO_2. Again, simply heating the sensor restored the film colour to its original form. Overall, for the 20 LB layer sensor, the frequency change was around 50 Hz over a time period of 600 seconds.

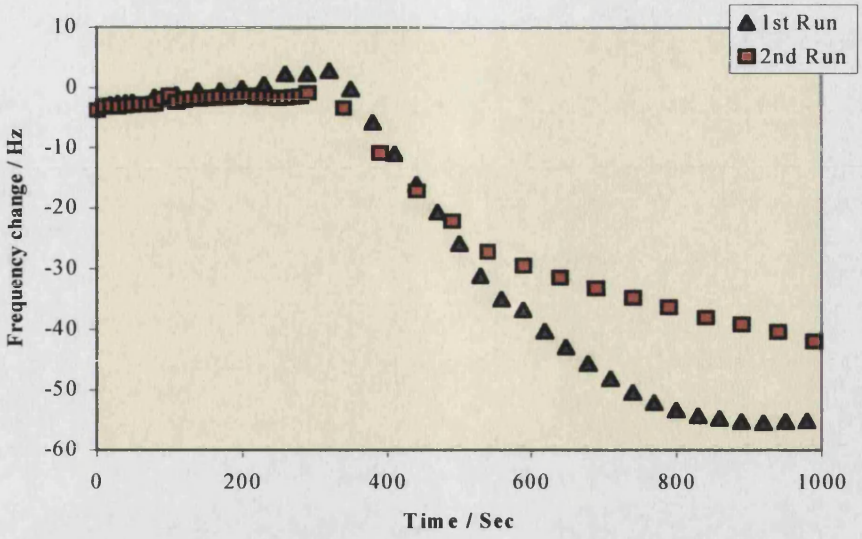

***Figure 4.18**: The response of the sensor coated with 20 LB layers to 100 ppm NO_x.*

The 30 LB layer sensor responded in much the same fashion and can be seen in Figure 4.19. The overall frequency change was between 80 to 90 Hz approximately three times that of the 10 LB layer sensor. Again the same colour change occurred which was reversible upon heating. The time period for the binding process was similar to the 20 LB layer sensor at 400 to 500 seconds both of which were slower than the 10 LB layer sensor. This is consistent with the response times of thin film sensors. As the thickness of the sensing film decreases so the response time decreases. The response times observed in the optical studies of this compound were of the order of 60-120 seconds. This is three times as fast as the QCM response time. Again further investigations on the response time and the factors effecting this would be particularly useful.

The response of the three sensors to NO_2 gas was very encouraging. The magnitude of the frequency shift induced by the binding of NO_2 correlated well with the number of LB layers deposited. This confirms that the deposited material was indeed binding the NO_2 gas and the response was not simply a physical interaction of the gas with the surface of the sensors. The colour change of the film associated with the NO_2 binding suggests that the film-gas interaction was chemical rather than physical and centred on the N=N double bond.

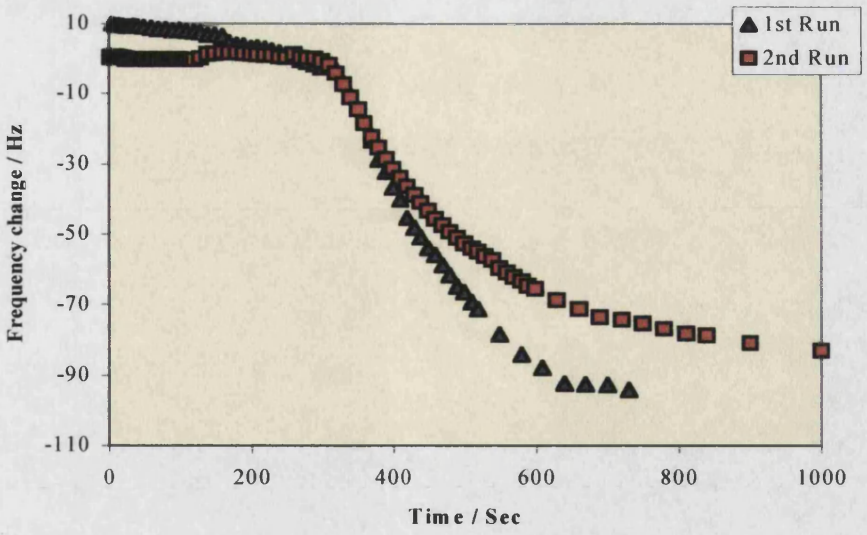

***Figure 4.19**: The response of the sensor coated with 20LB layers to 100 ppm NO_x.*

Figure 4.20 below shows the mass of the bound NO_2 plotted against the number of LB layers deposited. This clearly indicates the linear correlation between the number of gas molecules adsorbed and the total number of azo-binding sites available. This linear relation would be expected to break down as the number of LB layers increased due to the inaccessible nature of the lower films. The fact that the relationship holds up to 30 monolayers suggests that the azo-benzene film is highly porous and allows the NO_2 molecules to defuse freely throughout the layers.

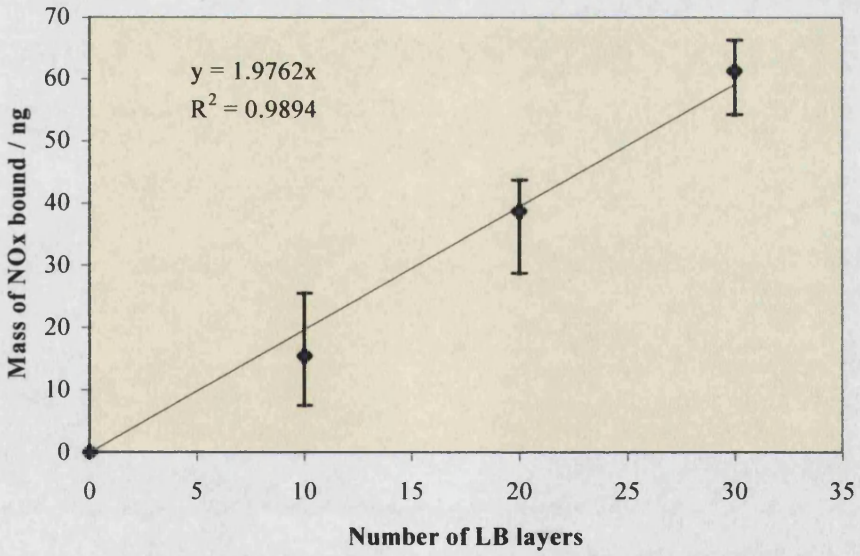

***Figure 4.20**: The response of the coated sensors to NO_x.*

4.6.5 Fractional Coverage

From the data obtained it is possible to work out a value for θ the fraction of available bindings sites occupied.

$$\theta = \frac{\text{Number of binding sites occupied}}{\text{Number of binding sites available}} = \frac{N_{Oc}}{N_{Av}} \qquad (41)$$

Assuming a 1:1 interaction between each azo-linkage in the dye molecules and the NO_2 gas the total number of sites occupied is equal to the total number of moles of NO_2 gas bound to the film, N_{Oc}. This can be calculated from the graph in Figure 4.20.

$$N_{Oc} = G_1 \text{ x } n / Mr_{NOx} \qquad (42)$$

Where $G_1 = 1.98 \text{ x } 10^{-9}$ g and is the gradient from Figure 4.20, n is the number of LB layers and Mr_{NOx} is the molecular weight of $NO_2 = 46$ g mol^{-1}.

The total number of binding sites available is equal to N_{Av}, the total number of moles of the azobenzene dye deposited. This can be calculated from Figure 4.16.

$$N_{Av} = G_2 \text{ x } n / Mr_{Azo} \qquad (43)$$

Where $G_2 = 4.95 \text{ x } 10^{-8}$ g and is the gradient from Figure 4.16, n is the number of LB layers and Mr_{Av} is the molecular weight of the azobenzene dye = 498 g mol^{-1}. Combining equations 41, 42 and 43 leads to an expression for θ:

$$\theta = G_1 \text{ x } Mr_{Azo} / G_2 \text{ x } Mr_{NOx} \qquad (45)$$

$$\theta = (1.98 \text{ x } 10^{-9} \text{ x } 498) / (4.95 \text{ x } 10^{-8} \text{ x } 46)$$

$$\theta = 0.433 \pm 0.018$$

The uncertainty in θ was calculated from the linear regression analysis performed on the data in Figures 4.16 and 4.20. This value compares well with the value predicted from the optical studies; however a direct comparison is not possible due to differing film composition.

4.6.6 Conclusion

AT-cut quartz resonators were coated with Langmuir-Blodgett, (LB), films of an azobenzene dye, see compound 5 Figure 4.14. The mass of the films were estimated to be 0.17 μg, 0.97 μg and 1.50 μg for 10, 20 and 30 Langmuir-Blodgett layers respectively. The sensors were utilised to determine θ; the ratio of occupied binding sites to the total available binding sites after the films were exposed to 100 ppm NO_x gas. This was found to be $\theta = 0.433 \pm 0.018$. The response of the sensor was monitored via the fundamental frequency change of the resonator and was slightly greater than expected. With the QCM driving circuit and frequency recording device employed for this study the sensitivity in the frequency reading was ± 0.5 Hz. This gives an overall sensitivity to NO_2 gas of about 1 ppm. With more sophisticated frequency recording devices this sensitivity could be reduced to ± 0.005 Hz. Combining this with the addition of further LB layers of the azobenzene dye and a sensor sensitive to sub ppb levels could be produced.

The response times were rather slow. The optical studies showed a response time of less than 100 seconds. Typically a 60 second exposure of a dip-coated film to 100 ppm NO_2 produced a 90% response. Exposure of the film for a further 600 seconds produced only a minor increase in the UV-Vis absorption peak associated with the NO_2 binding. This may be attributed to thinner film being employed for the earlier work. But as no data was available on the thickness of the films used for the optical studies a definite conclusion can not be drawn.

It was also interesting to observe the frequency-time relationship in the 10 LB layer sensor. The formation of the plateau a few seconds after exposure to NO_2 gas. It should be possible to use the QCM sensor to study the binding kinetics of the NO_2 gas. This could be particularly useful for observing any changes in morphology of the film due to the NO_2 binding and the heating process used to remove the gas once exposed.

Generally QCM based gas sensor offer great potential for the analysis of trace components in a gaseous environment. The QCM itself is a very simple way of coupling a sensitive coating to a transducer that converts chemical binding to a recordable signal. The sensitivity has been shown to be very low and the responses reproducible.

CONCLUSION

CHAPTER FIVE

The aims of the project were to synthesis chemical interfaces that displayed selective uptake capabilities for target compounds in the presence of potential contaminants and to couple these systems to QCM transducers. This was with the intention of developing selective chemical sensors for application in both liquid and gas phase environments. The systems investigated successfully demonstrated the usefulness of this approach to the advancement of such sensors; the ease of sensor fabrication, signal formation and data manipulation has all been highlighted.

5.1 The Liquid Phase $K^+_{(aq)}$ Sensor

The liquid phase sensors were design to respond to $K^+_{(aq)}$ selectively over the other Group I ions $Na^+_{(aq)}$ and $Li^+_{(aq)}$ with the chemical interface based on acrylic acid crown ether copolymer systems. Both the 15-crown-5 and 18-crown-6 containing copolymers were successfully synthesised and shown to preferentially bind $K^+_{(aq)}$ in the presence of the other Group I ions $Na^+_{(aq)}$ and $Li^+_{(aq)}$. The 18-crown-6 resin system was coated onto a QCM resonator and used as a $K^+_{(aq)}$ sensor. This is the first account of a crown ether based coating being employed with a QCM for the detection of cations. As discussed at the end of Chapter Three the sensor developed had an estimated detection limit of 0.2 ppm and a linear response range of 0-2000 ppm with zero response to either $Na^+_{(aq)}$ or $Li^+_{(aq)}$. These values are well within the operating criteria for commercial K^+ sensors. The markets for such devices are in the areas of water analysis [302] and physiological sensors. The concentration of K^+ in tap-water is typically in the range of 1-80 ppm [302]. In the human body the concentration of K^+ in blood serum is around 140 ppm [303] and bile around 500 ppm [303] with the most common interference arising from Na^+.

The standard devices employed for clinical and environmental analysis are atomic emission (AES) and atomic absorption spectrometers (AAS). These are extremely sensitive to metal cation concentrations but operate only in a limited concentration range, usually below 100 ppm. Samples are routinely diluted prior to analysis resulting in lengthy preparation time. The devices are expensive and can not perform continuous monitoring. Another consequence of using the AES and AAS

systems is their accessibility. The devices are not mobile and located away from the sample location; again this increases the sample time and cost. More mobile sensor systems have recently been employed for metal ion analysis. The potentiometric system discussed in section 1.1.2 is an example of this. The sensor is now used in many clinical applications bringing both health and economic benefits. The sensitivity of these potentiometric systems is comparable to the system developed here operating in the concentration range of 0.1-1000 ppm with the $K^+_{(aq)}$ selectivity imparted by a valinomycin based membrane. The QCM transducers offer more versatile sensor systems as the recognition and signal generation is combined in a single step. The transducers are also cheaper increasing the economic benefits.

The sensor described here is still far from any commercial application with a great deal of development work still required (this is discussed in section 5.3). However the potential use of the system would be to offer an alternative to the AAS and AES analysers. The sensor could also function as an on-line continuous system monitoring K^+ concentration in biological fluids where the current AAS and AES systems are impractical; for example during open-heart surgery [302]. Environmental applications of the QCM sensors are those concerned with the quick and easy water analysis out in-the-field and again continuous on-line monitoring of water quality in flow through systems.

This is the first account of a crown ether based copolymer being employed with the QCM as a selective cation sensor. It brings together the innovative use of a water compatible copolymer system with the QCM transducer for application in an aqueous environment. It has been demonstrated that such an approach is suitable to the development of liquid phase QCM based sensors and that such sensors possess the required selectivity and stability to operate in the ppm range. With improved design such as the inclusion of the reference and working electrodes in the same liquid sample, and response optimisation by increasing the crown ether loading and the mass of the copolymer coating, this range could be extended down to one part in 10^9. The copolymer system incorporated in the sensor design can be readily modified to include a variety of different host compounds and offers a general route to the production of an array of selective chemical sensors.

5.2 The Gas-Phase Sensors

Research in the field of gas phase piezoelectric sensors is progressing rapidly with the first major commercial applications already on the market. Marconi Applied Technologies have developed odour analysers based on QCM systems, for example the eNOSE 5000 [304]. As discussed in section 1.5 a variety of different adsorbent coatings have been studied, each with their own advantages and disadvantages. The cyclodextrins are one group of host compounds that to date have only had limited application.

The work conducted on the α-cyclodextrin and β-cyclodextrin demonstrates the potential of these hosts to function as selective binding interfaces coupled to the QCM transducer. Direct comparison with other systems is of limited practical use as no firm conclusions on sensor response or selectivity can be drawn. This is a consequence of the variety of operating conditions; transducer design and result presentation carried out in previous systems. However, such a comparison does help to illustrate the sensitivity of the cyclodextrin coating. Pinalli *et al.* [305] published data on a cavitand based QCM alcohol sensor. The sensor had a 60 Hz response to a 3000 ppm methanol vapour. The α-cyclodextrin coating employed here has a 950 Hz Sec peak area for a similar vapour concentration. The lower detection limit for the methanol system is estimated at 20 ppm. This compares well with the detection limits of 100 ppm quoted by Yang *et al.* [215] for VOCs utilising a cyclodextrin SAW device and 50 ppm quoted by Dickert *et al.* [176] the vapour phase detection of xylenes using cyclodextrin based coatings.

As discussed at the end of section 4.5 the response of the underivatsed cyclodextrin sensors is dominated by hydrogen bonding interactions. The cavity size formed a secondary factor adding subtle variations to the overall sensor response. The system could therefore operate as a functional group sensor indicating the presence of a hydrogen bond donor and acceptor in unknown vapour mixtures. The device can also be used to examine the interaction parameters of the cyclodextrin coating with different molecular probes in a similar fashion to GC and IGC systems. However, the final application envisaged at this stage of the investigation is that of an electronic tongue or electronic nose system with the cyclodextrin coating forming

part of an overall sensor array. The diversity of the response to a range of VOCs shows the suitability of the cyclodextrin coatings for such applications.

The work conducted on the NO_x sensor in section 4.6 again shows the capability of the QCM to operate as a chemical sensor in the low ppm region. The azobenzene dye utilised was developed to operate in an optical sensor with complementary information being obtained from both the optical and QCM sensor systems. The QCM forms an alternative transducer maintaining the ppm sensitivity and brining the economic benefits associated with the production and fabrication of QCM resonators. The commercial requirements for NO_x gas sensors are in the ppm-ppb concentration range and so slight improvements on the sensor response are still required. This could be achieved by using the SAW systems currently available. The section also illustrates the other aspects of the system, the possibility of obtaining absorption data and performing kinetic experiments on the reaction rates of surface absorption processes.

In summary, the work presented demonstrates the potential of QCM based systems to operate as selective chemical sensors in liquid phase and gas phase applications. The methodology employed for the sensor fabrication is both simple and versatile with the final sensors having low detection limits and broad operating ranges. The cyclodextrin surfaces investigated displayed selective absorption properties arising from the central cavity. The response profiles were reproducible and the coatings remained active after repeated exposure. The NO_x system illustrated the potential of the QCM to act as an alternative transducer to the more expensive optical system.

5.3 Future Work

The Liquid Phase $K^+_{(aq)}$ Sensor

The immediate work that could be conducted on the liquid phase $K^+_{(aq)}$ sensor would be the variation of the mass of the copolymer coating and the percentage crown ether content. These two variables would be expected to have a marked effect on the sensor response. The oscillation of a QCM resonator follows a linear frequency-mass

relationship for mass-loads (m_q/m_f) less than 0.02. This corresponds to a frequency change of 200 kHz. The coating employed for the current work was around 1 kHz. Increasing the mass of the copolymer coating would increase the available binding sites and so increase the sensor response. Similarly increasing the crown ether loading within the copolymer would also increase the number of binding sites. It would also be interesting to vary the cross-linker concentration in the sensor coating. Although this had only a minor effect on the uptake of the solid resins the dependence of the QCM operating frequency on the viscoelastic properties of the coating indicates that this may have a more significant effect on the sensor response. Similarly the work on the non cross-linked copolymer system should be continued. Lowering the temperature used to promote the amide links and the use of other amino-acid coupling agents are two of the most suitable directions to proceed.

The lifetime of the sensor also needs further investigation. The use of different cleaning procedures such as acid washing or even washing with a free crown ether solution may help to regenerate the sensor after exposure to concentrated $K^+_{(aq)}$ solution. It would also be interesting to alter the sensing conditions such as temperature and pH. As well as being important from a commercial point of view these would also enhance the understanding of the binding and recognition mechanism involved.

A more long-term direction would be to vary the host compound incorporated into the copolymer network. Targeting other metal ions, dissolved organic species and even anions are three possible sensor routes. Cryptands and porphyrins are two examples of host compounds that could be readily incorporated and have increased binding affinities towards metal ions compared to the crown ether systems currently employed. Work on anion receptors based on redox active metal centres in conjunction with amides has been published by Reinhoudt *et al.* [306] and Beer *et al.* [307]. These anion sensor systems could also be readily incorporated into a copolymer matrix in a similar fashion to the crown ethers. Molecularly imprinted polymers are another area with great potential in the field of QCM-based chemical sensors and offer systems with chiral recognition capabilities or organic compounds recognition such as explosives.

The Cyclodextrin System

The variation of the functional groups on the two rims of the cyclodextrin cavity is the obvious next step to extend the current work. This could be achieved simply and easily as several derivatised cyclodextrin are commercially available. A more long-term investigation would be to look at the orientation of the cyclodextrin cavities. Utilising the SAM technology discussed in section 3.8 ordered monolayers of the cyclodextrins could be formed on the gold electrodes of the QCM resonator [288][308]. These would be similar to the ordered monolayers of calixarenes synthesised by Cygan [309]. Tabushi *et al.* [310][311] developed a synthesis for thiol derivatised β-cyclodextrins. This involved capping the β-cylcodextrin ring with an aryltosylate group then opening the bridge with two benzenedithiol molecules. The final product possesses the thiol groups on the narrow rim of the cavity and is the ideal candidate to produce the SAM. An alternative synthesis of a thiol-cyclodextrin compound would be to use H_2S and Al_2O_3 [312]. This reaction selectively converts primary alcohols to the equivalent thiol and so the secondary and tertiary hydroxyl groups on the larger rim would remain intact. Again this would produce an ideal candidate for the formation of ordered cyclodextrin monolayers.

Another use of the cyclodextrin SAM could be in the application of the coated sensors in a liquid environment. For such an application the coating must be secured in some way to the resonator surface. There are several other methods available for this attachment, including covalent and non-covalent encapsulation in an inert matrix [313]. Dickert *et al.* [314] coated a QCM resonator with a cyclodextrin compound attached directly to a polymer support and used the resonator as a sensor for chlorobenzene in a liquid environment. Such sensors could operate as VOC detectors in both the liquid phase and in the gas phase offering a much more versatile sensor than the current electronic nose systems and the potential for the development of the electronic tongue.

General

On a commercial side the advantages of QCM based chemical sensor are the versatility and robust nature of the QCM transducer. It would be a relatively straightforward procedure to miniaturise the oscillating circuit and produce a small handheld device with interchangeable heads for sensing different species in different environments. QCM systems have been modified by several workers to operate with multiple resonators [305][315][316]. A modification to the QCM utilised throughout this work would be to combine the signals from several resonators as opposed to just the current reference and working system. This 'multi-channel' QCM would aid in the calibration of sensor response and data interpretation by eliminating unwanted signals and increasing the range of reference data. The system could also be used as a pattern recognition sensor combining information from several different coating materials.

The fabrication of novel QCM operating systems and resonator designs that are more appropriate for application as hand held chemical sensors is an essential requirement for the development of these devices. The miniaturisation of the electronic circuits and the incorporation of 'multi-channel' resonators are two possible ways forward to reach this final goal.

REFERENCES

CHAPTER SIX

1. Collins English Dictionary, Third Edition, HarperCollins Publishers, 1994
2. Hitchman ML, Hill HAO, *Chemistry in Britain,* **22**, 1117-1124, 1986
3. Heyrovsky J, *Chem. Listy*, **16**, 256, 1922
4. Faraday M, *Phil. Trans. Roy. Soc. London*, **1**, 55, 1834
5. Nernst W, *Z. Phys. Chem.* **4**, 372, 1889
6. PettovaNikolova M, Pohl JP, *Sensors and Actuators B-Chemical*, **46**, No 1, 66-71, 1998
7. Yamazoe N, Miura N, *Electrochemistry*, **67**, No 3, 224-231, 1999
8. Fleischer M, Meixner H, *Sensors and Actuators B-Chemical*, **52**, No 1-2, 179-187, 1998
9. Shimizu Y, Egashiva M, *MRS Bulletin*, **24**, No 6, 18-24, 1999
10. Aroutiounian VM, Aghababian GS, *Sensors and Actuators B-Chemical,* **50**, No 1, 80-84, 1998
11. Mosbacher CJ, *Res. and Dev.* **91**, 1986
12. Moss SD, Janata J, Johnson CC, *Anal. Chem.* **47**, 2238, 1975
13. Marco MP, Barcelo D, *Meas. Sci. Technol.* **7**, 1547-1562, 1996
14. Bogdanovskaya VA, Tarasevich MR, *Biosensors Bioelectronics,* **11**, No 9, 853-861, 1996
15. Green MJ, Hill HAO, *J. Chem. Soc. Faraday Trans 1*, **82**, No. 4, 1237-1243, 1986
16. King, Mason, Morrison, *Oxidases and Related Redox Systems: Proceedings of a Symposium Held in Amherst,* John Wiley and Sons Inc, U.S.A, volume 1, page 310, 1964
17. Tran-Minh C, Vallin D, *Anal. Chem.* **50**, 1874, 1978
18. Cobbold RSC, *Transducers for Biomedical Instruments*, Wiley, New York, 1974
19. Zemel JN, *Solid State Chemical Sensors*, Academic Press, New York, 1988
20. Ristic VM, *Principles of Acoustic Devices*, Wiley, New York, 1983
21. Janata J, *Principles of Chemical Sensors*, Plenum Press, NewYork, page 50, 1990
22. Zemel JN, Solid State Chemical Sensors, Academic Press, New York, 1985
23. Gentry SJ, *Catalytical Devices in Chemical Sensors*, Chapman and Hall, New York, 1988
24. Martin P, *Chemistry in Britain*, **35**, No 7, 33-36, 1999

25. Blood P, *Chemistry in Britain*, **35**, No 7, 38-40, 1999
26. Wilson J, Hawkes JFB, *Optoelectronics; An Introduction*, 2nd Edition, Prentice Hall International (UK) Ltd, 1989
27. Chan K, Ito H, Inaba H, *J. Lightwave Tech.* **LT-2**, 234-237, 1984
28. Chan K, Ito H, Inaba H, *Appl. Otics.* **23**, 3415-3420, 1984
29. Snel D, Pitt GD, *Proc. Int. Conf. On Opt. Tech. In flow Monitoring and Control*, The Hague (BHRA), 27-42, 1983
30. Kirkbright GF, Narayanaswamy R, Welti NA, *Analyst.* **109**, 1025-1028, 1984
31. Arnold MA, Ostler TJ, *Anal. Chem.* **58**, 1137-1140, 1986
32. Edmonds TE, *Chemical Sensors*, Blackie, Glasgow and London, 1988, pp 295
33. Karmarker KH, Guilbault GC, *Anal. Chim. Acta.* **75**, 111, 1975
34. Thomas RC, Yang HC, DiRubio CR, Ricco AJ, Crooks RM, *Langmuir,* **12**, 2239, 1996
35. Jane YS, Shih JS, *Analyst*, **120**, No 2, 517-522, 1995
36. Yokoyama K, Ikebukuro K,Tamyin E, Karube I, Ichiki N, Arikawa Y, *Anal. Chim. Acta.* **304**, 139, 1995
37. Menon A, Zhou R, Josse F, *IEEE Trans. Ultrason. Ferroelect. Freq. Contr.* **45**, No 5, 1416-1426, 1998
38. Abad JM, Pariente F, Hernandez L, Abtuna HD, Lorenzo E, *Anal. Chem.* **70**, No 14, 2848-2855, 1998
39. Yuanjin X, Changyin L, Kang C, Lihua N, Shouzhuo Y, *Anal. Chim. Acta.* **325**, 65-71, 1996
40. Plato (427-327 B.C.), *Timaeus*, Sec. 80c.
41. Ikeda T, *Fundamentals of Piezoelectricity*, Oxford University Press, page 1, 1990
42. Curie J, Curie P, *Bull. Soc. Min. Paris*, **3**, 90, 1880
43. Cady WG, *Piezoelectricity*, New Revised Edition, Dover Publications, Inc, New York, page 2, 1964
44. Hauy RJ, *Ann. Chim. et Phys.* **5**, 95-101, 1817
45. Becquerel AC, *Bull. Soc. Philomath. Paris*, **7** (series 3), 149, 1820
46. Suslick KS, *Ultrasound: Its chemical, physical and biological effects*, VCH Publishers Inc. USA, 1988
47. Pierce GW, Proc. *Am. Acad. Arts Sci.* **59**, 81, 1923
48. Cady WG, *J. Opt. Soc. Am.* **10**, 475, 1925

49. Jones DJ, Prasad SE, Wallace JB, *Key Engineering Materials*, **122-124**, 71-144, 1996

50. Giacovazzo C, *Fundamentals of Crystallography*, Oxford Science Publications, 1992

51. Alder JF, McCallum JJ, *Analyst*, **108**, 1169, 1983

52. O'Donnell M, Busse LJ, Miller JG, *Methods of Experimental Physics*, Vol. 19, 29-65, 1981

53. Deakin MR, Buttry DA, *Anal. Chem.* **61**, 1147A, 1989

54. McCallum JJ, *Analyst*, Vol. **114**, 1173-1189, 1989

55. Lu C, Czanderna AW, *Methods and Phenomena 7: Applications of Piezoelectric Quartz Crystal Microbalances*, Elsevier Science Publishers, Amsterdam, 1984, pp 27

56. Sauerbrey GZ, *Phys. Verhandl.* **8**, 113, 1957

57. Sauerbrey GZ, *Z. Phys.* **155**, 206, 1959

58. Strutt JW, *The Theory of Sound*, Rev. Ed., Dover, New York, 1945

59. Onoe M, *Proc. IRE*, **45**, 694, 1957

60. Oberg P, Lingensjo G, *Rev. Sci. Instrum.* **30**, 1053, 1959

61. Behrndt KH, Love RW, *Vacuum*, **12**, 1, 1962

62. Warner AW, Stockbridge CD, Walker RF (Ed.), *Vacuum Microbalance Techniques*, Vol 2, Plenum, New York, 1962 page 71

63. Stockbridge CD, *Vac. Microbalance Technol.* **3**, 55, 1963

64. EerNisse EP, *IEEE Trans.* SU-14, **59**, 1967

65. Miller JG, Bolef DI, *J. Appl. Phys.* **39**, 5815, 1968

66. Lu C, Lewis O, *J. Appl. Phys.* **43**, 4385, 1972

67. Lu C, *J. Vac. Sci. Technol.* **12**, 578, 1975

68. Hillier AC, Ward MD, *Anal. Chem.* **64**, 2539-2554, 1992

69. Ward MD, Delawski EJ, *Anal. Chem.* **63**, 886, 1991

70. Lide DR, *CRC Handbook of Chemistry and Physics*, 76th Edition, CRC Press, New York, 1995-1996, table 4-137

71. Lide DR, *CRC Handbook of Chemistry and Physics*, 76th Edition, CRC Press, New York, 1995-1996, table 12-192

72. Ullevig DM, Evans JF, Albrecht MG, *Anal. Chem.* **54**, 2341-2343, 1982

73. Lu C, Czanderna AW, *Methods and Phenomena 7: Applications of Piezoelectric Quartz Crystal Microbalances*, Elsevier Science Publishers, Amsterdam, 1984, pp 31-32

74. Daikhin L, Urbakh M, *Faraday Discuss.*, **107**, 27-28, 1997

75. Benes E, *J. Appl. Phys.* **Vol 56**, No 3, 1984

76. Miller JG, Bolef DI, *J. Appl. Phys.* **39**, 4589-4593, 1968

77. Z-Match is a registered trademark of Inficon Leybold-Heraeus Inc. East Syracuse, New York.

78. Reed CE, Kanazawa KK, Kaufman JH, *J. Appl. Phys.* **68**, 1993, 1991

79. Mecea VM, *Sensors and Actuators A-Physical*, **40**, 1-27, 1994

80. Lu C, Czanderna AW, *Methods and Phenomena 7: Applications of Piezoelectric Quartz Crystal Microbalances*, Elsevier Science Publishers, Amsterdam, 1984, pp 43-45

81. Slutsky LJ, Wade WH, *J. Chem. Phys.*, **36**, 10, 2688, 1962

82. King WH, *Anal. Chem.* **36**, 1735, 1964

83. Guilbault GG, Jordan JM, *CRC Crit. Rev. Anal. Chem.* **19**, 1, 1-28, 1988

84. Chuan RL, *J. Aerosol. Sci.* **1**, 111, 1970

85. Olin JG, Sern GJ, *Atmos. Environ.* **5**, 653, 1971

86. Mieure JP, Jones JL, *Talanta,* **16**, 149, 1969

87. Jones JL, Mieure JP, *Anal. Chem.*, **41**, 484, 1969

88. King WH, Camilli CT, Findeis AF, *Anal. Chem.* **40**, 1330, 1968

89. Vand C, *Acta. Crystallogr.* **6**, 797, 1953

90. Hammond DL, Benjaminson A, *IEEE Spectrum*, **6**, 53, 1969

91. King WH, Camilli CT, Findeis AF, *Anal. Chem.* **40**, 1330, 1968

92. Konash PL, Bastiaans GJ, *Anal. Chem.*, **52**, 1929-1931, 1980

93. Nomura T, Minemura A, *Nippon Kagaku Kaishi*, **1980**, 1621, 1980

94. Nomura T, Okuhara M, *Anal. Chimica. Acta.* **142**, 281-284, 1982

95. Nomura T, *Anal. Chim. Acta*, **124**, 81, 1981

96. Nomura T, Yamashita T, *Anal. Chim. Acta*, **143**, 243, 1982

97. Nomura T, Nagamune T, *Anal. Chim. Acta*, **155**, 231, 1983

98. Nomura T, Iijima M, *Anal. Chim. Acta*, **131**, 97, 1981

99. Nomura T, Maruyama, *Anal. Chim. Acta*, **147**, 365, 1983

100. Nomura T, Watanabe M, *Anal. Chim. Acta*, **175**, 107-116, 1985

101. Kanazawa KK, Gordon JG, *Anal. Chim. Acta*, **175**, 99-105, 1985

102. Kanazawa KK, Research Report, RJ 5125 (53236), 4/30/86, IBM Almaden Research Center

103. Bruckenstein S, Shay M, *Electrochimica Acta*, **30**, No 10, 1295-1300, 1985

104. Bruckenstein S, Hillman AR, *Handbook of surface Imaging and Visualisation* (Ed Hubbard AT), CRC Press, Boca Raton, 1995

105. Schumacher R, Angew. *Chem. Int. Engl.* **29**, 329-343, 1990

106. Kanazawa KK, Melroy OR, *IBM J. Res. Dev.* **37**, 157-171, 1993

107. Hinsberg WD, Willson CG, Kanazawa KK, *J. Electrochem. Soc.* **133** (7), 1448-1451, 1986

108. Price GJ, Buley JM, *Progress in Organic Coatings*, **19** (3), 265-274, SEP 16, 1991

109. Price GJ, Buley JM, *Journal of Macromolecular Science: Pure and Applied Chemistry*. **A31**, 1255-1262, Suppl. 6-7, 1994

110. Kurosawa S, Tawara E, Kamo N, Kobatake Y, *Anal. Chimica. Acta.* **230**, 41-49, 1990

111. Dunham GC, Nicholas HB, Danuta P, Janata J, *Anal. Chem.* **67**, 267-272, 1995

112. Ward MD, Delawaski E, *J. Anal. Chem.*, **63**, 886, 1991

113. Rodahl M, Hook F, Kasemo B, *Anal. Chem.* **68**, 2219-2227, 1996

114. Niemczyk TM, Martin SJ, Frye GC, Ricco AJ, *J. Appl. Phys.*, **64**, 5002, 1988

115. Yang M, Thompson M, *Anal. Chem.*, **65**, 3591-3597, 1993

116. Martin B, Hager HE, *J. Appl.. Phys.*, **65**, 2630-2635, 1989

117. Shana ZA, Josse F, *Anal. Chem.*, **66**, 1955-1964, 1994

118. Yao SZ, Zhou TA, *Anal. Chim. Acta*, **21**, 61-72, 1988

119. Josse F, Shana ZA, Zong H, *Proc. IEEE Ultrson. Symp.*, **1**, 425-430, 1993

120. Mecea VM, *Sensors and Actuators A-Physical*, **40**, 1-27, 1994

121. Wajid A, *Sensors and Actuators A-Physical*, **63**, 41-46, 1997

122. Lu C, Czanderna AW, *Methods and phenomena 7: Applications of Piezoelectric Quartz Crystal Microbalances*, Elsevier Science Publishers, Amsterdam, 1984

123. Finlayson-Pitts BJ, Pitts Jnr JN, *Atmospheric Chemistry; Fundamentals and Experimental Techniques*, Wiley New York, 1986

124. Alder JF, McCallum JJ, *The Analyst*, **108**, 1291, 1169-1189, 1983

125. Ali Z, *J. Therm. Anal. Cal.*, **55**, 397-412, 1999

126. Wessa T, Gopel W, *Fresenius J. Anal. Chem.*, **361**, 239-245, 1998

127. Cavic-Vlasak BA, Rajakovic LJV, *Fresenius J. Anal. Chem.*, **343**, 339-347, 1992

128. Zhang S, Chen ZK, Bao GW, Li SFY, *Talanta*, **45**, 4, 727-733, 1998

129. DeJesus DP, DeMedeiros GA, DoLago CL, *Quimica Nova*, **72**, 1, 32-37, 1999

130. Polo J, Ibbet E, Vilanova X, Bremzmes J, Correig X, *Electronics Letters*, **35**, 10, 772-773, 1999

131. D'Amico A, Palma A, Vetelino E, *Sensors and Actuators*, **3**, 1, 31-39, 1982

132. Bryant A, Poirier M, Riley G, Lee DL, Vetelino JF, *Sensors and Actuators*, **4**, 1, 105-111, 1983

133. Nieuwenhuizen MS, Harteveld JL. *Talanta*, **41**, 461, 1994

134. McGill RA, Abraham MH, Grate JW, *Chemtech*, **27**, 1994

135. Rajakovic LV, Bastic MB, Korenman YI, Tunikova SA, Belskih NV, *Anal. Chim. Acta*, **318**, 77-87, 1995

136. Paolesse R, DiNatale C, Macagnano A, Davide F, Boschi T, D'Amico A. *Sensors and Actuators B-Chemical*, **47**, 70-76, 1998

137. Chang P, Shih JS, *Anal. Chim. Acta*, **360**, 61-68, 1998

138. Xing WL, He XW, *Talanta*, **44**, 959-965, 1997

139. Hartmann J, Hauptmann P, Levi S, Dalcanale E, *Sensors and Actuators B-Chemical*, **35-36**, 154-157, 1996

140. Bruschi L, Delfitto G, Mistura G, *Rev. Sci. Inst.*, **70**, No1, Pt1, 153-157, 1999

141. Barnes C, D'Silva C, Jones J, Lewis T, *Sensors and Actuators A-Physical*, **31**, 159-163, 1992

142. Jones JP, Lewis TJ, *J. Chem. Soc. Faraday Trans.*, **91**, 18, 3147-3155, 1995

143. Bergveld P, *Sensors and Actuators A-Physical*, **56**, 1-2, 65-73, 1996

144. Cygan MT, Collins GE, Dunbar TD, Allara DL, Gibbs CG, Gutsche CD, *Anal. Chem.*, **71**, 142-148, 1999

145. Rosler S, Lucklum R, Borngraber R, Hartmann J, Hauptmann P, *Sensors and Actuators B-Chemical*, **48**, 415-424, 1998

146. Jane YS, Shih JS, *Analyst*, **120**, 2, 517-522, 1995

147. Menon A, Zhou R, Josse F, *IEEE Trans. Ultra. Ferroelectrics and Frequency Control*, **45**, 5, 1416-1426, 1998

148. Malitesta C, Losito I, Zambonin PG, *Anal. Chem.*, **71**, 1366-1370, 1999

149. Slutsky LJ, Wade WH, *J. Chem. Phys.*, **36**, 10, 2688, 1962

150. King WH, *Anal. Chem.*, **36**, 1735, 1964

151. King WH, U.S. Patent 3, 164, 004, January 5th, 1965

152. Guilbault GG, Jordan JM, *CRC Crit. Rev. Anal. Chem.*, **19**, 1, 1-28, 1988

153. Karasek FW, Tierney JM, *J. Chromatogr.*, **89**, 31, 1974

154. Janaghorbani M, Freund H, *Anal. Chem.*, **45**, 325, 1973

155. Edmonds TE, West TS, *Anal. Chem.*, **117**, 147, 1980

156. Karasek FW, Guy P, Hill HH, Tierney JM, *J. Chromatogr.*, **124**, 179, 1976

157. Schulz WW, King WH, *J. Chromatogr. Sci.*, **11**, 343, 1973

158. Konash PL, Bastiaans GJ, *Anal. Chem.*, **52**, 1929-1931, 1980

159. Tunoglu N, Caglar P, Wnek GE, *J. M. S. Pure Appl. Chem.*, **A35**, 4, 637-647, 1998

160. Rajakovic LV, Strdac S, *Analytica Chimica Acta*, **315**, 1-2, 83-91, 1995

161. Jia CR, Luo YZ, Pawliszyn J, *J. Micro. Separations*, **10**, 2, 167-173, 1998

162. Hierlemann A, Weimar U, Kraus G, Schweizer-Berberich M, Gopel W, *Sensors and Actuators B-Chemical*, **26**, 1-3, 126-134, 126, 1995

163. Hierlemann A, Schweizer-Berberich M, Weimar U, Kraus G, Pfau A, Gopel W, *Sensors Update: Sensor Technology Application Markets*, Baltes H, Gopel W, Hesse J (Eds.), VCH, Weinheim, 2, page 119, 1996,

164. Konig W, *HRC J. High Res. Chrom. Chromatogr. Commun.*, **5**, 588, 1982

165. Gopel W, *Sensors and Actuators B-Chemical*, **24**, 1-3, 17-32, 1995

166. Schierbaum KD, Gerlach A, Haug M, Gopel W, Sensors and Actuators A, 31, 1-3, 130-137, 1992

167. Zhou R, Haimbodi M, Everhart D, Josse F, *Sensors and Actuators B-Chemical*, **35-36**, 176-182, 1996

168. Menon A, Zhou R, Fabien J, *IEEE Transactions on Ultrasonics Ferroelectrics and Frequency Control*, **45**, 5, 1416-1426, 1998

169. Sun HT, Chen ZH, Wlodarski W, McCormick M, *Sensors and Actuators B-Chemical*, **35-36**, 146-153, 1996

170. Nanto H, Tsubakino S, Habara M, Kondo K, Morita T, Dougruchi Y, Nakazumi H, Waite RI, *Sensors and Actuators B-Chemical*, **34**, 312-316, 1996

171. Janata J, *Principles of Chemical Sensors*, Plenum Press, NewYork, 1990

172. Reinhoudt DN, Engbersen FJJ, Brzozka Z, Vlekkert HH, Honig GWN, Holterman HAJ, Verkerk UH, *Anal. Chem.*, **66**, 3618-3623, 1994

173. Visser HC, Reinhoudt DN, DeJong F, *Chem. Soc. Rev.*, **23**, 2, 75-81, 1994

174. Klok HA, Eibeck P, Moller M, Reinhoudt DN, *Macromolecules*, **30**, 4, 795-802, 1997

175. Tunca U, Yagci Y, *Prog. Polym. Sci.*, **19**, 233-286, 1994

176. Dickert FL, Hayden O, *Trends in Analytical Chemistry*, **18**, 3, 192-199, 1999

177. Malitesta C, Losito I, Zambonin G, *Anal. Chem.*, **71**, 1366-1370, 1999

178. Wulff G, Heide B, Helfmeier G, *J. Amer. Chem. Soc.*, 1089, 1986

179. Shea KJ, SaSaki DY, *J. Amer. Chem. Soc.*, **111**, 3442, 1989

180. Dickert FL, Thierer S, *Adv. Mater.*, **8**, 987, 1996

181. Dickert FL, Besenbock H, Tortschanoff M, *Adv. Mater.*, **10**, 149, 1998

182. Shinkai S, *J. Amer. Chem. Soc.*, **108**, 2409 1986

183. Gutsche CD, *Calixarenes: RSC Monographs in Supermolecular Chemistry*, No 1, Royal Society of Chemistry, Cambridge, 1989

184. Yilmaz A, Memon S, Yilmaz M, *J. Polym. Sci. A-Polym. Chem.*, **37**, 23, 4351-4355.

185. Schierbaum KD, *Sensors and Actuators B-Chemical*, **18**, 1-3, 71-76, 1994

186. Schierbaum KD, Gopel W, *Synthetic Metals*, **61**, 1-2, 37-45, 1993

187. Chen XL, He XW, Hu XB, Xu H, *Analyst*, **124**, 12, 1787-1790, 1999

188. O'Connor KM, Svehla G, Harris SJ, McKervey MA, *Talanta*, **39**, 1549, 1992

189. Chan WH, Lee AWM, Lee CM, Yau KW, Wang K, *Analyst*, **120**, 1963-1967, 1995.

190. Jin T, *Chem. Comm.*, **1**, 24, 2491-2492, 1999

191. Hartmann JH, Auge J, Hauptmann P, *Sensors and Actuators B-Chemical*, **18-19**, 429-433, 1994

192. Vicens J, Bohmer V, *Calixarenes: A Versatile Class of Macrocyclic Compounds*, Kluwer Academic Publishers, Dordrecht, 1993.

193. Lucklum R, Rosler S, Hartmann J, Hauptmann P, *Sensors and Actuators B-Chemical*, **35-36**, 103-111, 1996

194. Blair DS, Bando J, *Environ. Sci. Technol.*, **32**, 2, 294-298, 1998

195. Wink Th, van Zuilen SJ, Bult A, van Bennekom WP, *Analyst*, **122**, 43R-50R, 1997

196. Soncini P, Bonsignore S, Dalcanale E, Ugozzoli F, *J. Org. Chem.*, **57**, 4608, 1992

197. Vincenti M, Pelizzetti E, Dalcanale E, Soncini P, *Pure Appl. Chem.*, **65**, 1507, 1993

198. Chemical Sensors Special Issue, *Acc. Chem. Res.*, **31**, 5, 1998

199. Schierbaum KD, Weiss T, Thoden van Velzen EU, Engbersen JFJ, Reinhoult DN, Gopel W, Science, 265, 1413-1415, 1994.

200. Dickert FL, Baumler UPA, Zwissler GK, *Synthetic Metals*, **61**, 47-52, 1993

201. Dalcanale E, Hartmann J, *Sensors and Actuators B-Chemical*, **39**, 24-25, 1995

202. Grate JW, Patrash SJ, Abraham MH, Du CM, *Anal. Chem.*, **68**, 913-917, 1996

203. Dalcanale E, Soncini P, Bacchilega G, Ugozzoli F, *J. Chem. Soc. Chem. Commun.*, 500-502, 1989

204. Moran JR, Ericson JL, Dalcanale E, Bryant JA, Knobler CB, Cram DJ, *J. Amer. Chem. Soc.*, **113**, 5707-5714, 1991

205. Pinalli R, Nachtigall FF, Ugozzoli F, Dalcanale E, *Angew. Chem. Int. Ed.*, **38**, 16, 2377-2380, 1999

206. Grate JW, Patrash SJ, Abraham MH, Du CM, *Anal. Chem.*, **68**, 913-917, 1996

207. March J, *Advanced Organic Chemistry: Reactions, Mechanisms, and Structures*, Fourth Edition, John Wiley and Sons, New York, 1992, pages 89-91.

208. Atwood JL, Davies JED, MacNicol DD, *Inclusion Compounds*, Academic Press, London, **Vol. 2**, pages 231-260, 1984.

209. Konig WA, Lutz S, Hagen M, Krebber R, Wenz G, Baldenius K, Ehlers J, Dieck H, *J. High Res. Chromatorg.*, **12**, 35, 1989

210. Szente L, Szejtli J, *Analyst*, **Vol. 123**, 4, 735-741, 1998

211. Bugler J, Engbersen JFJ, Reinhoudt DN, *J. Org. Chem.*, **63**, 16, 5339-5344, 1998

212. He PA, Ye JN, Fang YH, Suzuki I, Osa T, *Analytica, Chimica Acta*, **337**, 2, 217-223, 1997

213. Ide J, Nakamoto T, Moriizumi T, *Sensors and Actuators A-Physical*, **49**, 1-2, 73-78, 1995.

214. Dickert FL, Tortschanoff M, Weber K, Zenkel M, *Fres. J. Anal. Chem.*, **362**, 1, 21-24, 1998

215. Yang X, Shi J, Johnson S, Swanson B, *Sensors and Actuators B-Chemical*, **45**, 1, 79-84, 1997.

216. Thomas RC, Hierlemann A, Staton AW, Hill M, Ricco AJ, *Anal. Chem.*, **71**, 16, 3615-3621, 1999.

217. Atwood JL, Davies JED, MacNicol DD, *Inclusion Compounds*, vol. 1, 1984

218. Reinbold J, Buhlmann K, Cammann K, *Sensors and Actuators B-Chemical*, **77-81**, 1994

219. Weber E, Skobridis K, Wierig A, Stathi S, Nassimbeni LR, Niven ML, *Angew. Chem. Int. Ed. Engl.*, **32**, 606, 1993

220. Flynn BR, Vaska L, *J. Chem. Soc. Chem. Commun.*, **703**, 1974.

221. Li PCH, Thompson M, *Analyst*, **120**, 2529-2535, 1995.

222. Li PCH, Thompson M, *Analyst*, **119**, 1947, 1994.

223. Kimura K, Maeda T, Shono T, *Analytical Letters*, **A11(10)**, 821-827, 1978

224. Machida Y, Nishi H, Nakamura K, Nakai H, Sato T, *Journal of Chromatography A*, **805**, 85-92, 1998

225. Lee D, Thomas JDR, *Talanta*, **41**, 6, 901-907, 1994

226. Lu CJ, Shih JS, *Analytica Chimica Acta*, **306**, 129-137, 1995

227. Xing WL, He XW, *Talanta*, **44**, 959-965, 1997

228. Battenberg A, Breidt VF, Vahrenkamp H, *Sensors and Actuators B-Chemical*, **30**, 29-34, 1996

229. Martin B, Hager HE, *J. Appl. Phys.*, **65**, 2630-2635, 1989

230. Barnes C, *Sensors and Actuators A-Physical*, **31**, 159-163, 1992

231. See section 1.5

232. Jia CR, Luo YZ, Pawliszyn J, *J. Micro. Separations*, **10**, 2, 167-173, 1998

233. Hunter TC, Price GJ, *The Analyst* **120** 1 161-165 1995

234. Lindsay D, Sherrington DC, Greig JA, Hancock RD, *React. Polym.*, **12** 59 1990

235. Pedersen CJ, *J. Amer. Chem. Soc.*, **89** 2495, 1967

236. Kimura K, Maeda T, Shono T, *Analytical Letters*, **10** 821-827 1978

237. Jia CR, Luo YZ, Pawlisyn J, *J. Micro. Separations*, **10(2)** 821-827 1998

238. Tunoglu N, Caglar P, Wnek GE, *J. M. S. Pure Appl. Chem.*, **A35(4)** 637-647 1998

239. Lu CJ, Shih JS, *Analytica Chimica Acta*, **306**, 129-137, 1995

240. Battenberg A, Breidt VF, Vahrenkamp H, *Sensors and Actuators B-Chemical*, **30**, 29-34, 1996

241. See section 3.6.2

242. Pedersen CJ, *J. Amer. Chem. Soc.*, **89**, 7017, 1967

243. Cram DJ, Cram JM, *Science*, **183**, 803, 1974

244. Sousa LR, Hoffmann DH, Kaplan L, Cram DJ, *J. Amer. Chem. Soc.*, **96**, 7100, 1974

245. Lehn J-M, Montavon F, *Tetrahedron Letters*, 4557, 1972

246. Cheney J, Lehn J-M, *J. Chem. Comm.*, 487, 1972

247. Gokel GW, *Monographs in Supramolecular Chemistry, No 3; Crown-Ethers and Cryptands*, The Royal Society of Chemistry, Cambridge, 1991

248. Saul Patai, *Supplement E; The Chemistry of Ether, Crown-Ether, Hydroxyl Groups and Their Sulphur Analogues*, John Wiley and Sons Ltd, USA, 1980

249. Tunca U, Y. Yagci, *Prog. Polym. Sci.*, Vol. **19**, 233, 1994

250. Atkins PW, *Physical Chemistry*, 4th Edition, Oxford University Press, page 885, 1990

251. Weast RC, *CRC Handbook of Chemistry*, Table F-216, 61st Edition, 1980-1981

252. Cotton FA, Wilkinson G, *Advanced Inorganic Chemistry*, 5th Edition, Wiley, New York, 1988

253. Wink TH, van-Zuilen SJ, Bult A, van-Bennekom WP, *Analyst*, **122**, 43R-50R, 1997

254. Weast RC, *CRC Handbook of Chemistry*, Table F-222, 61st Edition, 1980-1981

255. Barnes C, *Sensors and Actuators A-Physical*, **31**, 159-163, 1992

256. W. L. Xing, *Chemistry Letters*, 12, **1996**, 1065

257. Tamada K, Nagasawa J, Nakanishi F, Abe K, Hara M, Knoll W, Ishida T, Fukushima H, Miyashita S, Usui T, Koini T, Lee TR, *Thin Solid Films*, **327-329**, 150-155, 1998

258. Nuzzo RG, Dubois LH, Allara DL, *J. Amer. Chem. Soc.*, **112**, 558, 1990

259. Herdt GC, Czanderna AW, King DE, *Surface Science*, **1-3**, pp.L 371-L 374, 1996

260. Kim HJ, Kwak S, Kim YS, Seo BI, Kim ER, Lee H, *Thin Solid Films*, **327-329**, 191-194, 1998

261. Horacek J, Skladal P, *Analytica Chimica Acta*, **347**, 43-50, 1997

262. March J, *Advanced Organic Chemistry; Reactions, Mechanisms, and Structure*, pages 420-421, 4th Edition, John Wiley and Sons, New York, 1992

263. March J, *Advanced Organic Chemistry; Reactions, Mechanisms, and Structure*, pages 419, 4th Edition, John Wiley and Sons, New York, 1992

264. Yang Z, Gonzalez-Cortes, Jourquin G, Vire JC, Kauffmann JM, Delplancke JL, *Biosensors and Bioelectronics*, **10**, 789-795, 1995

265. Turyan I, Mandler D, *Israel Journal of Chemistry*, **37**, 225-233, 1997

266. Schneider TW, Buttry DA, *J. Amer. Chem. Soc.*, **115**, 12391-12397, 1993

267. See section 1.5

268. Atkins PW, *Physical Chemistry*, 4th Edition, Oxford University Press, page 752, 1990

269. Atkins PW, *Physical Chemistry*, 4th Edition, Oxford University Press, page 760, 1990

270. Townshend A, *Encyclopedia of Analytical Science*, Volume 2, page 835, table 2, Academic press Ltd, London, 1995

271. Lide DR, *CRC Handbook of chemistry*, Table 13-5, 74st Edition, 1993-1994

272. See table 3.1

273. See section 2.5 and 3.4.2

274. Townshend A, *Encyclopedia of Analytical Science*, Academic press Ltd, London, 1995

275. Bogdanovskaya VA, Tarasevich MR, *Biosensors Bioelectronics,* **11**, No 9, 853-861, 1996

276. See section 1.4.1

277. Atkins PW, *Physical Chemistry*, 4th Edition, Oxford University Press, page 885, 1990

278. Barrow GM, *Physical Chemistry*, 3rd Edition, McGraw-Hill Inc., USA, 1973

279. Dean JA, *Lange's Handbook of Chemistry*, Table 1.15, 14th Edition, McGraw-Hill INC, USA, 1992

280. Szejtli J, *Cylcodextrins and their Inclusion Complexes*, Akademiai Kiado, Budapest, Hungary, 1982

281. Swanson B, Johnson S, Shi J, Yang X, *Cyclodextrin-Based Microsensors for Volatile Organic Compounds*, 130-138, American Chemical Society, 1998

282. See section 1.8.6

283. Swanson B, Johnson S, Shi J, Yang X, *Cyclodextrin-Based Microsensors for Volatile Organic Compounds*, page 131, American Chemical Society, 1998

284. Jia CR, Luo YZ, Pawliszyn J, *J. Micro. Separations*, **10**, 2, 167-173, 1998

285. See section 1.4.1

286. Stephenson G, *Mathematical Methods For Science Students*, page 245, 2nd Edition, Longman Singapore Publishers Ltd, Singapore, 1992

287. These data was collected by Simona Negro

288. Easton CJ, Lincoln SF, *Modified Cyclodextrins: Scaffolds and Templates for Supramolecular Chemistry*, Imperial College Press, London, 1999

289. *Chemistry in Britain*, **34**, 11, 23, 1998

290. Radojevic M, *Chemistry in Britain*, **34**, 3, 30-33, 1998

291. Harrison RM, *Chemistry in Britain*, **30**, 987-991, 1994

292. Santos J, Serrini P, O'Beirn B, Manes L, *Sensors and Actuators B-Chemical*, **43**, 154-160, 1997

293. Where 1 ppb equals 0.001 cm^3 of the gas in 1 m^3 of air.

294. Cantalini C, Pelino M, Sun HT, Faccio M, Santucci S, Lozzi L, Passacantando M, *Sensors and Actuators B-Chemical*, **35-36**, 112-118, 1996

295. Miura N, Iio M, Lu G, Yamazoe N, *Sensors and Actuators B-Chemical*, **35-36**, 124-129, 1996

296. Finlayson-Pitts BJ, Pitts Jnr JN, *Atmospheric Chemistry; Fundamentals and Experimental Techniques*, Wiley, New York, 1986

297. Nagashima K, Meguro K, Hoba T, *Analyst*, **114**, 947-949, 1989

298. Jiang MRM, Weller MT, *Sensors and Actuators B-Chemical*, **30**, 3-6, 1996

299. Scheerder J, Walton DJ, Peterson IR, Miller LS, *Adv. Mater. Opt. Electron.*, **8**, 309-315, 1998

300. Walton DJ, Miller LS, Peterson IR, Bradford A, Worsfold O, Scheerder J, Parry DA, Forkan MG, Malins C, MacGraith BD, *Synthetic Metals*, **109**, 1-3, 91-96, 2000

301. Worsfold O, Walton DJ, Peterson IR, Miller LS, *Adv. Mater. Opt. Electron.*, **8**, 317-324, 1998

302. Townshend A, *Encyclopedia of Analytical Science*, Academic Press Ltd, London, 1995

303. Bogdanovskaya VA, Tarasevich MR, *Biosensors Bioelectronics,* **11**, No 9, 853-861, 1996

304. http://www.Marconitech.com/products/chem_s/chemprod.html

305. Pinalli R, Nachtigall FF, Ugozzoli F, Dalcanale E, *Angew. Chem. Int. Ed.*, **38**, 16, 2377-2380, 1999

306. Rudkevich DM, Verboom W, Brzozka Z, Palys MJ, Stauthamer WP Hummel GJ, Fanken SM, Harkema S, Engbersen JF, Reinhoudt DN, *J. A. Chem. Soc.*, **116**, 4341, 1994

307. Beer PD, Cadman J, Lloris JM, Martinez-Manez R, Padilla ME, Pardo T, Smith DK, Soto J, *J. Chem. Soc. Dalton Tans.*, **21**, 2, 127-133, 1999

308. Maeda Y, Fukuda T, Yamamoto H, Kitano H, *Langmuir*, **13**, 4187-4189, 1997

309. Cygan MT, Collins GE, Dunbar TD, Allara DL, Gibbs CG, Gutsche CD, *Anal. Chem.*, **71**, 142-148, 1999

310. Tabushi I, Kuroda Y, Mochizuki A, *J. Amer. Chem. Soc.*, **102**, 1152, 1980

311. Tabushi I, Kazuo Y, Tatsuya N, *J. Amer. Chem. Soc.*, **106**, 5267, 1984

312. March J, *Advanced Organic Chemistry: Reactions, Mechanisms, and Structure*, page 406, 4th Edition, John Wiley and Sons, New York, 1992

313. See section 1.7.2

314. Dickert FL, Tortschanoff M, Weber K, Zenkel M, *Fres. J. Anal. Chem.*, **362**, 1, 21-24, 1998

315. Rosler S, Lucklum R, Borngraber R, Hartmann J, Hauptmann P, *Sensors and Actuators B-Chemical*, **48**, 415-424, 1998

316. Lucklum R, Rosler S, Hartmann J, Hauptmann P, *Sensors and Actuators B-Chemical*, **35-36**, 103-111, 1996

APPENDICES

Appendix 1

Analysis of the cross-linked resins synthesised in section 2.4.2.

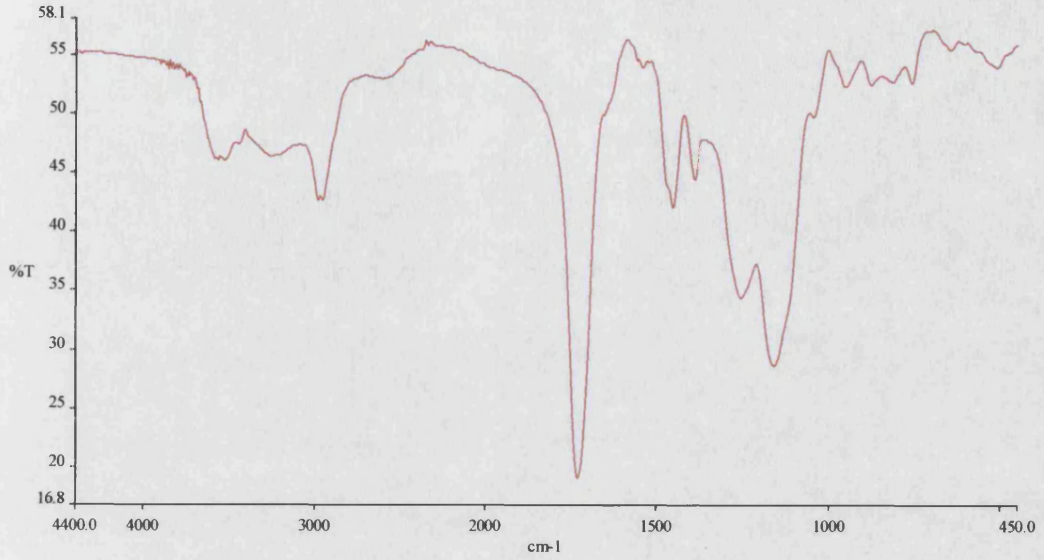

***Figure A1.1**: The KBr disc FTIR spectra of resin 18c6/70 after drying.*

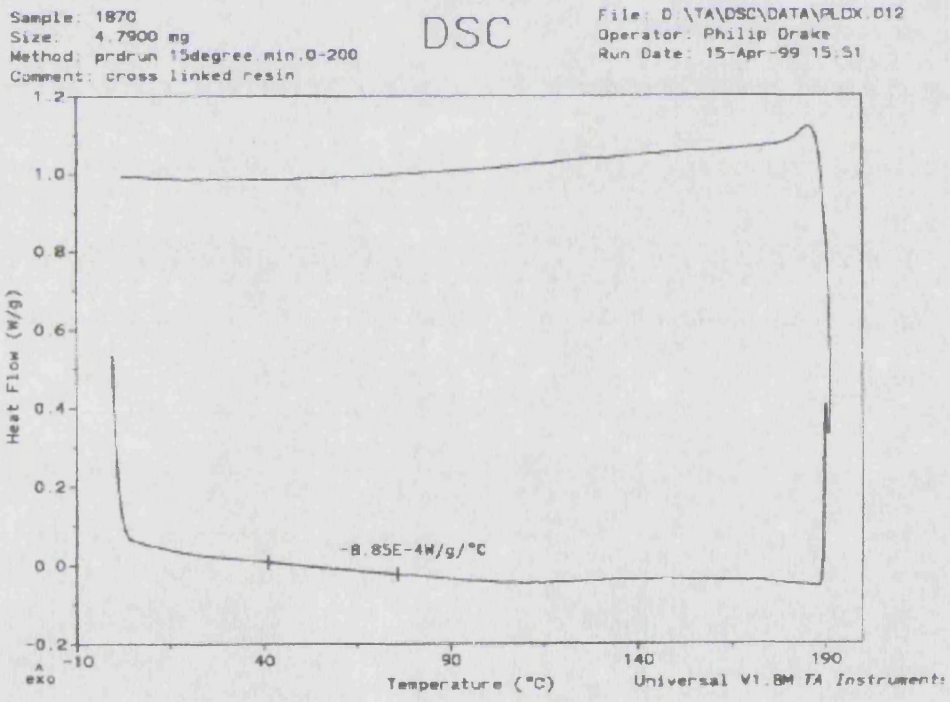

***Figure A1.2**: The DSC trace for resin 18c6/70 after drying at 70 °C.*

Appendix 2

Results from the uptake studies on the cross-linked resins.

Experiment 1: The uptake of $Na^+_{(aq)}$, $Li^+_{(aq)}$ and $K^+_{(aq)}$ were recorded individually with separate stock solutions.

Cross-linked Resin	Stock Used	Concentration		
		$Li^+_{(aq)}$ / ppm	$Na^+_{(aq)}$ / ppm	$K^+_{(aq)}$ / ppm
15c5/70	Stock1	49 (51)	48 (46)	34 (35)
15c5/30	Stock2	50	43	31
15c5/2	Stock2	49	44	30
18c6/70	Stock1	48 (51)	48 (44)	24 (25)
EG/70	Stock1	51 (52)	47 (46)	45 (46)
Stock1	-	52 (52)	49 (45)	45 (45)
Stock2	-	50	49	39

***Table A2.1**: The metal ion concentrations were recorded around 10 hours after exposure to the chelating resin. The numbers in brackets were recorded for the same sample after 2 weeks of continuous exposure.*

Experiment 2: The competitive uptake study. This time all three metal ions were in the same stock solution.

Cross-linked Resin	Mass / g	Concentration		
		$Li^+_{(aq)}$ / ppm	$Na^+_{(aq)}$ / ppm	$K^+_{(aq)}$ / ppm
15c5/70	1.002	60 (61)	51 (52)	51 (56)
15c5/30	0.998	52(52)	49(50)	36(46)
15c5/2	0.998	48(52)	50(50)	40(46)
18c6/70	1.014	53 (53)	45 (46)	32 (50)
18c6/30	1.001	52(52)	52(50)	26(45)
18c6/2	0.999	51(52)	52(50)	26(45)
EG/70	1.012	51(52)	49(50)	42(45)

***Table A2.2**: Uptake of $Li^+_{(aq)}$, $Na^+_{(aq)}$ and $K^+_{(aq)}$. All three ions were present in the same stock. The numbers in brackets indicate the stock solution concentration for that specific run.*

Experiment 3: Varying the concentration of the metal ion stock solution. Using 0.5 g of resin A and D and 10, 20, 50, 80, 150 and 200 ppm solutions.

Cross-linked Resin	Mass / g	Concentration		
		$Li^+_{(aq)}$ / ppm	$Na^+_{(aq)}$ / ppm	$K^+_{(aq)}$ / ppm
15c5/70	0.500	13(13)	11.7(11.6)	11.4(12.8)
	0.504	23(23)	14.5(14)	22(23)
	0.500	58 (57)	36 (37)	53 (55)
	0.501	92(93)	82(83)	89(91)
	0.506	180(180)	150(150)	165(165)
	0.506	230(230)	200(200)	220(220)
18c6/70	0.501	13(13)	12.2(11.6)	6.4(12.8)
	0.501	23(23)	14.5(14)	15.5(23)
	0.506	58 (57)	38 (37)	44 (55)
	0.500	90(93)	81(83)	74(91)
	0.499	180(180)	145(150)	150(165)
	0.510	230(230)	200(200)	200(220)

***Table A2.3**: Varying the concentration of the stock solutions The concentrations aimed for were 10, 20, 50, 80, 150 and 200 ppm of each metal ion. The numbers in brackets indicate the stock solution concentration for that specific run.*

Experiment 4: Varying the mass of the resin used keeping the initial metal ion concentration and volume constant. Using 50 ppm stock solutions and 0.5, 1.0, 1.5, 2.0, 2.5 g of resin A and D.

Cross-linked Resin	Mass / g	Concentration		
		$Li^+_{(aq)}$ / ppm	$Na^+_{(aq)}$ / ppm	$K^+_{(aq)}$ / ppm
15c5/70	0.500	58 (57)	36 (37)	53 (55)
	1.002	60 (61)	51 (52)	51 (56)
	1.499	60 (61)	51 (52)	50 (56)
	2.009	59 (61)	51 (52)	50 (56)
18c6/70	0.502	53 (53)	45 (46)	39 (50)
	1.014	53 (53)	45 (46)	32 (50)
	1.503	60 (61)	52 (52)	32 (56)
	2.000	58 (57)	50 (50)	30 (55)

***Table A2.4**: Varying the mass of the resin used from 0.5 g to 2.0 g. The numbers in brackets indicate the stock solution concentration for that specific run.*

Experiement 5: The kinetic uptake, see section 2.4 for the experimental detail.

Resin D, 1.343 g										
Concentration at t = 0 of $K^+_{(aq)}$ / ppm					69					
Time / minutes	2	5	8	12	16	20	24	28	37	200
Concentration $K^+_{(aq)}$ / ppm	19	17	16	19	16	17	17	16	16	15

***Table A2.5**: The uptake of $K^+_{(aq)}$ by resin D as a function of time.*

Appendix 3

X-PES data for the surface of an uncoated and polymer coated resonator. Figure A3.2 shows an increased peak associated with the presence of the carbon based coating. Also Figure A3.1 is representative of the spectra recorded for a resonator which failed to form SAM's. The large Si peak indicates surface contamination of the gold electrode preventing the reaction with the thiol compound used. Figure A3.2 shows the expected Au:Si peak ratio, this was recorded for a resonator that successfully formed SAMs.

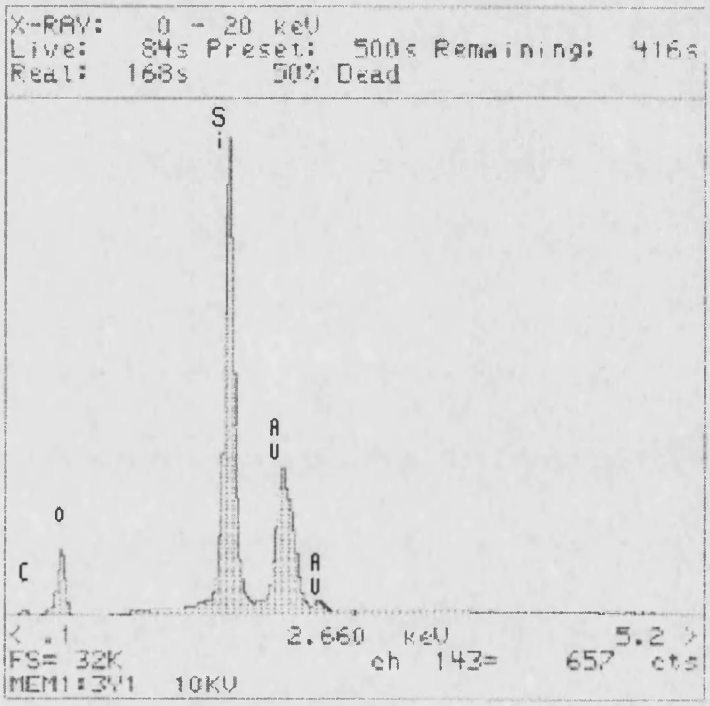

***Figure A3.1**: The X-PES spectra for an uncoated resonator showing the expected Si, O and Au peaks with only a minor C peak.*

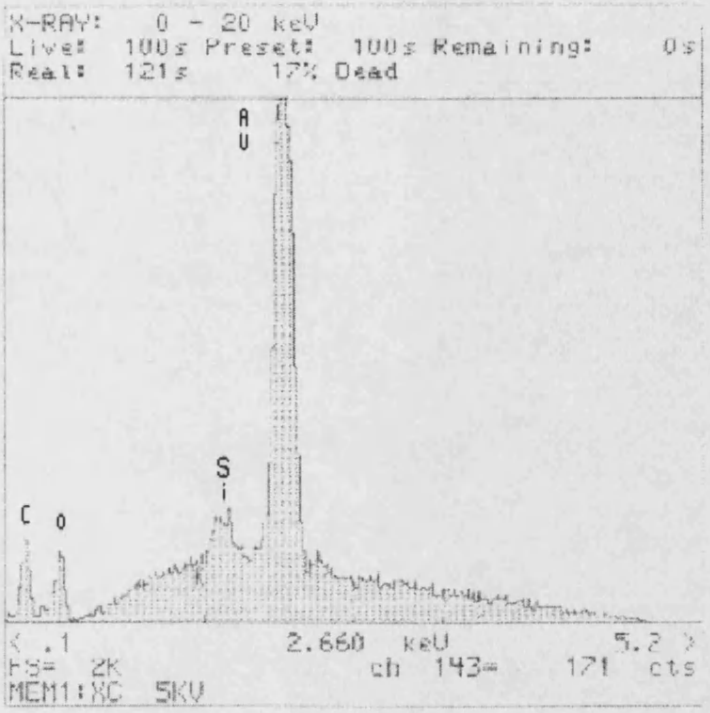

***Figure A3.2**: The X-PES spectra for a resonator coated with the cross-linked resin 18c6/70. This shows the increased carbon peak indicating the presence of the copolymer coating.*

Appendix 4

Figure A4.1 shows the overlay of two FTIR spectra of the cross-linked resin 18c6/70. They were recorded for the resin both before and after heating (red is after heating). The heating process is described in section 3.11.1 and involved placing the resin in a fan-assisted oven at a temperature of 180 °C for 24 hours. The spectra show no evidence for the thermal decomposition of the crown ether groups present in the copolymer network.

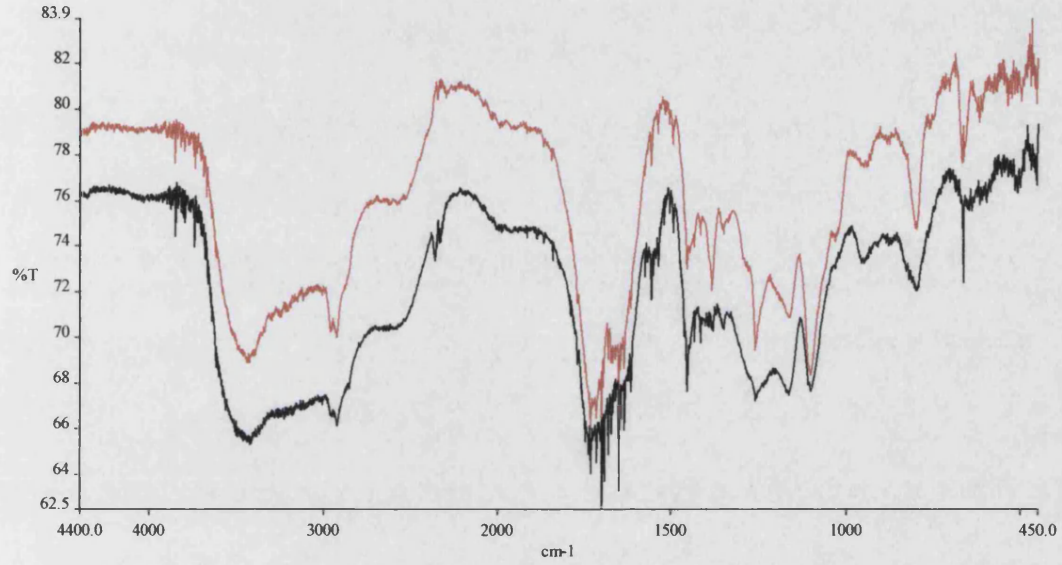

***Figure A4.1**: The FTIR spectra of resin 18c6/70 before and after heating. The red spectrum is after heating.*

Appendix 5

X-PES spectrum for coated resonators looking for evidence of K contamination in the saturated sensor. The three spectra are for a resonator prior to exposure to $K^+_{(aq)}$, after exposure to a saturated $K^+_{(aq)}$ solution and that of the saturated sensor respectively. The elemental labels in the spectra are those assigned to the associated peak. The regions of the spectra marked with a K represent the expected K peak position.

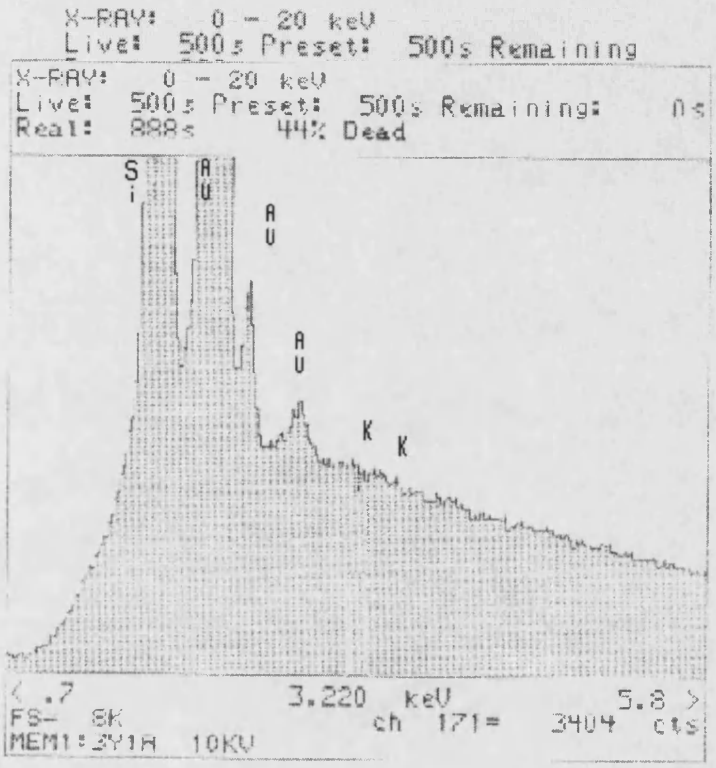

***Figure A5.1**: No $K^+_{(aq)}$ exposure.*

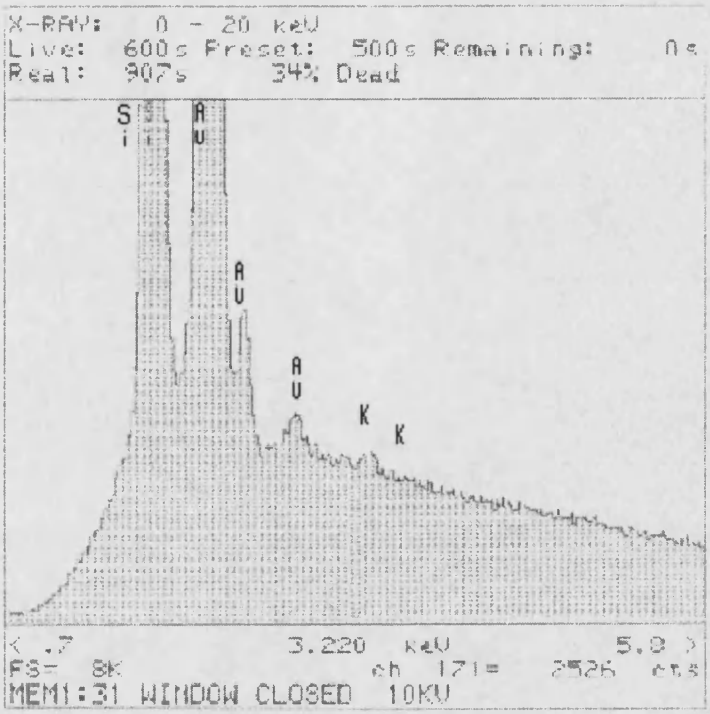

***Figure A5.2**: Exposed to concentrated $K^{+}_{(aq)}$ solution and rinsed.*

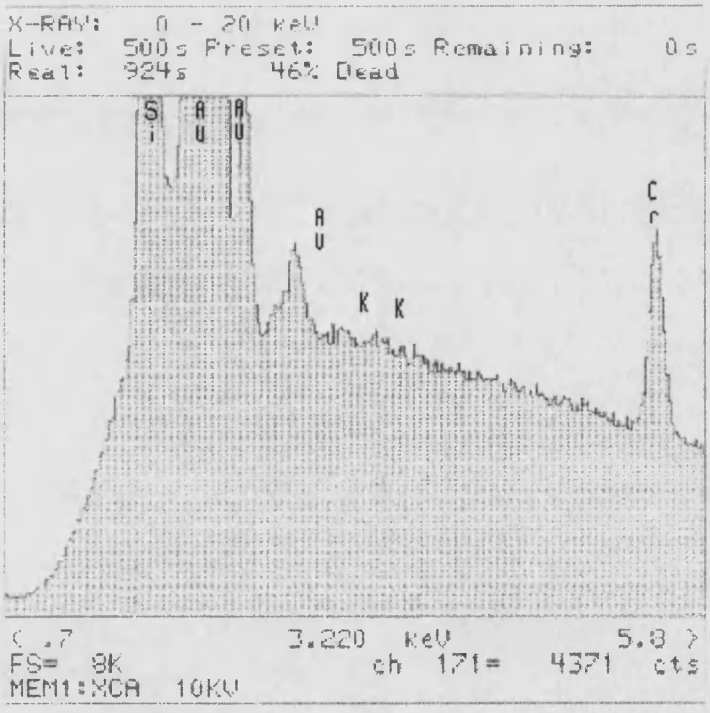

***Figure A5.3**: The saturated sensor.*

Appendix 6

The response factors calculated for the exposure resonators 1, 2 and 3 to a series of alcohol vapours. The figures associated with these tables can be seen in section 4.4. These are Figures 4.9, 4.10 and 4.11 respectively.

Resonator 1 α-cyclodextrin coated			
Solvent injected	**Regression analysis results;** Y = MX + C		
	M / Hz Sec μl^{-1}	**C / Hz Sec**	**R^2**
Methanol	4312.5	98.3	0.9781
Ethanol	2380.8	-141.8	0.9680
1-Propanol	1858.1	189.7	0.9982
1-Butanol	1651.9	279.6	0.9862
2-Propanol	239.4	160.8	0.9980
2-Butanol	677.5	224.2	0.9910
t-Butanol	158.6	221.8	0.9824

***Table A6.1**: The response factors of resonator 1 to a series of alcohols.*

Resonator 2 β-cyclodextrin coated			
Solvent injected	Regression analysis results; Y = MX + C		
	M / Hz Sec μl^{-1}	**C / Hz Sec**	**R^2**
Methanol	2394.6	264.6	0.9954
Ethanol	2380.8	-77.3	0.9930
1-Propanol	2429.7	-131.0	0.9922
1-Butanol	3294.6	12.2	0.9996
2-Propanol	1054.6	258.7	0.9901
2-Butanol	1994.0	138.1	0.9638
t-Butanol	1108.4	116.0	0.9951

***Table A6.2**: The response factors of resonator 2 to a series of alcohols.*

Resonator 3 amylose coated			
Solvent injected	**Regression analysis results;** Y = MX + C		
	M / Hz Sec μl^{-1}	**C / Hz Sec**	**R^2**
Methanol	1172.4	142.9	0.9776
Ethanol	1142.5	71.2	0.9563
1-Propanol	791.4	69.8	0.9537
1-Butanol	1647.6	171.7	0.9883
2-Propanol	722.65	98.5	0.9984
2-Butanol	976.1	267.1	0.9857
t-Butanol	1154.9	-95.8	0.9876

***Table A6.3**: The response factors of resonator 3 to a series of alcohols.*